IEEE 802.16 Metropolitan Area Network with SDMA Enhancement

Von der Fakultät für Elektrotechnik und Informationstechnik der Rheinisch-Westfälischen Technischen Hochschule Aachen zur Erlangung des akademischen Grades eines Doktors der Ingenieurwissenschaften genehmigte Dissertation

vorgelegt von

Diplom-Ingenieur Diplom-Kaufmann
Christian Hoymann

aus Essen

Berichter: Universitätsprofessor Dr.-Ing. Bernhard Walke
Universitätsprofessor Dr.-Ing. Bernhard Rembold

Tag der mündlichen Prüfung: 11. Juli 2008

AACHENER BEITRÄGE ZUR MOBIL- UND TELEKOMMUNIKATION

Herausgeber:
Universitätsprofessor Dr.-Ing. Bernhard Walke

Bibliografische Information Der Deutschen Bibliothek
Die Deutsche Bibliothek verzeichnet diese Publikation in der Deutschen Nationalbibliografie; detaillierte bibliografische Daten sind im Internet über http://dnb.ddb.de abrufbar.

1. Auflage 2008
ISBN: 3-86130-936-X
Aachener Beiträge zur Mobil- und Telekommunikation; Band 57

Wissenschaftsverlag Mainz
Süsterfeldstr. 83, 52072 Aachen
Telefon: 02 41 / 2 39 48 oder 02 41 / 87 34 34
Fax: 02 41 / 87 55 77
www.verlag-mainz.de

Herstellung: Druckerei Mainz GmbH,
Süsterfeldstr. 83, 52072 Aachen
Telefon 02 41 / 87 34 34; Fax: 02 41 / 87 55 77

Gedruckt auf chlorfrei gebleichtem Papier

"D82 (Diss. RWTH Aachen)"

ABSTRACT

Broadband access is the key driver of the telecommunications industry today. Customers all around the world demand this service to surf the World Wide Web (WWW) and to communicate by email. Furthermore, the classical Internet undergoes a shift towards a collaborative (second generation) Internet of people. The WWW is used as a platform to establish social networks and to share self-generated content. People download and upload rich multimedia content. They want to be connected.
In metropolitan areas, fixed Broadband Wireless Access (BWA) offers a cost-effective alternative to wired broadband access technology such as Digital Subscriber Line (DSL) and cable modem. In rural areas, fixed BWA can bridge the digital divide by bringing broadband services to remote places. Finally, BWA technology provides market potential for portable and mobile broadband services.
IEEE 802.16 (or WiMAX) is a promising radio access technology that performs similar to wired access systems and covers large geographic regions. The key feature to reach that goal is the integration of multi antenna techniques. Beamforming is the most promising MIMO technique since it allows for both, increased system capacity and extended cell coverage.
The thesis describes the developed comprehensive system concept to fully integrate Space Division Multiple Access (SDMA) technology into the IEEE 802.16 system. SDMA affects a large portion of the WiMAX system. Multiple antennas are required in the PHY layer to form adaptive patterns. Through the newly specified PHY Service Access Point (SAP) the enhanced PHY layer offers its beamforming services to the Medium Access Control (MAC) entities. The extended MAC protocol controls the additional spatial dimension. Multiple access based on Time Division Multiple Access (TDMA) and SDMA need to be coordinated. Besides the protocol, MAC algorithms are affected by beamforming and SDMA. The hierarchical TD-SD-OFDM scheduling algorithm proposed in this work optimizes resource allocation while observing strict real-time constraints. For multi-hop transmission a MAC extension is specified and evaluated. By leveraging SDMA on the feeder link, the proposed MAC frame structure strengthens the radio link, which is the bottleneck in most multi-hop systems. On the access link,

interference suppression by means of beamforming allows for a tight spatial reuse of the radio resource in Relay Station (RS) controlled subcells.
The introduced analytical evaluation illustrates the upper bounds of an OFDM-based IEEE 802.16 system in terms of coverage and throughput. It compares single-hop and multi-hop scenarios and illustrates the benefits of multi-hop operation. Furthermore, the thesis shows a possible implementation of an SDMA-enabled IEEE 802.16 system. Especially the prototypical TD-SD-OFDM scheduler can be seen as an exemplary reference implementation. The implementation is embedded in the event-driven system level simulator Wireless Network Simulator (WNS). The WNS is an open source simulation framework that is publicly available. The simulation tool comprises all aspects of the system, which are affected by SDMA. The presented simulative performance evaluation shows the enormous potential of beamforming and SDMA technologies. The thesis illustrates the enhanced throughput, the reduced packet delay, and the extended coverage of the SDMA-enabled WiMAX system. The major parameters that influence the system behavior are identified and evaluated.

KURZFASSUNG

Die Bereitstellung von breitbandigen Teilnehmeranschlüssen ist ein Hauptanliegen der heutigen Telekommunikations-Industrie. Kunden in aller Welt verlangen nach einem Zugang zum Internet. Dieser bietet die Möglichkeit Internet-basierte Dienste, paketvermittelte Telefonie oder zukünftige Anwendungen wie bspw. Fernsehen über das Internet Protokoll (IP) zu nutzen.
Eine breitbandige Funktechnik mit ortsfesten Teilnehmern (fixed broadband wireless access) kann in städtischen Gebieten eine kostengünstige Alternative zu drahtgebundenen Technologien wie DSL sein. In unterversorgten, ländlichen Gebieten bietet diese Technik die einzige Möglichkeit einen breitbandigen Anschluß zu erhalten. Eine mögliche nomadische Nutzung des breitbandigen Funkzugangs (mobile broadband) bietet darüber hinaus großes Marktpotential.
Die standardisierte Funktechnik IEEE 802.16, das so genannte WiMAX, bietet solche breitbandigen Teilnehmeranschlüsse an. Einerseits verspricht WiMAX die Abdeckung großer Flächen, andererseits eine Kapazität, die mit heutigen drahtgebundenen Techniken vergleichbar ist. Der Schlüssel zu diesen Eigenschaften liegt in der Unterstützung von Mehrantennen-Techniken, hier speziell der adaptiven Strahlformung, dem sog. Beamforming, und dem räumlichen Vielfachzugriff (engl. Space Division Multiple Access (SDMA)).
Die vorliegende Arbeit beschreibt ein vollständiges Systemkonzept, das den räumlichen Vielfachzugriff in die WiMAX Funktechnologie integriert. Diese Integration beeinflusst große Teile des Systems: Zuerst benötigt man Antennen-Arrays mit mehreren Antennenelementen. Die Richtcharakteristik des Arrays wird von der physikalischen Schicht adaptiv geformt. Die spezifizierten Dienstzugangspunkte bieten den darüber liegenden Medienzugriffsprotokollen Zugriff auf die Strahlformung. Über die angepassten Protokolle werden Informations- und Kontrollnachrichten ausgetauscht, die die zusätzliche räumliche Dimension berücksichtigen. Neben der zeitlichen Dimension verteilt die vorgestellte Bedienstrategie die Ressourcen zusätzlich in der räumlichen Dimension. Die wechselseitig auftretende Interferenz des räumlichen Vielfachzugriffs wird dabei reduziert. Aufgrund des hierarchischen Ansatzes bleibt der Rechenaufwand der entwickelten Bedienstrategie im sinnvollen Rahmen.

Des Weiteren wurde im Rahmen dieser Arbeit eine multihop-fähige MAC-Rahmenstruktur entwickelt. Diese Struktur erlaubt die Nutzung des räumlichen Vielfachzugriffs um die drahtlose Anbindung des Relays zu verbessern. Darüberhinaus bietet die aus der Strahlformung resultierende Unterdrückung der Interferenz die Möglichkeit, die Funkressourcen in den von Relays gebildeten Subzellen sehr effizient wieder zu verwenden.
Das Systemkonzept wurde im Rahmen der Open Source Entwicklungsumgebung Wireless Network Simulator (WNS) in einer prototypischen Implementierung umgesetzt. Die erzielten Simulationsergebnisse zeigen die Leistungsfähigkeit der adaptiven Strahlformung und des räumlichen Vielfachzugriffes basierend auf der Funktechnik WiMAX. Als Referenzszenario dient ein städtisches Gebiet mit guten Ausbreitungsbedingungen. Es wird gezeigt, dass die adaptive Steuerung der Richtcharakteristik eine Verdoppelung der Zellkapazität ermöglicht. Der räumliche Vielfachzugriff mit zwei parallelen Datenströmen bietet darüber hinaus eine Steigerung der Kapazität um 70% auf der Abwärtsstrecke und 40% auf der Aufwärtsstrecke. Die in dieser Arbeit vorgestellte Bedienstrategie nutzt die räumliche Dimension effektiv und verteilt die Funkressource darüber hinaus gerecht auf. Alle Teilnehmer des Netzes kommen in den Genuss einer erhöhten Zugangskapazität.
Die Simulationsergebnisse zeigen aber auch die Grenzen der adaptiven Strahlformung bzw. des räumlichen Vielfachzugriffs auf. Auf der Abwärtsstrecke reduziert sich die Sendeleistung, da diese auf alle parallel übertragenen Datenströme aufgeteilt wird. Auf der Aufwärtsstrecke skaliert die Nachbarzell-Interferenz mit der Anzahl paralleler Datenströme bzw. mit der Anzahl gleichzeitig aktiver Teilnehmer. Die maximal zulässige Anzahl paralleler Ströme ist daher ein kritischer Faktor. Im untersuchten Szenario mit neun Antennenelementen an der Basisstation sollten nicht mehr als vier zeitgleiche Ströme zugelassen werden.
Des Weiteren wird gezeigt, dass Mehrantennen-Funksysteme nicht mehr unter konventionellen Gesichtspunkten geplant und dimensioniert werden können. Heutige Funksysteme sind entweder Rausch- oder Interferenz-begrenzt. Allerdings ist die Signalqualität bei Nutzung von adaptiven Antennen-Arrays, z.B. während der Datenübertragung, unkritisch. Für alle untersuchten Zellradien und Gleichkanalabstände konnte eine zufriedenstellende Qualität festgestellt werden. Sogar ein Frequenz-Wiederverwendungsfaktor von eins ist möglich. Die Ergebnisse zeigen allerdings, dass die Qualität der Rundsendephase, während der Kontrollnachrichten ausgesendet werden, zum limitierenden Faktor wird. Die Rundsendephase wird mit einer omnidirektionalen Antennencha-

rakteristik abgestrahlt, der Gewinn der adaptiven Strahlformung steht also nicht zur Verfügung. Daher muss gerade in synchronisierten Funksystemen die Übertragung während der Rundsendephase besonders robust sein.

CONTENTS

CHAPTER 1

Introduction

1.1 Increasing Demand for Broadband Wireless Access

Broadband access is the key driver of the telecommunications industry today. Customers all around the world demand services offered by the WWW. Conventional applications such as web browsing and communication via email are well known and commonly used. Nowadays two major trends are changing the application landscape. First, Voice over IP (VoIP) is substituting classical circuit switched telephony. Mainly due to lower cost, VoIP is strongly demanded by private and business customers. Although VoIP does not require high throughput, it requires omnipresent radio access optimized for packet switched data transmission. Second, the classical Internet is revolutionized by what is called "Web 2.0". This refers to a collaborative (second generation) Internet of people. The WWW is used as a platform to share self-generated multimedia content and to establish social networks. In conventional WWW applications downlink traffic was the dominant factor. However, new applications generate a considerable amount of uplink traffic and they urge users to be online periodically or even continuously. Popular examples are, for instance, social networking platforms (Skype, Xing), auctions (ebay), and public knowledge databases (wikipedia). Definitely the highest demand for broadband capacity have content sharing platforms such as YouTube (video collection), Flickr (photo album), or Kazaa (file sharing).

People strongly demand web-based services. They use them regularly wherever they have a PC with broadband access, be it at home, in school/university, or in the office. All these places need to be connected. In metropolitan areas, wired access technologies, such as DSL or cable modem are already widely available. However, the wired infrastructure is owned by a few major players and access for third parties is restricted. In these markets, fixed BWA is a cost-effective alternative to wired technologies. Remote areas in newly developing or in developed countries lack a wired infrastructure. These

regions suffer from not being connected at all, they suffer from "the digital divide". Wired infrastructure is rather expensive and sometimes impossible to deploy, so fixed BWA is the preferred solution for these markets.
Besides the traditional fixed access, wireless technology offers the potential to provide portable and even mobile access. Hand-held devices such as mobile phones and PDAs become more and more powerful and computing devices such as laptop PCs become more and more mobile. Having powerful and mobile devices, people will demand portable and mobile BWA basically everywhere, e.g., in cafes, in busses, and on the streets.
Providing fixed and mobile broadband access economically to everyone everywhere is a major challenge. Up to now, some wireless systems such as Wireless Local Area Networks (WLANs) provide broadband access locally, others such as 2nd Generation (2G) and 3rd Generation (3G) systems cover large regions with narrow band access. WiMAX or IEEE 802.16 is a promising radio access technology that may reach both goals at once. It offers performances similar to wired broadband systems and at the same time it covers large geographic regions.

1.2 Enabling Technology: Multi-Antenna Systems

In order to reach the goal of true broadband access and wide area coverage, WiMAX comprises a set of promising features of modern wireless systems. The major technical features are a large channel bandwidth for high PHY layer capacity, OFDM transmission to overcome multipath propagation, TDMA/OFDMA multiple access schemes for time- and frequency-selective scheduling, and centrally controlled frame-based MAC to support Quality of Service (QoS). Multi-hop transmission overcomes challenging radio propagation conditions resulting from large link distances or heavy shadowing.
However, the most important feature of modern wireless systems is the integration of multi antenna techniques. These techniques offer a huge potential to boost system capacity: the achievable spectral efficiency of a multi-antenna link scales linearly with the number of antennas. In general, multiple antennas can be utilized in diverse manners:

Spatial Multiplexing allows for transmitting multiple data streams simultaneously from a multi-antenna sender to a multi-antenna receiver. Spatial multiplexing multiplies the capacity of a single link.

Diversity Coding allows for increasing the robustness of a transmission.

This extends the coverage of a link.

Beamforming allows for adaptively steering the antenna gain. It increases the carrier signal and reduces interference. The enhanced Signal to Interference plus Noise Ratio (SINR) can be used to achieve a larger transmission range or higher order Modulation and Coding Schemes (MCSs). Furthermore, beamforming allows for SDMA. An SDMA-enabled system provides access to several users simultaneously. This multiplies system capacity.

Spatial multiplexing is only applicable in high SINR regions, which limits the usage of spatial multiplexing to the inner area of a cell. Furthermore, multiple antennas are required at the transmitter and the receiver. Diversity coding is useful at the cell-edge where signal quality is poor. Since diversity coding utilizes the radio resource inefficiently it should not be used in situations where the SINR at the receiver is reasonable good, e.g., in the inner cell area or in Line-of-Sight (LOS) conditions.
Beamforming is the most promising multi-antenna technique since it allows for both, increased system capacity and extended cell coverage. The antenna gain of the adaptive array significantly enhances the signal quality at the cell edge, which results in extended coverage. In good SINR regions, SDMA allows for simultaneous data streams, which increases system capacity. Furthermore, beamforming and SDMA requires multi antennas only at the Base Station (BS). End-user devices do not need multiple antennas.
Initial drafts and the first version of the IEEE 802.16 standard supported multi-antenna techniques only rudimentarily [IEEE, 2003b]. Diversity coding was part of the OFDM-based PHY layer specification and an optional Advanced Antenna System (AAS) zone was foreseen. This AAS zone allowed for an allocation of subframes dedicated to conventional (non-AAS) and AAS-enabled Subscriber Stations (SSs). Besides that, nothing had been specified, so that the AAS option was simply a hook for a backward compatible integration of multi-antenna techniques in future versions of the standard. Hence, there was an obvious need to investigate beamforming techniques and to integrate them in the OFDM-based IEEE 802.16 specification. This is where the author was involved and where the work towards this thesis could contribute.

1.3 Contribution of the Thesis

The thesis describes a comprehensive system concept to fully integrate SDMA technology into the IEEE 802.16 system. SDMA mainly affects the following aspects of an IEEE 802.16 system:

PHY Layer: Multiple antennas form adaptive patterns when each antenna element is steered individually. The dynamic steering of beams is performed by an adequate beamforming algorithm. The chosen algorithm impacts the shape of the adaptive pattern.
The thesis investigates the influence of the number and the layout of antenna elements. For the given Reference Scenario a favorable solution is presented.

PHY SAP: A multi-antenna PHY layer offers enhanced services. These services are, for instance, (concurrent) transmission and reception through adaptive antenna patterns and SINR estimation for adaptive transmission and reception.
This thesis proposes an appropriate SAP that allows interchanging all necessary control information. Especially the additional spatial dimension and the requirements of the TD-SD-OFDM scheduler have been considered.

Standardized MAC Protocol: Resource allocation is announced by means of standardized MAC management messages. SDMA resource allocation gains another degree of freedom: the spatial domain. MAC management messages need to be extended in order to sufficiently consider this new dimension.
The presented extension of MAC management messages has been successfully contributed to the IEEE 802.16 standard. Hence, the outcome of this thesis has directly influenced the IEEE standardization [Hoymann and Piggin, 2004].

MAC Layer Algorithms Vendor-specific algorithms determine the behavior of the IEEE 802.16 system in terms of radio resource, radio link and medium access control. Some of these algorithms need to consider the additional spatial dimension offered by the SDMA-enabled PHY layer. Besides that, the interference characteristic of systems using adaptive patterns fundamentally changes. Intra-cell interference due to non-optimal antenna patterns is introduced. Inter-cell interference becomes much more bursty due to the main beams and side lobes of adaptive patterns. All this especially affects the scheduling algorithm. The thesis proposes a new scheduling architecture that is optimized for SDMA enabled systems. The hierarchical design allows for allocating resources efficiently in the time and spatial domain, while keeping the computational complexity within reasonable limits [Hoymann et al., 2007].

Multi-hop Operation Advanced multi-hop concepts also benefit from multi-antenna techniques. SDMA on the feeder link strengthens the bottleneck of most multi-hop systems. On the access link, interference suppression by means of beamforming allows for a tight spatial reuse of the radio resource between RS subcells.
The thesis presents a MAC layer concept that allows for multi-hop communication in IEEE 802.16. The proposal has two advantages. First, it is backward compatible. Hence, legacy WiMAX terminals can operate in such networks. Second, the concept allows integrating multi-antenna techniques. The current draft of IEEE 802.16j shows that the mobile multi-hop task group has been inspired by the publications, which were issued during the thesis work [Hoymann and Klagges, 2006; IEEE, 2008].

An analytical evaluation illustrates the upper bounds of an OFDM-based IEEE 802.16 system in terms of coverage and throughput. It compares single-hop and multi-hop scenarios and illustrates the benefits of multi-hop operation. The analytical evaluation supports the setup of the Reference Scenario, which is chosen for simulative performance evaluation.
Furthermore, the thesis shows a possible implementation of an SDMA-enabled IEEE 802.16 system. Especially the prototypical TD-SD-OFDM scheduler can be seen as an exemplary reference implementation. The implementation is embedded in an event-driven system level simulator. The simulation tool comprises all aspects of the system, which are affected by SDMA.
The performance evaluation by means of computer simulation shows the enormous potential of beamforming and SDMA technologies. The thesis presents the enhanced throughput, the reduced packet delay, and the extended coverage of the SDMA-enabled WiMAX system. The major parameters that influence the system behavior are identified and evaluated.

1.4 Outline

The following Chapter 2 summarizes background information on the history of the IEEE 802.16 technology and its predecessors within ETSI. It describes the relationship between the IEEE 802.16 standards committee and WiMAX as the corresponding industry forum. The current status of the IEEE 802.16 base standard, its amendments and active task groups are outlined. The chapter ends with a description of related and/or competing BWA technologies such as WiBro, LTE, or 1xEVDO.
Chapter 3 introduces the IEEE 802.16 base standard. It describes deployment concepts and foreseen frequency bands. The chapter goes into details on the OFDM-based PHY layer as well as on the MAC layer specification. Finally, system profiles narrow down the set of available options for testing purposes and for typical implementations.
Chapter 4 as one of the main chapters of this thesis derives a comprehensive system concept that fully integrates SDMA technology into the IEEE 802.16 system. It outlines all relevant aspects such as enhanced PHY layer operation, extended PHY SAP as well as MAC protocol specification, and sophisticated MAC layer algorithms.
A concept to integrate multi-hop operation by means of layer 2 relaying is given in Chapter 5. An approach for de-centrally controlled and one for centrally controlled RSs are outlined. Both concepts are further enhanced to fully support SDMA operation, which can be seen an enabling technology for an efficient operation of RSs.
Chapter 6 discusses an analytical approach to dimension cellular single-hop and multi-hop networks. The analysis compares single-hop and multi-hop deployments based on capacity and coverage. The chapter concludes by giving general guidelines, which propose to use multi-hop deployments in some scenarios, whereas it disadvises its deployments in others.
A possible implementation of an SDMA-enabled IEEE 802.16 system is given in Chapter 7. The implementation is based on the concept of Functional Unit Networks (FUNs). It is embedded in the event-driven simulation environment WNS, an open source software tool [openWNS, 2007].
Valuable performance evaluation results are given in Chapter 8. The results illustrate how the fundamental characteristics of interference and carrier signals change when SDMA is introduced. The performance of the implemented scheduling and interference estimation algorithms is outlined. Performance results of cellular IEEE 802.16 systems illustrate the potential of SDMA

technologies.
The thesis concludes with Chapter 9, where the main findings are summarized and the major results are highlighted.

CHAPTER 2

IEEE 802.16 – Overview

2.1 History

Shortly after the European Telecommunications Standards Institute (ETSI) Broadband Radio Access Networks (BRAN) started its effort on the standardization of BWA, the IEEE Standards Association (SA) established the IEEE 802.16 working group 1999. In the same year, both organizations agreed on a cooperation to harmonize their standards. IEEE 802.16 specified the initial standard for wireless metropolitan area networks operating in frequencies above 11 GHz. It was published in 2002 as IEEE 802.16-2001 [IEEE, 2002]. ETSI BRAN published its standard High Performance Radio Access Network (HiperACCESS) [ETSI, 2004, 2002c], which was based on the same single carrier physical layer as well.
In response to market needs and significant industry interest, the standardization efforts proceeded by extending the standard to licensed and license-exempt bands ranging from 2 to 11 GHz. Three additional PHY layers including one Single Carrier mode, an OFDM and a mode based on Orthogonal Frequency Division Multiple Access (OFDMA) were specified. The resulting amendment to the base standard was published in 2003 as IEEE 802.16a-2003 [IEEE, 2003b]. In the same year, ETSI published its corresponding standard named High Performance Metropolitan Area Network (HiperMAN), which applied OFDM only [ETSI, 2003a,b]. It was designed using the basic MAC of the IEEE 802.16 standard. HiperMAN was developed in close cooperation with IEEE 802.16, such that the HiperMAN standard and the OFDM based subset of the IEEE 802.16a-2003 standard interoperate seamlessly.
Further on, task group 802.16c developed an amendment for 10 to 66 GHz system profiles in order to aid interoperability specifications [IEEE, 2003c]. Working group IEEE 802.16d was set up to specify 2 to 11 GHz system profiles. Both groups additionally reviewed the corresponding standards to correct errors and inconsistencies. Before 802.16d could finish, the work

transitioned to a revision effort of IEEE standard 802.16-2001. The standard developed during this revision was published in 2004 as IEEE standard 802.16-2004 [IEEE, 2004a], replacing 802.16-2001, 802.16c-2002, and 802.16a-2003. From the date of publication, the new standard document supersedes the previous volumes.

2.2 WiMAX Forum

The Worldwide Interoperability for Microwave Access Forum is an industry-led, non-profit corporation formed to promote and certify compatibility and interoperability of broadband wireless products. Formed in 2001, member companies support the industry-wide acceptance of the IEEE 802.16 and ETSI HiperMAN standards in order to accelerate the introduction of these systems into the marketplace. By August 2006, more than 370 companies joined the WiMAX Forum, including equipment manufacturers, operators, system integrators, silicon and component makers, and application providers [WiMAX Forum, 2006a].

2.3 Current Status of Standardisation

2.3.1 IEEE 802.16-2004 - Base Document

The IEEE standard 802.16-2004 as it emerged out of the revision process is considered as the root document [IEEE, 2004a]. The basic MAC and four incompatible PHY layers are specified. An Asynchronous Transfer Mode (ATM) and a packet Convergence Sublayer (CS) as well as system profiles are part of the standard. It covers all frequency bands below 66 GHz. The process of standardisation finished in 2004. A corrigendum (IEEE 802.16-2004/Cor1-2005) corrects errors, inconsistencies, and ambiguities in the standard. It does not contain new material. The corrigendum was published along with the mobility amendment in 2006 [IEEE, 2006].

2.3.2 IEEE 802.16/Conformance

Conformance tests ensure that equipment is performing according to a general, independent and not according to a personal interpretation of the standard. Together with successful interoperability, verified conformance leads to certification. The final goal of certification is the global interoperability of fully functional equipment and systems. The conformance task group works out the general, independent conformance specifications for BSs and SSs based upon the 802.16 air interfaces. The documents describe the Protocol Implementation Conformance Statement (PICS), the Test Suite Structure and Test Purposes (TSS&TP), and the Radio Conformance Tests (RCT) needed to develop a standardized Abstract Test Suite (ATS). The documents are numbered and published as IEEE standard 802.16/Conformance01 to 802.16/Conformance04 [IEEE, 2003a, 2004c,d, 2007a].

2.3.3 IEEE 802.16.2 Coexistence

This task group provides a recommended practice for the design and coordinated deployment of BWA systems in order to control interference and facilitate coexistence among these systems and with other applicable systems that may be present. It analyzes appropriate coexistence scenarios and provides guidance for system design, deployment, coordination, and frequency usage. It generally addresses licensed spectrum between 2 and 66 GHz with particular focus on the range 23.5 to 43.5 GHz. The IEEE standard 802.16.2-2001 was published in 2001 [IEEE, 2001].
As the working group expanded the scope to include frequencies between 2 and 11 GHz, the standard amendment 802.16.2a was initiated. In 2003 the amendment was converted into a revision project. Along with additional material on coexistence between Point-to-Multipoint (PMP) and Point-to-Point (PTP) systems, the revision 802.16.2-2004 addresses licensed spectrum between 2 and 66 GHz in general, with an additional emphasis on 3.5 and 10.5 GHz [IEEE, 2004b]. The revision 802.16.2-2004 superceded the former version 802.16.2-2001.

2.3.4 IEEE 802.16e Mobility

In order to increase the market for BWA solutions, task group 802.16e takes advantage of the inherent mobility of wireless media. By providing enhancements to support SS moving at vehicular speed (Mobile SS (MS)), the specified system fills the gap between high data rate wireless LANs and high mobility cellular systems. The amendment IEEE 802.16e-2005 for a combined fixed and mobile operation in licensed bands below 6 GHz was published in 2006 [IEEE, 2006]. The published version of the mobility amendment also includes the corrigendum IEEE 802.16-2004/Cor1.

2.3.5 IEEE 802.16f / g / i Network Management

The purpose of the Network Management Task Groups is to provide 802.16 equipment with procedures and services to enable interoperable and efficient management of network resources, mobility, and spectrum. Within this group, the management plane behavior in 802.16 fixed and mobile devices is standardized. Amendment IEEE 802.16f-2005 defines a Management Information Base (MIB) for the MAC and PHY. It was published in 2005 [IEEE, 2005]. IEEE 802.16g creates standardized procedures and interfaces for the management of 802.16 devices [IEEE, 2007b]. Amendment IEEE 802.16i provides mobility enhancements to the MIB for the MAC and the PHY layer as well as associated management procedures.

2.3.6 IEEE 802.16h License Exempt

Task group 802.16h specifies improved coexistence mechanisms for license-exempt operation, as policies and MAC enhancements, to enable coexistence among systems based on IEEE 802.16. The amendment is not limited to license-exempt bands, but operation may take place in all bands where 802.16-2004 is applicable.

2.3.7 IEEE 802.16j Mobile Multi-hop Relay Task Group

The Mobile Multi-hop Relay group develops a relay mode for fixed and mobile terminals. 802.16 RS shall either extend the coverage or enhance the throughput of a BWA network by leveraging the higher throughput over multi-hop links. The multi-hop mode can also be used for self backhauling. BSs which do not have a backhaul connection could communicate with BSs that do. This will of course reduce the available bandwidth but it saves costs and extend network coverage into areas where connecting a BSs via a fixed lines is economically or technically not feasible.
Different from the existing Mesh mode, the Mobile Multi-hop Relay group focuses on tree structures and thus excluding inter-SS/MS communication. The RS mode shall be backward compatible to the PMP mode and shall support OFDMA. Fixed, nomadic and mobile RSs are taken into account, which may be owned and operated by the network operator, or which may be client terminals [IEEE, 2008].

2.3.8 IEEE 802.16m Advanced Air Interface

The ITU Radiocommunications Sector (ITU-R) develops advanced air interface specifications for mobile telecommunications. The requirements for these techniques are specified in cooperation with different stakeholders, such as 3GPP, 3GPP2, or IEEE. Initial proposals for these IMT-Advanced air interfaces are solicited for 2008. Standardization is expected to continue through 2009. The IEEE task group 802.16m seeks to develop an advanced IEEE 802.16 air interface that meets the requirements of International Mobile Telecommunications (IMT)-Advanced next generation mobile networks. The standard amends the IEEE 802.16 OFDMA specification to provide an advanced air interface for operation in licensed bands. That includes mobility support according to 802.16e and multi-hop capability specified in 802.16j. The amendment provides backward compatibility for legacy OFDMA equipment.

2.4 Related Technologies

2.4.1 ETSI BRAN HiperACCESS and HiperMAN

The Broadband Radio Access Networks (BRAN) technical committee of the European Telecommunications Standards Institute (ETSI) and IEEE working group 802.16 co-operate closely in order to harmonize the standards for BWA networks. ETSI BRAN standardizes the High Performance Radio Access Network (HiperACCESS) as well as the High Performance Metropolitan Area Network (HiperMAN) system.
HiperACCESS is a broadband multimedia fixed wireless access system to allow for a flexible and competitive alternative to wired access networks. HiperACCESS is based on single carrier transmission and is targeting high frequency bands, especially the 40.5 - 43.5 GHz band. The published specifications include the PHY and Data Link Control (DLC) layer specifications [ETSI, 2004, 2002c] as well as the convergence layers for the cell and packet based core networks [ETSI, 2002a,b,d,e]. Various conformance tests are specified for the PHY, for the DLC, and for the convergence layer.
HiperMAN is an OFDM based BWA system operating at radio frequencies between 2 and 11 GHz. Due to the close cooperation, HiperMAN and the OFDM based subset of IEEE 802.16a-2003 share the same MAC and PHY. Thus, they interoperate seamlessly. The published specifications include the

PHY and DLC layer specifications [ETSI, 2003a,b], electromagnetic compatibility and radio spectrum matters, and conformance test specifications.

2.4.2 Wireless Broadband (WiBro)

After the allocation of 100 MHz of spectrum in the 2.3 GHz band in 2002, the Telecommunications Technology Association (TTA) of Korea standardized the national Wireless Broadband (WiBro) system in 2004. Three licensed 27 MHz bands are allocated for three different operators, each band containing three 9 MHz channels. Thus, a frequency reuse factor of one allows for a cell structure with one to three sectors. The WiBro system supports mobile personal subscriber stations, such as cell phones, PDAs, handheld PCs, and laptop PCs moving with up to 60 km/h. The targeted throughput varies between a minimum of 128 Kilobits per Second (kbps) / 512 kbps and a maximum of 1 Mbps / 3 Mbps for uplink / downlink respectively. The WiBro specification is a subset of the IEEE standards 802.16-2004, 802.16e and 802.16-2004/Cor1. It is based on the OFDMA PHY layer using 1048 subcarriers in Time Division Duplex (TDD) mode. Harmonization activities work towards compatibility between the standards WiBro and WiMAX.

2.4.3 Evolution of 3G Systems

2.4.3.1 3GPP2: CDMA2000 / 1xEVDO

3GPP2 developed Evolution Data-Optimized (1xEVDO), also known as High Rate Packet Data (HRPD), as the data optimized evolution of CDMA2000. 1xEVDO is a data only system that is based on the same 1.25 MHz Frequency Division Duplex (FDD) channels as CDMA2000. In a 1.25 MHz channel 1xEVDO offers peak data rates of 2.4 Mbps (Rev 0) and 3.1 Mbps (Rev A) in the Downlink (DL) and 153.6 kbps (Rev 0) and 1.8 Mbps (Rev A) in the Uplink (UL). In order to achieve this significant increase in data throughput performance, the baseline CDMA2000 system is modified [3GPP2, 2002, 2005; WiMAX Forum, 2006b]:

- DL channel is changed from Code Division Multiplex (CDM) to Time Division Multiplex (TDM) to allow full transmission power to a single user
- DL power control is replaced by closed loop DL rate adaptation

- Adaptive Modulation and Coding (AMC), i.e., Turbo Codes as well as Quadrature Phase Shift Keying (QPSK), 8 Phase Shift Keying (PSK), 16 Quadrature Amplitude Modulation (QAM)
- Hybrid ARQ (HARQ)
- Fast DL scheduling
- Soft handoff is replaced by a more bandwidth efficient "virtual" soft handoff

The next evolutionary step following revision A is 1xEVDO-Rev B or data optimized multi-carrier. The enhancement increases DL spectral efficiency and data throughput by adding 64 QAM to the DL modulation scheme, which results in DL peak data rate for a 1.25 MHz carrier to 4.9 Mbps [3GPP2, 2007]. Furthermore, it allows for dynamic allocation of up to fifteen 1.25 MHz carriers in a 20 MHz bandwidth. By aggregating three carriers in a nominal 5 MHz channel bandwidth, 1xEVDO Rev B provides a peak DL rate of 14.7 Mbps and a peak UL data rate of 5.4 Mbps.
1xEVDO-Rev 0 had initial success in Korea and Japan beginning in 2003 with additional major deployments following in 2004 and 2005. The initial launch for 1xEVDO-Rev A with CDMA2000 UL enhancements took place in Korea and Japan in 2005. US deployments followed in 2006. Commercial deployments for 1xEVDO-Rev B are not anticipated until 2008 [WiMAX Forum, 2006b].

2.4.3.2 3GPP: UMTS / HSDPA / LTE

3rd Generation Partnership Project evolves its Wideband CDMA (WCDMA) system, called Universal Mobile Telecommunications System (UMTS), by including High Speed DL Packet Access (HSDPA) in the Release 5 specification. High Speed DL Packet Access (HSDPA) offers over the air DL peak data rate of up to 10.8 Mbps (up to 20 Mbps for MIMO systems) in a 5 MHz channel. With release 6, 3GPP has also defined UMTS enhancements for the UL. This is known as High Speed UL Packet Access (HSUPA) and the combination of HSDPA and HSUPA is known simply as High Speed Packet Access (HSPA). The maximum possible UL peak data rate is 5.76 Mbps. In order to improve the support of high data rate packet switched services, the following advanced features are introduced [Döttling et al., 2006; Forkel, 2005]:

- A new shared High Speed DL Shared Channel (HS-DSCH) allowing for multi-code operation and an Enhanced Dedicated Transport Channel (E-DCH) for UL

- Short frame sizes enabling Adaptive Modulation and Coding with fast Channel Quality Indicator (CQI) feedback. AMC includes Convolutional and Turbo Codes as well as QPSK and 16 QAM,
- Fast HARQ with incremental redundancy
- Fast scheduling to exploit multi-user diversity
- De-centralized architecture where protocol functionality is moved from the Radio Network Controller (RNC) to the base transceiver station (Node-B) thus reducing latency

3GPP's work on the Long-Term Evolution (LTE) of the 3G mobile system started in 2004. The LTE project develops a framework for the evolution of the 3GPP radio access technology (Evolved UTRA (E-UTRA) and Evolved UTRAN (E-UTRAN)) towards a high data rate, low latency and packet optimized radio access technology. The development and the final selection of techniques and the architecture is based on detailed requirements [3GPP, 2006a; Ekstrom et al., 2006]:

Control-plane capacity Support of at least 200 users per cell in the active state for spectrum allocations up to 5 MHz

User-plane latency Less than 5 ms in unload condition (i.e. single user with single data stream) for small Internet Protocol (IP) packets

User throughput Average user throughput per MHz, 3 to 4 times Release 6 HSDPA in DL and 2 to 3 times in UL

Mobility E-UTRAN is optimized for low mobile speed from 0 to 15 km/h. Higher mobile speed between 15 and 120 km/h is supported with high performance. Mobility across the cellular network is maintained at speeds from 120 to 350 km/h

Coverage Throughput, spectrum efficiency and mobility targets mentioned above are met for 5 km cell radius, and with a slight degradation for 30 km cells. Cells ranging up to 100 km are not excluded.

Spectrum flexibility E-UTRAN operates in spectrum allocations of different sizes, including 1.25, 2.5, 5, 10, 15, and 20 MHz in both UL and DL. Operation in paired and unpaired spectrum is supported. Two center frequencies are considered, i.e., the UMTS core frequency band at 2.0 GHz and also the Global System for Mobile Communication (GSM) band at 900 MHz.

Architecture and migration The E-UTRAN architecture is packet based, although it supports real-time and conversational class traffic

Radio Resource Management Enhanced support for end-to-end QoS. Support of load sharing and policy management across different radio access technologies

Complexity A minimum number of options and no redundant mandatory features

The final technical specification of the new air interface and the layout of the new architecture will be available in 2008. Reference [3GPP, 2006b] gives details of the physical layer considered by 3GPP. LTE is based on OFDMA in DL and on Single Carrier (SC)-Frequency Division Multiple Access (FDMA) in UL [Dahlman et al., 2007]:

Downlink OFDMA OFDMA allows for a highly flexible resource allocation in the time and frequency domain and it is scalable for the different considered bandwidths. The transmission time interval is further reduced compared to HSDPA, which ensures low latency and enables fast packet scheduling. Either consecutive or non-consecutive subcarriers/time positions are supported by the scheduler. A report of a channel quality indicator enables frequency selective scheduling. AMC supports QPSK, 16QAM, and 64QAM. The final LTE system supports MIMO techniques with 2x2 or 4x4 antennas as well as interference coordination among cells.

Uplink SC-FDMA The low Peak to Average Power Ratio (PAPR) SC-FDMA achieves uplink inter-user orthogonality and enables efficient frequency-domain equalization at the receiver side. Frequency adaptive scheduling is supported. The UL also supports MIMO techniques and interference coordination among cells.

The first commercial launch of HSDPA-based services was announced in December 2005 and operators in Europe and Japan started to promote services based on HSDPA in 2006. HSUPA availability is expected in 2008. 3GPP concludes the 3G LTE specification in March 2008. Most of the involved companies anticipate an initial deployment around the year 2010 [Döttling et al., 2006; WiMAX Forum, 2006b].

CHAPTER 3

IEEE 802.16 – Metropolitan Area Network Base Standard

3.1 Scope of 802.16

Wireless last mile technology is becoming a challenging competitor to conventional broadband wired last mile access systems such as DSL, cable modems and even fiber optic cables. The Institute of Electrical and Electronics Engineers developed a standard for BWA systems namely IEEE 802.16. The amendments to the base standard enhance the system to support advanced antennas systems, mobile SSs as well as mesh and multi-hop deployments. This broadens the system's applicability far beyond the pure fixed wireless last mile access.
The wireless Metropolitan Area Network (MAN) IEEE 802.16 specifies four different physical (PHY) layers including two SC modes, an OFDM and a mode based on OFDMA [IEEE, 2004a]. One SC mode, which is specified for frequency bands between 10 and 66 GHz targets LOS communication whereas all other modes are designed for frequency bands below 11 GHz that additionally covers Non Line-of-Sight (NLOS) links.
The OFDM based transmission mode of the IEEE 802.16 standard was developed in close cooperation with the European Telecommunications Standards Institute (ETSI) whose standard is named High Performance Metropolitan Area Network (HiperMAN) [ETSI, 2003a,b]. Thus, the HiperMAN standard and the OFDM based transmission mode of IEEE 802.16 are nearly identical. Both OFDM based physical layers should comply with each other and a global OFDM system should emerge [Koffman and Roman, 2002]. Both standards form the basis for the WiMAX certified technology. The WiMAX Forum is an industry-led, non-profit corporation formed to promote and certify compatibility and interoperability of broadband wireless products such as IEEE 802.16 and HiperMAN [WiMAX Forum, 2006a].
The main advantage of BWA technologies over wired systems such as DSL and cable modem results mainly from the high costs of the labor-intensive

deployment of cables. ”A 200-square-kilometer service area costs a DSL provider over $11 million. The same area can be served wirelessly for about $450,000” [Cherry, 2003]. Apart from being wireless the above-mentioned BWA systems IEEE 802.16 and HiperMAN is designed to meet today’s most promising challenges: NLOS operation capability cuts the deployment costs. Large cells radii allow for rapidly deployable infrastructure networks. This decreases time to market for new broadband services, which is crucial for the success of new operators. Networks become even more scalable by utilizing the optional Mesh deployment. The system performance enables operators to offer services requiring high peak bit rates. A substantial QoS support for packet-based services is provided by the system.

3.1.1 Deployment Concept

WiMAX’s network deployment consists of a PMP architecture where BS are the central, controlling units. On the one hand, they are connected to the operator’s core network and on the other hand they provide the wireless interface towards SS (see Figure 3.1). The BS’s connection to the core network is not part of the WiMAX network itself. It can be achieved by using cable or radio links. Available are for instance DS3/E3 services provided by the Plesiochronous respectively Synchronous Digital Hierarchy, Frame Relay or DSL [Orthman, 2005]. Alternatively, the WiMAX network itself can establish the backhaul to connect BSs wirelessly to the fixed network.

In the PMP deployment, each SS has a direct link to its BS. The wireless link might have LOS or NLOS characteristics. A repeater might even reinforce the signal. WiMAX business models foresee a variety of potential markets [Orthman, 2005]. Thus, WiMAX can provide high-speed Internet access for residential customers, Small Office, Home Office (SOHO). It can alternatively supply Small and Medium-Sized Enterprise (SME) with DSL or leased line services. As local loop bypass, it will carry packet data as well as circuit switched voice. Cellular operators will have the opportunity to replace its wired backhaul partly by a WiMAX network. Possibly even more relevant is the potential as backhaul for WLAN hot spots. Such 802.11 access points do need a high capacity, cost-efficient backhaul solution for their rapid growth. Other applications for WiMAX can be public safety services and private networks.

The IEEE standard foresees an optional Mesh deployment. Within the Mesh

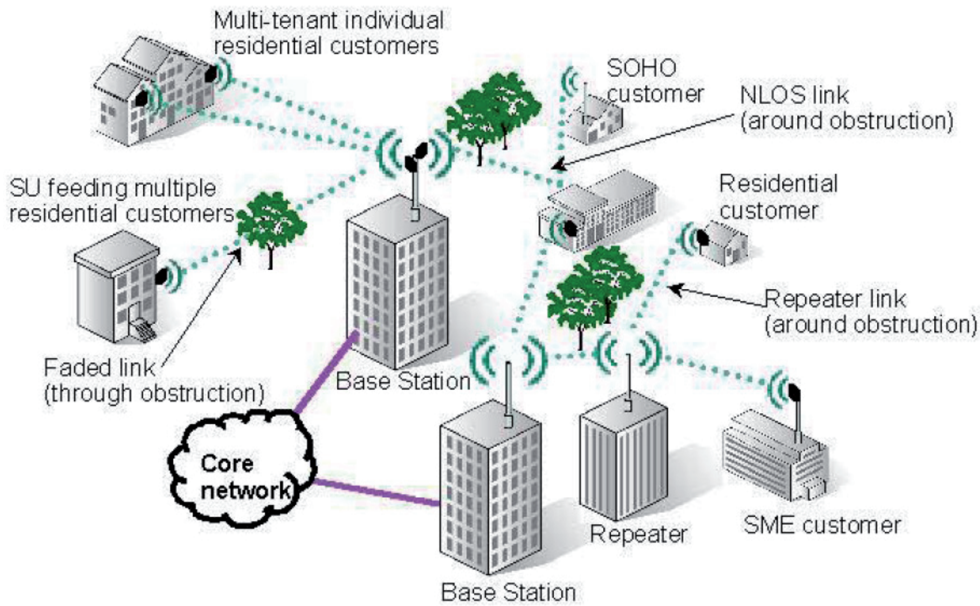

Figure 3.1: Deployment Concept

deployment, SSs do no longer need a direct link to the BS, but they might be associated to a RS that forwards data further to/from the BS. Section 3.3.2.9 gives a description of the optional Mesh mode and its benefits.

3.1.2 Target Frequency Bands

Since the electromagnetic propagation conditions in the huge foreseen frequency range are not uniform, the IEEE 802.16 standard targets two different frequency regions, i.e., 10 - 66 GHz and below 11 GHz.
At high frequencies, LOS radio propagation is required, since the wavelength is short and hence the attenuation owing to shadowing is severe. Under LOS condition, the effect of multipath propagation can be neglected. Only the main path carries significant energy. Another advantage at high frequencies is that system bandwidth is typically large compared to radio services operated at lower carrier frequencies. For BWA system bandwidth is in the order of 25 to 28 MHz. Frequency bands preferred by the Electronic Communications Committee (ECC)/ of the European Conference of Postal and Telecommunications Administrations (CEPT) for BWA ranges from 24.5 to 26.5 GHz and from 27.5 to 29.5 GHz [ERC, 2000, 2001]. Other potential bands are identified at 31.8 to 33.4 GHz and at 40.5 to 43.5 GHz [ERC, 1999,

2001].
Below 11 GHz, the radio propagation conditions allow for NLOS system operation. Thus, the system has to deal with shadowing and multipath propagation, which results in variations of the received signal power resulting from both, long-term and short-term fading. In license-exempt bands, users competing in the band may cause interference, hence regulation limits the allowed transmission power more restrictively compared to unlicensed bands. The interference has to be handled by the system, e.g., by means of an advanced power management or Dynamic Frequency Selection (DFS).
Since a single harmonized frequency band below 11 GHz is not available, [IEEE, 2004a] and [CEP, 1998] recommend different bands, depending on the region of interest. Licensed bands are available at 2.5 and 3.5 GHz in the majority of all countries. Some regions, e.g. Europe, additionally allocate bandwidth at 10 GHz as preferred bands for BWA [CEP, 1996]. Due to the suitable amount of low cost spectrum, license-exempt frequency bands at 2.4 and 5.7 GHz have been targeted nearly world-wide, see Figure 3.2.
Radio frequency technology for these frequencies is inexpensive since it is well known from 802.11a/b/g devices. License-exempt spectrum is strategically important for enabling grass root deployments in underserved, low populated rural and remote markets. However, other users of the license-exempt spectrum might cause severe interference.
New bands of interest are especially located at lower frequencies. The WiMAX Forum advances the allocation of licensed and license-exempt spectrum in lower frequency bands. Sub 1 GHz frequency bands, especially vacant or analog TV spectrum, are expected to become available after television stations' transition from analog to digital broadcasting will have been finished. In the U.S., the Federal Communications Commission (FCC) has already allocated spectrum for BWA in the 700 MHz range [WiMAX Forum, 2006a]. In India, vendors are pushing for the 700 MHz bands, so that a special Radio Frequency (RF) profile (refer to Section 3.4.3) may be specified.

3.1.3 Reference Model

The IEEE reference model follows general IEEE 802 guidelines and specifies only the MAC and the PHY layer. Higher layer protocols as well as the management plane are outside the scope of the standard. Figure 3.3 shows that the MAC comprises three sublayers.
The Convergence Sublayer (CS) interfaces higher layers. It classifies exter-

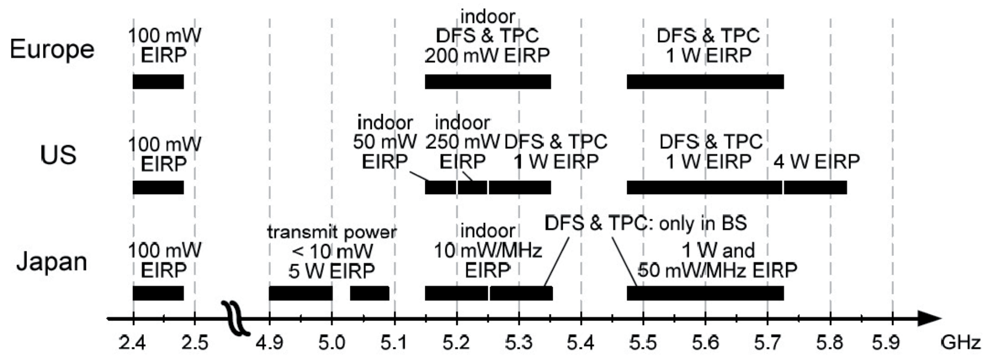

(a) Regulatory Restrictions for Unlicensed Operation

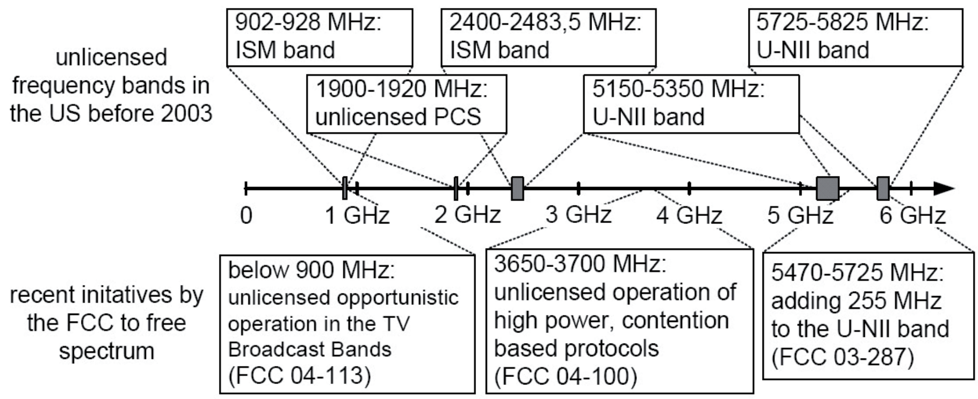

(b) Unlicensed Frequencies in the United States

Figure 3.2: Frequency Bands and Regulatory Restrictions of Unlicensed Operation (a) and Available Spectrum for Unlicensed Operation in the US (b) [Walke et al., 2006]

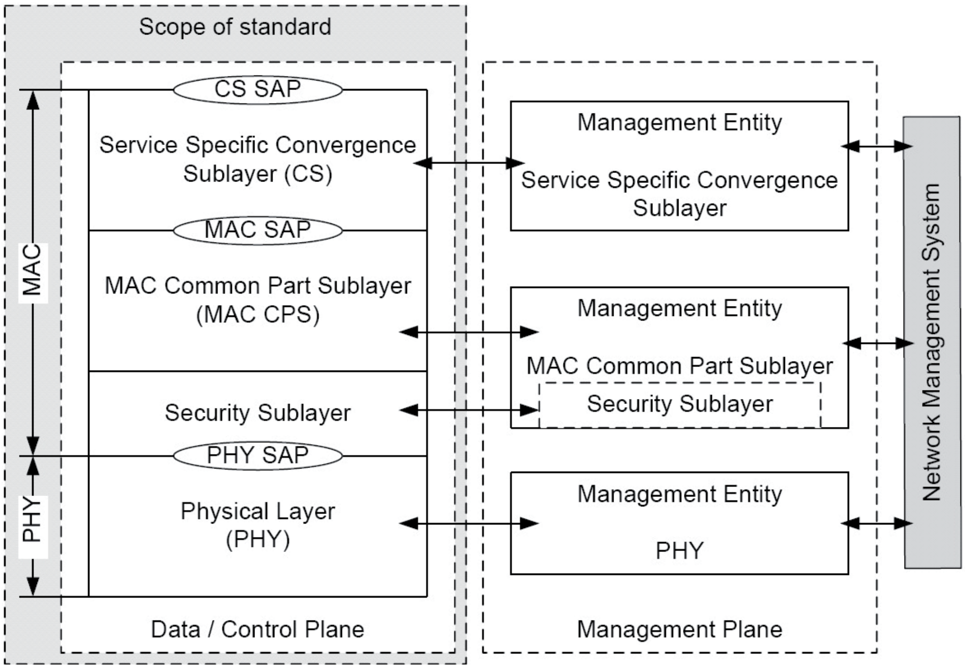

Figure 3.3: IEEE 802.16 Reference Model and Scope of Standard [IEEE, 2004a]

nal Service Data Units (SDUs) and associating them to the proper MAC connection. The CS may also process SDUs, e.g., to reduce overhead by performing Payload Header Suppression (PHS). Two CS specifications are provided for interfacing ATM as well as packet based protocols such as IP, Point-to-Point Protocol (PPP), or IEEE 802.3 (Ethernet). Both CSs are outlined in 3.3.1.

The MAC Common Part Sublayer (CPS) carries key functions such as system and channel access, connection management, and the application of QoS. Section 3.3.2 details the CPS.

Below the MAC CPS resides the security sublayer that provides authentication, secure key exchange, and encryption.

The IEEE 802.16 PHY specification defines multiple PHY layers, each appropriate to a particular frequency range and application. Thus, it is left free to develop, implement and deploy optimized systems with respect to available frequency bands, cell planning, equipment cost, and targeted services. Another reason for having several PHY specifications was the lack of support for a single one during standardization. The development of the supported PHY specifications is outlined in Chapter 2. The OFDM PHY, which is PHY layer of interest in this thesis, is described in Section 3.2.

3.2 IEEE 802.16 OFDM Based PHY Layer

The initial version of the 802.16 standard (IEEE 802.16-2001) specified only one Single Carrier (SC) PHY. It targets frequency bands between 10 and 66 GHz, in which LOS communication is mandatory due to the propagation characteristics. The current standard (IEEE 802.16-2004) specifies three additional PHY techniques. They were designed for frequency bands below 11 GHz that allow for NLOS links. The new modes include a Single Carrier below 11 GHz (SCa) and two multicarrier MCSs based on OFDM and OFDMA.
The OFDM based transmission mode has been standardized in close cooperation with the ETSI standard HiperMAN. Both OFDM based protocols shall comply with each other in order to form the basis for the WiMAX certified technology. In the following, the OFDM based PHY layer is presented in detail.

3.2.1 OFDM Basics

An OFDM system splits the available system bandwidth into orthogonal subcarriers. By reducing the bandwidth per subcarrier by a factor of N, the symbol duration becomes N times longer. Thus, the symbol becomes relatively robust to delay spread caused by multipath propagation. The introduction of a guard time, called Cyclic Prefix (CP), nearly eliminates the influence of delay spread if it is well designed in its length. Nevertheless, OFDM systems are highly sensitive to frequency offset errors, which destroy the orthogonality of subcarriers. Furthermore, the addition of a multitude of harmonic sinusoidal waves results in a high peak to average power ratio. Thus, the transceiver's power amplifier has to be linear over a wide range of power.
In OFDM transmission, each single subcarrier band can be seen as a narrowband flat fading channel. This allows for a relatively simple equalizer at the receiver. For instance, equalization might be performed by means of only one complex division per subcarrier.
The IEEE 802.16 OFDM PHY was designed for both, LOS and NLOS operation in frequency bands below 11 GHz. It can operate in licensed and license-exempt spectrum. Under license-exempt operation, the system makes

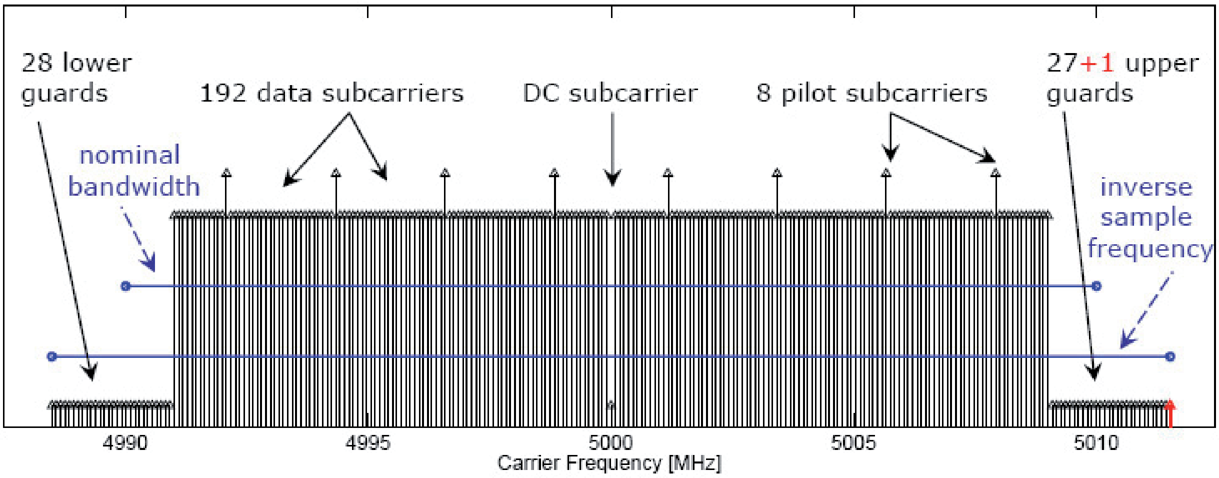

Figure 3.4: OFDM Subcarrier Spacing, 20 MHz Example with 5 GHz Center Frequency [IEEE, 2004a]

use of transmit spectral masks and channelization schemes specified for the unlicensed spectrum. These special features are captioned under the name Wireless High Speed Unlicensed MAN (HUMAN).

Link distances, i.e., cell sizes vary strongly based on the frequency bands used, the allowed transmit power, the environment, propagation conditions and antenna gain. The system targets distances between 2 and 4 km for NLOS and up to 15 km for LOS.

For the IEEE 802.16 OFDM PHY, Time Division Duplex (TDD) and Frequency Division Duplex (FDD) variants are defined. Channel bandwidths vary typically between 1.75 and 20 MHz. The actual sampling frequency depends on the chosen channel bandwidth and is slightly higher than the nominal bandwidth (see Figure 3.4). The OFDM PHY is based on a 256-point Fast Fourier Transform (FFT), resulting in 256 subcarriers. Thus, the subcarrier spacing is calculated to one 256^{th} of the sampling frequency. Eight subcarriers are used for pilot tones, 55 subcarriers are used as guard carriers. On the guard carriers and on the Direct Current (DC) subcarrier nothing is transmitted at all. Due to the even number of subcarriers, the upmost subcarrier spacing remains unused and can be seen as the 28^{th} upper guard carrier. The remaining 192 data carriers are used for data transmission.

Figure 3.5 shows the basic modules of an IEEE 802.16 transmitter-receiver chain. In the following the different modules and their corresponding functionality are outlined. The very first block MAC Source represents the MAC

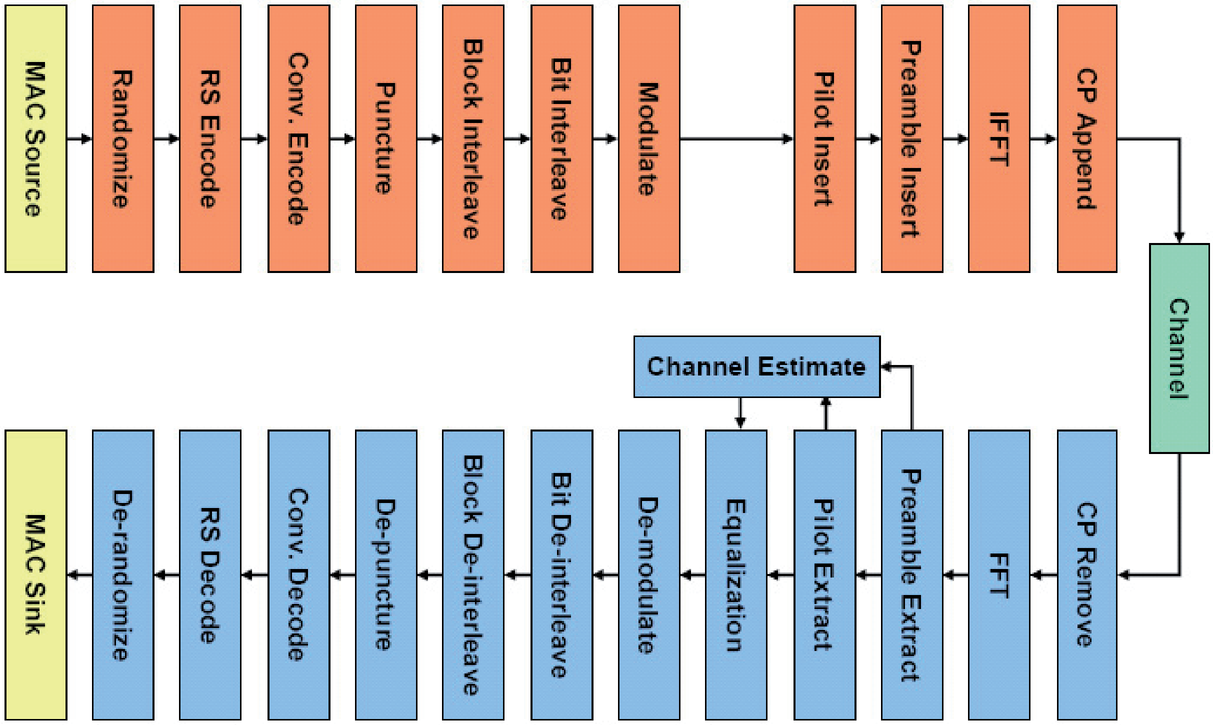

Figure 3.5: 802.16 Transmitter-Receiver Chain

layer. It generates the current MAC frame. The frame is converted into a bit stream, which is given to the first block of the PHY layer, i.e., the Randomizer.

3.2.2 Randomizer

The Randomizer (or Scrambler) adds a pseudo-random binary sequence to the original DL and UL bit stream. This random bit sequence avoids long rows of zeros or ones for a better coding performance of the following Forward Error Correction (FEC) modules. The addition is processed on each burst independently. The pseudo-random binary sequence generator is initialized with the BS Identifier (BSID), the MCS used for the burst and the frame number. At the end of each burst, the Randomizer adds padding bytes (0xFF) to end up on an OFDM symbol boundary. For the following convolutional coder to start and end in the well-known and predefined all-zeros state the module appends one tail byte of zeros (0x00).

Table 3.1: Modulation and Coding Schemes and Resulting Block Sizes

Modulation	Overall coding rate	Uncoded block size	Coded block size
BPSK	1/2	12 byte	24 byte
QPSK	1/2	24 byte	48 byte
	3/4	36 byte	48 byte
16-QAM	1/2	48 byte	96 byte
	3/4	72 byte	96 byte
64-QAM	2/3	96 byte	144 byte

3.2.3 Forward Error Correction

The Forward Error Correction (FEC) scheme consists of the concatenation of a Relay Station (RS) outer code and an inner Convolutional Code (CC). A concatenated code has been specified in order to achieve a superior error correction performance for a given complexity compared to a single but longer code.
The Reed-Solomon (RS) coder corrects burst errors at byte level. The actually applied code depends on the MCS and is derived, i.e. shortened, from a systematic RS (N=255, K=239, T=8) code using the Galois field (28). N is the number of overall bytes after encoding, K is the number of data bytes before encoding, and T stands for the number of data bytes that can be corrected. The RS code is particularly useful for OFDM links in the presence of multipath propagation, since bursty errors might occur frequently.
The CC corrects independent bit errors. A CC code can easily and efficiently be decoded, e.g., using the Viterbi algorithm. The CC decoder can benefit from softbit input generated by the demodulation and depuncturing blocks. The concatenation of both codes is made rate-compatible by the following puncturing module. Based on four puncturing patterns, bits are removed to realize different code rates. The punctured bits are replaced at the receiver side either as hard (either 1 or 0) or soft bits (no information, i.e., a value of 0.5). The support of Block Turbo Code (BTC) and Convolutional Turbo Code (CTC) is optional. Table 3.1 shows the resulting data block sizes for each MCS.

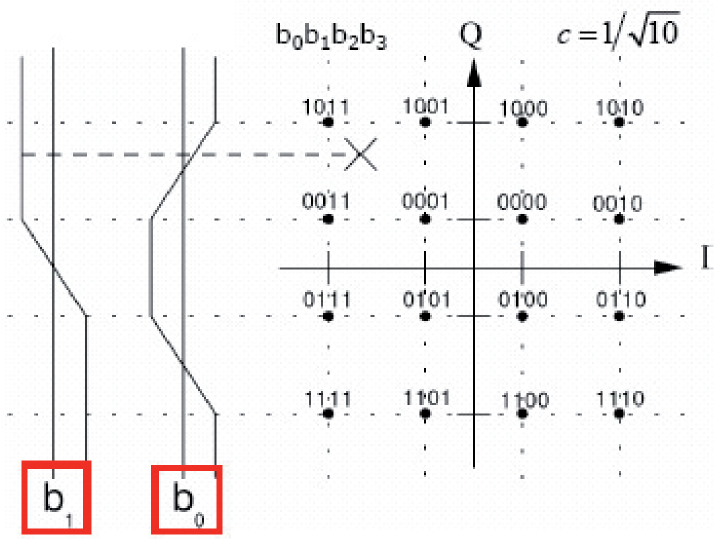

Figure 3.6: 16 QAM Constellation Diagram with Soft Bit Generation

3.2.4 Interleaving

The Interleaver is composed of a block and a bit interleaver. The block interleaver maps adjacent coded bits onto non-adjacent subcarriers to overcome burst errors. This can be done by writing the bit stream into 12 rows of an array rows-wise and by reading the bits out column-wise. Alternatively, a deterministic formula can be applied to modify the indices of the bits. The bit interleaver maps adjacent coded bits alternately onto less and more significant bits of the constellation to avoid long runs of unreliable bits. This has an impact only for QAM modulation where a single bit, e.g. using 16-QAM, can either switch once (more significant bit) or twice (less significant bit) while moving through the constellation diagram (see bits b_0 and b_1 in Figure 3.6).

3.2.5 Modulation

The block Modulate converts the bits into complex constellation points. Figure 3.6 shows the mapping of bits to complex symbols being composed of the inphase (I) and quadrature (Q) component of a 16-QAM constellation diagram. The amplitude and phase of the complex symbol become the amplitude and phase of the corresponding subcarrier in the Inverse Fast Fourier Transform (IFFT) block. The amplitude of the constellation point

is normalized to achieve equal average power (factor c in Figure 3.6).
The constellation points are subsequently modulated onto the data subcarriers in order of increasing frequency offset. The first point is modulated onto the subcarrier with the lowest offset. Per default, all 192 data subcarriers are modulated. However, the optional subchannelization mode allows to allocate individual subchannels, i.e., groups of subcarriers. Unused data subcarriers are not modulated at all. The optional subchannelization mode is outlined in Section 3.2.10.
Binary Phase Shift Keying (BPSK), QPSK, 16-QAM and 64-QAM are the modulation schemes specified by the 802.16 standard. The FEC options are paired with the modulation schemes to form burst profiles, i.e., MCSs of varying robustness and efficiency. The possible MCS are listed in Table 3.1. The demodulator at the receiver side can convert the perceived constellation points of the subcarriers either in hard or soft bits (refer to Figure 3.6). Soft bits generated by the demodulator as well as soft bits introduced by the depuncturing block can increase the performance of the convolutional decoder.

3.2.6 Pilot Tones & Preambles

In between the 192 data subcarriers eight subcarriers are inserted for pilot tones. These subcarriers are BPSK modulated with a pseudo-random binary sequence. The actual BPSK constellation point depends on the random sequence initialization and on the pilot tone subcarrier index. Since the receiver knows the modulation of the pilot tones very well, this knowledge can be used for channel estimation, synchronization, and tracking of frequency offsets during the regular reception of an OFDM symbol. The remaining subcarriers which are not used for data transmission, i.e., 55 guard carriers and the DC carrier are not modulated at all.
Preambles can be appended either in the frequency domain, i.e., before the IFFT block or in the time domain, i.e., after the IFFT. Preambles and midambles are pre-defined training symbols and are therefore used for frame time- and frequency synchronization and for channel estimation purposes. Preambles are composed of QPSK modulated subcarriers. Only every second or every fourth subcarrier is used so that the resulting time domain waveform consists of two, respectively, four repetitive parts.
The long preamble consists of two consecutive OFDM symbols. A long preamble is appended at the beginning of each DL subframe to indicate the

start of the MAC frame and it is used to transmit initial ranging messages in contention-based uplink slots during the network entry procedure.
Short preambles consist of only one OFDM symbol. Short preambles precede UL bursts and, optionally, DL bursts. As UL midambles, they may be included periodically in UL bursts. Short preambles might be cyclically shifted by an integer number of samples.
By means of the cyclic shift, concurrently transmitted preambles become separately detectable. The preamble modification can be used by Space Division Multiple Access (SDMA) techniques such as joint detection and pre-distortion. The cyclic shift can also be leveraged by other advanced antenna techniques, e.g. space-time codes.

3.2.7 Inverse Fast Fourier Transform

The Inverse Fast Fourier Transform (IFFT) module creates the OFDM waveform by transforming the complex constellation points from the frequency domain into the time domain. Since a 256 IFFT is used, the addition of 256 individual subcarrier waveforms composes the resulting OFDM waveform. As an example, Figure 3.7a shows three separated subcarriers, which are modulated with the complex values 1+i. The resulting phase shift of 45° represents the QPSK modulated bit sequence bx00. Figure 3.7b shows the sum of three subcarriers. In general, the addition of all 256 sinusoidal waves results in a high Peak to Average Power Ratio (PAPR). For instance, the worst case PAPR of a QPSK modulated OFDM symbol (with an oversampling factor L=1) is 23 dB. Typical PAPRs vary between 8 and 13 dB. PAPR reduction techniques can reduce this value by 2 to 4 dB [Han and Lee, 2005]. Still, the transceiver's power amplifier has to be linear over a wide range of power.

3.2.8 Cyclic Prefix

The phenomenon of delay spread is due to multipath scattering and causes inter-symbol interference and inter-carrier interference. In order to preserve the orthogonality of subcarriers a Cyclic Prefix (CP) is introduced in front of every useful part of an OFDM symbol [van Nee and Prasad, 2000]. As Figure 3.8 indicates, the CP extends the useful OFDM symbol time by copying the last portion of the OFDM waveform to the front of the symbol. Different CP lengths, measured in ratios of CP duration to useful symbol duration,

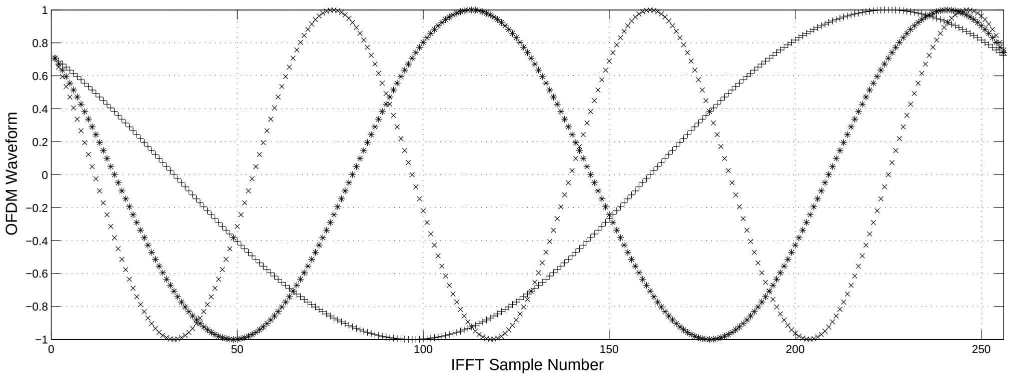

(a) Three separated modulated subcarriers

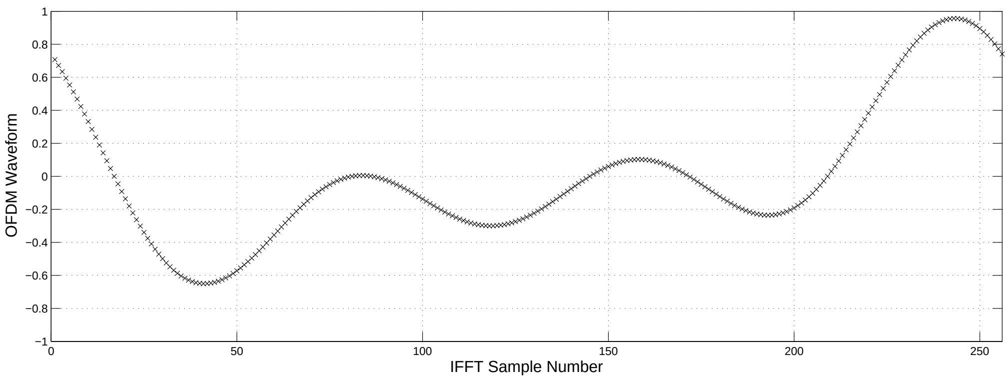

(b) Sum of three modulated subcarriers

Figure 3.7: Modulated Subcarriers that form the OFDM Waveform

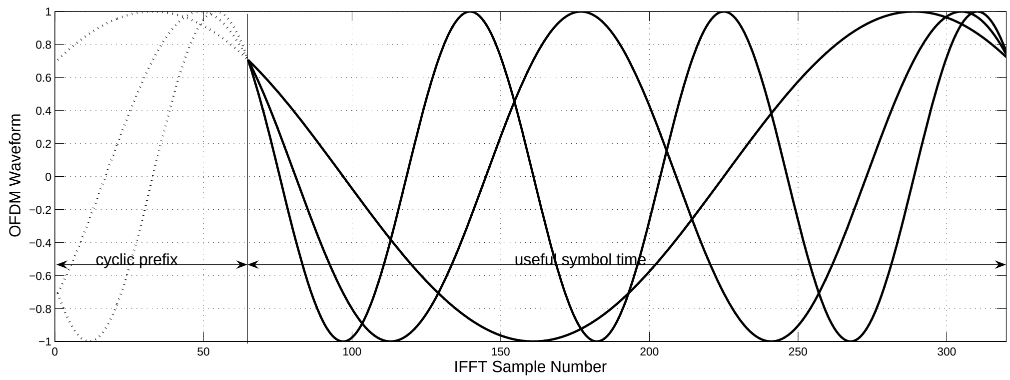

Figure 3.8: Cyclic Extension of the OFDM Waveform

are defined. Values of 1/4, 1/8, 1/16, and 1/32 are specified.
By extending the OFDM symbol, the samples required for performing the IFFT at the receiver can be taken anywhere over the length of the extended symbol. Thus, the CP provides multipath immunity as well as a tolerance for symbol time synchronization errors. As a draw-back, the overhead introduced by the cyclic extension results in a reduced Signal to Interference plus Noise Ratio (SINR) [Engels, 2002].
In the targeted frequency bands, radio communication benefits significantly from the ability to operate under obstructed LOS and NLOS conditions. It is therefore necessary to choose a CP larger than the maximum delay spread but still as short as possible. Table 3.2 lists common maximum delay spread values in different types of environment. These delay spread values remain unchanged for any operating frequency above 30 MHz, since the wavelengths become much smaller than man-made architectural structures. Recent measurements do confirm the values for frequency bands between 800 MHz and 6 GHz [Kepler et al., 2002; van Nee and Prasad, 2000].

3.2.9 Power Control

Power control is supported for the UL channel. The received power level is first calibrated during initial ranging. However, it may vary during operation due to distance loss or power fluctuations. The objective of the power control algorithm is to bring the received power density (received power per active subcarrier) from a given subscriber to a desired level. To do so, the BS feeds back power measurements to the SS. This is done during periodic ranging

Table 3.2: Delay Spread Values

Type of environment	Max. delay spread
In-building (house, office)	$< 0.1\ \mu s$
Large building (factory, malls)	$< 0.2\ \mu s$
Open area	$< 0.2\ \mu s$
Suburban area LOS	0.2 - $1.0\ \mu s$
NLOS	0.4 - $2.0\ \mu s$
Urban area	1.0 - $3.0\ \mu s$

intervals with a Ranging Response (RNG-RSP) or anytime with a Fast Power Control (FPC) message. The SS adapts its transmission power accordingly. The algorithm's implementation is not specified, it is vendor-specific.

3.2.10 Optional Subchannelization Mode

Subchannelized transmission in the UL is a SS-specific option. The SS's capability to decode such transmissions is negotiated during the network entry (SS basic capability encodings). Subchannelized transmission may occur in three different states.

Initial Ranging During initial ranging, a SS successively increases its transmit power until it receives the BS response, which allows proceeding the network entry. SSs that exceed their maximum power level during initial ranging can access a ranging slot using subchannelization. To do so, the SS transmits a regular long preamble on the entire bandwidth, followed by a subchannelized preamble on a single subchannel, i.e., $1/16$ of the bandwidth. Both preambles are transmitted using the same total power. As a result the spectral density of the subchannelized preamble is increased by a factor of 16 (about 12 dB).
The increased spectral density during initial ranging tackles the imbalanced link budget of DL and UL transmissions. In general, the BS has a higher transmit power and a higher transmitter antenna gain so that the DL transmissions have a larger coverage than the UL transmissions. The increased spectral density enlarges the SSs' transmission range on single subchannels. Thus, the BS is able to detect the new SS during initial ranging.

Bandwidth Requests Contention slots for bandwidth requests are allocated

either for the entire bandwidth or for individual subchannels. The exact width (in subchannels) and length (in OFDM symbols) is defined in the Uplink Channel Descriptor (UCD) message broadcasted by the BS. During the transmission on subchannel basis, i.e., a focused contention bandwidth request, the amplitude of each of the four subcarriers in use can be boosted above its normal amplitude, i.e., the amplitude used during a noncontention OFDM symbol. The boost in Dezibel (dB) is indicated in the current UCD.
Like the focus of transmission power onto single subchannels during initial ranging, the power boost during contention based bandwidth requests leads to an increased transmission range of SSs. Thus, BSs are able to detect the bandwidth request of SSs. Besides the increased range, the number of contention slots is increased by four if only four subchannels are used instead of the entire 16 channels. With the increased number of slots the collision probability decreases.

UL Data Transmission If subchannelized UL data transmission is negotiated during network entry, the BS can allocate an UL burst based on individual subchannels to a SS. The corresponding UL MAP Information Element (IE), transmitted by the BS contains the subchannel index.
Subchannelization during regular user data transmission allows for flexible resource allocation because resources can be scheduled in smaller units in the time and frequency domain. It enables the exploitation of frequency selectivity by means of frequency selective scheduling. Furthermore, it offers the opportunity for a simultaneous usage of the same UL channel by more than one BS.
The usage of subchannels may also reduce the overhead due to preambles. This is accomplished since the subchannelized preamble is still one OFDM symbol long but the length of the following data part is increased proportionally to the decreased number of allocated subcarriers. As a result, the ratio of user data length to preamble length is increased. This is especially useful with high rate MCSs, where data packet transmissions become very short. Subchannelization for the DL was introduced to the standard with the mobility amendment IEEE [2006].

3.3 IEEE 802.16 Medium Access Control

The scope of the IEEE 802.16 standard comprises the data and control plane of the MAC and the PHY layer as illustrated in Figure 3.3. The MAC includes a service-specific convergence sublayer that interfaces higher layers. The MAC Common Part Sublayer (CPS) carries the key functions and below resides the security sublayer. The management plane is specified in three IEEE network management standard amendments (IEEE 802.16f / g / i) for the Fixed as well as the Mobile Management Information Base and for Procedures and Services (refer to Section 2.3.5).

3.3.1 Service Specific Convergence Sublayer

The Service Specific Convergence Sublayer (CS) provides any transformation or mapping of external network data, received through the CS Service Access Point (SAP). This includes classifying external network SDU and if required processing SDUs. Classifying incoming SDUs means to associate them with the proper connection identified by the Connection Identifier (CID) (shown in Figure 3.9). Since a CID is associated with a certain QoS, the association of an SDU to a CID facilitates the delivery with the corresponding QoS constraints. The CS processes higher layer SDUs to suppress unused higher layer protocol information. After classification and Payload Header Suppression (PHS), the SDU is delivered to the corresponding MAC CPS SAP. At the receiving CS entity, the suppressed header is reconstructed before it is handed to the higher layer protocol via the SAP. Since PHS is an optional feature, incoming SDUs can also be delivered without any modifications. The standard provides two CS specifications, an ATM and a Packet CS.

3.3.1.1 Packet Convergence Sublayer

The Packet CS is used for packet-based higher layer protocols such as Internet Protocol (IP), Point-to-Point Protocol (PPP) and IEEE 802.3 (Ethernet). Classification of SDUs is based on classifiers that consist of a reference to a CID, a classifier priority and a set of protocol-specific matching criteria. As matching criteria the characteristical protocol entries such as IP or Ethernet source / destination address, protocol source / destination port range, IP type of service / differentiated services codepoint, or the IEEE 802.1D-1998

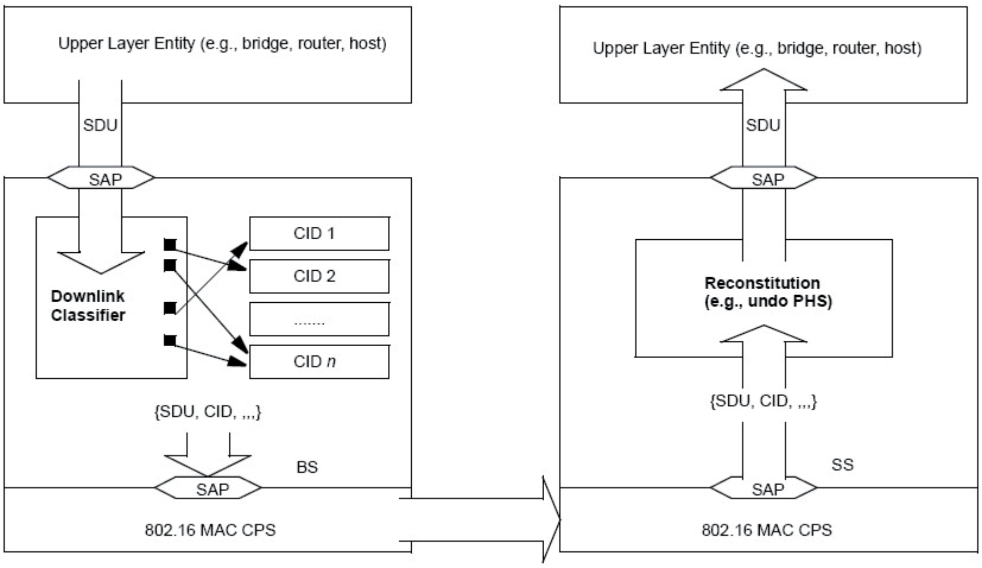

Figure 3.9: Service Specific Convergence Sublayer [IEEE, 2004a]

user priority can be used. If several classifier rules match with an incoming SDU, the classifier priority specifies which rule is to be applied.
Since the Packet CS handles various higher layer protocols, various header entries might have to be suppressed and reconstructed. Therefore, the optional PHS functionality defines a mechanism to suppress specific bytes of an unspecified SDU adaptively. All bytes of a specific region (PHS Field) will be suppressed by the sending entity unless they are marked by the PHS Mask. Compressed Packet CS SDUs are prefixed with an 8-bit PHS Index. The receiving entity reassambles the original SDU by adding the bytes that are stored in the PHS Field associated to the CID.

3.3.1.2 ATM Convergence Sublayer

Classification within the ATM CS depends on the switching mode of the corresponding ATM connection. A pair of values, i.e., Virtual Path Identifier (VPI) and Virtual Connection Identifier (VCI), uniquely identifies an ATM cell. If virtual path switched mode is applied, ATM cells having a certain VPI are mapped to the associated MAC connection. Thus, ATM cells with different VCI are transmitted on one single MAC connection. If the ATM connection operates in VCI switched mode, the combination of VCI and VPI is mapped to the CID of the connection on which it is transported. Thus, in the ATM CS the classifier's matching criteria is either the combination of

VCI and VPI or the VPI only.
The optional PHS mode also depends on the switching mode of the ATM connection. In virtual path switched mode, the 5-byte ATM header is compressed to a 3-byte header containing, amongst others, the VCI. Thus, the VPI is suppressed. In virtual channel switched mode, both the VPI and the VCI is suppressed resulting in a compressed ATM header of only one byte. The receiving ATM CS entity reconstructs the original ATM header by adding the corresponding VPI and/or VCI and by recalculating the header checksum.

3.3.2 Medium Access Control Common Part Sublayer

The MAC Common Part Sublayer (CPS) provides system access, bandwidth allocation, connection establishment, and connection maintenance. From the CS it receives data classified to particular CIDs. QoS is applied to transmission and scheduling of data over the PHY layer.
IEEE 802.16 is optimized for Point-to-Multipoint (PMP) configurations where several Subscriber Stations (SSs) are associated with a central Base Station (BS). As an option, the standard allows for a flexible Mesh deployment where direct communication between stations is possible. Since the Mesh frame structure is not compatible with the PMP frame, the Mesh deployment is especially foreseen for wireless backhaul networks based on IEEE 802.16. Additional to PMP, an amendment for multi-hop communication in tree-based deployments is specified (refer to Section 2.3.7). The introduction of RSs, which decode and forward data, extends the coverage area of a BS or increases the achievable capacity within a given area. The multi-hop amendment requires being PMP compliant so that legacy SS will be able to participate in relay enhanced networks.
Section 3.2 outlines that the IEEE 802.16 standard specifies four different PHY layers, while one single MAC is controlling the access to the medium. Hence, the MAC protocol is PHY layer independent in general, but some mechanisms are PHY specific. PHY specific parts mainly focus on the MAC frame structure and the corresponding signaling messages. Wherever necessary, the OFDM specific part of the MAC protocol is described in the following.

3.3.2.1 Duplex Modes

Two duplexing techniques are specified for 802.16, i.e., Time Division Duplex (TDD) and Frequency Division Duplex (FDD). FDD operation is possible in paired frequency bands, which are typically allocated in licensed spectrum. Thus, DL and UL operates on separate frequency channels. The capacity (a)symmetry between DL and UL is predefined by the spectrum allocation and is therefore static. DL and UL capacity cannot be changed during operation. In full-duplex FDD, stations receive and transmit simultaneously on both channels. Therefore two RF filters, two oscillators and two synthesizers are necessary. On the one hand, the increased need for components makes FDD devices more power consuming and more costly. On the other hand, the MAC software can be less complex since DL and UL are not strictly synchronized [Bisla et al., 2004]. In order to avoid costly hardware a Half-Duplex FDD (HFDD) mode is supported. In HFDD DL and UL are still on separate frequency channels, but stations do not transmit and receive simultaneously. The resulting radio complexity is comparable to the complexity of TDD devices. A desirable network deployment, in which the BSs operate in FDD and the SSs in HFDD, combines the possibility to utilize both channels simultaneously with competitive user devices.
TDD overcomes the static (a)symmetry inherent to FDD by time-sharing the same frequency channel for DL and UL transmission. Hence, capacity can be dynamically assigned by shifting the switching point between DL and UL in time. However, cell individual switching points in cellular deployments result in severe mobile to mobile interference, also known as the near-far problem. Thus, a system wide partitioning in DL and UL, which is valid for all cells is favorable. Since stations do not receive and transmit at the same time, a single RF filter, one oscillator and one synthesizer is necessary. This results in cost- and power efficient devices, but the MAC scheduler tends to be more complicated since it has to synchronize many users' time slots in both DL and UL direction [Bisla et al., 2004]. In order to switch between receive and transmit phases turnaround gaps have to be introduced between both phases. Assuming moderate mobility, the reciprocity of the wireless channel can be exploited in TDD systems. This feature is highly attractive because the station's transmitter can take advantage of the channel knowledge available at the station's receiver. A detailed overview on pros and cons of duplexing modes can be found in [Falconer et al., 2006]. In IEEE 802.16 TDD mode is mandatory for operation in license-exempt spectrum.

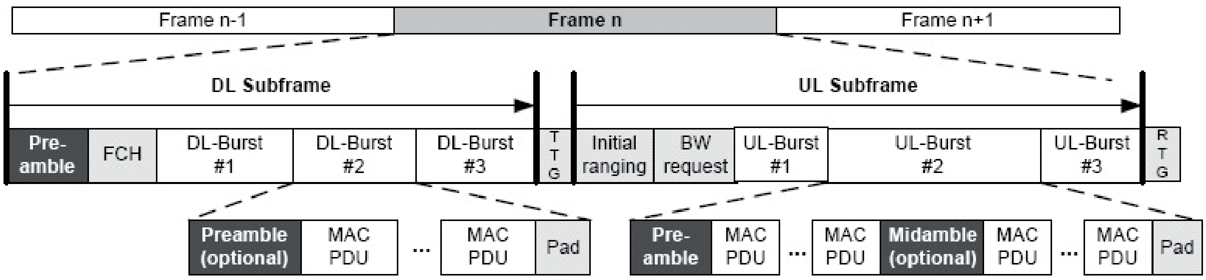

Figure 3.10: IEEE 802.16 MAC Frame in TDD Mode

3.3.2.2 Frame structure

IEEE 802.16 supports a frame-based transmission. The frame duration may vary between 2.5 to 20 ms but a highly dynamic variation is not foreseen during normal operation. A frame duration change forces all SSs to resynchronize. Figure 3.10 illustrates the frame structure of an OFDM-based MAC layer operating in TDD mode. Each frame consists of a DL subframe and an UL subframe. The DL subframe always precedes the UL subframe. Subframes are separated by Receive / Transmit Transition Gaps (RTGs) and Transmit / Receive Transition Gaps (TTGs), respectively. The gaps allow stations to switch their PHY processors between transmit and receive states. The partitioning between DL and UL may vary dynamically to efficiently handle an asymmetric traffic load. In FDD, similar DL and UL subframes are used, but they are located on separate frequency channels.

The DL subframe consists of only one PHY transmission starting with a preamble. The long preamble at the beginning of each frame is composed of two OFDM symbols. It is used by the SSs for time and frequency synchronization. The following Frame Control Header (FCH) occupies one OFDM symbol and describes the following DL subframe. The FCH is followed by one or multiple DL bursts, which should be ordered by decreasing modulation robustness. While the burst with the most robust modulation, e.g., BPSK, is transmitted first, the last burst is modulated using the highest MCS that is supported, e.g., 64 QAM. This ordering should simplify the PHY and improve the synchronization of SSs. Each DL burst consists of MAC Protocol Data Units (PDUs) scheduled for DL transmission. Optionally, a DL burst might start with a short preamble. A short preamble is one OFDM symbol long and allows for an enhanced synchronization and channel estimation at the receiving SSs. MAC PDUs transmitted within the same

DL burst are all encoded and modulated using the same MCS. Nevertheless, PDUs of one DL burst might be associated to different connections and / or SSs. In DL as well as in UL direction the burst length is an integer number of the OFDM symbol length so that burst and OFDM symbol boundaries match each other. In order to end up on OFDM symbol boundaries, padding bytes (0xFF) are added at the end of each burst.

The UL subframe consists of contention intervals and one or multiple PHY transmissions, each transmitted from a different SS. One contention interval may be scheduled for initial ranging and another one for bandwidth request purposes. In order to reduce the probability of collisions, contention intervals are slotted. Initial ranging slots allow SSs to enter the system by requesting the basic management CIDs, by adjusting its power level and frequency offset and by receiving its timing offset. Since the SSs that are accessing the initial ranging contention slots do not have their timing offset yet, the appropriate slot duration depends on the intended cell radius. The slot duration should be at least long enough to transmit a long preamble followed by an initial ranging management message, which is coded and modulated with the most robust MCS (BPSK $^1/_2$), plus the Round Trip Delay (RTD).

SSs access the second type of contention slots in order to transmit bandwidth requests. Hence, SSs can adapt the requested UL capacity to their varying traffic load. The slot duration of bandwidth request slots may be shorter than the duration of initial ranging slots. Taking the right timing offset into account, only a short preamble plus a bandwidth request header is transmitted. Numerous mechanisms to allocate UL resources more efficiently are foreseen in 802.16. These mechanisms include, for instance, dedicated bandwidth request slots, piggybacked request or unsolicited resource grants.

Besides contention phases, the UL subframe contains one or multiple UL bursts. Each burst starts with a short preamble. For better synchronization and channel estimation at the receiving BS, optional midambles might be periodically included in the UL burst. Like in the DL, all PDUs transmitted within one single burst are coded and modulated with the same MCS. An UL burst is transmitted by one single SS. Thus, PDUs are associated to connections of only one SS. Analog to the DL, padding bytes are added at the end of each UL burst to end up on OFDM symbol boundaries.

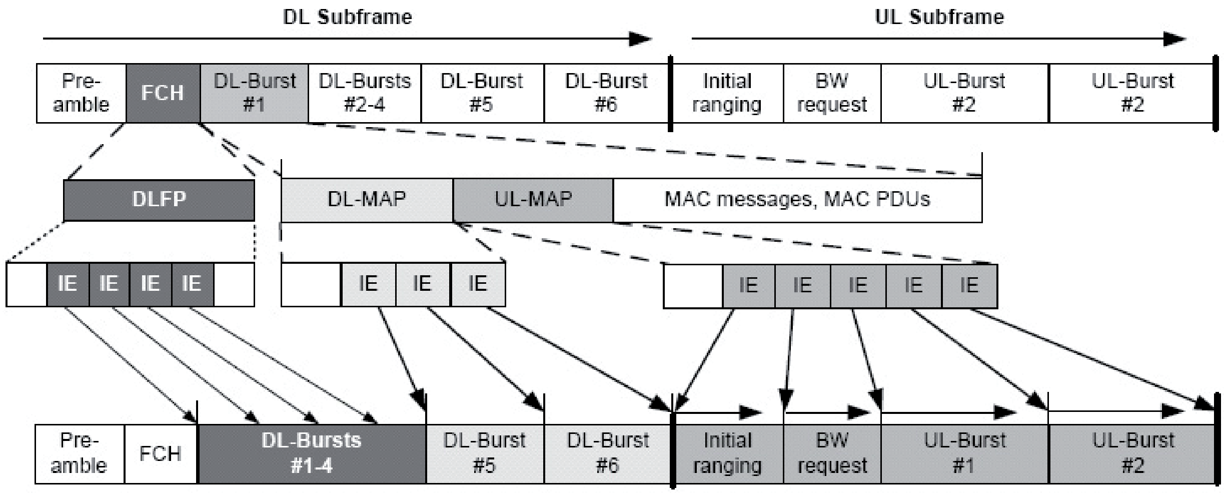

Figure 3.11: IEEE 802.16 References of MAC Management Messages

3.3.2.3 Frame Control

Since the MAC frame is dynamically composed of various bursts, the BS broadcasts MAC management messages to describe the current realization of the MAC frame. SSs receive these messages and gather the information needed to receive and transmit PDUs. Figure 3.11 shows the basic MAC management messages used to specify the current MAC frame realization. The management messages contain time references to the corresponding elements of the MAC frame. Arrows in Figure 3.11 indicate these references, such as burst start times and burst lengths.

The FCH and the DL MAP define the access to the DL subframe. The FCH is composed of the Downlink Frame Prefix (DLFP). The DLFP specifies up to four DL bursts, which are directly following the FCH. The FCH, whose length is one OFDM symbol, is transmitted with the mandatory MCS BPSK 1/2. Taking the zero tail byte for the CC into account, the size of the DLFP results in 11 byte. The DLFP contains four Information Elements (IEs), each IE specifying one DL burst.

The DLFP IE contains the length and the MCS of the corresponding DL burst. The MCS is not given directly, but as a reference to a certain burst profile, which is named Downlink Interval Usage Code (DIUC). A burst profile is a detailed description of the corresponding MCS. It is contained in the Downlink Channel Descriptor (DCD). The DCD defines the characteristic of the physical DL channel. It is occasionally broadcasted by the BS. The burst profile details the specific coding algorithm (RS+CC, BTC or CTC), the code rate, and the modulation scheme. Since the start time of a burst is not explicitly included in the IE, it has to be calculated as the sum of all burst lengths of the preceding bursts. The IE additionally informs whether the optional preamble is transmitted at the beginning of the DL burst or not. If the DL subframe consists of four or less bursts, the DLFP is sufficient to specify the entire subframe. However, if the DL subframe is made up of more than four bursts, an additional DL MAP has to be transmitted that specifies the remaining bursts.

The very first DL burst contains the broadcast MAC control messages, i.e., DL- and UL MAP as well as DL- and UL channel descriptor (DCD and UCD). Analog to the DCD, the UCD defines the characteristic of the physical UL channel. If it is applicable to all SSs within the intended coverage area of the BS, the first DL burst may be coded with a more efficient MCS than BPSK $1/2$. This reduces the overhead due to signaling, but is also reduces the potential coverage area of the BS.

If present, the DL MAP is included in the very first PDU of the first DL burst, thus, it immediately follows the FCH. Among others, the DL MAP contains one IE for each burst of the DL subframe that has not been described by the FCH yet. The information included in the DL MAP is relevant only for the DL subframe of the current MAC frame. Figure 3.12a shows that the DL MAP IE is made up of four entries, the CID of the addressee of the burst, the DIUC, the start time of the burst and a bit to indicate whether the optional preamble is prepended to the DL burst. If all PDUs of one burst are intended for only one SS, the burst is directly addressed to this SS. No other SS need to decode this particular burst. If the specified DL burst contains MAC PDUs for several SSs, the CID of the corresponding DL MAP IE is set to a multicast or the broadcast CID. All addressed SSs have to start decoding the burst at the specified start time with the given MCS. The information to which connection the received MAC PDUs are associated can be taken from the MAC header of the particular PDU. Like in the DLFP, the DIUC is a reference to the burst profile used for the corresponding burst. The start time of the following DL burst is automatically taken as the end of the current one. That means the burst duration is implicitly given by subtracting the burst start time from the start time of the following burst. This calculation strictly relies on a sequential nature of bursts. The last IE indicates the end of the MAP and refers to the end of the subframe. Besides the start time, which is set to the end of the DL subframe, this last IE is

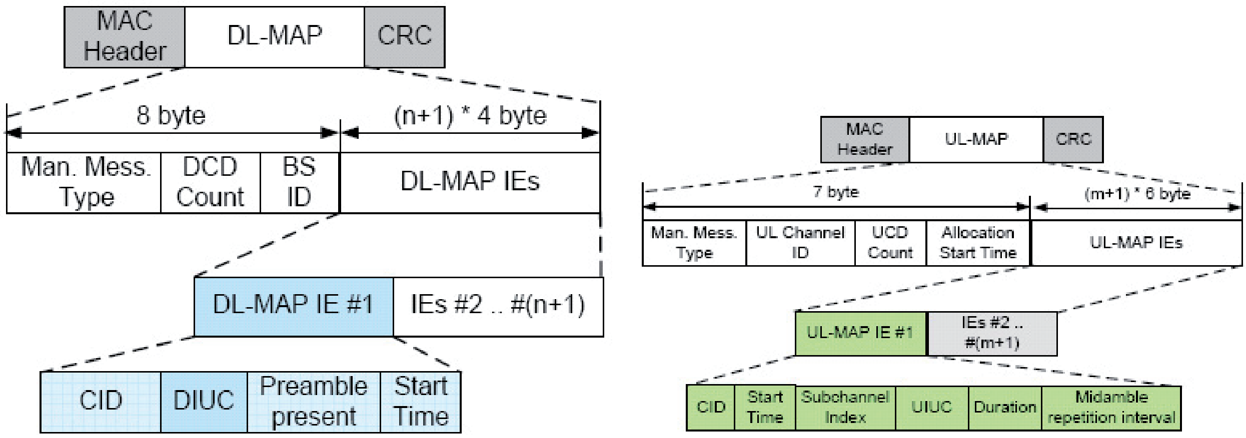

(a) DL MAP **(b)** UL MAP

Figure 3.12: MAC PDUs Containing DL- and UL MAP (OFDM-specific)

empty.
Optionally, the DL MAP IE might be extended so that it contains additional information for one specific purpose. For instance, by means of a Channel Measurement IE, a BS can request a channel measurement report. If bursts of the DL subframe are transmitted with Space Time Coding (STC) or Advanced Antenna System (AAS) techniques, they can be identified by means of the AAS IE and the STC IE respectively. A Physical Modifier IE indicates a cyclic shift of the following optional DL preambles. Like that, the reception of concurrent DL bursts sent by the BS in SDMA mode might be enhanced (refer to Section 4). The Concurrent Transmission IE contains the burst duration. The explicit indication of the duration overcomes the restriction of the sequential nature of DL bursts. Knowing the start time and the duration, the BS is able to flexibly arrange concurrent DL bursts for SDMA [Hoymann, 2006].
The UL MAP, which is shown in Figure 3.12b, allocates access to the UL subframe. Like the DL MAP, the UL MAP contains IEs to specify the bursts. Depending on the effective start time of the corresponding UL subframe (included in the UL MAP as Allocation Start Time), the UL MAP is relevant for the UL subframe of the current or of the following MAC frame. Each UL MAP IE specifies one UL burst including the contention intervals for initial ranging as well as for bandwidth request.
The UL MAP IE consists of six elements (refer to Figure 3.12b). The CID is the unique address of the SS that is scheduled for the particular UL burst.

The start time and the duration of the corresponding UL burst are given. Hence, unlike the regular DL subframe the UL subframe does not rely on a sequential structure of bursts. UL bursts do not end implicitly at the beginning of the following one. Thus, idle times can be included in between two bursts by starting the second one delayed. For SDMA operation, UL bursts might be scheduled concurrently by specifying the same start time for more than one burst. The subchannel index is used to indicate which OFDM subcarriers shall be used for the transmission. Subchannelization can only be used if the SS is able to transmit on a subchannel basis. This capability has to be negotiated during the network entry. Analog to the DIUC, the Uplink Interval Usage Code (UIUC) is a reference to a burst profile. The UCD message, which contains the burst profiles, is occasionally broadcasted. The profile details the coding algorithm, the code rate, and the modulation scheme that should be used by the SS to transmit the corresponding UL burst. In addition to the mandatory short preamble at the beginning of each UL burst, midambles might be included in the UL burst on a periodic basis. The request to include midambles is indicated by the midamble repetition interval. Together with the preamble, the midambles allow for an enhanced synchronization and channel estimation at the BS.
Like the DL MAP IE, the UL MAP IE can be extended for specific purposes, such as the request to change the SS's transmit power, the switch to AAS enabled traffic, or the indication of the cyclic shift of preambles and midambles. The cyclic shift allows for an enhanced joint detection of SSs during the UL subframe. The above described FCH and the MAPs are PHY layer independent, while the detailed inner structure of the DLFP and the IEs are PHY specific.

3.3.2.4 Protocol Data Unit Format

MAC PDUs carry user data, i.e., SDUs from the Convergence Sublayer, as well as MAC management messages. PDUs consist of a fixed-length MAC header, a variable-length payload and a 32-bit Cyclic Redundancy Check (CRC). The CRC is optional for PDUs that contain user data but it is mandatory for PDUs that carry MAC management messages. The size of the MAC header is six byte. Thus, the minimum size of a PDU, which is composed of the header only, is six byte. The length field, which is included in the header, specifies the entire length of the PDU including header, payload, and CRC. Since the length field is encoded with 11 bit,

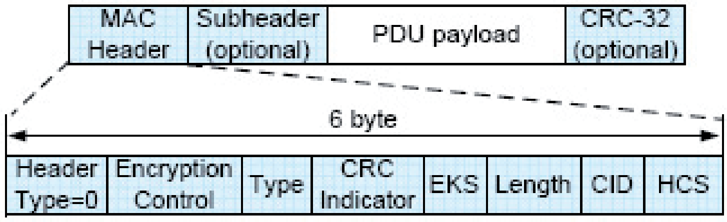

Figure 3.13: MAC PDU with Generic MAC Header Format

the maximum possible PDU length is 2047 byte. Thus, the variable PDU payload may range up to 2041 byte. This allows the MAC protocol to tunnel various higher layer traffic types without knowledge of the format of those messages. The structure of a MAC PDU is shown in Figure 3.13.
Two different header formats are defined, the Generic MAC and the Bandwidth Request Header format. The generic header is used for any PDU that contains user data or management messages. It is composed of eight fields (refer to Figure 3.13): The header type identifies the generic header format. The encryption control field indicates if the payload is encrypted. If it is encrypted, the entry Encryption Key Sequence (EKS) field gives a reference to the encryption key that has been used. The type field is a set of bits that indicates subheaders and special PDU payload, such as Automatic Repeat Request (ARQ) feedback payload, mesh, packing and fragmentation subheaders. Some subheaders directly follow the generic header, while others might occur within the payload. The presence of the CRC at the end of the PDU is denoted by the CRC indicator. The CID field contains the identifier of the associated connection. The Header Check Sequence (HCS) is used to detect errors in the MAC header.
The bandwidth request header is only used by SSs to request bandwidth in the UL subframe. The corresponding header format contains entries to identify the connection, for which bandwidth is requested and to specify the amount of data that is waiting for transmission. The type of the request can be either incremental or aggregate.

3.3.2.5 Automatic Repeat Request

The IEEE 802.16 Automatic Repeat Request (ARQ) mechanism is an optional part of the MAC protocol. By means of the connection setup procedure, ARQ functionality can be enabled on a connection basis. Four different ARQ mechanisms with different types of Acknowledgments (ACKs) are defined in the standard: a selective, a cumulative, a cumulative with selective, and a cumulative with block sequence ACK.

All ARQ mechanisms are working on numbered ARQ blocks. For this purpose, the SDU, which is transmitted on an ARQ-enabled connection, is logically partitioned into fixed-size ARQ blocks. The SDU is prefixed with a fragmentation or a packing subheader. On ARQ-enabled connections, the Fragment Sequence Number (FSN), which is contained in the subheader, becomes the Block Sequence Number (BSN). The BSN is set to the number of the first logical ARQ block of the SDU. Then, the compound of the subheader and the SDU is ready for transmission or retransmission. It is also possible to fragment SDUs, which have been partitioned into ARQ blocks, but fragmentation shall only occur on ARQ block boundaries.

ARQ feedback, i.e., positive or negative ACK, is transmitted either as a standalone MAC management message or piggybacked. The format of the ARQ feedback depends on the type of the ARQ in use. The feedback message of the cumulative ARQ, which has the smallest size, contains the BSN of the last successfully received ARQ block. The feedback of the other ARQ types contains one or more bitmaps to acknowledge ARQ blocks. The message of the selective ARQ contains up to four 16-bit bitmaps that selectively acknowledge ARQ blocks. The message format of the selective with cumulative ARQ equals the one of the selective ARQ. Its feedback additionally acknowledges received blocks cumulatively, which are not covered by the bitmaps. The ACK format of the block sequence ARQ type is optimized to acknowledge entire sequences of ARQ blocks at once.

3.3.2.6 Connection Management and Quality of Service

The MAC protocol of IEEE 802.16 is connection-oriented. All services are mapped to connections in order to provide procedures for requesting bandwidth, associating QoS, transporting and routing data, and all other mechanisms associated with the services.

In order to describe the connection management in 802.16, one has to define two terms with a slightly different meaning: a service flow and a connection. The 802.16 standard defines a service flow as a MAC transport service that provides unidirectional transport of packets. It is identified by a 32-bit Service Flow Identifier (SFID). If a SS or a BS wants to use the transport service and the chosen service flow is admitted, then a connection

is established and a 16-bit CID is assigned to the service flow. Thus, a service flow can be called connection once the transport service is realized. The activation of a service flow, i.e., the establishment of a connection, follows a two-phase activation model that is often utilized in telephony applications. First, the initiating station conserves network resources, such as bandwidth or memory, for an admitted connection request. Once the complete end-to-end connectivity has been established, the resources are activated. The process of activation performs policy checks and admission control on resources as quickly as possible. If possible, this is done before the far end of a connection request is informed. This procedure should prevent potential theft-of-service scenarios.
A service flow has several attributes. It has at least an SFID and a direction. A service flow is characterized by a set of QoS parameters. Due to the activation model, three different QoS parameter sets can be distinguished. First, the Provisioned QoS Parameter Set is provided, e.g., by the network management system. The BS (and optionally the SS) may choose to activate the service flow by requesting the activation. Following the two-phase activation process, the BS checks the SS's authorization, admits the flow, and conserves resources. The Admitted QoS Parameter Set defines the set of parameters, for which resources have been reserved. The level of admitted QoS is always lower than the level of provisioned QoS. A CID has been associated to a service flow having a non-zero admitted QoS parameter set. The type of an admitted service flow may remain admitted for a while or it migrates to active. The type changes to active once both peer entities have confirmed the end-to-end connectivity. The service flow now has a non-zero Active QoS Parameter Set. Again, the activated level of QoS is lower than the admitted level of QoS of the service flow.
The QoS parameter sets may contain various parameters. The standard foresees traffic performance parameters, such as the maximum traffic burst length, the minimum reserved traffic rate, the tolerated jitter, the maximum latency, or a maximum sustained peak traffic rate. Other parameters affect the data plane configuration. Such parameters may configure the ARQ mechanism or specify the convergence sublayer including Payload Header Suppression. Additionally, the 802.16 standard contains a hook to encode vendor-specific parameters.
The corresponding message exchange follows a three-way handshake of Dynamic Service Addition (DSA) MAC management messages. The exchange takes place on the SS's primary management connection. A similar

message exchange is specified for the modification of existing connections. By means of the Dynamic Service Change (DSC) mechanism, QoS parameters can be modified if the request is accepted. However, only QoS parameters that regard the traffic performance can be modified. The ones that configure the data plane are exempt from modification. Finally, connections can be released by exchanging Dynamic Service Deletion (DSD) management messages.

3.3.2.7 Burst Profile Management

UL and DL transmissions are associated with a burst profile. The burst profile details the specific coding algorithm, the code rate, and the modulation scheme of the corresponding DL and UL burst respectively. The BS has full control about the association of burst profiles to DL and UL transmissions. The BS decides about the burst profile based on the signal quality, i.e., SINR perceived during the transmission.

The BS can measure the UL SINR during the reception of UL bursts. Thus, the BS chooses the proper burst profile based on the measured SINRs of one or more previous UL transmissions. The UL burst profile, which a SS should use during a given UL burst, is specified in the UL MAP. In the DL, the BS cannot measure the SINR perceived at the receiving SS. Therefore, the SS measures the DL SINR and signals this information back to the BS. In order to reduce the signaling overhead, not every measured value it transmitted. Each SS monitors the observed DL SINR and compares its mean value with the allowed range of operation. If the mean SINR leaves the allowed range, the SS requests a change of the burst profile. The range of operation is defined by DL SINR thresholds. Each burst profile has mandatory entry and exit thresholds, which are encoded in the DCD message. Figure 3.14 shows the thresholds of an example burst profile A. If a SS receives DL bursts with the profile B, but the mean SINR is higher than the entry threshold of profile A, the SS requests the change to the more efficient profile A. If, after a while, the mean SINR drops again and if it passes the exit threshold of profile A, the SS request the change to the more robust profile B. The resulting DL burst profile, which a BS applies during the transmission of a DL burst, is specified in the DL MAP.

The standard defines two methods to request a change of the burst profile. If the SS has a granted UL allocation, i.e., if an UL burst is scheduled for its basic management CID, the SS sends a DL burst profile change request

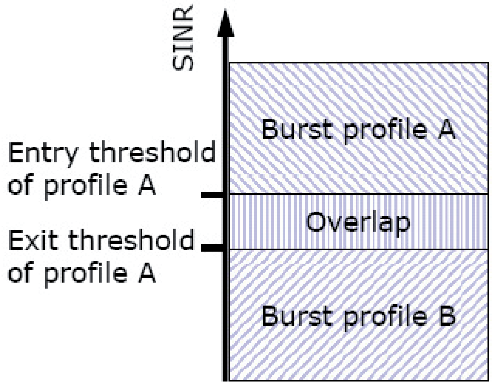

Figure 3.14: DL Burst Profile Entry and Exit Thresholds

(*DBPC-REQ*) in that burst. The BS responds with the corresponding *DBPC-RSP* message. If no UL allocation is available, the SS uses the initial ranging contention slots. It sends a Ranging Request (RNG-REQ) message, which is addressed to the basic management CID, and the BS responds with the corresponding RNG-RSP.

3.3.2.8 Bandwidth Requests and Uplink Scheduling Services

To allow for an adaptive UL transmission of data streams, which may have variable throughput requirements, the standard defines different types of bandwidth request mechanisms. In general, the request mechanisms follow a semi-distributed QoS approach, i.e., bandwidth is requested on connection basis (individual transport CID), but it is granted per SS (basic management CID). By partitioning the granted bandwidth to different connections, even the SS has to maintain QoS and fairness among connections [Cicconetti et al., 2006].

One way of requesting bandwidth is to transmit a preamble plus a bandwidth request header during a contention interval. The interval can be either addressed to the broadcast or a multicast CID. The bandwidth request header requests the transmission of data for a given transport CID. The amount of data, which is encoded in the message, specifies the aggregate number of bytes waiting for transmission. This request can also be transmitted during any regular UL burst dedicated to the SS's basic management CID. In such bursts, the same bandwidth request header is transmitted as a standalone MAC management message, which specifies either the aggregated or incremental amount of data.

Another way to request bandwidth is piggybacking. A SS sends a grant management subheader piggybacked to a regular PDU. This subheader requests bandwidth for the same UL connection (transport CID) that carries the PDU. Thus, this mechanism can only be used for connections, which currently have UL allocations. Piggyback requests can specify incremental requests only.

BSs can also trigger bandwidth requests. To do so, BSs individually poll SSs by allocating UL bursts specifically for UL bandwidth requests. Regular UL MAP IEs specify these UL bursts, but the bursts have only the size of a preamble plus a bandwidth request header. Thus, SSs have the opportunity to send a bandwidth request header that lists the current amount of UL data. By means of the poll-me bit, a SS can stimulate the BS to poll it. The poll-me bit is part of the grant management subheader. By setting this bit, the SS indicates its need to be polled. Thus, the SS can transmit a bandwidth request header to request bandwidth for any CID.

In the above-mentioned mechanisms, SSs request bandwidth so that the BS assigns resources on demand. Nevertheless, the BS can also grant UL allocations to SSs without prior notice. For that purpose, it assigns an UL burst to the SS's basic management CID.

In order to allocate UL bandwidth efficiently, UL scheduling services specify which type of UL bandwidth request shall be used for the corresponding connection. Four types of scheduling services allow for different levels of flexibility and efficiency. The type of the scheduling service and the corresponding parameters are negotiated during the connection setup. They are part of the QoS parameter set that individually characterizes each service flow.

Unsolicited Grant Service

The Unsolicited Grant Service (UGS) supports real-time data streams that generate fixed-size data packets on a periodic basis, such as T1 / E1 or Voice over IP (VoIP) without silence suppression. The scheduling service assigns fixed-size grants, i.e., UL bursts, at periodic intervals. These UL bursts shall be used for data transmission. The size of the grants and the duration of the time period is specified by the QoS parameter set associated to the service flow. Since service flows using UGS are prohibited from using contention-based request mechanisms, signaling overhead and latency due to bandwidth requests is eliminated.

Real-Time Polling Service

The Real-Time Polling Service (rtPS) supports real-time streams that generate variable size SDUs on a periodic basis, such as MPEG video. Using this scheduling service the BS periodically grants UL allocations. The size of the UL bursts meets the flow's real-time needs and it allows the SS to specify the size of the desired grant. Thus, during the granted UL allocation, the SS sends PDUs containing user data and it requests bandwidth for the next grant either by means of a standalone bandwidth request header or by means of a piggybacked subheader. The minimum and maximum data rate as well as the allowed latency is specified by the QoS parameter set that is associated to the rtPS service flow. Service flows using rtPS are prohibited from using contention-based bandwidth request opportunities. This service requires more signaling overhead than UGS, but supports variable grant sizes for optimum data transport efficiency.

Non-Real-Time Polling Service

The Non-Real-Time Polling Service (nrtPS) supports streams of delay-tolerant SDUs for which a minimum throughput is required, such as File Transfer Protocol (FTP). The scheduling service offers unicast polls on a regular basis. Minimum and maximum data rates are specified by the corresponding QoS parameter set. Besides polling, contention-based bandwidth request opportunities may be used by service flows using nrtPS.

Best Effort Service

The Best Effort (BE) service supports data streams that require no specific QoS. Service flows using BE scheduling services can be handled on a space-available basis. Thus, BE connections can use contention-based request opportunities. Only a maximum traffic rate is given in the QoS parameter set of the service flow.

3.3.2.9 Optional Mesh Mode

IEEE 802.16 mesh networks were intended to be used as backhaul networks. Its ease of deployment (cost advantage of RSs and scalability) makes mesh networks interesting for operators. Frequency spectrum that has been allocated to an operator can be used not only to connect SSs but also to

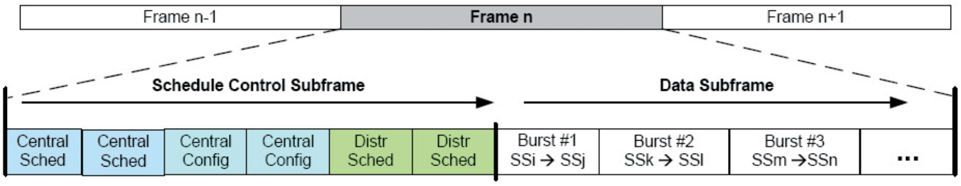

Figure 3.15: 802.16 Mesh MAC Frame Structure

interconnect several BSs. No cabling or leased lines are needed anymore and the capital and/or operation expenditures are hence reduced. For a relay deployment only power supply is needed.
The IEEE 802.16 mesh mode is an optional feature of the standard. In contrast to the mandatory PMP configuration where traffic only occurs between the BS and SSs, in the mesh mode traffic can be routed through other SSs and can occur directly between SSs. Such SSs are called Mesh SSs. The BS that is connected to the backhaul network is called Mesh BS. All PDUs, i.e., data and control messages are forwarded in the time domain by the Mesh SSs.
All Mesh communications are in the context of a link which is established between two nodes. Thus, the PMP frame structure composed of a DL- and an UL subframe is replaced by a structure based on bursts scheduled for the transmission between two nodes. Figure 3.15 shows that PDUs containing user data are transmitted during bursts of the data subframe and PDUs containing scheduling control messages are transmitted during the schedule control subframe. Instead of the schedule control subframe a network control subframe is included in the frame periodically. The network control subframe provides a basic level of communication between nodes, e.g., for synchronization, initial network entry and exchange of neighborhood lists. The schedule control subframe is used for the coordination of the scheduling. Access to the network and the schedule control subframe is based on a standardized scheduling algorithm so that no collisions occur [Bayer et al., 2006]. Depending on the configuration of the SSs, scheduling can be done on the basis of distributed scheduling, on the basis of centralized scheduling, or on a combination of both.
Using centralized scheduling, the Mesh BS gathers resource requests from all Mesh SSs within a certain hop range. The BS determines the amount of granted resources for each link in the network both in DL and UL, and

communicates these grants to all Mesh SSs within the hop range. The collection of bandwidth requests and the broadcast of the final schedule is done in the corresponding Centralized Scheduling Bursts of the Schedule Control Subframe (refer to Figure 3.15). However, increased overhead due to signalling overhead sent to a central device may occur.
Using distributed scheduling, all nodes including the Mesh BS coordinate their transmissions in their two-hop neighborhood and broadcast their schedules (available resources, requests and grants) to all neighbors. All nodes ensure that the resulting transmissions do not cause collisions with the data and control traffic scheduled by any other node in their two-hop neighborhood. The corresponding signalling messages (three-way handshake) are transmitted either in the corresponding distributed scheduling bursts of the Scheduling Control Subframe or during a contention burst of the Data Subframe. If the signalling is done during the control subframe, it is called coordinated distributed scheduling. If it is done during the data subframe, it is called un-coordinated distributed scheduling. Using uncoordinated distributed scheduling collisions might affect the latency and the overhead of the signalling messages.

3.4 System Profiles

The standard contains various optional features such as ARQ, PHS, and CRC capability. Their implementation is left to the equipment manufacturer. Besides that, many configuration parameters are not fixed so that devices can operate with different duplexing modes, have different channel bandwidths or operate in different spectrum bands. To reduce the implementation complexity, the WiMAX Forum started to define system profiles. These profiles list sets of features and parameters that are assumed in typical implementation cases. Additionally, the process to certify standard conformance and interoperability, i.e., the WiMAX forum certification, is based on these profiles. The WiMAX system profiles were transferred to the IEEE standardization group [IEEE, 2003c], which finalized the profiles and included them in the standard document.
A system profile consists of a set of profiles, each one listing features for a specific purpose. Thus, a system profile is composed of a MAC, a PHY and an RF profile as well as the duplexing selection and a power class. A profile specifies optional features of the standard as “required” or “conditionally

required". It does not change the "mandatory" status if it is specified in the standard. Options that do not appear in the profile remain optional. The standard contains separate profiles for the different PHY layer specifications SC, SCa, OFDM, and OFDMA. This section exemplarily outlines the OFDM system profiles.

3.4.1 MAC Profiles

Two MAC profiles are defined, one for PMP (called *profM3_PMP*) and another one for mesh deployments (called *profM3_Mesh*). Both profiles require a Packet CS that supports IP Version 4 (IPv4) and Ethernet traffic. CRC capability is necessary as well. The profile *profM3_PMP* demands the uplink scheduling services BE and nrtPS, whereas *profM3_Mesh* only requests the BE service. The Mesh profile additionally requires ARQ functionality. Other features, such as PHS or AAS remain optional.

3.4.2 Physical Layer Profiles

The PHY layer profiles follow the naming convention *profP3_BW* where BW is the provisioned channel bandwidth, which is the intended channelization as well. Profiles for 1.75, 3.5, 5.5, and 7 MHz bandwidth define the operation in licensed bands and *profP3_10* defines the license-exempt operation with 10 MHz channel bandwidth. All profiles require specific minimum performance level of the transmitter and the receiver. BSs operating in PMP mode shall support frame durations of 5, 10 and 20 ms. SSs shall allow for transition gaps (TTG and RTG), smaller than 100 μs. Licensed operation additionally requires 64 QAM modulation capability, whereas unlicensed operation requires Dynamic Frequency Selection (DFS).

3.4.3 RF Profiles, Duplexing Modes and Power Classes

RF profiles are defined for license-exempt operation only. Three RF profiles define 10 MHz channels in the middle U-NII (5.275-5.335 GHz), the upper U-NII (5.740-5.830 GHz), and in the CEPT band C (5.735-5.835 GHz). The duplexing mode is either TDD or FDD, furthermore, SSs in FDD are either half- or full-duplex. The power classes specify the range of the devices' transmit power. The intended transmit power classes vary from below 14 dBm (for class *profC3_0*) up to above 23 dBm (for class *profC3_23*).

CHAPTER 4

SDMA-Enhanced Metropolitan Area Network

As one of the first standards IEEE 802.16 includes means to integrate adaptive antenna techniques. Comparable approaches were later standardized by the 3GPP for UMTS or by the IEEE for 802.11n. These advanced antenna techniques have a significant impact on the capacity and service quality provided by wireless links and the efficient use of the available spectrum [Ghosh et al., 2005]. An initial approach to support space division multiple access techniques in wireless ATM systems has been presented in [Vornefeld et al., 1999].

Systems that operate with smart antennas must fulfil several requirements. First, the PHY layer must be able to dynamically adapt its receive and transmit characteristics by smart antenna algorithms. Second, the enhanced PHY layer has to offer its new services to the MAC layer via the PHY SAP. Third, the MAC protocol has to cope with the new features, e.g., the spatial domain of SDMA. Last, the MAC behavior, which is not standardized is affected as well. Vendor-specific algorithms, such as scheduling or link adaptation, have to work efficiently under the new constraints, e.g., the intra-cell interference generated by SDMA. These four aspects, which enable a system to operate with smart antennas, are detailed in the following sections.

4.1 PHY Layer Comprising Smart Antennas

4.1.1 Introduction to Smart Antennas

Smart or adaptive antennas control their pattern, by means of feedback control, while the antenna is operating [Compton, 1988]. Adaptive antennas are built as arrays, rather than continuous aperture antennas, because the pattern of an array is easily controlled by adjusting the amplitude and phase of the signal of each element before transmitting the signals. The individual antenna elements are spatially separated and arranged in a specific geometric layout,e.g., on a line or circle. The distances between the elements are typically on a scale of $\lambda/2$, where λ is the wavelength of the carrier

signal. However, adaptive arrays do not require uniform element spacings or identical element patterns in the array. They can operate with somewhat arbitrary element patterns, polarizations, and spacings.
Adaptive antennas systems can be said to date from the 1950s. In 1956, the use of phase-locked loops for combining the signals from different receive antennas in a diversity system was proposed [Altman and Sichak, 1956] . A phase-locked loop array is adaptive because the antenna pattern is controlled by the incoming signal direction. The array automatically forms a beam that tracks the signal. However, such an array can only track one signal at a time and a strong interference signal can easily capture the beam of the antenna [Compton, 1988].

4.1.1.1 Smart Antennas at the Base Station

A smart antenna at the BS can be used to improve the link quality for a single data stream in UL (Single Input Multiple Output (SIMO)) and DL (Multiple Input Single Output (MISO)). It may also be used to form multiple adaptive beams to provide SDMA for different subscriber stations at the same time.

Single User: To improve the link to one specific SS, diversity coding algorithms can be used. Well proven techniques are Maximum Ratio Combining (MRC) [Jakes, 1974] in UL and STC [Alamouti, 1998; Tarokh et al., 1998] in DL. These techniques increase diversity and thus reduce the Bit Error Ratio (BER). A higher data rate might be achieved through higher order modulation schemes. Diversity coding techniques are introduced in Section 4.1.2.1.
Beamforming techniques can be used alternatively for DL to maximize SINR. By focussing the transmitted energy, these techniques either maximize the carrier signal, or they minimize the inter-cell interference. Section 4.1.2.3 describes beamforming techniques.

Multi User: To improve the links to several SSs simultaneously, smart antenna form concurrent, independent beams for different SSs [Godara, 1997a]. Concurrent beams are orthogonal, i.e., the mutual intra-cell interference is suppressed. SSs access the radio resources by means of SDMA.

4.1.1.2 Smart Antennas at Base Station and Subscriber Station

Transmissions further benefit from adaptive antennas at both ends, the BS and the SS. One link is then a point-to-point MIMO system. If several links are active at the same time, it is a multi user MIMO system.

Single User: For point-to-point MIMO systems three processing schemes are promising. Spatial multiplexing uses, e.g., the Bell Labs Layered Space Time (BLAST) algorithm developed by Foschini [Foschini, 1996]). Eigenbeamforming is based on a Singular Value Decomposition (SVD) of the channel matrix [Raleigh and Cioffi, 1998]. Spatial Multiplexing is introduced in Section 4.1.2.2.

Multi User: To exploit several MIMO links at once, a multi user version of Eigenbeamforming exists [Kim and Cioffi, 2000].

4.1.1.3 Benefits of Smart Antennas

Smart antennas offer a variety of improvements for wireless systems [Godara, 1997a]:

Managing Delay Spread and Multipath Fading: Focusing the transmitted energy to the required direction helps to reduce multipath reflections, which cause delay spread. In the receive mode, multipath reflections may be resolved by exploiting their temporal or spatial structure.

Reducing Co-channel Interference: Suppressing the radiated energy towards the direction of co-channel receivers, reduces the inter-cell interference. In receive mode, the gathered inter-cell interference can be suppressed.

Improving Capacity: Providing concurrent channels/beams to multiple SSs increases the capacity. Spatial multiplexing offers an increased single-user data rate. Improving system capacity without allocating additional spectrum directly converts to higher spectral efficiency.

Reducing Outage Probability: Adaptive antennas reduce the outage probability by decreasing cochannel interference and by leveraging several independent transmission paths.

Increasing Transmission Efficiency: The directivity of an array reduce the radiated energy. This allows the use of electronic components of lower power rating.

Extending Coverage: Depending on regulations, it is possible to increase transmission power density leading to larger range.

These advantages can of course be traded for each other. The gains achievable with multiple antenna systems can be classified as follows [Pauraj et al., 2003]:

The array gain is the average increase in signal power at the receiver due to a coherent combination of the signals received at all antenna elements. It is proportional to the number of receive antennas. If channel knowledge is available at the transmitter, the array gain can also be exploited in systems with multiple antennas at the transmitter.

The diversity gain depends on the number of transmit and receive antennas as well as the propagation channel characteristics, i.e. the number of independently fading branches (diversity order). The maximum diversity order of a flat-fading MIMO channel is equal to the product of the number of receive and transmit antennas. Transmit diversity with multiple transmit antennas can, for instance, be exploited via STC and does not require any channel knowledge at the transmitter.

The interference reduction gain can be achieved at the receiver and the transmitter by (spatially) suppressing other co-channel interferers. It requires an estimate of the channel of the desired user.

The spatial multiplexing gain can be obtained by sending multiple data streams to a single user in a MIMO system or to multiple co-channel SSs in an SDMA system. These techniques take advantage of several independent spatial channels through which different data streams can be transmitted.

4.1.2 Smart Antenna Algorithms

This section reviews and introduces algorithms that are used by antenna arrays. The schemes fall into three categories, corresponding to the maximization of the following criteria [Alexiou and Haardt, 2004]:

Diversity: In the case of maximization of diversity, joint encoding, e.g., STC, is applied and thereby the level of redundancy between transmit antennas is increased as each antenna transmits a differently encoded fully redundant version of the same signal.

Data Rate: The maximization of data rate is achieved by performing spatial multiplexing, i.e. by sending independent data streams over the transmit antennas.

SINR: The maximization of SINR is achieved through focusing energy into the desired directions and minimizing energy towards all other directions. Beamforming allows spatial access to the radio channel by means of different approaches, for example based on directional parameters.

4.1.2.1 Diversity Coding

Diversity exploits the random nature of radio propagation by finding independent or at least highly uncorrelated signal paths for communication. If one radio path undergoes a fade, another independent path may have a strong signal. By decreasing the sensitivity to fading, diversity coding allows the use of higher-level modulation to increase the effective data rate. It is effective when the system capacity is limited by multipath fading.
Common forms of diversity are:

Temporal diversity: Replicas of the signal are transmitted in different time slots, where the separation between the time slots is greater than the coherence time of the channel.

Frequency diversity: Replicas of the signal are transmitted in different frequency bands, where the separation between the frequency bands is greater than the coherence bandwidth of the channel.

Antenna diversity: Antennas with large enough spacing lead to uncorrelated channels. The transmission of replicas of the signal over these spatial channels leads to spatial diversity.

Diversity reception methods are for example selection diversity, feedback diversity, equal gain combining and maximal ratio combining [Jakes, 1974]. MRC produces an output Signal to Noise Ratio (SNR) equal to the sum of the individual SNRs. This technique gives the best statistical reduction of fading of any known linear diversity combiner [Rappaport, 2001].

4.1.2.1.1 Space Time Coding

Space-Time Codes were developed in the form of Space Time Trellis Codes (STTCs), which require a multidimensional Viterbi algorithm for decoding at the receiver. These codes can provide diversity equal to the number of

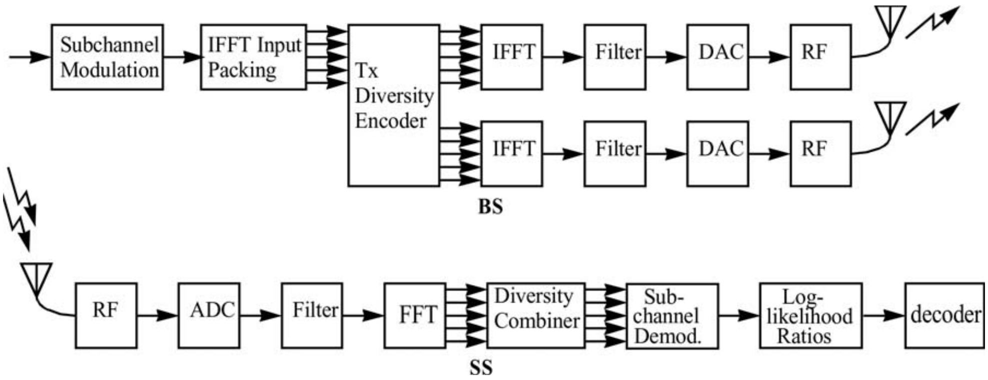

Figure 4.1: Alamouti Space-Time Coding Option in IEEE 802.16 [IEEE, 2004a]

transmit antennas as well as coding gain depending on the complexity of the code without loss in bandwidth efficiency. Space Time Block Codes (STBCs) offer the same diversity as the STTCs but do not provide coding gain. STBCs are often the preferred solution against STTC, as their decoding only requires linear processing [Alexiou and Haardt, 2004].
Alamouti proposed the most famous STBC using two transmit antennas [Alamouti, 1998]. The STBC achieves the same diversity advantage as MRC. STBC is defined as a mapping operation of a block of input symbols into the space and time domains, creating orthogonal sequences that are transmitted from different transmit antennas. The decoding is achieved using a decoder based upon the Maximum Likelihood (ML) detection rule. Figure 4.1 illustrates the Alamouti scheme, which is included in the IEEE 802.16-2004 standard.
At a given symbol period, two signals are simultaneously sent by the two transmit antennas. The signal transmitted by antenna 1 is s_1 and the one transmitted by antenna 2 is s_2. During the next symbol period, the signal $-s_2^*$ is transmitted from antenna 1 and s_1^* is transmitted from antenna 2, where * denotes the complex conjugate. The Alamouti code matrix is thus orthogonal:

$$S = \begin{pmatrix} s_1 & s_2 \\ -s_2^* & s_1^* \end{pmatrix}$$

The Alamouti scheme was generalized in [Tarokh et al., 1999] for an arbitrary number of transmit antennas. Furthermore, the concept can be expanded for the case of M receivers. It is then possible to provide a diversity order of

$2M$ with two transmit antennas and M receive antennas [Alamouti, 1998].

4.1.2.1.2 Space Frequency Coding

Broadband systems offer frequency diversity. In OFDM systems, frequency diversity is exploited by interleaving coded bits over different subcarriers. Channel coding deals with the resulting random bit errors.
Combining STC with OFDM simultaneously exploits spatial and frequency diversity. Hence, data is coded across antennas and subcarriers. This is known as Space Frequency Coding (SFC). In [Bölcskei and Paulraj, 2001] it is shown, that SFC can outperform traditional STC.

4.1.2.2 Spatial Multiplexing

By means of spatial multiplexing two SSs with n antennas each, are able to establish up to n orthogonal channels between each other. Each channel has about the same data rate as that of a single Single Input Single Output (SISO) channel.

4.1.2.2.1 BLAST

The BLAST scheme [Foschini, 1996] leads to theoretical data rates, which grow linearly with the number of antennas. This assumes equal numbers of transmit and receive antennas and an independent Rayleigh scattering environment.
A single data stream is splitted into n substreams, and each substream is independently encoded into symbols and fed to its respective (ordinary QAM) transmitter. The total radiated power is held constant compared to the single transmitter case (independent of n). The receivers are also individually conventional QAM receivers.
An essential feature of BLAST is that no explicit orthogonalization of the transmitted signals is imposed by the transmit structure at all. Instead, the propagation environment itself, which is assumed to exhibit significant multipath propagation, is exploited to achieve the signal decorrelation necessary to separate the co-channel signals [Foschini, 1996].
For detection of the different data streams, linear combinatorial nulling could be performed (according to the zero-forcing or minimum mean square error criterion). But superior performance is obtained if nonlinear techniques are used. The proposed technique exploits the timing synchronism inherent in

the system model to perform symbol cancelation as well as linear nulling [Foschini, 1996]. In this case, the order in which the components are detected, becomes important. It is shown that the best performance is achieved with the "best first" cancelation approach, where iteratively the strongest signal is detected and canceled.

4.1.2.2.2 Eigenbeamforming

Eigenbeamforming was presented in [Raleigh and Cioffi, 1998] and [Telatar, 1999]. The technique is based on the SVD theorem, which states that any matrix $H \in \mathbf{C}$ can be decomposed into three components, each with some special property, as follows:

$$H = U\Lambda V^H \tag{4.1}$$

U and V are unitary matrices. The matrix Λ is a diagonal matrix with non-negative definite elements. The properties of U, V and Λ can be geometrically explained. In a complex-valued multi-dimensional vector space, a transformation of a vector by a unitary matrix represents a pure rotation of the original vector. This means the power of the signals represented by the vector is conserved under this transformation. Similarly a diagonal matrix represents a pure scaling (and no rotation) of the vector. Thus, it represents a pure power scaling of the signal represented by the vector. When viewed in the light of a communications system model, a rotational transformation of the complex vector signal from a transmit-antenna array represents cross coupling when received by an appropriate receive-antenna array. A pure scaling has no cross-coupling at all and offers only a power loss.
The Eigenbeamforming method uses the SVD of the channel matrix to establish parallel independent (non-interfering) spatial sub-channels. Both transmitter and receiver need to know the channel matrix. The transmitter performs a prefiltering of the transmit vector with the matrix V, the receiver applies the filter U^H. Because the Hermitian of a unitary matrix is its inverse, the transmission line between transmitter and receiver is diagonalized.
In a rich scattering case with good separation between antenna elements, the maximum possible number of spatial subchannels created will be equal to the rank of the matrix channel, which is again the minimum of the number of Tx and Rx antennas.

4.1.2.3 Spatial Filtering and Interference Cancelation

The algorithms described in the following refer to a common signal model, which is described in the next Section 4.1.2.3.1. The beamforming algorithms introduced thereafter are narrow-band beamformers. In a multicarrier system such as OFDM, these techniques can be applied on subcarrier basis.

4.1.2.3.1 Signal Model and Array Covariance Matrix

Consider an array of M omnidirectional elements immersed in a homogeneous media in the far field of M uncorrelated sinusoidal point sources of frequency f_0. Let the origin of the coordinate system be taken as the time reference (refer to Figure 4.2). Thus, the time taken by a plane wave arriving from the i^{th} source in direction (ϕ_i, θ_i) and measured from the l^{th} element to the origin is given by

$$\tau_l(\phi_i, \theta_i) = \frac{\vec{r}_l \cdot \hat{\vec{v}}(\phi_i, \theta_i)}{c} \tag{4.2}$$

where $\vec{r}_l$ is the position of the l^{th} element, $\hat{\vec{v}}(\phi_i, \theta_i)$ is the unit vector in direction (ϕ_i, θ_i), and c is the speed of propagation of the plane wave front. For a linear array of equispaced elements with element spacing Δx aligned with the x-axis such that the first element is situated at the origin, it becomes

$$\tau_l(\phi_i, \theta_i) = \frac{\Delta x}{c} l \cos\phi_i \sin\theta_i \tag{4.3}$$

The signal induced on the reference element due to the i^{th} source is normally expressed in complex notation as

$$m_i(t) e^{j2\pi f_0 t} \tag{4.4}$$

with $m_i(t)$ denoting the complex modulation function. Assuming that the wavefront on the l^{th} element arrives $\tau_l(\phi_i, \theta_i)$ seconds before it arrives at the reference element, the signal induced on the l^{th} element due to the i^{th} source can be expressed as

$$m_i(t) e^{j2\pi f_0 (t + \tau_l(\phi_i, \theta_i))} \tag{4.5}$$

The expression is based upon the narrow-band assumption for array signal processing, which assumes that the array dimensions are small enough for the

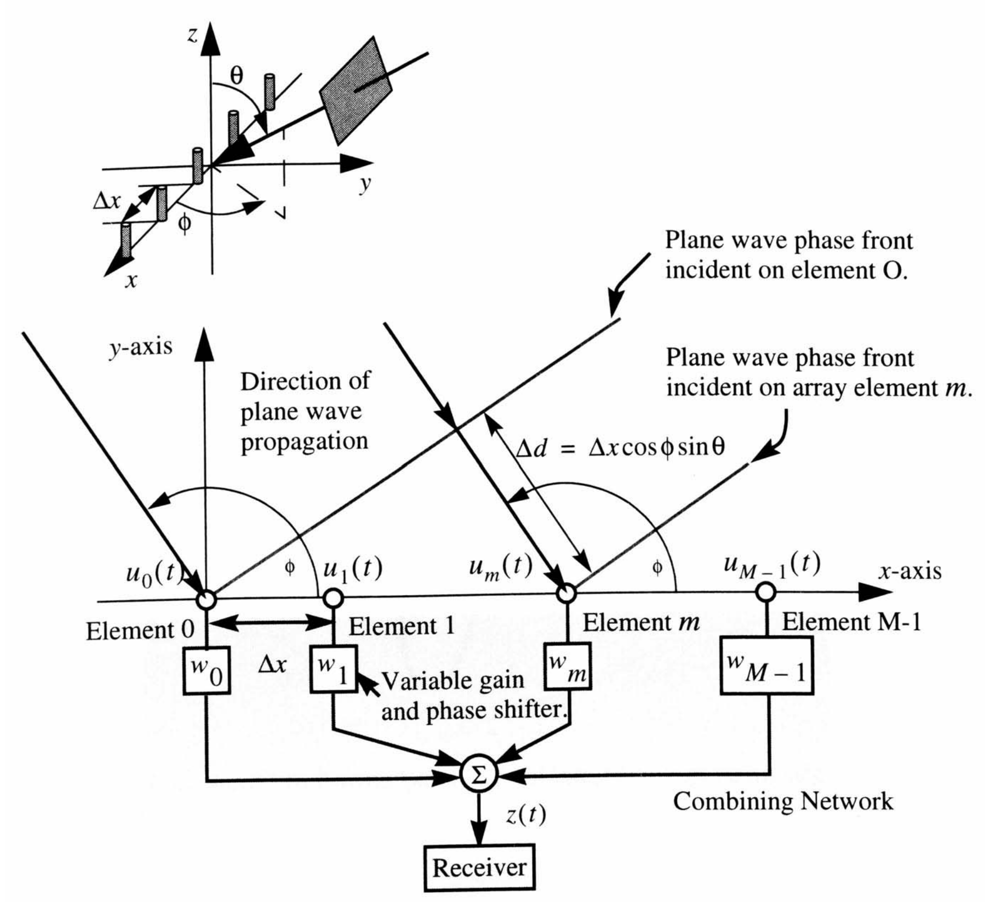

Figure 4.2: Plane Wave incident on Uniform Linear Array [Liberti and Rappaport, 1999]

modulating function to stay almost constant during $\tau_l(\phi_i, \theta_i)$ seconds, that is, the approximation $m_i(t) \approx m_i(t + \tau_l(\phi_i, \theta_i))$ holds. Figure 4.2 illustrates the scenario.

Let x_l denote the total signal induced due to all N directional sources and background noise on the l^{th} element. Then it is given by

$$x_l = \sum_{i=1}^{N} m_i(t) e^{j2\pi f_0 (t + \tau_l(\phi_i, \theta_i))} + n_l(t) \tag{4.6}$$

where $n_l(t)$ is a random noise component on the l^{th} element, which includes background noise and electronic noise generated in the l^{th} channel. It is assumed to be temporally white with zero mean and variance σ_n^2.

Consider the narrow-band beamformer of Figure 4.2, where signals from each element are multiplied by a complex weight w_l and summed to form the array output. The array output is given by

$$z(t) = \sum_{l=0}^{M-1} w_l^* x_l(t) \tag{4.7}$$

where $*$ denotes the complex conjugate. Denoting the weights of the beamformer as

$$\vec{w} = (w_0, w_1, \ldots, w_{M-1})^T \tag{4.8}$$

and signals induced on all elements as

$$\vec{x}(t) = (x_0(t), x_1(t), \ldots, x_{M-1}(t))^T \tag{4.9}$$

the output of the beamformer becomes

$$z(t) = \vec{w}^H \vec{x}(t). \tag{4.10}$$

The notation w^H denotes the Hermitian adjoint (complex conjugate transpose) of w. If the components of $\vec{x}(t)$ can be modeled as zero mean stationary processes, then for a given $\vec{w}$ the mean output power of the processor is given by

$$P(\vec{w}) = E[z(t)z^*(t)] = \vec{w}^H R \vec{w} \tag{4.11}$$

where $E[\cdot]$ denotes the expectation operator and R is the array correlation matrix defined by

$$R = E[\vec{x}(t)\vec{x}^H(t)]. \tag{4.12}$$

Elements of this matrix denote the correlation between various elements. Denote the steering vector associated with the direction (ϕ_i, θ_i) of the i^{th} source by an M-dimensional complex vector $\vec{s}_i$ as

$$\vec{s}_i = (e^{j2\pi f_0 \tau_0(\phi_i,\theta_i)}, \ldots, e^{j2\pi f_0 \tau_{(M-1)}(\phi_i,\theta_i)})^T. \tag{4.13}$$

Then R can be expressed as

$$R = \sum_{i=1}^{N} p_i \vec{s}_i \vec{s}_i^H + \sigma_n^2 I \tag{4.14}$$

where I is the identity matrix and p_i denotes the power of the i^{th} source measured at one of the elements of the array. p_i is the variance of the complex modulating function $m_i(t)$ when it is modeled as a zero mean low-pass random process. Using matrix notation, the correlation matrix R may be expressed in the following compact form:

$$R = ASA^H + \sigma_n^2 I \tag{4.15}$$

where columns of the $M \times N$ matrix A are made up of steering vectors, i.e.

$$A = (\vec{s}_1, \vec{s}_2, \ldots, \vec{s}_N) \tag{4.16}$$

and the $N \times N$ matrix S denotes the source correlation. For uncorrelated sources, it is a diagonal matrix with

$$S_{ij} = \begin{cases} p_i, & i = j \\ 0, & i \neq j \end{cases} \tag{4.17}$$

Sometimes, it is useful to express R in terms of its eigenvalues and their associated eigenvectors. The eigenvalues of R can be divided into two sets when the environment consists of uncorrelated directional sources and uncorrelated white noise.

The eigenvalues contained in one set are of equal values. Their value does not depend upon the directional sources and is equal to the variance of the white noise. The eigenvalues contained in the second set are a function of the parameters of the directional sources, and their number is equal to the number of these sources. Each eigenvalue of this set is associated with a directional source, and its value changes with the change in the source power of this source. The eigenvalues of this set are bigger than those associated with white noise. Sometimes, these eigenvalues are referred to as the signal eigenvalues, and the others belonging to the first set are referred to as the noise eigenvalues. Thus, the R of an array of M elements immersed in N directional sources and the white noise has N signal eigenvalues and $M - N$ noise eigenvalues.

R can be spectrally decomposed into

$$R = \sum_{l=1}^{M} \lambda_l \vec{U}_l \vec{U}_l^H + \sigma_n^2 I, \tag{4.18}$$

where the λ_l are the eigenvalues and $\vec{U}_l$ the corresponding unit-norm eigenvectors.

4.1.2.3.2 Conventional Beamforming

A conventional beamformer applies weights of equal magnitude. The phases are selected to steer the array in a particular direction (ϕ_0, θ_0), known as the look direction. With $\vec{s}_0$ denoting the steering vector in the look direction, the array weights are given by

$$\vec{w}_c = \frac{1}{M}\vec{s}_0. \tag{4.19}$$

The array with these weights has unity response in the look direction, that is, the mean output power of the processor due to a source in the look direction is the same as the source power arriving at the array (input power). The signals received at the antenna elements are added up in phase.
In an environment consisting of only uncorrelated noise and no directional interferences, this beamformer provides maximum SNR. For uncorrelated noise, the noise covariance matrix is given by $R_N = \sigma_n^2 I$ and the output noise power of the beamformer

$$P_N = \vec{w}_c^H R_N \vec{w}_c = \frac{\sigma_n^2}{M}. \tag{4.20}$$

This shows that the noise power at the array output is M times less than that present on each element. Thus, the processor with unity gain in the signal direction has reduced the uncorrelated noise by M, yielding the output SNR $= p_s M/\sigma_n^2$. As the input SNR is p_s/σ_n^2, this provides an array gain equal to M, the number of elements in the array.
This performance is degraded when there is directional interference, as this interference might be in the direction of a side lobe.

4.1.2.3.3 Null-Steering Beamforming - Zero Forcing

A null-steering beamformer is used to cancel plane waves arriving from known directions and thus produces nulls in the response pattern in the Direction of Arrival (DoA) of the plane wave.
This may be done by estimating the weights of a beamformer using suitable constraints. Assume that $\vec{s}_0$ is the steering vector in the direction where unity

response is required and that $\vec{s}_1, \ldots, \vec{s}_k$ are k steering vectors associated with k directions where nulls are required. The desired weight vector is the solution of following simultaneous equations:

$$\vec{w}^H \vec{s}_0 = 1 \tag{4.21}$$
$$\vec{w}^H \vec{s}_i = 0; \quad i = 1, \ldots, k. \tag{4.22}$$

Using matrix notation, this becomes

$$\vec{w}^H A = \vec{e}_1^T \tag{4.23}$$

For $k = M - 1$, A is a square matrix. Assuming that the inverse of A exists, which requires that all steering vectors are linearly independent, the solution for the weight vector is given by

$$\vec{w}^H = \vec{e}_1^T A^{-1}. \tag{4.24}$$

In case the steering vectors are not linearly independent, A is not invertible, and its pseudo inverse can be used in its place:

$$\vec{w}^H = \vec{e}_1^T A^H (AA^H)^{-1} \tag{4.25}$$

Though the beam pattern produced by this beamformer has nulls in the directions of interferences, it is not designed to minimize the uncorrelated noise at the array output.

4.1.2.3.4 Optimal Beamforming

The null-steering scheme described above requires knowledge of the directions of interference sources, and the beamformer using the weights estimated by this scheme does not maximize the output SINR. The optimal beamforming method described in this section overcomes these limitations. The algorithm is also known as Minimum Variance Distortionless Response (MVDR) beamformer [Godara, 1997b].
For an unconstrained array, the weights that optimize the output SINR are

$$\hat{\vec{w}} = \mu_0 R_N^{-1} \vec{s}_0. \tag{4.26}$$

As noise covariance matrix R_N does not contain any signal from the look direction. For an array constrained to have a unit response in the look direction, the constant μ_0 becomes

$$\mu_0 = \frac{1}{\vec{s}_0^H R_N^{-1} \vec{s}_0} \tag{4.27}$$

This beamformer is also known as the Maximum Likelihood filter, as it finds the ML estimate of the power of the signal source, assuming all sources as interferences.
If the noise-alone matrix is not available, the total R (signal plus noise) can be used instead. In the absence of errors, the processor performs identically in both cases. The weights are then

$$\hat{\vec{w}} = \frac{R^{-1}\vec{s}_0}{\vec{s}_0^H R^{-1} \vec{s}_0}. \tag{4.28}$$

These weights are the solution of the following optimization problem:

$$\begin{array}{ll} \text{minimize} & \vec{w}^H R \vec{w} \\ \text{subject to} & \vec{w}^H \vec{s}_0 = 1. \end{array}$$

Thus, the processor weights are selected by minimizing the mean output power of the processor while maintaining unity response in the look direction. The constraint ensures that the signal passes through the processor undistorted. Therefore, the output signal power is the same as the look-direction source power. The minimization process then minimizes the total noise, including interferences and uncorrelated noise. Minimizing the total output noise while keeping the output signal constant is the same as maximizing the output SNR.
The processor with these weights is referred to as the optimal processor. The output SINR $\hat{\alpha}$ of the optimal processor is given by

$$\hat{\alpha} = p_s \vec{s}_0^H R_N^{-1} \vec{s}_0. \tag{4.29}$$

For the optimal beamformer to operate as described above and to maximize the SINR by canceling interferences, the number of interferences must be less than or equal to $M-2$, as an array with M elements has $M-1$ degrees of freedom (free parameters, possibilities to place nulls or maxima) and one has been utilized by the constraint in the look direction. This may not be

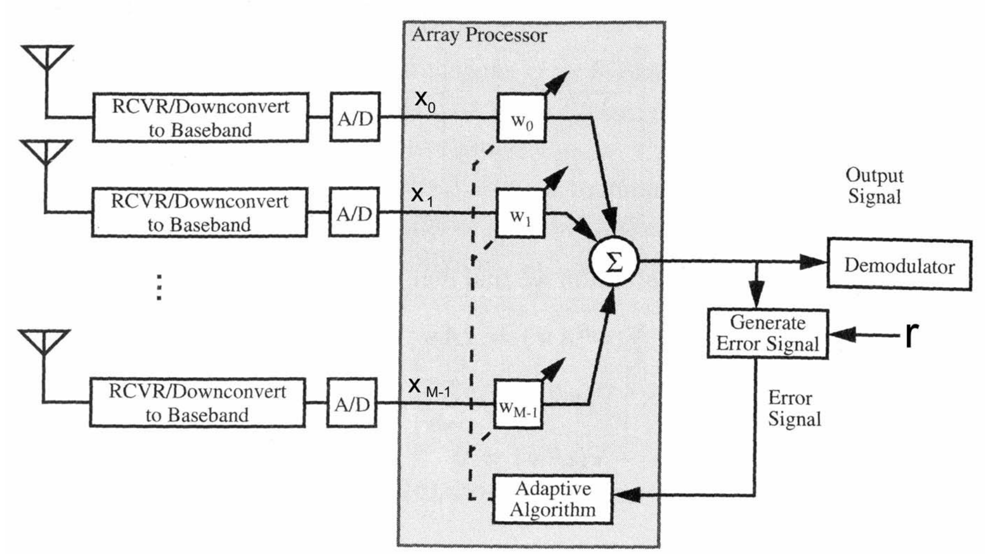

Figure 4.3: Adaptive Array with Generated Error Signal. Adapted from [Liberti and Rappaport, 1999].

true when multipath exists, and the beamformer may not be able to achieve the maximization of the output SINR by suppressing every interference. However, suppressing parts of the interference is still an improvement.

4.1.2.3.5 Optimization Using Reference Signal

The optimal beamformer described above needs the knowledge of the direction of the desired signal. This can be substituted by the knowledge of a reference signal.

The array output is subtracted from an available reference signal $r(t)$ to generate an error signal $\epsilon(t) = r(t) - \vec{w}^H \vec{x}(t)$, which is used to control the weights (see figure 4.3). Weights are adjusted such that the Mean Squared Error (MSE) between the array output and the reference signal is minimized. The MSE is given by

$$\text{MSE} = E[|\epsilon(t)|^2] = E[|r(t)|^2] + \vec{w}^H R \vec{w} - 2\vec{w}^H \vec{z} \tag{4.30}$$

where $\vec{z} = E[\vec{x}(t)r(t)]$ is the correlation between the reference signal and the array signal vector $x(t)$.

The MSE surface is a quadratic function of $\vec{w}$ and is minimized by setting its gradient with respect to $\vec{w}$ equal to zero, yielding the solution

$$\hat{\vec{w}}_{MSE} = R^{-1}\vec{z}. \tag{4.31}$$

The Minimum Mean Squared Error (MMSE) of the processor, also known as the Wiener filter, using these weights is given by

$$\text{MMSE} = E[|r(t)|^2] - \vec{z}^H R^{-1}\vec{z}. \tag{4.32}$$

The MSE minimization scheme (the Wiener filter) is a closed-loop method compared to the open-loop scheme of MVDR (the ML filter) described in the previous section. In general, the Wiener filter provides higher output SINR compared to the ML filter in the presence of a weak signal source. As the input signal power becomes large compared to the background noise, the two processors give almost the same results. The increased SINR by the Wiener filter is achieved at the cost of signal distortion caused by the filter. The required reference signal for the Wiener filter may be generated in a number of ways. A synchronisation signal, e.g., the preamble may be used for initial weight estimation, followed by the use of the detected signal as reference signal. A user specific sequence might also be used.

4.1.2.3.6 Multi User Eigenbeamforming

Multi User Eigenbeamforming, also known as MU-SVD was proposed in [Kim and Cioffi, 2000]. It is assumed that all stations have antenna arrays, although it is not necessary that they have the same number of elements.

Beamforming is typically used to suppress the interference, but it is not always able to process a multipath signal optimally, especially when the paths from each user arrive in an alternating fashion. It also loses antenna diversity since it steers the angle of gain to only one direction of interest (and this path could be fading). By choosing one direction, the system may not fully exploit all the path gains, thus reducing achievable data rates. This is overcome by multi user Eigenbeamforming.

Using Eigenbeamforming (see subsection 4.1.2.2.2), a SVD of the channel matrix is used to coordinate the space domain to collect the signal power in order to maximize SINR, in which sense the SVD filter is a spatial MRC filter.

Using MU-SVD, all stations perform the prefiltering derived from the SVD of their own channel matrix. The BS can then perform the postfiltering

for each link in parallel. This corresponds to a matched filter approach collecting all multipath components for all links. However, the received signals are severely corrupted by interference, due to the correlation of the matched filters. A linear multi user detector can then be used, for example a decorrelator or an MMSE detector. A multi-stage detector for successive cancelation could be used alternatively (see Section 4.1.2.2.1).
[Kim and Cioffi, 2000] also proposes a modified version of MU-SVD by considering another multi user detector. Another criterion is proposed to diagonalize the covariance matrix of the matched filters at the expense of losing gains for the desired signal. This method is shown to further reduce the BER.

4.1.2.4 Algorithm Selection

In most deployments, only BSs have antenna arrays because antenna arrays are too big and too costly for (mobile) SSs. This avoids the usage of spatial multiplexing techniques, since they require multiple antennas at both nodes. Beamforming performs well for high element or channel correlation, whereas diversity coding and spatial multiplexing are interesting in low element/channel correlation environments [Alexiou and Haardt, 2004]. Highly correlated transmission channels can be found in rural and suburban scenarios, especially with LOS or over-the-rooftop antennas. Due to the multipath environment, channels tend to be uncorrelated in urban scenarios. Since the intended scenarios for initial WiMAX deployments are rural and suburban scenarios the beamforming approach has been chosen for this work. The optimal beamforming algorithm has been implemented in the simulation environment, which is introduced in Chapter 7.
As described in Section 4.1.2.3.4, the optimal beamformer calculates a beam pattern that realizes a gain of one in the direction of the desired SS. As the algorithm minimizes the total radiated energy, it reduces the antenna gain towards undesired SSs. Figure 4.4 shows the beam patterns for a two SS environment. The size of the side lobes can be influenced by assuming a different noise level when building the array correlation matrix.
Figure 4.4 shows two exemplary beam patterns for a 9-element Uniform Linear Array (ULA) and Uniform Circular Array (UCA). The difference is in the position of the antenna elements. In a ULA they are aligned in a line. As Figure 4.4a shows, the ULA array allows thin beam widths but has the disadvantage of always exhibiting a symmetry with respect to the array's

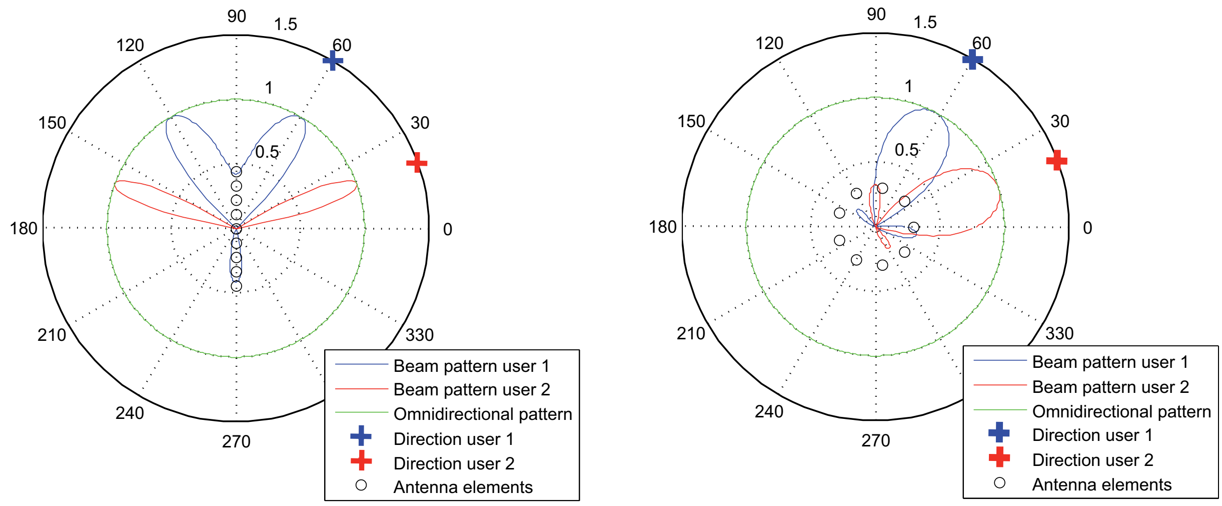

(a) Uniform Linear Array **(b)** Uniform Circular Array

Figure 4.4: Radiation patterns for 9-element circular and linear antenna arrays

axis. Thus, ULAs are usually used in sectorized deployments where only one sector is served by the array. In contrast, the UCA shown in Figure 4.4b features slightly wider beams but is better suited for the deployment at the base station of an unsectorized cell. The UCA is used for the performance evaluation in Chapter 8.

4.1.3 Spatial Filtering for Interference Reduction

A beamforming antenna can focus the transmit power to the desired directions and reduce the inter-cell interference. Figure 4.4 shows the benefits of a beamforming antenna compared to an omnidirectional one. The conventional omnidirectional antenna emits the same amount of energy into all directions (green pattern). The beamforming patterns in contrast, only radiate the full energy into the direction of the desired SS. In all other directions the emitted power is significantly reduced or even close to zero.
This is advantageous both in receive and transmit mode. When the beamforming station is receiving, it still gets the same desired signal strength (the carrier), but collects significantly less interference from other directions. Thus, the SINR is increased. While transmitting, the station emits less total energy while the same power will arrive at the desired receiving SS. The advantage is a reduced inter-cell interference. This technique is called

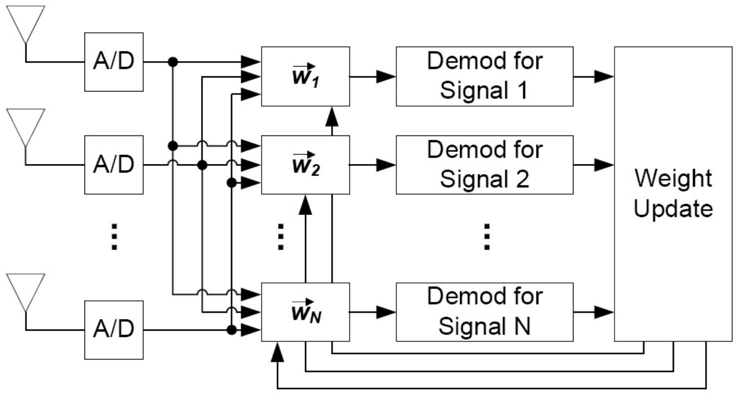

Figure 4.5: Beamforming System supporting N parallel beams [Liberti and Rappaport, 1999]

Spatial Filtering for Interference Reduction (SFIR) and is often proposed to reduce the Cluster Order in cellular systems.

4.1.4 Space Division Multiple Access

The term SDMA denotes the possibility for multiple, spatially separable SSs to access the medium at the same time, on the same frequency. This can be realized using a beamforming system as depicted in Figure 4.5. The linear nature of an antenna allows a superposition of several signals onto one antenna element. If the beam patterns (resulting from the corresponding weight vectors $\vec{w}_1, \vec{w}_2 \dots \vec{w}_N$) have high gains in the direction of the desired SSs and low gains in the directions of concurrent, undesired SSs, each station will receive its signal with a sufficient SINR. An example SDMA transmission to two SSs is given in Figure 4.4: SS 1 (located at an azimuth angle of 60°) and SS 2 (located at an azimuth angle of 20°) can be served simultaneously because each SS's pattern has a null set in the other SS's direction. In the uplink, when SS 1 and 2 concurrently transmit to the beamforming station, joint detection techniques of the beamforming system allow the parallel reception. This can be seen as setting "receive beam patterns".
Figure 4.6 summarizes how the different transmission techniques can be used by the base stations of a clustered cellular deployment. With conventional omnidirectional antennas the BS transmits in all directions. In SFIR, multiple antennas form a beam to serve one particular SS at a time. With SDMA, multiple beams serve multiple SSs simultaneously.

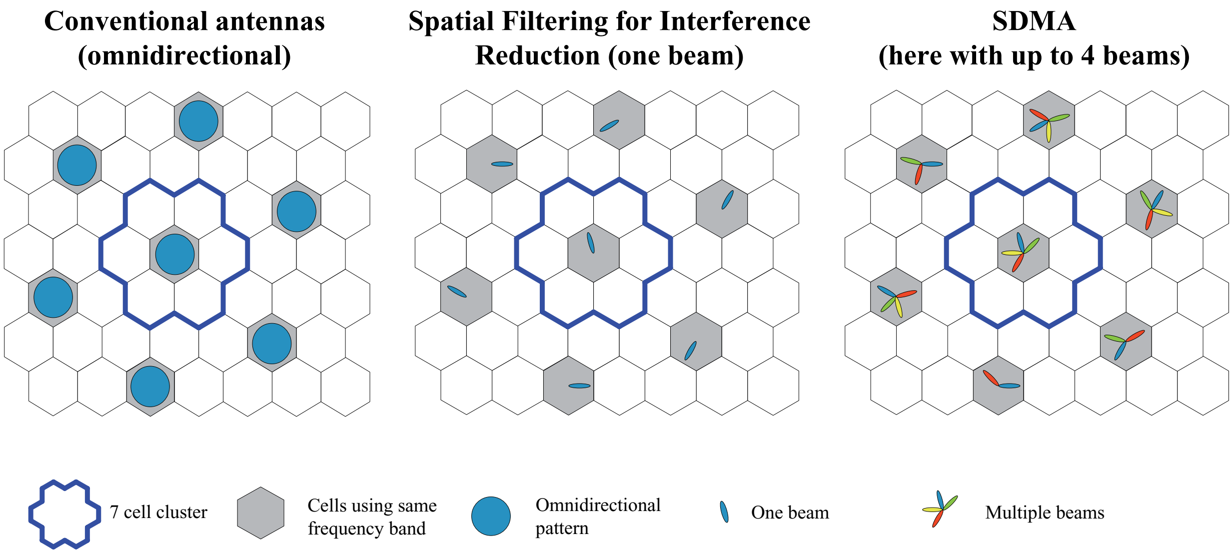

Figure 4.6: Comparison of omnidirectional, SFIR and SDMA mode

4.2 PHY Service Access Point

Specifications for both, MAC and PHY SAPs were part of the first draft standards. However, during the standardization process, SAPs were intended to become implementation-specific. Consequently, they were removed. The PHY SAP was deleted without substitution and the MAC SAP went to the annex as an informative example [IEEE, 2004a]. Thereupon, the PHY SAP (at least the PHY SAP of the data plane) was defined by manufacturers [Intel, 2006]. Within the working group 802.16g management and control SAPs were again incorporated in the standard. Furthermore, a Generic Packet Convergence Sublayer (GPCS) SAP was introduced there [IEEE, 2007b].
The available SAP do not support beamforming and SDMA sufficiently. Hence, the following section proposes a PHY SAP that supports SDMA transmission and reception. The specification of the SAP comprises all necessary service primitives. Service primitives are used by MAC layer entities to access SDMA related PHY-layer functionality such as SINR estimation and Tx/Rx beam steering.

4.2.1 Service Primitives

The services of the PHY layer are provided to the MAC layer at the PHY SAP. By means of service primitives, the MAC layer can pass control information and user data to the PHY. The PHY can give feedback to the MAC and deliver the received data. Therefore, several primitives are specified [Intel, 2006].

An example usage of service primitives for DL transmission is shown in Figure 4.7. The MAC sends the *PHY_TXSTART.req*. This primitive contains the *TXVECTOR*, which is a description of the following DL subframe. The *TXVECTOR* provides all information necessary for encoding, modulation, and transmission of data bursts. Its content is comparable to the DL-MAP. The reception is acknowledged by the the *PHY_TXSTART.conf* primitive. Afterwards, the MAC sends PHY SDUs, which contain data (MAC PDUs) for the DL bursts. The PHY confirms the reception. Finally, it indicates the periodic frame start *PHY_TXSTART.ind* and the end of the DL subframe *PHY_TXEND.ind*. The reception at the SS is controlled by the corresponding primitives. Service primitives for BS reception are shown in Figure 4.9.

4.2.2 Smart Antenna Specific Service Primitives

An antenna array steered by smart algorithms allows for applying optimized antenna patterns in DL (beamforming) and in UL (joint detection). The MAC needs to control the pattern since it has to schedule the SSs and the applied antenna patterns must correspond to the schedule. The schedule is based on feedback information offered by the PHY. Thus, sophisticated services have to be provided at the PHY SAP. Basically, two different services are needed:

- Provide SINR estimates needed for link adaptation and for spatial separation
- Allow antenna pattern control for omnidirectional, SFIR, or SDMA transmission and reception

4.2.2.1 SINR Feedback

Smart MAC scheduling strategies are necessary to fully benefit from the capabilities of a smart antenna enhanced PHY layer in the presence of inter- and intra-cell interference [Hoymann et al., 2006b]. The scheduling strategy

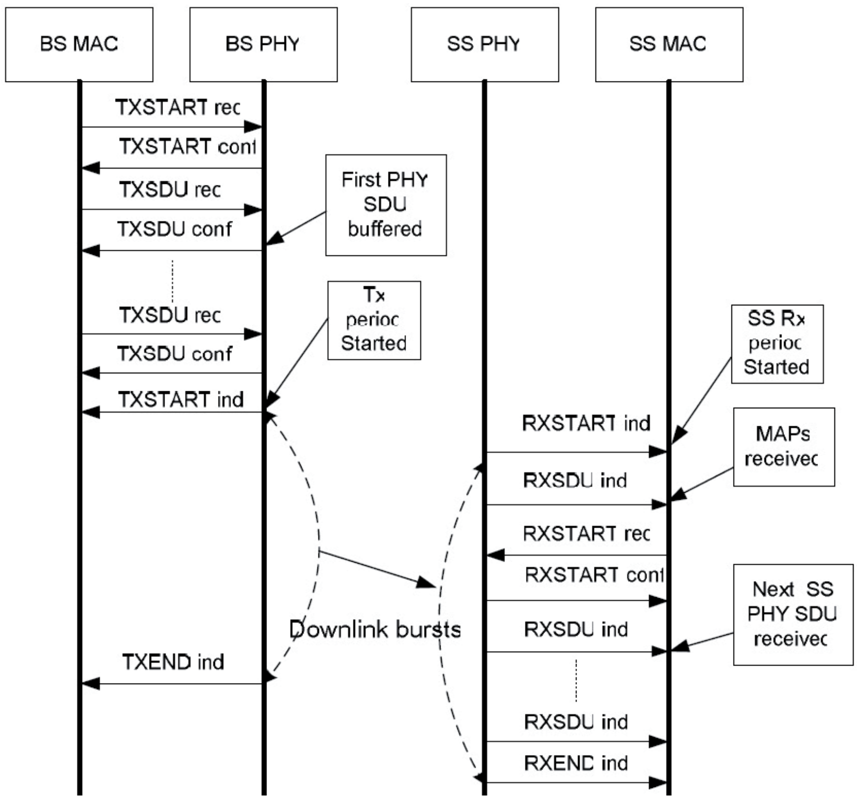

Figure 4.7: Service primitives for BS transmission [Intel, 2006]

has to take the current interference situation into account. It should not schedule stations in parallel that are not sufficiently separable by the smart antenna. Stations, which do interfere each other heavily, should be arranged in TDMA mode. An intelligent scheduler needs to acquire information about the current interference situation and about the spatial separability of SSs (refer to Section 4.4). For this, the estimated SINR seems to be a good measure [Hara, 2001; Shad et al., 2001]. It can be directly converted into a desired MCS and thus into the throughput of the link. More accurate MCS selection algorithms for multicarrier systems take the estimated mean SINR plus an additional indicator such as the variance of the subcarrier SINRs into account [Lampe et al., 2003].
Furthermore, SINR estimates can be used without further knowledge about the applied antenna algorithm. Sophisticated algorithms and antennas with a lot of elements are able to accurately steer the antenna pattern, which results in valuable SINR estimates. Antennas with less elements or with simple algorithms produce less powerful patterns, which results in lower SINR estimates. Hence, the MAC scheduling becomes almost independent from the PHY algorithms.

4.2.2.1.1 SDMA Transmit Case

When a conventional BS transmits using an omnidirectional antenna, it estimates the SINR at the receiver. To do so, the carrier strength at the SS is needed: In FDD systems, which operate DL and UL on separate frequency channels, the SSs signal the received carrier signal strength back to the BS. In TDD systems, which operate DL and UL on the same frequency channel, the reciprocity of the channel can be used to calculate it. In any case, the level of interference and noise at the SS has to be signaled or it has to be estimated.
A beamforming BS operating in SDMA mode has to additionally consider the intra-cell interference, which is generated when the BS concurrently transmits to other SSs. Figure 4.8a illustrates all relevant signals during SDMA transmission. An optimized beam pattern is applied at the BS that maximizes the desired signal S to SS A. All other patterns, which are optimized for concurrent transmissions to other SSs, say SS B, try to minimize the intra-cell interference I_{intra} to SS A. Inter-cell interference I_{inter}^{SS} generated by BSs of neighbor cells is received as well.
During SDMA transmission, the desired signal S and the intra-cell interfer-

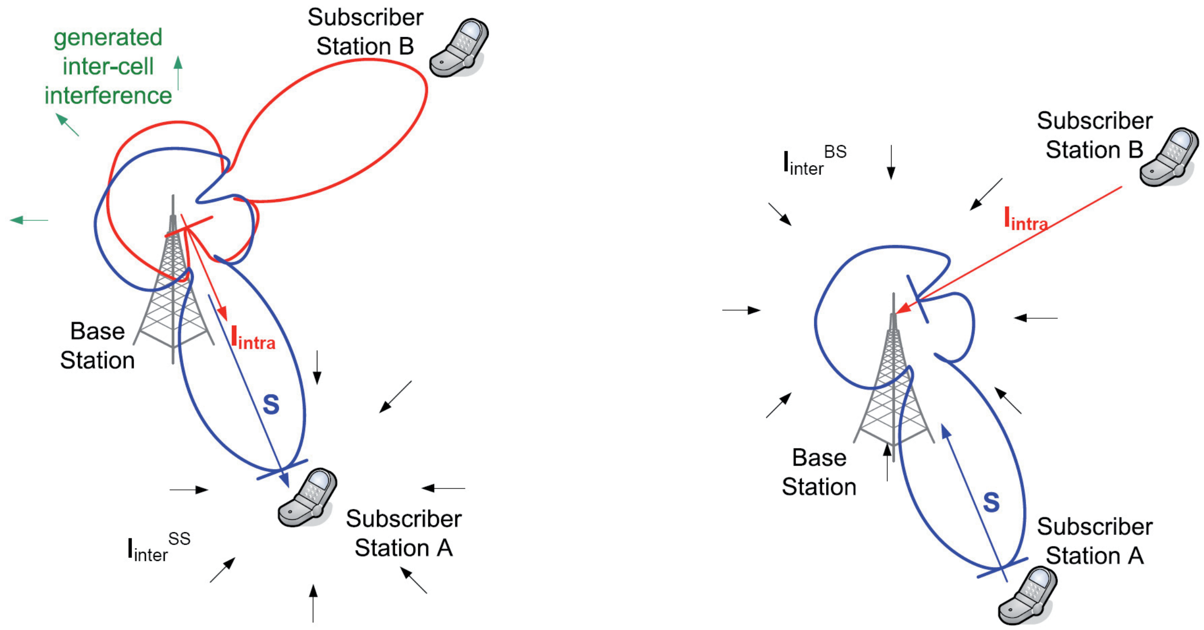

(a) SDMA transmission **(b)** SDMA reception

Figure 4.8: Relevant signals during SDMA operation

ence I_{intra} is filtered through the corresponding optimized beam patterns, denoted by the superscript ^{opt}. Since it is presumed that the SS is receiving omnidirectionally, the inter-cell interference is not filtered. By reducing the side-lobes of the BS's antenna patterns the inter-cell interference caused in neighbor cells can be minimized. Receiver noise at the SS N^{SS} has to be considered as well. The resulting SINR is given by

$$SINR_{Tx} = \frac{S^{opt}}{N^{SS} + I^{SS}_{inter} + \sum\limits_{\substack{other\,Tx\\patterns}} I^{opt}_{intra}} \tag{4.33}$$

The signal strengths of S^{opt} and I^{opt}_{intra} can be calculated by the PHY based on both, the Channel State Information (CSI) and the optimized antenna patterns. In TDD systems, the DL CSI is gained by estimating the UL channel during preamble reception. UL preambles are send in front of every UL burst and rather inactive SSs can be (periodically) scheduled to transmit a preamble only. Figure 4.9 illustrates the service primitives that are necessary for UL channel estimation.

The interference and the noise level at the SS (N^{SS}, I^{SS}_{inter}) has to be passed

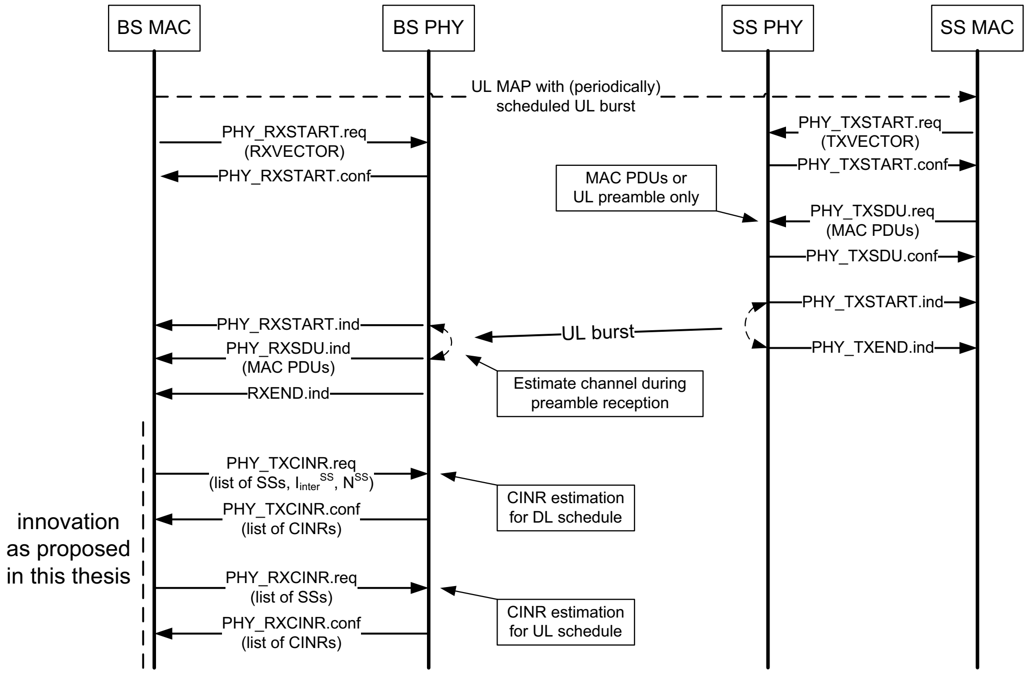

Figure 4.9: Service primitives for channel estimation and request of SINR estimates

to the SS MAC layer by means of conventional service primitives used for communicating measurements. Then, they have to be signaled from the SS to the BS by means of MAC management messages. Alternatively, they can be estimated at the BS. Both values are handed to the BS PHY as parameters of the newly proposed service primitive *PHY_TXSINR.req* shown in Figure 4.9. The third parameter is a list of SSs for which the SINRs are requested. If this list contains only one SS, the SINR for the SFIR mode is estimated, if the list contains several SSs, the SINR level for each SS in SDMA mode is estimated. The second primitive proposed for supporting smart antennas, i.e., *PHY_TXSINR.conf* passes these SINR estimates to the MAC layer. Based on these feedback information the MAC layer can schedule resource allocations (MCS selection and spatial grouping) in the DL subframe. Sophisticated SDMA scheduling algorithms are outlined in Section 4.4.
In FDD systems, the BS cannot estimate the DL channel during preamble reception in UL. The DL CSI has to be acquired at the SS and signaled to the BS. To do so, a service primitive would be necessary at the SS to handover the CSI from the PHY to the MAC layer and a MAC management

message would be needed to transmit the CSI to the peer MAC entity at the BS. Currently, these two service primitives are not contained in the standard.

4.2.2.1.2 SDMA Receive Case

The SINR during reception of a conventional BS is estimated by taking the SINR perceived during the last reception. When applying smart antennas, the received signal strength depends on the current antenna pattern and on simultaneous SDMA transmissions, which might differ from the previous reception.
Figure 4.8b illustrates all relevant signals during concurrent reception of data from spatially separated SSs. An optimized antenna pattern is applied at the BS. It maximizes the desired signal S from SS A and minimizes the intra-cell interference I_{intra} from SS B, which is concurrently transmitting. If more than one station is scheduled to transmit in SDMA, all intra-cell interferers have to be counted as well. The third component is the interference I_{inter}^{BS} generated by neighbor cells. All these signals are filtered through the optimized pattern, denoted by the superscript ^{opt} . Finally, the receiver noise at the BS N^{BS} has to be taken into account. The result is given by

$$SINR_{Rx} \quad = \quad \frac{S^{opt}}{N^{BS} + I_{inter}^{BS,\,opt} + \sum\limits_{\substack{SDMA \\ SSs}} I_{intra}^{opt}} \tag{4.34}$$

In the receive case, the strengths of all relevant signals are available at the BS PHY or can be calculated there from the CSI. Neither in FDD nor in TDD systems any additional information has to be provided.
Figure 4.9 illustrates the newly proposed service primitives that are needed to acquire SINR estimates for the receive case. The primitive *PHY_RXSINR.req* contains the list of SSs which are foreseen for (concurrent) reception. The primitive *PHY_RXSINR.conf* passes the requested SINR estimates to the MAC layer. The MAC layer can now schedule the UL subframe.

4.2.2.2 Smart Antenna Control

Frame descriptors are used by the MAC to communicate the structure of individual frames to the PHY [Intel, 2006]. The DL frame descriptor

(TXVECTOR) describes the structure of and burst allocations in a DL subframe, while the UL frame descriptor (RXVECTOR) describes the structure of and burst allocations in the UL subframe. The TXVECTOR provides all of the information that the PHY needs to modulate and encode the DL bursts that are to be transmitted. As shown in Figure 4.9 the TXVECTOR is handed to the PHY layer at the beginning of each frame. Since its content is similar to the DL-MAP, it contains the start time, the MCS, the address of the SS, and a bit to indicate the optional preamble (refer to Section 3.3.2.3). In SDMA mode the Extended Concurrent Transmission DL-MAP IE is used, which additionally contains the length of the burst. This field must be included in the TXVECTOR as well.

Besides this information, the smart antenna has to be controlled. Bursts are sent one after another by means of omnidirectional or adaptive antenna patterns (SFIR). Alternatively, bursts are transmitted simultaneously to other bursts by means of adaptive pattern (SDMA). Therefore, the TXVECTOR needs to indicate the type of transmission. The OFDMA PHY SAP specified by Intel already includes one bit to indicate SDMA in the AAS zone contained in reference [Intel, 2006]. However, another bit is required to differentiate between omnidirectional transmission and SFIR. For SFIR (and SDMA) bursts, an antenna pattern has to be calculated that optimizes the transmission to the (set of) station(s). If the channel has not changed since the last transmission, the previously used pattern can be applied.

In order to fasten the PHY processing, the MAC could signal the identifiers of concurrent SSs for each SDMA burst. Although, the TXVECTOR already contains this information, it might be beneficial, if the PHY does not need to search through all bursts looking for concurrent transmissions. A set of identifiers could be provided for each SDMA burst.

The RXVECTOR describes the UL subframe. It provides information for demodulation and decoding of received UL bursts. Its content equals the UL-MAP, thus it includes the burst duration, the start time, the MCS, the address of the SS, and a bit to indicate the optional midamble (refer to Section 3.3.2.3). This information allows for SDMA reception.

In order to control the smart antenna, the type of reception (omnidirectional, SFIR, or SDMA) needs to be indicated by the RXVECTOR. Like the TXVECTOR, the RXVECTOR might include the identifiers of simultaneously transmitting SSs to fasten the PHY processing.

4.3 MAC Protocol Enhancements to IEEE 802.16

The MAC protocol of IEEE 802.16 coordinates the access to the wireless medium and provides the basis for the communication between peer MAC entities. By means of MAC management messages the protocol allows remote stations to exchange management related data. These messages are standardized so that multi-vendor equipment can be operated.
SDMA operation affects the MAC protocol only with regards to the MAC frame control: the schedule of the DL and the UL subframe becomes two-dimensional, i.e, resources are now scheduled in time and additionally in space dimensions. The original standard MAC protocol was only able to communicate a one-dimensional schedule. All other features of the protocol, e.g., measurement reports, network entry, or connection management are not affected by the adaptive SDMA concept presented in this chapter. Hence, they do not need to be modified. The new features to control SDMA operation are meanwhile contained in the standard based on a contribution by the author [Hoymann and Piggin, 2004].

4.3.1 History of SDMA Support in IEEE 802.16a-2003

The first version of the IEEE 802.16a MAC frame for OFDM was not designed to support SDMA techniques [Hoymann, 2006; Hoymann et al., 2003]. Figure 4.10 illustrates how the IEEE 802.16a-2003 MAC management messages for frame control could be leveraged to allow for SDMA transmission at least in DL direction. Different antenna patterns, which are drawn above the frame are applied at the BS's antenna array during a particular burst. Inside DL burst 1, the DL- and the UL-MAP is highlighted. The arrows coming out of the MAPs show the timing information which is included in the MAPs, i.e., start time in the DL-MAP and burst duration in the UL-MAP [IEEE, 2003b].
As indicated by the antenna pattern, the first part of the frame (preamble, FCH and DL burst 1) is sent omnidirectionally because all SSs need to keep track of the broadcast information (DLFP, MAPs). At the beginning of DL burst 2 the antenna characteristic is adapted. Thus, the BS can send one data stream containing DL burst 2a in the direction of a SS while a different data stream containing DL burst 2b is sent in the direction of another SS. The number of data streams is only limited by the capability of the antenna array to form beams which sufficiently separate the different signals. Due to

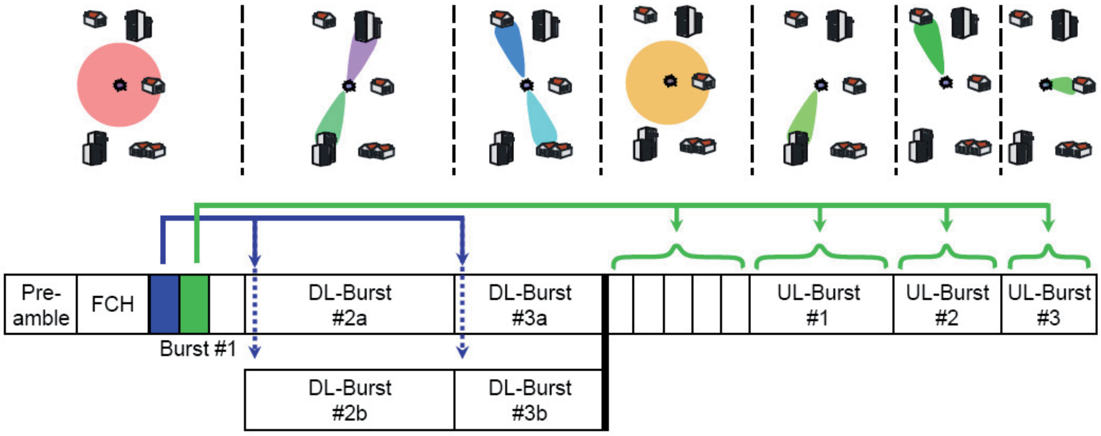

Figure 4.10: SDMA support of IEEE 802.16a-2003

the content of the DL MAP IE, parallel transmissions are restricted to have the same start time, the same MCS, and the same burst duration. After DL burst 2 the antenna pattern changes again. Within DL burst 3 other SSs are served. The BS sends individual data streams, i.e., DL burst 3a and 3b to the corresponding SSs simultaneously.

The UL subframe starts with contention slots. During this phase the BS antenna array has to receive omnidirectionally. After the contention slots, dedicated UL transmission bursts are following. In IEEE 802.16a-2003 the UL MAP IE only contains the burst duration as time information. The start time is calculated as the addition of all durations of preceding bursts. This behavior leads to a succession of UL transmission bursts. There is no way to communicate a simultaneous transmission of different SSs. However, the BS antenna array can be used to increase the receiver SINR by optimizing the antenna pattern.

Summing up, a simultaneous transmission of data is only possible in DL direction. Start times, durations and MCSs of simultaneously transmitted bursts must be equal. In UL direction a concurrent reception of data is not possible [Hoymann, 2006; Hoymann et al., 2003].

4.3.2 MAC Frame Control for SDMA

The first MAC management message that specifies the following DL subframe is the DLFP, which is transmitted in the FCH. In order to specify up to four bursts, the DLFP IE contains the start time and the MCS. The DL MAP

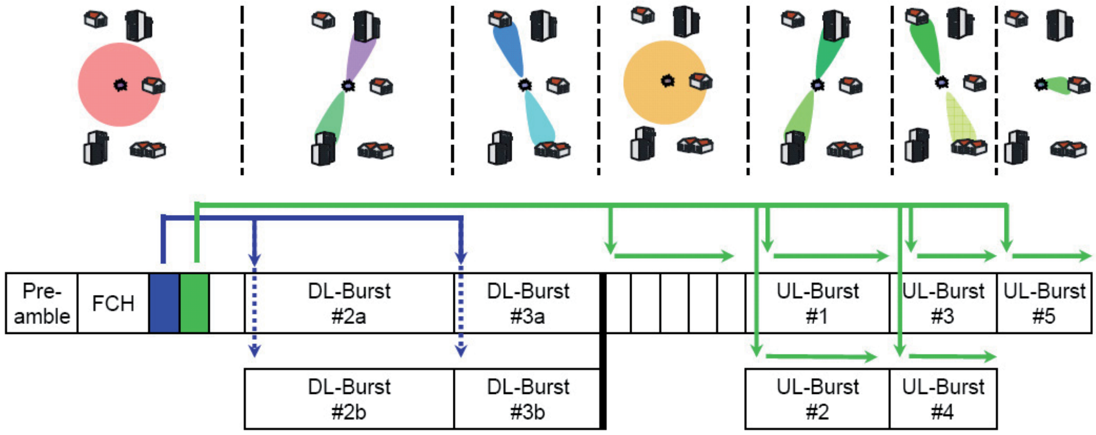

Figure 4.11: SDMA support of IEEE 802.16-2004 using basic DL MAP IEs

in the very first burst determines the remaining DL subframe (for details refer to Section 3.3.2.3). The basic DL-MAP IE contains the start time only and no burst duration. Regarding the control of concurrent DL bursts, the DLFP and the DL MAP IEs restrict SDMA transmissions like the former standard IEEE 802.16a-2003.

Figure 4.11 shows the enhanced MAC frame developed in this work [Hoymann, 2006]. The control and management elements of the frame, the DL preamble, the FCH and DL burst 1, are still sent omnidirectionally as indicated by the antenna pattern shown in the pictogram above the frame structure. The restrictions mentioned for the DL subframe are still valid.

Compared to IEEE 802.16a-2003, the UL MAP IE has been enhanced to include the bursts' start times as specified in IEEE 802.16-2004. Besides the duration and the CID, the start time of a burst enables the BS to schedule UL bursts concurrently. By giving the start time explicitly, SSs do not need to calculate it. Thus, the UL subframe does not rely on a sequential structure. It can now be signaled by the BS that SSs transmit simultaneously, separated in space. This is indicated by the arrows shown above the frame pointing from the UL-MAP to the corresponding UL burst.

Additional to the mandatory preambles appended to each UL burst, midambles might be included in the UL burst on a periodic basis. Together with the UL preamble the midambles allow for an advanced joint detection of SSs by the BS during the UL subframe. In order to differentiate between simultaneously transmitted pre-/midambles coming from different SSs they might be shifted cyclically. Each SS generate unique pre-/midambles to

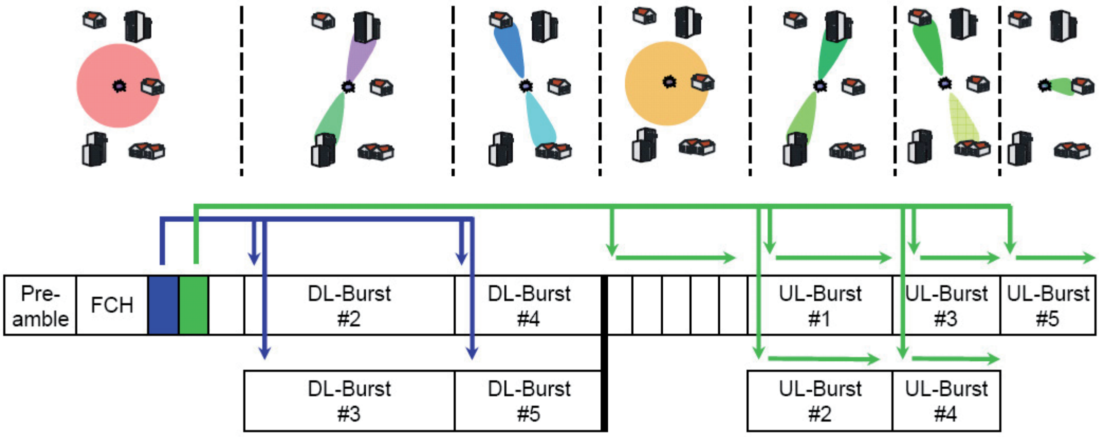

Figure 4.12: SDMA support of IEEE 802.16-2004 using concurrent transmission DL MAP IEs

improve the capability of the BS to jointly detect simultaneous bursts.
In order to extend the system range, especially during the broadcast phase, the robust modulation BPSK in conjunction with code rate $1/2$ has been introduced. This new MCS is mandatory for basic control elements and tries to overcome the difference in range between omnidirectional broadcast and adaptive directional unicast transmissions.

4.3.2.1 Extended DL MAP Concurrent Transmission IE Format

In order to enable a fully flexible DL transmission of simultaneous bursts, the DL MAP IE has to be extended. The possibility to use the extended "DL-MAP concurrent transmission IE format" has been included during the revision of the standard [Hoymann and Piggin, 2004]. The extension allows specifying the duration of the corresponding DL burst explicitly.
The first part of the frame, the DL preamble, the FCH and the burst 1, is again sent omnidirectionally. In Figure 4.12 the enhanced MAC frame can be seen. The DL-MAP included in DL burst 1 is now specifying the start time as well as the addressee, i.e., the CID, of each DL burst. By extending the DL-MAP IE with the IE for concurrent transmission, the burst duration can be specified additionally. This is indicated by the arrows shown above the frame. Now, the duration of DL bursts transmitted in parallel and even their MCSs might be different.
Optionally, a short preamble should be appended to the DL burst additionally to the long preamble at the beginning of the DL subframe. This short

preamble is used by the SSs for channel estimation and synchronization purposes. The antenna pattern of the BS's transmit antenna array is different for broadcast and unicast transmissions. The SS's channel estimation during the broadcast phase cannot be used to equalize the signal during unicast transmissions. Furthermore, the optional short preambles might be cyclically shifted so that concurrent preambles can be differentiated by the receiving SS.

4.4 SDMA Scheduling

TDMA systems can arbitrarily assign different SSs to different time slots because time slots are orthogonal as they do not overlap. Usually they are even separated by guard times. Thus, mutual interference for SSs assigned to distinct TDMA slots can be ruled out. The dimension time can be considered as being nearly perfectly orthogonal. Using other multiple access schemes, such as Frequency Division Multiple Access (FDMA) or Code Division Multiple Access (CDMA), SSs are scheduled onto different frequency (sub-) bands or orthogonal spreading codes are assigned to different SSs. Thus, channel assignments in the frequency or code domain can be considered nearly orthogonal, too.
For the spatial dimension, the picture is different. Even though the number of antenna elements limits the spatial dimension, modeling TDMA-SDMA resources as a two-dimensional cube with orthogonal access is not suitable. SSs cannot be arbitrarily scheduled for parallel SDMA transmissions at the same time because their spatial separability by the beamforming antenna array depends on their relative spatial positions.
To overcome this problem, a hierarchical scheduling approach is introduced in the following that first computes a spatial grouping of SSs that can be well separated by the BS's beamforming antenna. The result of this grouping is a set of spatial groups of SSs. SSs of the same group can be separated and thus be served at the same time. SSs from different groups are not spatially separable so that SSs of different groups have to be separated in the time domain. Consequently, the spatial groups are scheduled using conventional scheduling methods.
The separation of the scheduling process into two hierarchical stages, additionally adds flexibility and simplicity to the scheduling process. The grouping process is independent from the TDMA scheduling and vice versa.

Thus, spatial grouping and group scheduling procedures can be combined and interchanged freely in accordance with the specific needs of the target system.
The approach to build spatial groups of SSs has also been proposed in previous publications. Vornefeld and others were the first to propose groupings of SSs to establish "spatially compatible groups" taking their QoS requirements into account [Vornefeld, 2000]. Fuchs et al. proposes a grouping algorithm for multi-user MIMO systems, which also computes groups that are served in different time or frequency slots [Fuchs et al., 2005]. The first approach of a hierarchical grouping and scheduling algorithm for an SDMA enhanced IEEE 802.16 systems has been presented in [Hoymann et al., 2006b]. The first part of the hierarchical scheduling process, i.e., the spatial grouping was detailed in [Hoymann et al., 2007]. Different grouping strategies are outlined and their computational complexity is analyzed. A system level performance evaluation of an SDMA-enabled cellular IEEE 802.16 system that employs the presented tree-based spatial grouping algorithm together with proportional fair scheduling in the time domain can be found in [Pabst et al., 2007].
The authors of [Shad et al., 2001] propose to construct intelligent space-time frames under the constraint of requiring a minimum SINR for each user, which implicitly leads to a grouping of SSs for parallel transmission in one time slot, too. The impact of beamforming capable antennas on channel allocation at the MAC layer is examined in [Koutsopoulos et al., 2003]. TDMA, CDMA, and OFDMA medium access schemes are discussed and greedy heuristics are used to assign SSs to spatial channels. Yin and Liu improve a greedy scheduling strategy introduced in [Shad et al., 2001] to also take several QoS parameters into account [Yin and Liu, 2002]. An overview of the state of the art in this field is given in [Bartolomé Calvo, 2004].

4.4.1 Spatial Grouping

As introduced above, the first step in the combined TDMA-SDMA scheduling process is a spatial grouping process that partitions the set of SSs into groups of SSs. The SSs of a group are well separable by the beamforming antenna and can therefore be co-scheduled for the same TDMA resource. This section first defines the characteristics of such a grouping. Second a metric to compare the performance of different groupings is introduced. Finally, the grouping algorithms are presented and their performance and runtime complexities are discussed.

4.4.1.1 Definition of a Spatial Grouping

In mathematical terms, a spatial grouping is a partition $\mathcal{P} = \{G_1, G_2 ...\}$ of the set of all SSs U. Every SS $u_i \in U$ belongs to exactly one spatial group $G_j \subseteq U$. A combination of groups has to fulfill the two conditions defining a partition:

1. all groups have to be mutually exclusive, i.e., no SS can be in more than one group
2. the groups have to be collectively exhaustive, i.e., every SS from the set of all SSs has to be covered by a group

In a scheduler, not every possible partition is allowed as a valid grouping. On the one hand, the smart antenna system supports only a limited number of concurrent beamforming transmissions. If the maximum number of supported beams is denoted by k, only partitions $\mathcal{P}$ whose subsets G_j have cardinalities that are limited by k, i.e., $|G_j| \leq k \quad \forall G_j \in \mathcal{P}$ are allowed. On the other hand, a partition is invalid if it leaves a SS unserved. This might occur when SSs that are not well separable are grouped together. In this case, the mutual interference might become such high that one or several SSs perceive an SINR that is not sufficient for successful decoding. Considering such a grouping would contradict the objective to achieve high system throughput while serving all SSs.

4.4.1.2 A Performance Metric for Spatial Groupings

In order to be able to compare different groupings and to choose "the best" grouping, a metric that assigns a quantitative value to a grouping is necessary. In the end, utilizing SDMA should increase the system throughput compared to the non-SDMA, i.e., the TDMA case. Therefore, a metric should use the achievable throughput capacity (gain) relative to the non-SDMA case as the central performance measure.
Grouping SSs into one group that fits into a TDMA slot, which would otherwise be occupied by only a single SS, seems to increase the possible throughput in that time slot. However, the grouping comes at a cost: As explained before, the SSs' SINR will suffer when they are co-scheduled with other group members. Depending on the decrease in SINR and the link

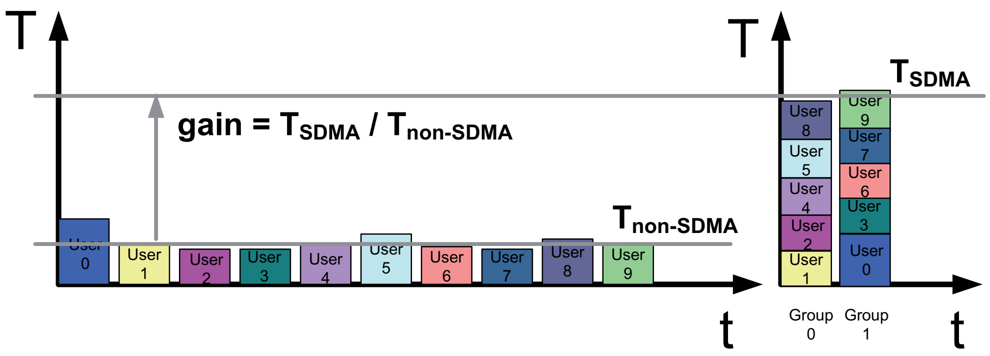

Figure 4.13: Example SDMA throughput (T) gain realized by grouping 10 SSs into 2 groups

adaptation of the specific system, a reduced SINR value might lead to a lower data rate for the SS.

The proposed grouping metric considers both effects. Equation (4.35) defines the throughput gain of a spatial grouping

$$gain = \frac{\sum_{i=1}^{n} Throughput_{SDMA}(u_i)}{\sum_{i=1}^{n} Throughput_{NON-SDMA}(u_i)} \frac{|U|}{|\mathcal{P}|} \tag{4.35}$$

that might be lower than 1.0. The gain is the ratio between the number of SSs $|U| = n$ and the number of groups $|\mathcal{P}|$ in a grouping $\mathcal{P}$ where instead of $|U| = n$ only $|\mathcal{P}|$ time slots are needed to carry the traffic of a saturated system. Figure 4.13 shows an exemplary grouping of 10 SSs into 2 groups. Even though some groups experience slightly lower throughput rates ($T_{SDMA} \leq T_{NON-SDMA}$), a gain appears possible to be achieved because only 2 instead of 10 time slots are needed to carry the same amount of data.

4.4.1.3 NP-Hardness of Optimal Grouping

The NP-completeness of the problem to allocate SSs to time slots such that the total frame capacity is maximized is shown in [Shad et al., 2001]. SSs allocated to the same time slot form what is called a spatial group in this thesis. The number of co-scheduled SSs is limited by a number k of possible parallel beams. Shad et al. require that SSs need to reach a minimum SINR threshold to be served successfully. To prove the NP-hardness of the grouping problem, they provide a polynomial time reduction of the well-known NP-complete problem to find a *minimum graph coloring* to the

optimal slot allocation problem. Another proof for the NP-completeness of the optimal grouping problem is given in [Zhang, 2002].
The NP-completeness of the optimal grouping problem means that most probably (unless $P = NP$ holds, which is strongly disbelieved by most computer scientists) there cannot be an efficient deterministic algorithm that would find an optimal solution in polynomially bounded time. This motivates the use of heuristics to find a close-to-optimal solution in polynomial time. Before such heuristics are presented in Sections 4.4.2.2 and 4.4.2.3, the complexity of the spatial grouping is discussed.

Complexity analysis of spatial groups candidate set size

This section examines how many different groups of co-scheduled SSs G_i exist and how many different partitions $\mathcal{P}$ could be constructed therefrom. n SSs are assumed to be grouped into different spatial groups (subsets), each comprising a maximum of k SSs. Then, there are $\sum_{i=1}^{k} \binom{n}{i}$ possible groups of up to k SSs because $\binom{n}{i}$ is the number of distinct i-element subsets of an n-element set. Unfortunately, there is no closed form for this sum [Graham et al., 1994, p. 165] so its asymptotic growth is studied.
Even though there is no closed form for the partial sum ($\leq k$ SSs per group), the solution for the sum of all $0...n$ element subsets is known to be $\sum_{i=0}^{n} \binom{n}{i} = 2^n$. This is a first upper bound for the number of possible groups. Since exponential growth with n is not satisfying, the binomial coefficient $\binom{n}{i}$ is bounded more tightly [Cormen et al., 1990, p. 102]:

$$\left(\frac{n}{i}\right)^i \leq \binom{n}{i} \leq \left(\frac{en}{i}\right)^i \tag{4.36}$$

As only the asymptotic behavior for $n \to \infty$ is interesting, only the biggest term of the partial sum is considered. It is reasonable to assume that k is fixed because the number of parallel transmissions is limited by the number of antenna elements at the BS. This number is usually smaller than the number of possible SSs in a cell. Therefore, in the following k is assumed to be fixed and small compared to n.
Assuming fixed k and $n > 2k$, the biggest term of the partial sum is $\binom{n}{k}$ which is bounded using Eq. (4.36)

$$\left(\frac{n}{k}\right)^k \leq \binom{n}{k} \leq \left(\frac{en}{k}\right)^k \tag{4.37}$$

Table 4.1: Candidate set size $\sum_{i=1}^{k} \binom{n}{i}$ for different values of n and k

	n=								
k	5	8	10	12	15	20	25	50	100
1	5	8	10	12	15	20	25	50	100
2	15	36	55	78	120	210	325	1,275	5,050
3	25	92	175	298	575	1,350	2,625	20,875	166,750
4	30	162	385	793	1,940	6,195	15,275	251,175	4,087,975
5	31	218	637	1,585	4,943	21,699	68,405	2,369,935	79,375,495
6	31	246	847	2,509	9,948	60,459	245,505	18,260,635	1,271,427,895

This gives, up to a constant factor, both a lower and an upper bound for the asymptotic growth of the number of possible groups when n is variable and k is fixed. Using the common notation [Cormen et al., 1990], it was thus shown that the function describing the number of possible groups is in $O(n^k)$.
Table 4.1 shows how the number of possible groups grows with an increasing number of SSs n for fixed values of k. A simulator would have to invert the antenna array correlation matrix for each group of SSs once in order to calculate the SINRs of every group member. This matrix inversion is a very complex operation. Table 4.1 gives an impression how the runtime of algorithms that generate all possible groups will evolve with (n,k).
According to what is said in Section 4.4.1.1, the number of valid spatial groups might be considerably smaller than the number of subsets with up to k elements because for SDMA grouping purposes, groups that create so much interference that one group member cannot be served, are discarded. Thus, in the following it is assumed that the number of candidate groups is only bounded from above, i.e., that it is in $O(n^k)$.

4.4.2 Grouping Algorithms and their Complexity

Four different grouping algorithms have been evaluated based on its implementations in the WiMAX MAC Layer (WiMAC) simulator (see Section 7.2). In the following, each of the four grouping algorithms is presented and the respective complexity is discussed. Then, their performance is compared by means of the grouping gain, Eq.(4.35). An outlook presenting adaptive grouping algorithms for real mobile communication systems concludes this section.

4.4.2.1 Optimal Grouper

The optimal grouper finds the best grouping with an exhaustive search. In the *first* step, it generates all possible candidate groups, i.e., all subsets G_j of the n-element SS set U. For each group the SINRs of all SSs are estimated, mapped to throughput rates, and the throughput rates are summed up to a group total. Groups that leave some SSs unserved are discarded.
In the *second* step, the optimal grouper enumerates all possible combinations of these candidate groups that would form a valid partition (grouping) according to Section 4.4.1.1. Note that a partition is only valid if all SSs can achieve an SINR threshold that allows data transmission. An exhaustive search of all group combinations that would form a valid partition of the set of all SSs is performed.
For every valid partition, the grouping gain as described in Eq. (4.35) is calculated and compared to the best grouping found so far. Finally, the best grouping is returned as the result of the optimal grouper.

Complexity Analysis

In the first step, SINR calculations for all groups, which are in ($O(n^k)$), have to be performed. Then, all possible partitions consisting of these groups have to be evaluated to find the optimal solution. If no groups from the candidate set of groups are removed then the number of partitions is exactly the number of possible set partitions of an n-element set into subsets of size $\leq k$ which is denoted by $G(n,k)$. Usually, some groups are so unfortunate that at least one SS does not reach the SINR threshold so that these groups are removed from the candidate set. Thus, the total number of set partitions $G(n,k)$ serves as an upper bound for the number of possible groupings.
The explosive growth of the total number of such set partitions can be seen in table 4.2 where the number of set partitions with subset sizes $\leq k$ is shown for different values of n. The non-italic entries in this table were generated by the optimal grouper algorithm as it is implemented in the WiMAC simulator. The removal of invalid groups was temporally switched off to obtain the theoretical number of such set partitions. The *italic* entries are either taken from integer sequence tables or are calculated using the exponential generating function given below. The On-Line Encyclopedia of Integer Sequences (OEIS) contains the sequences for $k = 2$, 3, and 4 as entries *A000085*, *A0001680*, and *A0001681*, respectively [Sloane, 2006].

Table 4.2: Number of possible set partitions of an n-element set into subsets of size $\leq k$. All numbers calculated by optimal grouper module, except those in *italics*, which are taken from sequence tables or are computed [Sloane, 2006].

	$n=$											
k	1	2	3	4	5	6	7	8	9	10	11	12
2	1	2	4	10	26	76	232	764	2,620	9,496	35,696	140,152
3	1	2	5	14	46	166	652	2,780	12,644	61,136	312,676	*1,680,592*
4	1	2	5	15	51	196	827	3,795	18,755	99,146	556,711	*3,305,017*
5	1	2	5	15	52	202	869	4,075	20,645	112,124	648,649	*3,976,633*
6	*1*	2	5	15	52	203	876	4,131	21,065	115,274	672,673	*4,163,743*

As we can see in Table 4.2, the number of possible partitions grows rapidly with an increasing number of SSs n. With a growing group size limit k, the number of partitions also grows but at a much slower pace. A current standard PC is only able to generate in the order of 1,000,000 partitions in a few minutes. This runtime complexity disqualifies the optimal grouper from being used in a real system where grouping decisions have to be made in milliseconds. Nevertheless, the results obtained by the optimal grouper are a valuable bound for the grouping performance reached by other grouping algorithms we study in the following.

The entry for the sequence $G(n{,}3)$ (*A0001680*) in the OEIS references a paper [Mansour, 2002] that proves the general Exponential Generating Function (e.g.f.) for the integer sequences $G(n{,}k)$.

$$\text{e.g.f.}: \sum_{n=0}^{\infty} G(n{,}k)\frac{x^n}{n!} = e^{\left(\sum_{i=1}^{k} x^i/i!\right)} \tag{4.38}$$

This exponential generating function correctly describes the number of partitions to be evaluated by the optimal grouper if no group is removed from the candidate set because one of its members would fail to meet the SINR threshold. To calculate the actual numbers from Eq. (4.38), a computer algebra tool like, e.g., *PARI/GP* function can be used [pari/gp].

By applying methods from [Odlyzko, 1995] an asymptotic bound for $G(n{,}k)$ with $n \to \infty$ can be derived from the e.g.f., see Eq. (4.38). However, a loose upper bound is also given by the *Bell numbers* $B(n)$ that describe the total number of set partitions of an n-element set into subsets of any size. Thus, $B(n)$ might also include partitions with groups of size larger than k and is therefore too big: $G(n{,}k) \leq B(n)$. Figure 4.14 shows that for the partition

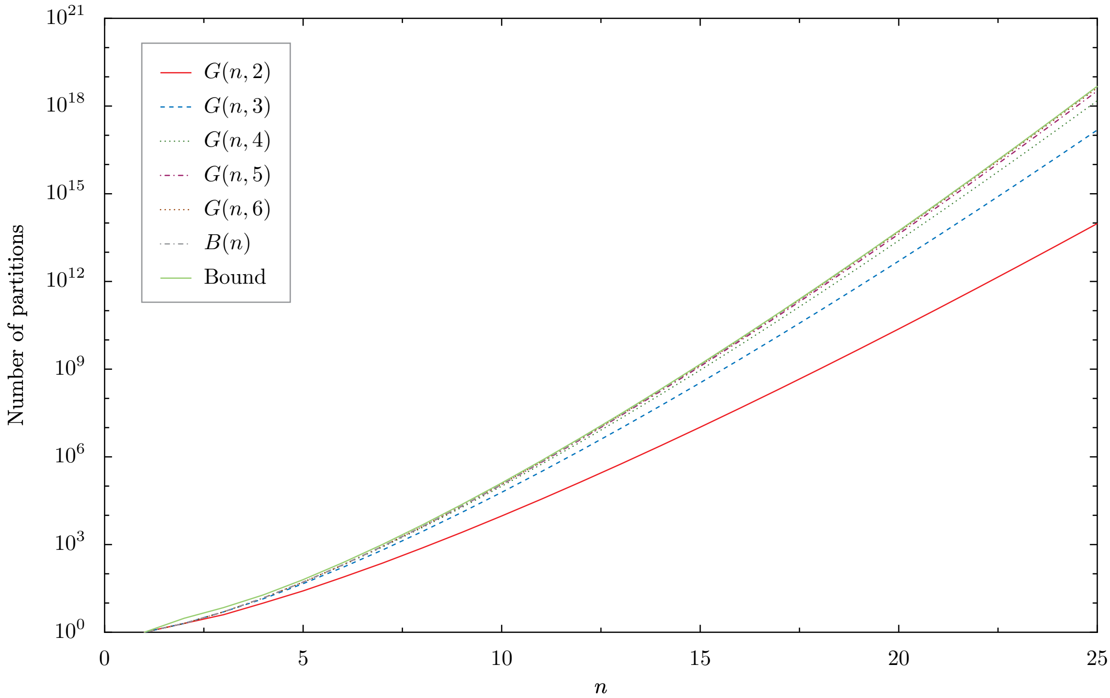

Figure 4.14: Growth of partition functions, *Bell numbers*, and bounding function

functions $G(n{,}k)$ with $k > 3$ this approximation fits well. An e.g.f. for the *Bell numbers* is given by [Odlyzko, 1995]:

$$\sum_{n=0}^{\infty} B(n)\frac{x^n}{n!} = e^{(e^x-1)} \tag{4.39}$$

As expected, for $k = n$ and $n \to \infty$ the e.g.f. for the number $G(n{,}k)$ of set partitions with limited subset sizes converges to the e.g.f. for the *Bell numbers*. This can be seen from the exponential generating functions given in Eq. (4.38) and (4.39), when considering the definition of the exponential function e^x as a power series:

$$e^x = \sum_{i=0}^{\infty} \frac{x^i}{i!}$$

According to [Graham et al., 1994] the *Bell numbers* $B(n)$ are asymptotically equal to the following exponential function:

$$\frac{m(n)^n e^{m(n)-n-1/2}}{\sqrt{\ln(n)}} \quad \text{with} \;\; m(n)\ln\left(m(n)\right) = n - \frac{1}{2} \tag{4.40}$$

where $m(n)$ is defined implicitly as given above. For values of $n = 1...25$ this function was evaluated and plotted together with the exact *Bell numbers*, as derived from the e.g.f., see Eq. (4.39). The resulting graphs and those of the partition function $G(n,k)$ for $k = 2...6$ are shown in Figure 4.14, which visualizes the super-exponential growth of possible partitions $G(n,k)$ with growing n. The implemented optimal grouper can enumerate all $G(10,4)$ groupings (with groups limited to 4 members) in a few seconds, which means that enumerating all $G(12,4)$ 12-SS groupings is a matter of minutes. But for SS sets with more than 15 SSs the optimal grouper would have to work for days. Clearly, this renders its use impossible in real life systems. Even as a benchmark for the performance of other grouping algorithms it is only useful for SS sets with ≤ 15 SSs.

4.4.2.2 Greedy Grouper

The greedy grouper is a grouping heuristic. It does not strive to find the optimal solution but tries to find a close-to-optimal solution by applying a simple criterion.

Similar to the optimal grouper introduced in the previous section, the greedy grouper also generates the whole candidate set of spatial groups in a first step. Section 4.4.1.3 shows that $O(n^k)$ SINR estimations have to be conducted. In a second step the algorithm sorts the candidate set of spatial groups G_1,...,G_m by decreasing group throughput. That is, the group that provides the highest throughput will become G_1 whereas group G_m will experience the lowest throughput total.

Then the greedy property of the algorithm comes into play: starting with an empty grouping, the algorithm successively adds the next compatible candidate group in the order of decreasing group throughput until a complete grouping has been constructed. By definition of a spatial grouping, see Section 4.4.1.1, a group may only be added if none of its members is already included in one of the previously selected groups.

Taking the highest group throughput as the criterion to choose the next group is motivated by the objective to achieve a high average throughput per group in the final grouping. In most cases the greedy grouper will not find the optimal solution. An example case of a 9-SS set that is to be grouped into groups with maximum 4 SSs each shows the potential drawback. A greedy algorithm would probably first choose two 4-SS groups and would then select the remaining SS in a third group. An optimal grouper might also select three groups but might go for three 3-SS groups. Grouping 4 SSs into one group will usually hurt their SINRs more than grouping 3 SSs into one group but this negative impact might still allow a 4-SS group to obtain more total throughput than a 3-SS group. Therefore, 4-SS groups can have higher throughputs than 3-SS groups but a single SS group would offset this advantage and make the greedy group average worse. Thus, with the same number of groups – and that means with the same number of TDMA slots – the greedy grouper would realize a sub-optimal grouping gain. In Section 4.4.3.2 the performance of the different grouping algorithms in terms of achievable grouping gain will be evaluated.

Complexity Analysis

The greedy grouper conducts SINR estimations for the entire candidate set size whose cardinality is in $O(n^k)$ (see Section 4.4.1.3).
The partitioning complexity of the greedy grouper is in

$$O(n^k \log(n^k)) = O(n^k \, k \log(n)) = O(n^k \log(n)) \tag{4.41}$$

because it has to sort the candidate set whose cardinality is in $O(n^k)$. In general, sorting algorithms need $O(m \log(m))$ in the worst case to sort m values.
In practice though, the SINR estimations conducted when constructing the candidate set need much more (floating point) operations than the sorting of the candidate groups. So unless n becomes very large, the SINR estimations in the first step of operation are the performance bottleneck of the greedy grouper.
The complexity of the greedy grouper, see Eq. (4.41), is a big improvement over the super-exponential growth of the optimal grouper. But it still has to perform $O(n^k)$ SINR estimations when constructing the candidate set of all spatial groups.

4.4.2.3 Tree-Based Grouping Heuristics

The tree-based grouper presented in this section reduces the computational complexity of the greedy grouper. It will be shown that only $O(n^3)$ SINR estimations, regardless of the group size limit k, are needed. The tree-based grouper is therefore much faster for $k \geq 4$ while achieving a similar or even slightly better grouping performance (see Section 4.4.3.2).
This tree-based algorithm was originally proposed by *Fuchs, Del Galdo and Haardt* [Fuchs et al., 2005]. In contrast to the original paper different metrics are applied in the following. The reason is that the authors of [Fuchs et al., 2005] assume perfect channel knowledge in the form of channel transfer function matrices of the wireless multi-user MIMO system. Since this information is not available in the MAC layer, the metrics used in the following are based on more abstract measures, such as the grouping gain metric introduced in Eq. (4.35).
Two main improvements contribute to the efficiency of this algorithm. The first stems from limiting the number of SINR estimations. The optimal and greedy groupers must calculate SINRs of all $O(n^k)$ possible spatial groups. As shown below, the tree-based grouper only needs to calculate $O(n^3)$ group SINR values regardless of the group size limit k. The second improvement is obtained by limiting the number of groupings that are evaluated. To find a good grouping more than one is evaluated (as the greedy grouper does) but significantly less than the super-exponentially growing number of groupings that the optimal grouper considers.
The tree-based grouping algorithm constructs its groupings as levels of a tree. It starts with a grouping that serves each SS in its own group. This trivial grouping forms the first level of the tree. From there, the algorithm builds higher levels by joining two groups. The criterion to select the two groups can be chosen arbitrarily in the form of a utility function that reflects how much the grouping can benefit from merging two groups. If this utility function is simply the evaluation of the new group's SINRs then the grouping algorithm can determine an accurate estimate of the achieved gain by mapping the SINRs to throughputs. But it is also possible to use other utility functions that do not perform SINR calculations. A utility function that is based on the DoA azimuth angles of the group members is exemplarily given at the end of this subsection. For the remainder of this subsection, an SINR based utility function is assumed.
Figure 4.15 shows an example tree that groups a set of five SSs $U =$

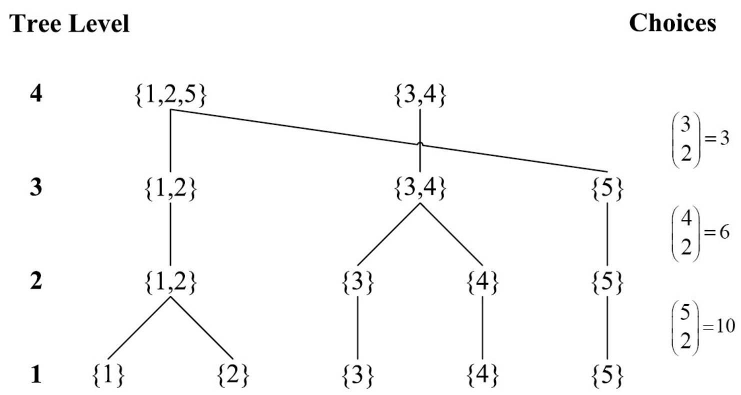

Figure 4.15: Tree-based grouping of a 5-SS set into groups ≤ 3 [Fuchs et al., 2005]

{1,2,3,4,5}. On the lowest level (tree level 1), all SSs form separate groups. Then, all $\binom{5}{2}$ combinations to join two groups are evaluated and the union with the highest utility is chosen, {1,2} in this example. The resulting grouping forms level 2. At this level, $\binom{4}{2}$ choices are possible and SSs 3 and 4 are joined next. Finally, from level 3 to level 4 only three choices remain and the union {1,2,5} delivering the highest utility is chosen. The grouping ends here because the group size limit is three and no more groups could be joined to form a valid grouping.

As a last step, all groupings corresponding to the tree levels are evaluated and the grouping with the highest grouping gain as defined in Eq. (4.35) is chosen. If the utility function does not directly rely on an SINR estimation, from which a total group throughput could be computed, SINR values for all groupings have to be computed first.

Complexity Analysis

This section examines how often the utility function has to calculate the gain of a candidate group when constructing the tree levels. If the regarded utility function is based on SINR estimations a SINR estimation with its matrix inversion has to be conducted every time the utility is calculated. Thus, the resulting complexity is directly comparable with the complexity of constructing the candidate set (see Section 4.4.1.3) which is a necessary first step when using either the greedy or the optimal grouper.

A tree has at most n levels because starting with the trivial grouping consisting of n groups at the lowest level, two groups get merged when constructing the next-higher level until only one group at the top of the tree

is left. If the number of beams is limited to $k < n$ then the tree has even less levels because before reaching the top it gets impossible to merge two groups due to the group size restriction. For the following upper bound on the number of group-mergers we will assume that the tree has n levels. On the bottom level, two groups from a set of n groups have to be chosen, for which there are exactly $\binom{n}{2}$ possibilities. On the penultimate level, there is only $\binom{2}{2} = 1$ choice to merge the only two remaining groups. Thus, on the way from bottom to top $\sum_{l=2}^{n} \binom{l}{2}$ joinable groups are evaluated by the utility function.
In contrast to the greedy and the optimal grouping algorithms, the tree-based grouper reduces the spatial groups candidate set size and not only the sorting complexity of the SINR estimates.
Using the "upper summation" identity for binomial coefficients [Graham et al., 1994]

$$\sum_{i=0}^{n} \binom{i}{m} = \binom{n+1}{m+1}, \; m,n \in \mathbb{N}$$

Eq. (4.42) can be obtained as a closed form using Eq. (4.37). Thus, the tree-based grouper has complexity $O(n^3)$.

$$\sum_{l=2}^{n} \binom{l}{2} = \binom{n+1}{3} \leq \left(\frac{e\,(n+1)}{3}\right)^3 \tag{4.42}$$

$$= O(n^3) \tag{4.43}$$

$O(n^3)$ is a true upper bound for groupings that are limited to group sizes $k < n$. The number of joins is dominated by the choices on the lower part of the tree whereas near the top there are only few choices. Thus, the simplification to consider trees of height n instead of height $n - \lceil \frac{n}{k} \rceil + 1$ is justified. The tree-based grouper has $O(n^3)$ complexity regarding the number of SINR estimations and therefore performs asymptotically better than both greedy and optimal groupers.
The tree based grouper does not need to partition the different groups, because each level of the tree is already a valid partition according to Section 4.4.1.1. However, the grouper needs to extract the groups with the highest

utility function at each level of the tree. There are at most n tree levels and the lowest level has n entries. So the "partitioning complexity" is bounded by $O(n^2)$ (compare Table 4.3).

DoA-Based Utility Functions

The idea of this utility function is that two SSs can be grouped together if their angular distance as seen from the beamforming antenna is bigger than a certain threshold value α_{th}. The width of the minimum angular distance depends on the width of the antenna's main beam. If the SSs' azimuth angles get too close, the beam towards SS A could hit SS B or, if the beamforming antenna enforces nulls towards co-scheduled SSs, the beams would not intersect but could not be pointed directly towards the SSs any more. Algorithms like ESPRIT, MUSIC or SAGE can extract the DoA estimates from the phase and amplitude differences of the signals received at the different antenna elements [Godara, 1997b; Molisch, 2005].
The utility of grouping SSs A and B together could be defined as follows:

$$utility(SS_A, SS_B) = \begin{cases} 0 & \text{if } |\measuredangle(A,B)| < \alpha_{th} \\ \frac{|\measuredangle(A,B)|}{\alpha_{th}} & \text{else} \end{cases}$$

$\measuredangle(A,B)$ denotes the minimum angle between SS A and SS B be it positive or negative. This utility function avoids the grouping of SSs that are closer than the threshold α_{th} and aims at realizing a maximal angular distance of up to 180°. From this utility function for grouping two individual SSs together, a utility function for joining two groups of SSs can be derived by considering the minimum angle between any SS of the first group and each SS of the second group.
In the context of channel allocation in SDMA systems, a similar utility function (there defined as a cost) is presented in [Hartmann, 2004]. It also takes into account the ratio of the radial distances of the SSs because the beam towards SS A should not only avoid hitting SS B directly but also steer clear from B's local scattering zone around the SS.

4.4.3 Comparison of Grouping Performance and Complexity

This section examines how the grouping algorithms presented above perform with respect to the achievable grouping gain, Eq. (4.35).

The grouping gain is indirectly measured in the system evaluations presented in Chapter 8. There, the grouping gain is responsible for the system throughput increase when parallel transmissions to k SSs is enabled. But in these simulations, many different factors influence the final throughput results. That makes it hard to attribute the resulting gains to the different groupers. Therefore, *Monte Carlo* simulation were conducted where users are randomly placed onto a scenario without considering any traffic or other system dependent parameters. The setup of the *Monte Carlo* simulation is described in the following section and the results are presented thereafter.

4.4.3.1 Setup of Monte Carlo Simulation

Each randomly generated scenario consists of a map area 1000 by 1000 m wide with the beamforming BS in the center. For each scenario snapshot, n SSs are created at map positions that are randomly generated following a uniform distribution. Free space propagation path loss is assumed and the transmit power is chosen in a way that SSs at the corners of the map will receive an SINR that is just sufficient for the most robust MCS (BPSK 1/2) as defined by the standard [IEEE, 2004a]. Link adaptation is applied according to the SINR thresholds of the standard.
In order to model the characteristics of the antenna array, the optimized antenna pattern has to be calculated. The algorithm in use (MVDR) is an optimal beamformer that minimizes the total power while maintaining unity response in look direction which leads to a "nulling" of co-scheduled interferers (refer to Section 4.1.2.3.4).
Figure 4.16 shows an example scenario setup with 10 randomly distributed SSs and a BS with a 9-element Uniform Circular Array at the center. The beam patterns used to transmit in parallel to a 5-SS group $\{1,2,4,5,8\}$ are plotted. The beamforming algorithm's property to place nulls in the direction of co-scheduled SSs is clearly visible. The negative side of placing nulls in the direction of co-scheduled SSs is also visible: the beams towards SSs 1 and 2, respectively, do not fully hit the desired SSs because the beam width is too wide to allow placing a null in the direction of the other SS. Besides minimal intra-cell interference that is caused by not perfectly nulling co-scheduled SSs, this pushing-away effect is the main cause for reduced SINRs when grouping SSs together.

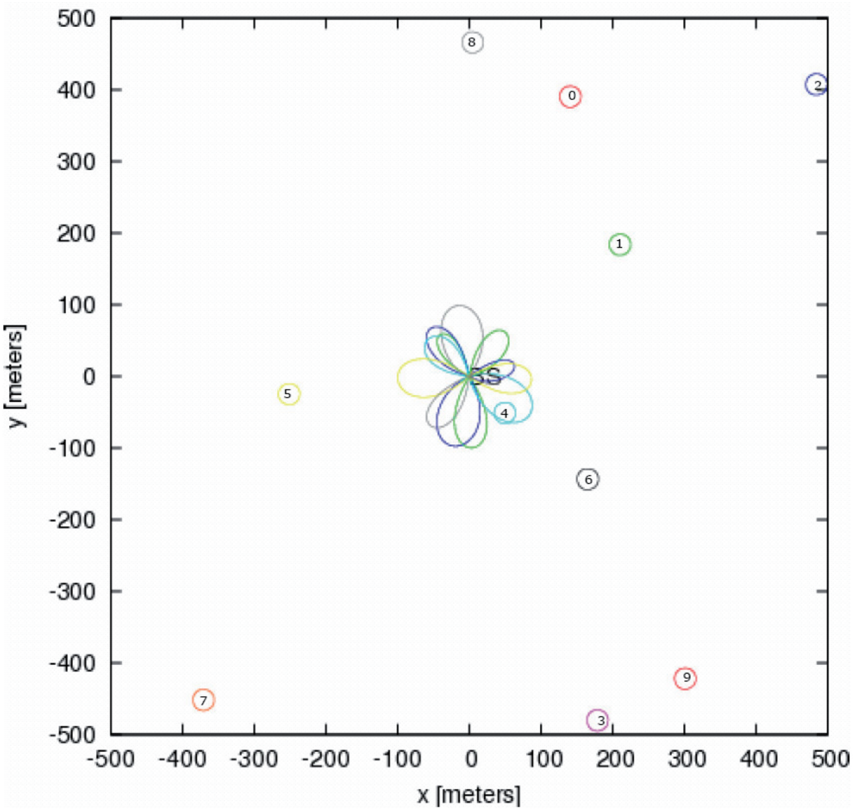

Figure 4.16: Random *Monte Carlo* snapshot: Beamforming antenna with beams for group $G = \{1,2,4,5,8\}$

4.4.3.2 Grouping Performance of the Spatial Groupers

In order to analyze the performance of the implemented grouping algorithms, 5000 snapshots of the above described scenario have been created and have been fed into the spatial grouper implementation. A 9-element UCA is assumed and up to $k = 4$ SSs were allowed per group.
In Figure 4.17 the Complementary Cumulative Distribution Functions (CCDFs) of the achieved grouping gains are plotted. These graphs show the probability that a grouper delivers a grouping gain higher than a certain value for any randomly generated scenario. As the scenario comprises 10 SSs, a minimum of three groups is required to partition the SS set into groups with sizes $\leq k$. Therefore, the maximum gain is $3.\overline{3}$, which is achieved when the grouper has been able to find a grouping of all 10 SSs into three groups so that the mutual interference is so low that all SSs can obtain the same MCS they get when served individually. An SINR that is better than in the non-SDMA case cannot be achieved because the patterns are normalized to the Equivalent Isotropic Radiated Power (EIRP) by adapting the Tx power.
Besides the above introduced groupers (optimal grouper, greedy grouper, and tree-based grouper with the two different utility functions), the distribution function of a random grouper is plotted. This "grouper" is a by-product of the exhaustive search for the optimal grouping and shows which grouping gain could be expected from simply guessing a valid grouping. It therefore marks the lower bound of the expected grouping gain. Note that, the grouping gain of the random grouper almost never drops below the non-SDMA reference gain, i.e., a grouping gain of one. The average gain is 1.81 (see Table 4.3).
The upper bound for the possibly achievable grouping gain is marked by the optimal grouper. As it exhaustively searches the solution space of all valid groupings, no grouper can yield a higher gain. In the *Monte Carlo* scenarios, it yields an average grouping gain of 3.19.
The curves of most interest in Figure 4.17 are those for the heuristics. As Table 4.3 shows, the average grouping gains are almost identical with the tree-based SINR-grouper scoring the highest average of 2.93. This value is only 8% smaller than that of the optimal grouper, whereas the necessary Central Processing Unit (CPU) time is just 2.3% of the total optimal grouper runtime for $n = 10$ SSs.
The graph of the greedy grouper has a striking step near a grouping gain of 2.5. As discussed in Section 4.4.2.2, the greedy grouper selects the high data rate groups first. It often has to add a very small group as the last one.

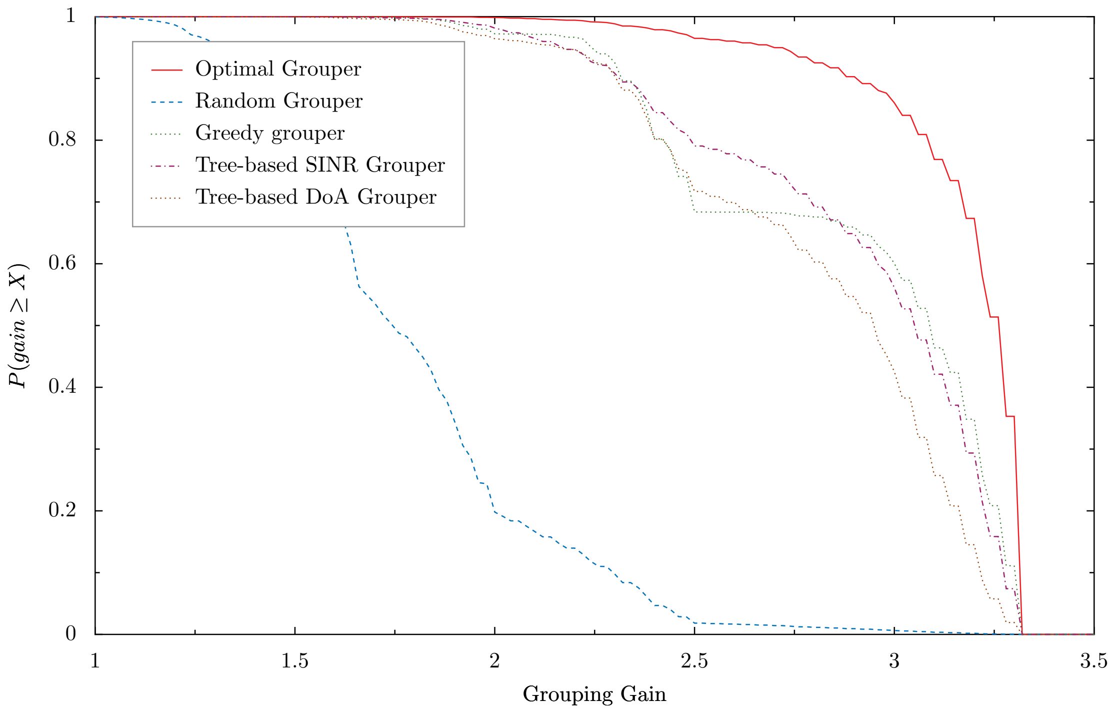

Figure 4.17: CCDFs of grouping gains achieved by different grouping algorithms for 5000 different randomly generated scenario realizations ($n = 10$ SSs, maximum $k = 4$ parallel SSs, 9 antenna elements)

Like this, one additional group may be necessary to cover n SSs with k-sized groups. Here, 10 SSs could be covered by three groups, so that an additional fourth group leads to a grouping gain of 2.5 if the groups themselves are so flawless that all SSs obtain their non-SDMA data rates.
In Table 4.3 the average gains and grouping algorithms runtimes for 5000 snapshots of the 10 and 12 SS scenario are listed. The actual runtimes on a standard PC (Intel Pentium4) for the implementations reflect the algorithmic complexity as discussed before. The optimal grouper's runtime increases rapidly, i.e., super-exponentially, whereas the greedy grouper shows a slightly higher growth rate than the two tree-based algorithms.

4.4.4 Further Reduction of Grouping Runtime

Runtimes even for the tree-based groupers are probably still too long to be conducted every frame in a BS. A grouping mainly depends on the instantaneous channel conditions of the active SSs. If fast-fading is not taken into account or is filtered by working with average SINR values, channel

Table 4.3: Comparison of actual runtimes, gains, and corresponding complexities for different groupers. Basis: 5000 randomly generated scenario snapshots with 10 and 12 SSs and max. k=4 SSs per group

Grouper type	$n = 10$		$n = 12$		Partitioning Complexity	Number of SINR Est.
	Runtime	Avg. Gain	Runtime	Avg. Gain		
Optimal	11,410 s	3.19	559,510 s	3.66	super-exp.	$O(n^k)$
Random	≈ 0 s	1.81	≈ 0 s	1.86	$O(n)$	$O(n)$
Greedy	1,055 s	2.92	2,332 s	3.00	$O(n^k \log(n))$	$O(n^k)$
Tree-based SINR	260 s	2.93	430 s	3.13	$O(n^2)$	$O(n^3)$
Tree-based DoA	77 s	2.83	107 s	2.86	$O(n^2)$	$O(n^3)$

conditions only vary when the SSs are mobile. This causes their SINR values to slowly change over time. Even assuming vehicular speeds, the channel coherence time, during which the channel conditions remains unchanged, is much larger than just a single frame duration, say 10 ms. Thus, a spatial grouping remains valid for a period of time longer than one frame and it is sufficient for the BS to compute it on a larger time scale. What can change on a short time scale though, is the set of active SSs. Especially when the traffic is bursty, SSs may have data to transmit in one frame but not in the next or vice versa. Constructing a grouping of SSs, some of which do not have any more packets to send, leads to a suboptimal grouping. However, the grouping would still be valid. On the contrary, SSs that have not been included in a group but become active before the next grouping takes place, cannot be served before. Their QoS needs may be considered when dimensioning the grouping repetition interval.

For some grouping algorithms, computing a new grouping when a SS enters or leaves the system is not as computationally expensive as computing a new grouping from scratch. For example, the tree-based algorithm introduced first builds the whole tree and then selects the grouping that corresponds to the best tree level. Starting with the previously chosen tree level, the SS can be added as a new group or removed from its group and only the next higher and lower levels are re-built [Fuchs et al., 2005]. This approach assumes that solutions to similar problems can be found with a local search starting in the vicinity of the previous solution. The time necessary to update the grouping can be expected to be much shorter than that needed to re-compute a whole tree.

The most promising approach for a beamforming BS will probably be the exploitation of all knowledge it has, be it a priori knowledge about its environment or knowledge it has learned from past groupings. An example source of a priori knowledge is the deployment concept used for the system. A BS with some fixed SSs may explicitly this knowledge. A grouping can be computed or configured beforehand and the resulting groups will never change. Groups for other mobile SSs will be added to these. Other characteristics of the BS's surroundings that cannot be configured a priori might be learned during operation. For example, actual SINR measurements that are signaled back from SSs can be taken as an input to calibrate future SINR estimations. In addition, user behavior patterns could be derived to find, e.g., all fixed SSs who continuously generate traffic. Thus, their grouping could be pre-calculated as well.

Further improvements of the spatial grouping concept should consider more parameters besides the grouping gain as defined above. If QoS requirements are provided by the SS, the grouper could restrict the solution space by only considering groups where a SS reaches a certain SINR threshold, for example. Or, on the contrary, if the grouper knows that a SS has low SINR demands, it can group more aggressively [Vornefeld et al., 1999].

4.4.5 TDMA Scheduling of Spatial Groups

The previous sections discussed the first step in the proposed scheduling process, i.e., the spatial grouping. This section focuses on the second step, i.e., how these spatial groups are assigned to TDMA slots.

In a packet oriented system, the task of the packet scheduler is to decide into which frame and at which position in a frame a data packet is placed for transmission. The data packets might have varying sizes resulting in varying transmission durations. In general, a frame cannot be completely filled with packets, there is always some capacity left unused. Two closely related optimization goals for the scheduler are first, to minimize the unused capacity of the frame, and second, to select and order packets for transmission such that the throughput capacity of the frame is maximized. These problems are related to the classical *bin packing* problem [Coffman, Jr. et al., 1997], that asks for an assignment of a set of items of varying sizes to a minimal number of fixed-size bins. The bin packing problem is known to be NP-hard. As a scheduling decision has to be found on a frame-by-frame basis, an extensive search for an optimal solution is not feasible and heuristics have

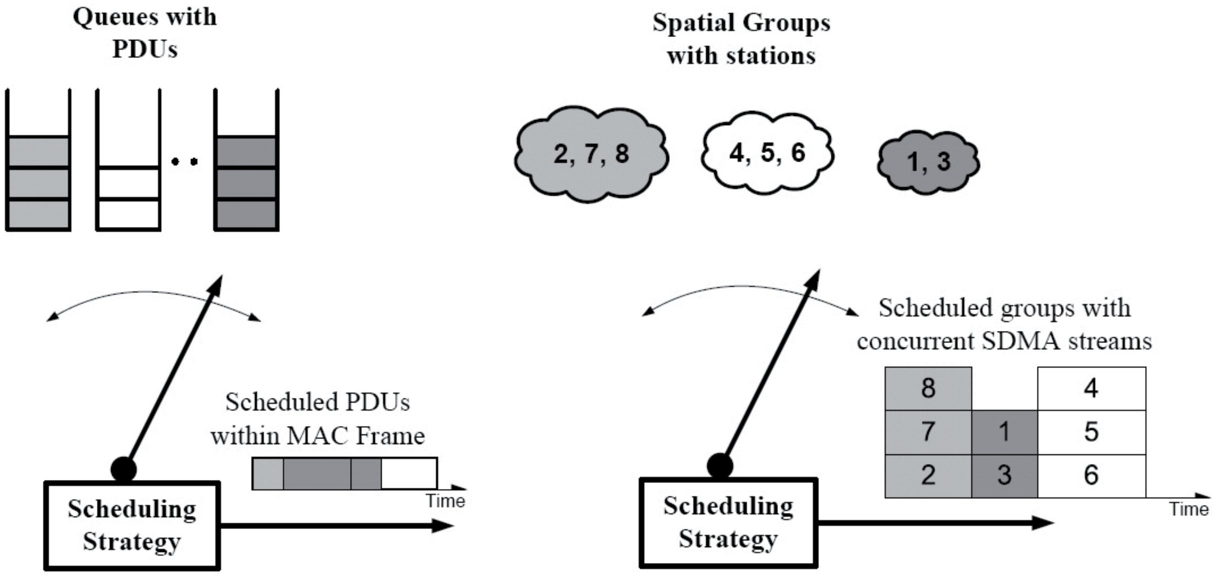

(a) Packet Scheduler **(b)** Group Scheduler

Figure 4.18: Schematic view on classical packet and hierarchical group scheduler

to be applied instead.

Servers in communication networks can be represented by a queueing model as depicted in Figure 4.18a. PDUs arriving from higher layers are classified according to some criterion (destination, data flow, QoS, etc.) in order to append a PDU to the corresponding queue. When the scheduler is ready to schedule packets for the next frame, it retrieves the Head of the Line (HoL) packet from one of the queues. The order in which the queues are emptied depends on the specific scheduling strategy. The strategy can take into account priorities, past data rate experienced by a SS, specific QoS requirements, etc.

Queueing models for trunked communication systems allow scheduling channels in parallel, e.g., as known from the Erlang model [Walke, 2001]. The difference to a model representing spatial multiplexing is that the number of channels in the Erlang model is fixed whilst the number of spatial multiplexing data streams may change over time, see Figure 4.18b. There a group specifies the number of channels provided in parallel.

Wireless scheduling algorithms in addition should take the current condition of the wireless channel into account. The link quality and consequently the error rate and achievable capacity of the wireless channel fluctuate owing to slow/fast fading, shadowing, and varying inter-cell interference levels. Some concepts have been suggested in the literature [Bharghavan et al., 1999; Fattah and Leung, 2002] to adapt wireline scheduling strategies for use in wireless communication systems. Channel-aware scheduler needs an indicator for its SSs' channel states. Furthermore, a wireless scheduling algorithm should fulfill the following requirements [Fattah and Leung, 2002] :

- **Efficient link utilization:** The algorithm should, e.g., not schedule a packet for a currently bad link.
- **Delay bound:** Some applications need guaranteed max. delay.
- **Fairness of opportunities scheduled to SSs/sessions** There should not only be fairness between error-free sessions (short-term fairness) but also between error-free and error-prone sessions.
- **Throughput guarantees:** For error-free sessions the scheduler must be able to always guarantee a certain throughput. For error-prone sessions it has to achieve the desired throughput on a long time scale.
- **Computational complexity:** The scheduling algorithm has to be efficiently implementable to allow for execution on very short time scales, e.g., in IEEE 802.16 a complete frame that lasts between 2 and 20 ms has to be scheduled in that time span.
- **Graceful service degradation:** In cases when the throughput of a sessions has to be reduced, e.g., system overload or when lagging sessions are given the chance to catch up, the degradation should be smooth and not result in an abrupt transmission stop.
- **Isolation:** Ill-behaved sessions, e.g., flooding attempts, should not affect other sessions. They have to be isolated.
- **Energy consumption:** User terminals usually run on batteries so the algorithm should try to conserve their power, e.g., by not requiring too many feedback messages or by scheduling transmissions in a way that sleeping period opportunities for the terminal are long.
- **Scalability:** The algorithm should scale well with the number of sessions and/or the number of resources.

Only some of these criteria have been taken into account in the following, namely efficiency, throughput, delay, computational complexity, and fairness.

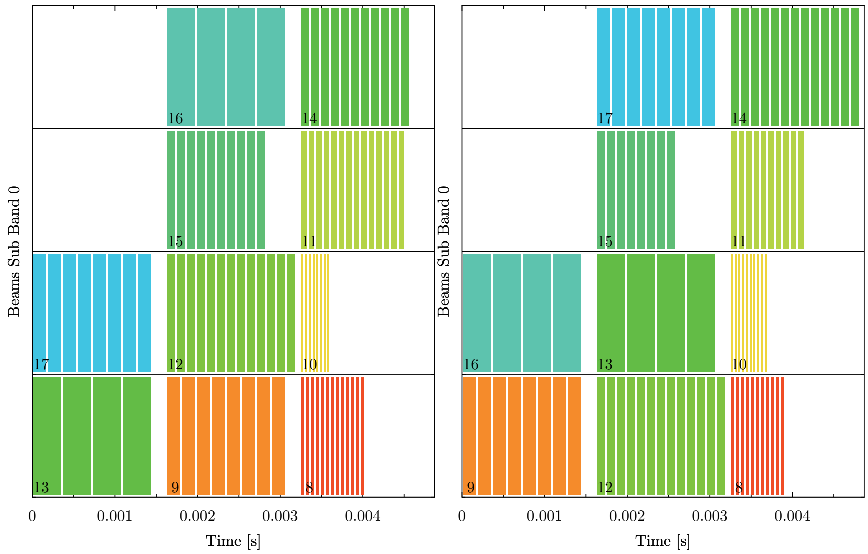

(a) $t = n$ **(b)** $t = n + 1$

Figure 4.19: Two consecutive frames for the RR scheduler with 10 SSs and max. 4 beams

4.4.5.1 Scheduling Disciplines

The algorithms presented in the following subsections are channel-aware versions of classical scheduling disciplines. Channel state scheduling discipline decides whether to serve a user during the current frame with a chosen MCS or not. The implementation complexity of the schedulers (especially in comparison to the grouper) is low and it scales with the number of SSs.

Round Robin

Round Robin (RR) serves SSs in frame based rounds. Because all SSs of the current round are given the chance to transmit before the next round starts anew, RR inherently assures a certain degree of fairness. While RR is widely known, there exist many different definitions and variants of it. Here, we will assume that the spatial groups of SSs are given equal time burst lengths during a frame.
Assuming a queueing model (see Figure 4.18) and a spatial grouper the scheduler determines the time length of the frame it has to fill and divides it by the number of groups it has retrieved from the grouper to determine the length of each burst. Each group is assigned to one of the bursts and the

bursts are filled with the SS's data packets.
Every SS that is served in SDMA is assigned a beamforming transmitter unit that transmits its data with a beam that is optimized for it. The spatial grouper computes the optimal beamforming weight vector for each SS and also provides an SINR estimation. Based on this SINR estimation the scheduler can select a MCS. With the associated data rate, the transmission duration of each packet is known so that the scheduler is able to determine the length of the group's burst resulting from the packet in the group taking the largest transmission time.
In Figure 4.19 example *RR* schedules for two consecutive frames are shown over time. The y-axis is divided into four parts representing the beamforming based transmitter units of the system (or the spatial domain). The colored boxes represent the scheduled packets. Note that the small white spacings in between the packets were just added for visualization purposes whereas the white space after a burst of packets indicates time in the frame that is not used for transmission. The colors allow to distinguish the different SSs, which are numbered from 8-17. The spatial grouping returned from the grouper in this example is {{13,17}, {9,12,15,16},{8,10,11,14}} for the first, and {{9,16},{12,13,15,17},{8,10,11,14}} for the second frame. In both examples, the grouping consists of three groups so that three bursts of equal duration are scheduled. In this example, all packets are assumed to have fixed lengths in bits. Therefore, the different transmission times visible in Figure 4.19 stem from different achievable data rates.

Exhaustive Round Robin

Under the *Exhaustive Round Robin (RR)* discipline the individual groups are not assigned bursts of equal time duration. Instead, a group is served until there are no more packets left in the respective queue. Only then bursts are scheduled for the other groups.
Figure 4.20 shows, by the example of two consecutive frames, how *Exhaustive RR* scheduling is working. In each frame only one single burst is scheduled so that the round consisting of 10 SSs will have to be continued in subsequent frames. What can be seen at a glance is that, in the first frame, a lot of transmission capacity of the frame is left unused resulting from of an uneven traffic and data rate distribution inside the group. SS 12 keeps transmitting even though the three parallel SSs have already run out of backlogged packets in the first frame.

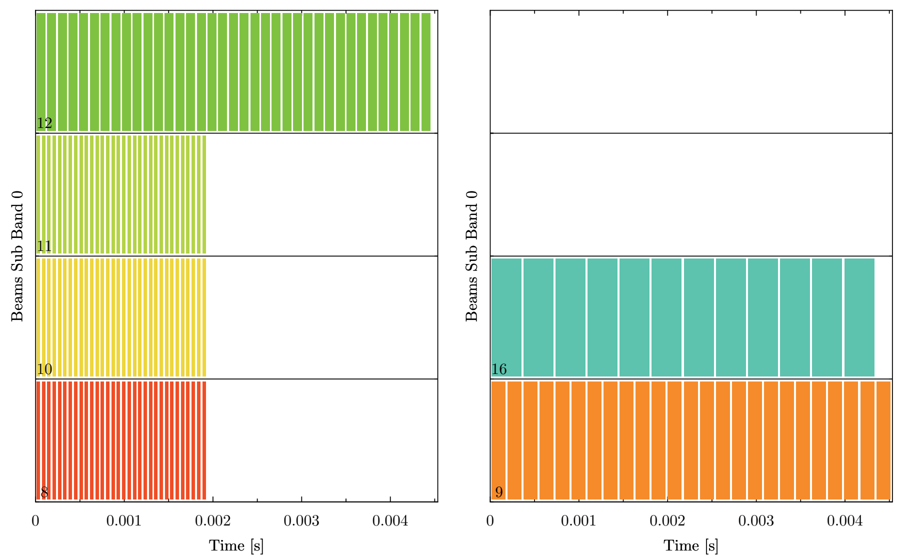

(a) $t = n$ **(b)** $t = n + 1$

Figure 4.20: Two consecutive frames for the *Exhaustive RR* scheduler with 10 SSs and max. 4 beams

In the second frame (Figure 4.20b), SSs 9 and 16 are the only ones in the spatial group. Thus, according to the spatial grouper, there is no better grouping that serves these two together with other SSs.
When comparing the performances of the RR and the *Exhaustive RR* schedulers, it appears that *RR* is always preferable to Exhaustive RR because it produces less delay. However, the *Exhaustive RR* scheduler requires less overhead because fewer bursts per frame have to be controlled.

Proportional Fair

The *Proportional Fair (PF)* scheduling strategy aims at a tradeoff between fairness and throughput. The throughput optimization is realized by preferring groups of SSs for which the grouper has estimated high SINR values, thus promising high throughput. The fairness is achieved by considering the past data rate that a SSs has experienced. This way, not only groups that promise high throughput in the future, but also those that have experienced throughput below average in the past, are taken into account by the scheduling decision.
The actual importance of a user in view of the scheduler is defined by the

ratio of its future and past data rates. The future data rate of a group is easily derived from the estimated data rates of the group members. Determining the past data rate is more difficult. The reason is that groupings may change on a frame-by-frame basis. Therefore, the members of a current group may have belonged to a different group in the past. When choosing members' past data rates as a criterion, high data rate SSs might starve SSs with low data rates. Therefore, the group's total future throughput and the minimum past group member throughput was taken for computing the groups importance in the view of the scheduler

$$importance(G_j) = \frac{\sum_{u \in G_j} EstimatedRate(u)}{1 + \beta \min_{u \in G_j} \{PastRate(u)\}} \tag{4.44}$$

This ratio is computed for every spatial group G_j obtained from the grouper. The groups are then served in order of descending importance. The factor β determines how much influence the past data rates have on the group's importance. The algorithm implemented in the WiMAC takes the past data rates into account using an exponential smoothing, thus reducing the weight of the preceding frames the more the larger the past time value is

$$PastRate_t = \alpha \, CurrentRate + (1 - \alpha) \, PastRate_{t-1} \qquad 0 \leq \alpha \leq 1 \tag{4.45}$$

In order to avoid intra-group inefficient use of the spatial channels like those observed in Figure 4.20a, the PF algorithm has been implemented to finish a group's burst duration once the first group member has run out of backlogged packets. The effect of this approach can be seen in Figure 4.21. In the first frame, all backlogged packets for SS 10 have been scheduled into the first burst. To avoid idle beamforming transmitter units, the other group members are scheduled to end transmission of packets synchronous to SS 10. Then the group with the next highest importance is scheduled. Again, the corresponding burst is terminated when SS 12 has run out of packets. The last group is not cut off when one member has run out of data unless a new grouping of the remaining SSs is done and offers a new group to schedule. This can be observed at the end of the second frame, when packets for SSs 8 and 11, who had previously been scheduled together with SSs 10 and 15, are transmitted.

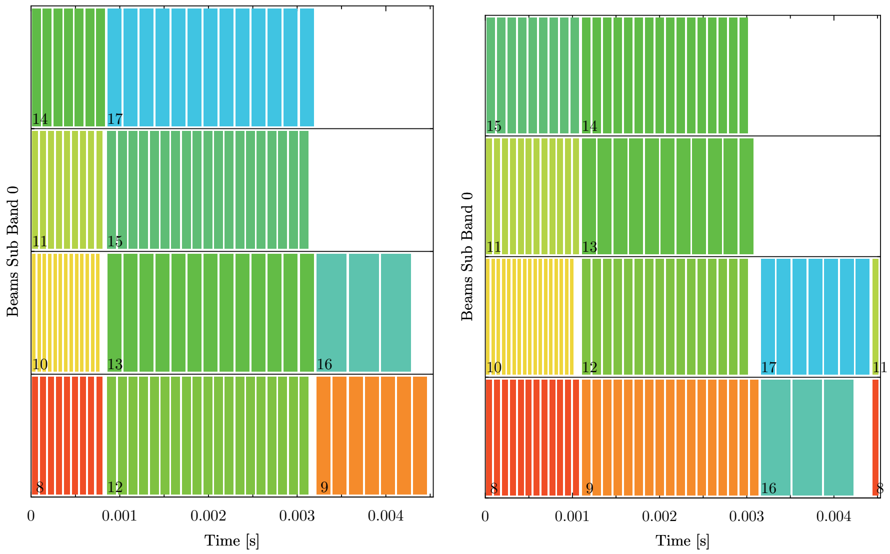

(a) $t = n$ **(b)** $t = n + 1$

Figure 4.21: Two consecutive frames for the *PF* scheduler with 10 SSs and max. 4 beams

Max Throughput

This scheduling discipline results from PF when using $\beta = 0, \alpha = 1$. To have always the best grouping of users served, the WiMAC implementation of the *Max Throughput* triggers a re-grouping of the active set of SS once a SS has left the set.

4.4.5.2 QoS Scheduling

There are many possible QoS parameters. Assuring a maximum delay, e.g., for VoIP services, as well as providing minimum throughput guarantees are the most interesting ones.
In order to facilitate delay guarantees, time-stamps that indicate the transmission deadline (= arrival time + max. delay) have to be added to every queued packet. In combination with a priority queue, the group scheduler then has to schedule the groups or SSs that have the most urgent packets waiting. For throughput guarantees the past data rates of individual SSs have to be monitored (similar to the *PF* scheduler). Different service classes can be supported by assigning fixed priorities to SSs.
The hierarchical SDMA scheduler can only schedule groups of SSs. When

it chooses one SS for transmission based on some QoS criterion, it also schedules the other SSs of the group at the same time or it wastes frame capacity by serving the SS individually.

4.5 Interference Reduction by Means of Smart Antennas

4.5.1 Adaptive vs. fixed Space-Time Sectorization

Advanced antennas can improve cellular radio systems in various ways (see Sections 4.1.3 and 4.1.4). Furthermore, switched beam antennas, which have a fixed antenna pattern, can be used for sectorization. Switched beam sectorization can increase capacity [Ho et al., 1998] and can be adapted to CDMA systems [Giuliano et al., 2002; Saraydar and Yener, 2001]. It is known from [Walke and Briechle, 1985] that adaptive sectorization may be employed in the time domain. There, spatial multiplexing has been proposed to serve TDMA channels in parallel for channel or packet based transmission. Section 6.1.1 describes sectorization as an established technique for reducing the interference level in cellular wireless networks. The cell is subdivided into sectors. Each sector is covered by a sector antenna. An individual frequency channel is assigned to each sector and an individual MAC protocol is controlling the access to the wireless channel. Sectorization reduces the number of interfering co-channel cells which increases the achievable SINR (see Eq. (6.3)). Sectorization is also foreseen to allow for scalability in WiMAX deployments [Fong et al., 2004].

The developed adaptive Space-Time Sectorization (STS) in this work for the WiMAX system divides the cell into sectors [Hoymann and Wolz, 2006]. But each sector is not covered by an individual sector antenna but served by the smart antenna using its adapted antenna pattern. Furthermore, the sectors are not separated in frequency, but in time. Thus, all sectors are operating on the same band but in different time slots. In the WiMAX system, these time slots correspond to MAC frames. This method results in the same interference reduction as conventional sectorization but it avoids its major disadvantages such as frequency channel allocation to sectors, the deployment of several sector antennas per site, the operation of different MAC entities per each sector, and thus the necessity for a SS to handover between sectors.

Figure 4.22 shows a cell that is divided into three 120° sectors. In conventional sectorization one third of the spectrum is allocated to each sector permanently.

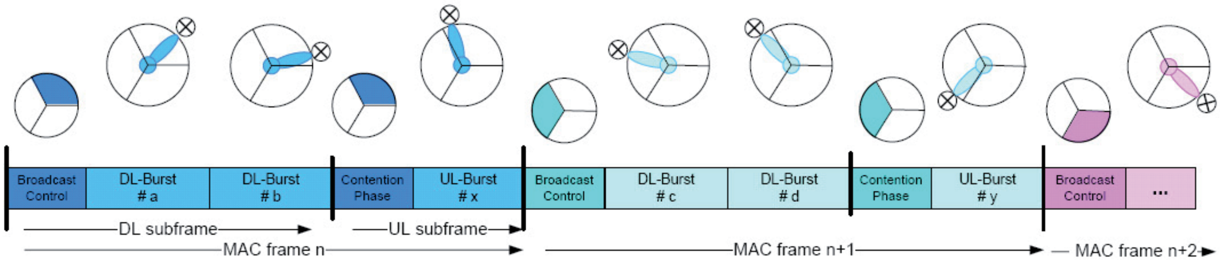

Figure 4.22: MAC frame and corresponding antenna pattern of space-time sectorization scheme

The new space-time scheme allocates the entire spectrum to each sector for one third of the time. Thus, the sectors are alternately served in the sequence of MAC frames, namely n, n+1, n+2. This alternating frame assignment to sectors can be arranged simply by scheduling the bursts of SSs located in the first sector within the corresponding numbered MAC frames, while bursts of SSs from the second sector are scheduled during their appropriate frames. After three subsequent MAC frames all sectors are served and the cycle repeats.
Even though sectors do have a specific shape reflected by conventional sector antennas, the antenna pattern that is applied during reception or transmission must not have the shape of the sector permanently. Figure 4.22 illustrates that only during broadcast and contention phases the antenna pattern must be shaped according to the shape of the sector. During unicast transmission periods, the antenna array is optimized to point to the proper SS.
By employing adaptive beams instead of sector antennas, a sector becomes a logically defined area, i.e., one sector refers to a group of SSs served within a distinctive time duration. No sector-specific hardware is deployed, such as sector antennas that predefine the shape of the sector. Furthermore, only one MAC entity serves all sectors. Hence, the number and shape of sectors can be changed adaptively during the operation simply by scheduling MAC frames at the BS according to the current needs. Like this, it is possible to adapt the shape of the sectors, for instance, to a varying traffic load of a network, even if the load follows the cycle of busy hours of a workday. It is also possible to re-shape the sectors of a cell to adapt the network to environmental and topology changes in the coverage area. A newly build office building might cause a re-optimization of the network sectorization,

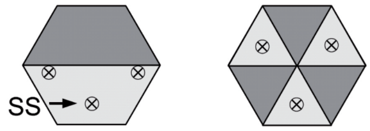

Figure 4.23: Reshaped space-time sectors

resulting in an adaptive re-shaping of the sectors [Giuliano et al., 2002].
Some shapes promise to improve a potential SDMA operation, as SSs can be served in parallel which have a greater angular width between them. Figure 4.23 shows two exemplary shapes of a logical two-sector cell ("light and dark"). The first shape allows a separation between three SSs that is limited to 60°, whereas the second shape allows for a separation of 120° when three SSs are served in parallel.
The geometric shape of a logical sector is limited only by the capability of the smart antenna. The angular width of the sector must be larger than the angular width of a single beam formed by the smart antenna. Otherwise transmit power is radiated to adjacent sectors where it causes interference. Other factors might affect the system performance, e.g., in order to benefit from multi-user diversity, the sectors must contain a considerable amount of SSs. Like in conventional sectorization, a reduced number of SSs per sector results in a reduced trunking gain. If the sector should be served in SDMA, the angular width of a sector must be large enough to exploit the spatial separability of SSs within one sector. Thus, the shape of a sector should take these trade-offs into account.
If a cellular network is operating in SDMA mode, STS does not only reduce the interference but it also significantly narrows down the solution space of grouping algorithms, since it needs to find an optimized solution only for the subset of SSs belonging to the same sector.

4.5.2 WiMAX MAC Frame Structure to Support Space-Time Sectorization

Operating in STS, transmissions have to be organized accordingly and the WiMAX MAC frame structure must be standard compliant. In IEEE 802.16 a SS periodically expects a preamble for time- and frequency synchronization followed by the FCH. The period between subsequent preambles is expected to be frame duration occasionally signaled in a MAC management message (DCD). At the beginning of the first DL burst, an UL- and a DL-MAP is

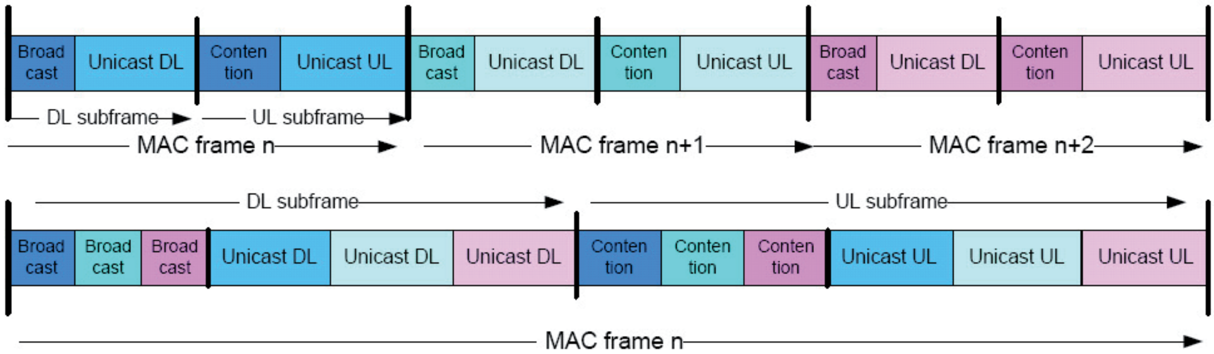

Figure 4.24: MAC frame structures

required that specifies access to the DL- and UL subframes, respectively. With respect to the proposed scheme, two types of phases are to distinguish in the MAC frame: broadcast and contention phases on one hand and the unicast DL and UL transmission phases on the other. Thus, each SS expects to receive the following sequence periodically: broadcast, unicast DL, contention, unicast UL. Figure 4.24 outlines two potential WiMAX MAC frame structures that both are organized to support STS. The same example cell with three space-time sectors, shown in Figure 4.22, is assumed. The colors of the phases indicate which sector is currently served.

The upper frame in Figure 4.24 is an arrangement of three shorter MAC frames, each fully standard-compliant. Since the broadcast messages are transmitted, by means of the proper antenna pattern, in the corresponding sector only, SSs receive information only every third MAC frame. Thus, the frame duration experienced by the SS, i.e., the difference between two consecutively received preambles, is three times the length of a single frame. This frame duration has to be signaled by the DCD so that SSs do not get confused. The MAPs received during the broadcast phase specify only the short MAC frame dedicated to the respective sector. The time intervals where the other sectors are served, i.e., for the other two frames, is left blank in the MAP. It appears to be unused.

The lower frame structure in Figure 4.24 is a rearrangement of the first. It can be seen that the same phases occur but in a different order. Here all broadcast phases are clustered together and transmitted subsequently. All other phases, such as the DL and UL unicast as well as the contention phase are subsequently arranged, too. Now the frame duration experienced by the SSs is the length of the long frame. But, the perceived frame start times are shifted by the duration of one or two broadcast phases. Note that the preamble is transmitted strictly periodically. Thus, the (in principle) variable sized broadcast phase becomes fixed size in this structure. The frame is experienced by a SS as follows: it starts with the preamble/FCH combination followed by one burst containing other signaling messages such as MAPs. After an interval that is not scheduled for DL transmission, the DL bursts containing unicast PDUs are transmitted. Again, the other sectors are served during the interval that seems to be unused. Then, another silent interval occurs followed by the contention phase. The unicast UL transmissions are scheduled again surrounded by two periods of silence.

4.5.2.1 Challenges of Space-Time Sectorization

Compared to a regular non-sectorized WiMAX system with the same frame duration or a system with fixed sectors, each served by its own antenna, the presented STS scheme introduces slightly higher delay since the perceived frame duration is three times the nominal one. A TDD system, that leverages the reciprocity of the channel, estimates the wireless channel in UL and uses the gathered channel state information for the DL. Such a system, e.g., a SDMA system, might suffer from the higher time distances between UL and DL transmissions.

Applying sectors in space-time domain requires synchronization of BSs so that the frame start and the switching point between DL and UL subframes are fixed and synchronized throughout the network. Otherwise co-channel cells would generate much more mutual interference and the impact of interference reduction by STS would degrade.

Imperfections in the antenna pattern applied during the broadcast and contention phases might decreases the benefit of the proposed scheme. It was mentioned that during these phases the antenna pattern has to be shaped so that the entire sector is covered but signals from/to neighboring sectors are suppressed. Imperfect patterns result in an increased level of interference.

4.5.3 Coordination Across Base Stations

Inter-cell interference can be reduced by coordinating transmissions of co-channel BS, RSs and SSs. Coordination offers huge potential for future wireless systems, especially to reduce handover time, avoid/average/smooth interference, advanced coding, and load balancing [Falconer et al., 2006].

Coordinating adaptive antennas of neighbor BSs may reduce mutual interference. If a BS is aware of co-channel SSs it may influence its antenna pattern and schedule transmissions accordingly.
If a BS knows the position/CSI of all co-channel SSs that are interfered during reception it can adapt its transmit antenna pattern to minimize the transmit power in the direction of interfered SSs in co-channel cells. In UL, the receive pattern can also be adapted to reduce co-channel interference. In order to get the information, the neighbor cells have to transmit their location or, alternatively, the BS needs to acquire the transmission times of UL bursts of co-channel SSs in order to periodically estimate the CSI itself. All SSs could be taken into account for the antenna pattern optimization.
If a BS knows the entire schedule of co-channel BSs, it would be able to coordinate its own schedule, accordingly. The antenna pattern needs to consider only those SSs that are currently transmitting or receiving. Under light to medium system load, a BS might schedule time slots currently not used by other BSs. SSs at the cell edge that are timewise highly interfered could be scheduled to be served when the interfering BS is transmitting into other directions. Coordination of DL and UL schedules across BSs is only possible, if the resource allocation is quite static for a certain period of time, i.e., some frame durations.

CHAPTER 5

Multi-hop Operation

WiMAX networks are foreseen to cover diverse geographic regions. On the one hand they shall cover urban areas where a high density of buildings and indoor usage prevent LOS radio propagation conditions. On the other hand WiMAX networks shall provide access over large geographic regions in remote rural areas, where over the rooftop deployment of Tx and Rx antennas allow for LOS radio propagation. In both scenarios it might be challenging to cover the entire service area. In order to cope with diverse radio propagation conditions, RSs have been introduced to standard IEEE 802.16. RS may enhance the link quality leading to throughput enhancements, see Figure 6.9b and coverage extensions see Figure 6.9a [Esseling et al., 2005]. Due to the enhanced coverage and the increased cell capacity, RSs promise a cost-efficient deployment and service [Pabst et al., 2004].

Several multi-hop concepts for frame-based MAC protocols have been developed so far. The ETSI-BRAN High Performance Local Area Network Type 2 (HiperLAN/2) standard that is similar to the HiperMAN standard mentioned in Section 3.1 contains a direct mode that allows terminals to communicate directly similar to the mesh mode described in Section 3.3.2.9. The HiperLAN/2 Access Point (AP) is coordinating the access, so both terminals must be in the coverage area of the AP's broadcast channel [ETSI, 2001]. Another concept, called the beacon concept, relies on the HiperLAN/2 option for sector antennas, where an AP transmits the broadcast messages and the following MAC frame through each sector antenna sequentially [Zirwas et al., 2002]. The third proposal, the subframe concept, realizes multi-hop communication without a need to extend the standard. The AP allocates periods within its MAC frame to be used by RSs. The RS can use the related frame capacity to act as an AP itself, thus generating an individual MAC frame (called subframe) for the terminals associated to the RS [Esseling et al., 2000].

The Task Group IEEE 802.16j aims at specifying enhancements for a mobile multi-hop operation without any modifications to SSs. Thus, the frame

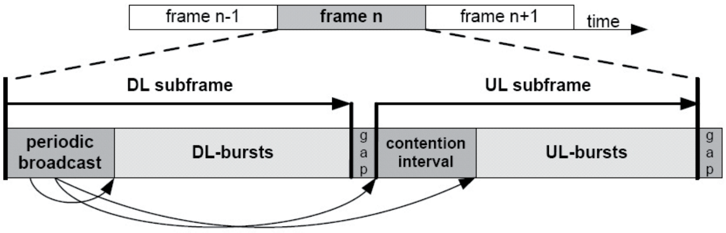

Figure 5.1: PMP MAC frame structure

structure shall be PMPs compatible and the MAC management procedures, such as association or handover, shall not be modified. Unlike the 802.16 mesh mode, the task group 802.16 aims at a tree-based radio network deployment only.
According to the requirements of the IEEE 802.16j task group, this thesis presents two concepts to support multi-hop communication in 802.16 networks. It focusses on decode and forward RSs that decode the received data packets, process them in the MAC layer, e.g., for ARQ operation, and forward them to the next hop. Both concepts apply time domain forwarding, where packets are received and forwarded on the same frequency channel. Thus, a RS only needs one transmit and one receive chain. Although the concepts presented focus on OFDM, they can be easily applied to OFDMA, too, which is the target PHY layer of task group 802.16j. Only the control elements, for instance, the DL- and UL-MAP would have to be modified. The principle frame structure remains valid as presented in the following.

5.1 Legacy PMP MAC Frame Structure

IEEE 802.16 supports a frame-based transmission as explained in Section 3.3.2. Figure 5.1 presents the frame structure of the OFDM PHY layer operating in TDD mode: each frame consists of a DL subframe and an UL subframe. Subframes are separated by gaps. The DL subframe starts with the periodic broadcast of control information. The arrows in Figure 5.1 indicate the references of the DL- and UL-MAP to the corresponding DL- and UL bursts. During the DL bursts MAC PDUs are transmitted. The UL subframe consists of intervals for contention-based access and one or multiple UL bursts.

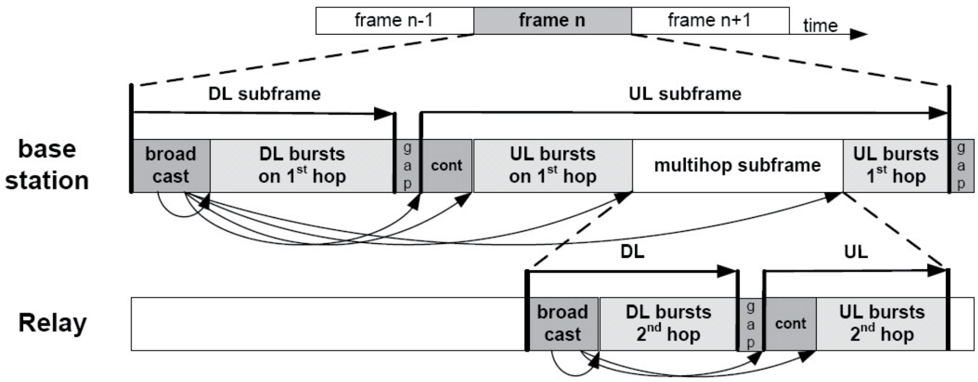

Figure 5.2: Multi-hop subframe embedded in an 802.16 MAC frame

5.2 Self-Controlled Relay Stations

In the self-controlled relaying approach, the RS has full control over the SSs that are associated to it. The entire functionality required for multi-hop operation is encapsulated in the RS. The BS is not affected. For the BS, a RS appears like an ordinary SS. For SSs the RS appears to be a regular BS.

5.2.1 Subframe Structure

The self-controlled concept applies the HiperLAN/2 subframe concept [ETSI, 2001] to the 802.16 system. During the multi-hop subframe interval, see Fig. 5.2, the BS does schedule neither DL nor UL traffic. Instead, it dedicates the interval to the control of the RS. The RS itself builds up an entire MAC frame. This frame, called *multi-hop subframe*, is a standard compliant 802.16 MAC frame.
Figure 5.2 shows the modified 802.16 frame with the embedded multi-hop subframe. The frame starts with the DL subframe composed of the broadcast phase and DL bursts. The DL bursts contain PDUs transmitted to SSs that are associated to the BS directly. For the BS, the RS appears to be a regular SSs. All DL bursts are specified by means of the DL MAP. Thus, DL bursts serve SSs and RSs on the first hop.
The UL subframe starts with a contention interval followed by UL bursts. SSs, which are close to the BS, use contention slots for network entry or bandwidth requests. The following UL bursts are scheduled for UL transmissions of SSs on the first hop. Some of these UL bursts are scheduled for RSs. Within these bursts, RSs can transmit its UL traffic to the BS. Another UL burst is

not addressed to UL transmission at all, but it is reserved for the multi-hop subframe. The broadcast phase specifies this burst by means of a regular UL MAP IE (indicated by an arrow in Figure 5.2). Here, the UIUC of that IE does not address a station but it indicates the multi-hop subframe for a specific RS. Therefore, a certain range of UIUC values should be reserved for multi-hop subframe allocations.
Since the frame structure of the multi-hop subframe is standard compliant, it is again divided into a DL and an UL subframe. The DL part starts with the broadcast of control information. The corresponding management messages are only relevant for the SSs associated to the respective RS. As the arrows in Figure 5.2 indicate, the DL MAP defines access to the second hop DL channel and the UL MAP schedules UL bursts on the second hop. The following DL bursts of the multi-hop subframe contain PDUs for SSs on the second hop. UL bursts are scheduled for UL data on the second hop. A gap divides the DL and the UL part of the multi-hop subframe. SSs close to the RS can access the contention slots scheduled at the beginning of the UL part of the multi-hop subframe to enter the network or to request bandwidth.
Since the broadcast phase must occur periodically, the BS has to schedule the multi-hop subframe at fixed time intervals. This can be accomplished since 802.16 provides a scheduling service that has been designed to support real-time data streams that generate data packets on a periodic basis. This so-called Unsolicited Grant Service assigns UL bursts at periodic intervals. A RS may use the periodic UL burst to establish its multi-hop subframe. Note that it is not sufficient to schedule the multi-hop subframe periodically on a frame basis. It must be scheduled periodically on OFDM symbol level. The UGS scheduling service should be implemented accordingly. The size and the duration of the burst can be specified by the QoS parameter set associated to the corresponding UL connection.
SSs that are close to the BS only notice the BS's frame, whereas SSs near the RS observe the RS's (sub)frame as if it was a regular frame. SSs that perceive both broadcast control phases seem to be in between two neighbored cells. Therefore, they will associate to the cell that they receive loudest. The association of SSs to the RS is handled by means of the standard compliant initial ranging procedure.

The subframe concept can be configured so that the multi-hop subframe appears to be an individual frame. To do so, the multi-hop subframe is located at the very end of the BS's MAC frame. The length of the multi-hop subframe is exactly half of the length of the BS's MAC frame and the multi-hop subframe occurs every regular BS MAC frame. Thus, the main frame and the multi-hop subframe appear to be two subsequent MAC frames. The experienced MAC frame period is half of the regular BS's MAC frame duration. Every second frame is dedicated to the BS and the frames in between are dedicated to the RS. Of course, the described configuration can be extended to more than one RS per BS. This configuration equals the *Time Sharing Wireless Router* concept presented in [Wijaya, 2005]. This configuration allows for synchronized broadcast phases within the whole system.

5.2.2 Distributed Connection Management

Multi-hop communication introduces a need for connection management at the RS. The RS has to forward bypassing packets in DL (away from the BS) and in UL (towards the BS) direction hop by hop. It has to maintain a control connection to exchange signaling information between a SS served multi-hop and the BS and it possibly receives and transmits data packets on its own.

The concept of *Connection Masquerading* suits the self-controlled relaying approach. Acting as a regular BS the RS provides all necessary procedures to setup transport and management connections for the remote SSs. For the BS, the RS appears to be an ordinary SS, thus it can setup and release transport connections applying standard procedures. Besides the transport connections, the RS maintains its management connections.

Figure 5.3 shows an example of the masqueraded connection management. The RS establishes its control connections to the BS. It uses these connections to exchange signaling information, such as connection management or periodic measurement reports. The RS in Figure 5.3 has also set up transport connections to receive and transmit data packets from/to the BS. On the right side of the RS, the remote SSs have established management and transport connections to the RS as well. The contention-based network entry process and the registration of SSs is handled by the RS itself. The backbone network, to which the RS communicates via its transport connections, assists the process of authentication and authorization.

For each transport connection that a SS sets up, the RS opens an associated connection to the BS. Both connections have the same QoS requirements.

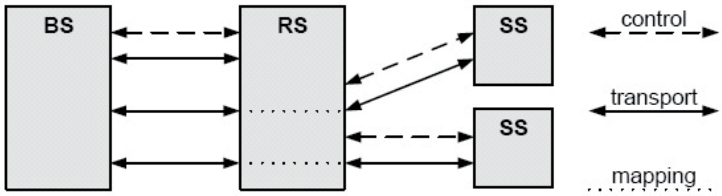

Figure 5.3: Connection masquerading

The BS is not aware that the connection corresponds to a remote SS. The RS masquerades the transport connection. It maintains a table to map the CID of one hop to the CID of the other and vice versa. Figure 5.3 indicates this mapping. All protocol functionality that maintains the packet transmission, such as ARQ, Segmentation and Reassembly (SAR), or burst profile management, is performed on link basis.

5.3 Centrally Controlled Relay Stations

The centrally controlled relaying approach is an alternative concept where the BS has full control over all its RSs' operation, hereby fully controlling the so called Relay Enhanced Cell (REC). The BS directly controls all SSs and all RSs that are associated to the BS. The complexity of the RS can be reduced since it just forwards packets hop by hop. It does not perform any other MAC management functions to allow for multi-hop operation.

5.3.1 Centralized MAC Frame Structure

Figure 5.4 shows the centralized multi-hop frame. The BS periodically transmits broadcast control information. The DL preamble indicates the frame start. The following management messages, i.e., FCH and MAPs, specify the entire MAC frame including the bursts scheduled on the second and on any subsequent hop. In order to calculate an appropriate schedule, the BS needs to know which connections of the entire REC are active, which QoS requirements they have, and which connections request UL bandwidth. Having received the broadcast information, the RS filters it and forwards only the relevant subset of information to its subcell. Figure 5.4 shows that the forwarded MAPs only specify the bursts that are scheduled for data transmission on the second hop served by a given RS. Before the RS starts

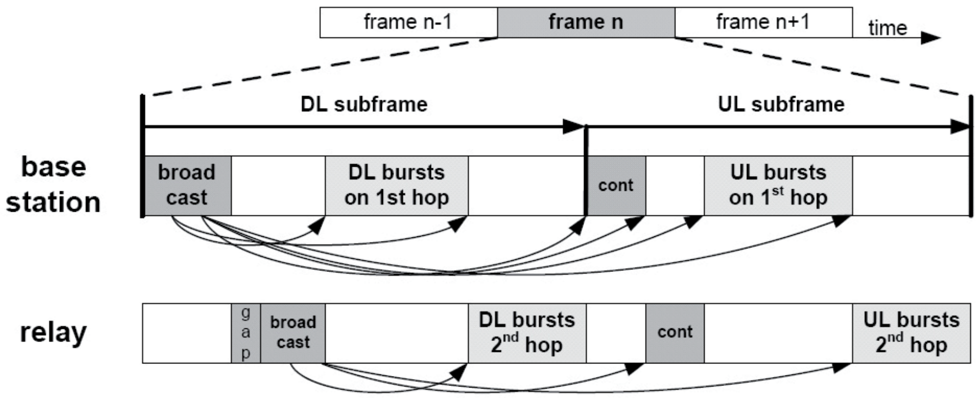

Figure 5.4: Centralized multi-hop MAC frame

transmitting the management messages, it sends the periodic DL preamble. Like in the subframe concept, the RS's frame start time has to be strictly periodic. In order to guarantee the periodic behavior and to allow the RS to process the BS's broadcast information a gap is introduced between the BS's and the RS's broadcast phase.

DL bursts for data transmission follow the broadcast phases. The BS may schedule bursts for any hop. The UL subframe succeeds the DL subframe. Again, phases for data transmission on any hop may be scheduled alternately. This ordering of transmission phases assures that all SSs that are associated either to the BS (single-hop) or to the RS (2-hop) do experience a regular, standard compliant MAC frame. They can associate, open connections, and they can receive and transmit data according to the IEEE 802.16-2004 protocol. Since there might be more than one RS in a REC, the BS needs to consider that in its resource scheduling. Using time-domain separation of RSs' channel access, the BS controlled MAC frame looks as shown in Fig. 4.22, lower part. The only difference is that resources are scheduled there to sectors whilst resources are scheduled here to RSs.

5.3.2 Central Connection Management

With centrally controlled RSs the BS manages the SSs' control and transport connections. RSs just forward packets to the BS and SSs, respectively. Figure 5.5 shows the schematic connection management at the RS. The RS itself has both control and transport connections to the BS.

Furthermore, each connection on the second hop corresponds to a connection

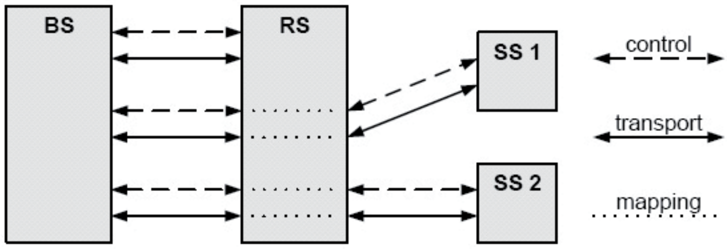

Figure 5.5: 1-to-1 mapping of connections

on the first hop. Every time a SSs establishes a management connection to the RS, the RS establishes a corresponding management connections to the BS. Each setup of a SS's transport connection results in a new transport connection of the RS. The mapping is realized by mapping tables.
After the synchronization of a new SS to the RS, it starts the ranging process by sending the ranging request during the RS's contention interval. The RS forwards this message to the BS through its own control connection. The BS processes the request and responds to the SSs via the RS. The BS entirely handles the following network entry. Currently, the standard compliant message exchange does not comprise all necessary information for the network entry. Using the 1-to-1 mapping, two management CIDs have to be assigned instead of one. One CID is required to identify the connection on the first hop and the other for the second hop. Since the BS schedules both hops, it needs to be aware which CID corresponds to which hop. The set-up of transport connections follows the same principle. The RS just forwards the request and the BS assigns the transport CIDs. All other signaling messages, such as UL bandwidth requests and measurement reports have to be transmitted from the SSs to the BS by means of the RS. Thus, the BS gathers all necessary information to schedule DL and UL bursts for the RSs and for the SSs. It periodically broadcasts the FCH and the MAPs and all nodes behave accordingly.

5.4 Pros and Cons of Self- and Centrally Controlled Relay Stations

Self-controlled RSs require BS functionality and corresponding processing capability. Due to the distributed control, signaling overhead can be reduced when compared to centrally controlled RSs. Since self-controlled RSs behave

like SSs from the BS perspective, the 802.16 air interface specification does not need to be modified much, however, from a network perspective self-controlled RSs and SSs are rather different so that the WiMAX network management requires major modification.
Centrally controlled RSs require less processing power because control functionality is located at the BS. Since the centrally controlled RS is different to a SS the 802.16 specification requires modification, however, WiMAX network management does not need to be modified much. Finally, a central control of RSs offers potential for optimization across RS subcells. Due to the listed advantages, the frame structure of non-transparent relays in IEEE 802.16j has been based on the concept of centrally-control RSs as proposed by the author [Hoymann et al., 2006a; IEEE, 2008].

5.5 Smart Antenna Enhanced Multi-hop Operation

5.5.1 SDMA at the Base Station

Chapter 4 outlined that in a conventional single-hop, SDMA capable 802.16 system, the BSs might operate in SDMA and thus increase capacity. However, SDMA operation is also beneficial in REC.
In a multi-hop scenario, SDMA operation on the first hop (BS-to-RS) hardly differs from the single-hop case. BSs schedule and serve SSs simultaneously. Figure 5.6 shows the MAC frame of an SDMA enabled multi-hop system where DL and UL bursts of the first hop are scheduled in parallel. The necessary feedback to schedule SSs is available at the BS.
Not only SSs can be served in SDMA mode, but also the DL or UL transmission to/from RSs can be scheduled in parallel as shown by the parallel multi-hop subframes in Figure 5.6. This has several major advantages. First, in multi-hop links the first hop is the bottleneck. Besides the regular traffic of the BS, the entire traffic of one or several RS subcells has to be transmitted to/from the BS. Operating RSs in SDMA enhances capacity of these links and increases the capacity of a multi-hop system. Second, RSs are fixed and separated in space. Thus, they can be effectively separated by the antenna array. The intra-cell interference can be significantly reduced. Third, the scheduling complexity can be decreased. The SDMA scheduler can first calculate an optimal spatial grouping for the RSs and afterwards calculate the grouping for the remaining SSs to be served by the RS. The grouping of RSs is quite static, thus is does not need to be updated frequently. By

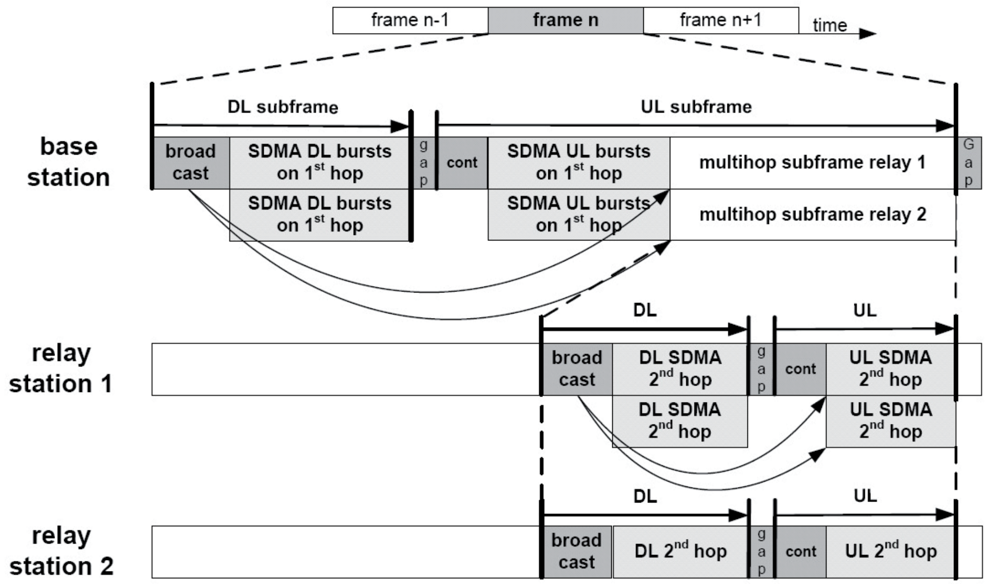

Figure 5.6: Subframe concept for SDM and SDMA mode of operation

processing the RSs independently, the number of remaining stations and thus the scheduling complexity decreases.
In the centrally-controlled approach (see Section 5.3), the BS is aware of the RSs. Using the subframe concept (Section 5.2), the BS does not necessarily know which station is a RS. This information could be communicated during the association procedure.

5.5.2 SDMA at the Relay Station

Provided that a RS has smart antennas that allow for beamforming in DL or joint detection in UL, SDMA operation is also possible in a subcell controlled by a RS.
In a centrally-controlled approach, the subcell is under the control of the BS. The BS schedules the SSs even if they are on the second or third hop. In order to build up a proper SDMA schedule, the BS needs to get all required information about the spatial separability of SSs on remote hops. This information is collected by the RS and afterwards signaled to the BS. This causes additional signalling overhead.
If the RS has the control about its subcell, as it is the case in the self-controlled operation, it can schedule and serve SSs simultaneously. Therefore, a RS needs to have all capabilities to operate in SDMA, such as an extended

scheduler and an enhanced PHY SAP. Like this, RSs can acquire the necessary knowledge about the wireless channel. SDMA operation of RSs on the second hop does not differ from the SDMA operation of BSs on the first hop.
The multi-hop subframe of RS 1 in Figure 5.6 shows an SDMA setup. DL and UL bursts are scheduled in parallel. The two arrows in the figure shows that the concurrent SDMA transmissions are indicate by MAP IEs.

5.5.3 Spatial Reuse of Subcells

The introduction of multi-hop communication allows to convert capacity of the inner cell to an increased SINR in the outer areas of the cell. The capacity reduction is due to the duplicated transmission of data and due to the increased signalling overhead. Figure 5.6 shows that the multi-hop subframe requires additional allocations of the radio resource.
In general, RSs and therewith their coverage areas are located apart from each other. In urban scenarios with high signal shadowing, RSs may be shadowed from each other so that RSs may operate in Space Division Multiplex (SDM), i.e., the multi-hop subframes are scheduled in parallel. Figure 5.6 shows the MAC frame for the SDM operation of two RSs. It can be seen that the multi-hop subframe of RS 1 is scheduled in parallel to the subframe of RS 2. The arrows indicate that the multi-hop subframes are controlled by regular UL MAP IEs. The additional overhead due to the duplicated transmission and the signalling overhead is reduced. SDM mode allows efficiently utilizing the radio resource, which promises to significantly increase capacity (see Section 6.4). However, care has to be taken that the mutual interference between simultaneously operating RSs stays within reasonable limits. This can be accomplished, e.g., with directive antennas at the RS (see Section 6.2.6).

CHAPTER 6

Performance Analysis

6.1 Dimensioning Cellular 802.16 Networks

This section investigates the SINR in a cellular 802.16 network. For dimensioning purposes, especially the UL and DL SINR seen from and at the most distant SS is interesting, respectively. Interference is generated by co-channel cells that utilize the same frequency channel. In the considered network, DL and UL channels are assumed to be perfectly separated either by a FDD or by a fully synchronized TDD scheme. Thus, in DL, neighbor BSs cause interference, while in UL, interference is generated by SSs of neighbor cells.

6.1.1 Clustering and Sectorization

In order to avoid interference in cellular networks, frequency channels used within one cell can only be reused after a sufficient reuse distance. Hence, cells are combined to clusters, in which frequency channels or groups of channels are uniquely assigned to cells. The number of unique frequency channels is named Cluster Order (CO). The frequency usage pattern of the entire cluster is regularly repeated throughout the network. Like this, the distance to co-channel cells can be increased. Figure 6.1a shows a cellular network with $CO = 3$. The distance to co-channel cells D is a function of the cell radius R and CO [Eberspächer and Vögel, 1999]:

$$D = R\sqrt{3\,CO} \tag{6.1}$$

According to [Walke, 2001], the SIR only depends on CO if noise is neglected and if the neighbor SSs are assumed to be centrally located in their cells. With an increasing CO, the Signal to Interference Ratio (SIR) at a central BS receiving a signal from a SS at the cell border is increasing. With γ as the pathloss coefficient, the SIR is

$$\frac{S}{I} = \frac{1}{6}\left(\frac{D}{R}\right)^{\gamma} = \frac{1}{6}\,(3\,CO)^{\frac{\gamma}{2}} \tag{6.2}$$

Dividing cells into sectors reduces interference in cellular networks. Each sector is covered by a sector antenna. An individual frequency channel is assigned to each sector and an individual MAC protocol is controlling the access to the wireless channel. The sectorization of cells and the frequency assignment is periodically repeated all over the network coverage area. A sophisticated way to allow for sectorization with adaptive antennas has been introduced in Section 4.5.1.
Because the power emitted backwards from the BS sector antenna is minimized, the number of interfering co-channel cells seen by a sector antenna can be reduced. Figure 6.1b shows a cellular network with 3-sectored cells. It can be seen that only two co-channel cells are visible for the receiving BS sector antenna instead of six in Figure 6.1a. Furthermore, a SS at the border of a cell receives only interference power from the most distant co-channel BSs. Thus, the number of interferers and the strength of interference can be reduced by sectorization. Analog to Eq. (6.2) the expected SIR in a sectorized and clustered cell can be calculated, where m is the number of sectors [Walke, 2001]:

$$\left(\frac{S}{I}\right)_{sectorization} = \frac{m}{6}\left(\frac{D}{R}\right)^{\gamma} = m\left(\frac{S}{I}\right)_{non-sectorization} \tag{6.3}$$

For the example given in Figure 6.1b, $m = 3$ sectors per cell increase the SIR by a factor of three. The drawback of sectorization is that the channel group assigned in Figure 6.1a to a cell must be allocated to the three sectors in Figure 6.1b so that each sector has its own channels exclusively. This results in a lower trunking gain and reduced cell capacity. Furthermore, several sector antennas have to be deployed at each BS and the control of each MAC entity per sector causes overhead. Since interference is reduced when introducing sectorization, CO can be reduced and thereby the number of channels per sector increased. If well dimensioned, sector systems are always preferential.
Equations (6.2) and (6.3) do not consider noise and assume that all co-channel interferers are equally distant. In the following analysis, the effect of noise is considered and positions of interfering BSs and SSs are modeled more accurately, separately for UL and DL.

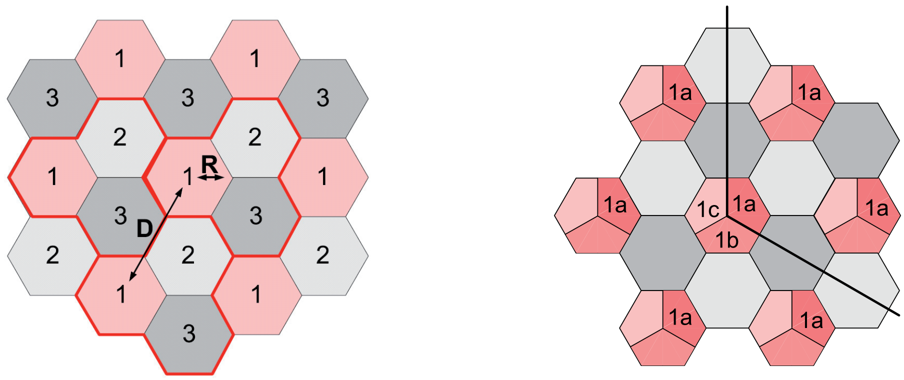

(a) Hexagonal cells with $CO = 3$

(b) 3-sectored cells using $CO = 3$

Figure 6.1: Cellular network

6.1.2 Mean UL Interference Generated by a Co-channel Cell

In UL, SSs of co-channel cells generate interference. These SSs can be assumed randomly distributed within the cell area. Sometimes, they are closer to the co-channel cell, and sometimes they are farther away. In order to model co-channel interference more accurately, the mean interference generated by a co-channel cell is calculated by assuming a planar transmitter with the shape of the hexagonal cell. The transmit power is assumed equally distributed all over the cell surface area.

A comparable approach to model interference has been developed in [Habetha and Wiegert, 2001]. The mean interference is estimated as the integral over the cell area. However, circular cells are assumed and the effect of noise is not considered. Sectorization has not been considered there.

Figure 6.2 shows the cell of interest on the right and a co-channel cell that generates interference on the left. Since we are interested in the interference to the BS in the right hand cell, only SSs in the left hand cell are of concern. The mean interference level that is received by the BS located at x_0, y_0, can be calculated by assuming that each area element of the left hand cell transmits with the same fraction of interference power. According to its distance to the BS of interest, each fraction of the interference power is attenuated by the pathloss. Thus, each area element of the distant interfering cell generates a fraction of the overall received interference power. By integrating over the

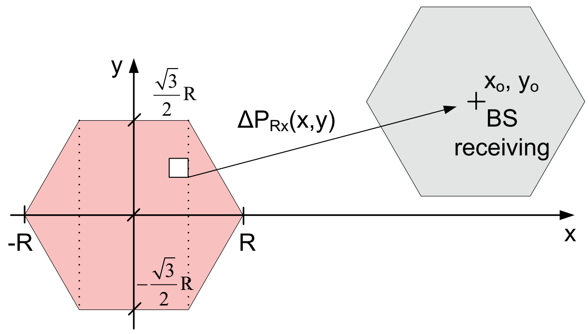

Figure 6.2: Interference received from a co-channel cell

cell area, the mean level of interference power $\overline{P_{R_x}}$ can be calculated.

$$\overline{P_{R_x}} = \int_{area} \Delta P_{R_x}(x,y) = \int_x \int_y \frac{P_{T_x} * G_{T_x} G_{R_x}}{area} \, pathloss(x,y)\, dy\, dx \quad (6.4)$$

$$\begin{aligned} \overline{P_{R_x}} &= \int_{area} \Delta P_{R_x}(x,y) \\ &= \int_x \int_y \frac{P_{T_x} * G_{T_x} G_{R_x}}{area} \, pathloss(x,y)\, dy\, dx \end{aligned} \quad (6.5)$$

Where $\Delta P_{R_x}(x,y)$ is the interfering power per area element. The location independent mean level of interference power P_{T_x} is assumed to result from uniformly distributed SSs. Each fraction of the interference power is attenuated by the pathloss and it is amplified by the antenna gain of the transmitter G_{T_x} and the receiver G_{R_x}.
The surface area of a hexagonal cell and the one-slope pathloss model with the pathloss coefficient γ are known

$$area = \frac{3}{2}\sqrt{3}R^2 \quad ; \quad pathloss(x,y) = \beta\, D^{-\gamma} = \beta\, \sqrt{(y-y_0)^2 + (x-x_0)^2}^{\,-\gamma} \quad (6.6)$$

The values of x_0, y_0 depend on the re-use distance that depends on the cell radius and CO see Eq. (6.1). Table 6.1 lists x_0, y_0 for the most common COs, which are the same for all six co-channel cells.

Table 6.1: Co-channel distances of various COs

$ClusterOrder$	x_0	y_0	$D = \sqrt{x_0^2 + y_0^2} = \sqrt{3k}R$
1	0	$\sqrt{3}R$	$\sqrt{3}R$
3	$3R$	0	$3R$
4	0	$2\sqrt{3}R$	$2\sqrt{3}R$
7	$3R$	$2\sqrt{3}R$	$\sqrt{21}R$
12	$6R$	0	$6R$

The receive power per area element only depends on the variables x and y, all other characters are fixed, so that Eq. (6.4) can be written as

$$\overline{P_{R_x}} = \int_{area} \frac{P_{T_x} * G_{T_x} G_{R_x}}{\frac{3}{2}\sqrt{3}R^2} \beta \left[(y - y_0)^2 + (x - x_0)^2\right]^{-\frac{\gamma}{2}} \tag{6.7}$$

To integrate over the cell area it is divided into three parts, see Figure 6.2, resulting in

$$\begin{aligned} \overline{P_{R_x}} &= \int_{-R}^{-\frac{R}{2}} \int_{-\sqrt{3}x-\sqrt{3}R}^{\sqrt{3}x+\sqrt{3}R} \Delta P_{R_x} \, dydx \\ &+ \int_{-\frac{R}{2}}^{\frac{R}{2}} \int_{-\frac{\sqrt{3}}{2}R}^{\frac{\sqrt{3}}{2}R} \Delta P_{R_x} \, dydx \\ &+ \int_{\frac{R}{2}}^{R} \int_{\sqrt{3}x-\sqrt{3}R}^{-\sqrt{3}x+\sqrt{3}R} \Delta P_{R_x} \, dydx \end{aligned} \tag{6.8}$$

Unfortunately, the sum of double integrals in Eq. (6.8) cannot be solved in closed form. Thus, it has been implemented in Matlab in order to be calculated numerically. The chosen granularity of the sum is set to $1/10000$ of the cell radius. This small granularity results in an error of 0.02 % of the integral compared to the size of the surface area when calculated by summation. If a circular instead of a hexagonal cell area is assumed, the integral can be solved in closed form for certain γ values [Habetha and Wiegert, 2001].

For the pathloss, the suburban C1 Metropol pathloss model from the IST - WINNER project is chosen [IST-WINNER, 2006], which has also been implemented in the simulation environment WNS described in Chapter 8.

The C1 Metropol is a composition of two models, a LOS and a NLOS model. NLOS propagation is modeled by a one-slope model with the parameters given in Eq. (6.9) and LOS by a two-slope model. However, the antenna height is assumed to be such high that the break-point distance between the two LOS slopes is beyond the distances of interest in the following analysis. As a result, a one-slope model remains for LOS propagation, see Eq. (6.10).

$$\text{NLOS:} \qquad \beta = 10^{-\frac{27.7}{10}} = 1.698 * 10^{-3} \qquad \gamma = \frac{40.2}{10} = 4.02 \tag{6.9}$$

$$\text{LOS:} \qquad \beta = 10^{-\frac{41.9}{10}} = 6.457 * 10^{-5} \qquad \gamma = \frac{23.8}{10} = 2.38 \tag{6.10}$$

In order to evaluate the interference generated by a co-channel cell, the mean receive power $\overline{P_{R_x}}$ is normalized to the receive power P_{R_x} of a single SS located at the center (0,0) of the co-channel cell, see Eq. (6.11). A correction factor results to be applied to a model where a central source of interference is assumed. In the following analysis the UL interference is calculated as if the co-channel SS is located in the center of the cell, and the resulting interference is corrected then by the interference correction factor.

$$\begin{aligned} 1 + \mathit{interference\ correction} &= \frac{\overline{P_{R_x}}}{P_{R_x}} = \frac{\overline{P_{R_x}}}{P_{T_x} * G_{T_x} G_{R_x} * \mathit{pathloss}(0,0)} \\ &= \frac{1}{\mathit{pathloss}(0,0)} \int_x \int_y \frac{\mathit{pathloss}(x,y)}{\mathit{area}}\, dy\, dx \end{aligned} \tag{6.11}$$

The first row of Tables 6.2 and 6.3 (one sector per cell) gives the interference correction factor in percent for the LOS and NLOS cases, respectively. The correction factor is independent of the cell radius, although this is not directly visible from the calculation. Although the cell radius is part of the limits of the integral, its influence disappears when normalizing to the interference power P_{R_x} in Eq. (6.11).

By comparing the content of the first rows of Tables 6.2 and 6.3 it can be seen that under LOS propagation the required correction is lower than for NLOS scenarios. This is due to the higher pathloss coefficient γ, which causes a non-linear attenuation. Besides on the pathloss coefficient, the correction factor depends on the CO. With higher COs, the co-channel distance increases. The more distant the co-channel cell, the more it appears

Table 6.2: Interference correction factor for LOS scenarios in [%]

$ClusterOrder \rightarrow$ sectors per cell $\downarrow$	1	3	4	7	12
1	24.89	7.12	5.22	2.92	1.68
2	-21.48	-15.38	-13.56	-8.52	-8.82
3	-41.04	-27.50	-24.28	-20.90	-15.33
6	-48.18	-33.66	-30.12	-24.04	-19.51

Table 6.3: Interference correction factor for NLOS scenarios in [%]

$ClusterOrder \rightarrow$ sectors per cell $\downarrow$	1	3	4	7	12
1	89.70	21.83	15.65	8.55	4.86
2	-21.97	-20.75	-18.71	-11.70	-13.37
3	-57.46	-41.00	-36.72	-32.28	-24.16
6	-65.98	-49.37	-44.91	-36.79	-30.45

to be like a point source of interference. Under LOS pathloss the values range from 24.89 % to 1.68 % and in the NLOS case the values range from 89.7 % to 4.86 %. That means, e.g., the mean interference of a distant LOS cell is between 1.68 % and 24.89 % larger than the interference generated by an interferer located in the center of the cell.

When sectorized cells are used the geometry and location of co-channel cells have to be considered. The shape of a sector and the relative position of interfering sectors depend on the number of sectors per cell and on the CO. Figures 6.1b and 6.3 show examples of different shapes of sectors and different relative positions between the sectors.
Since the interference power of a co-channel sector is always directed away from the BS of interest, the respective SSs of the sector generating UL interference are always farther away from the interfered BS than the center of the co-channel cell is. This leads to higher pathloss and a reduced interference level.
Analog to the calculation presented for non-sectorized cells, the mean interference generated by a co-channel sector can be derived by Eq. (6.4) where the *area* now refers to the area of a sector. Integrating x and y over the

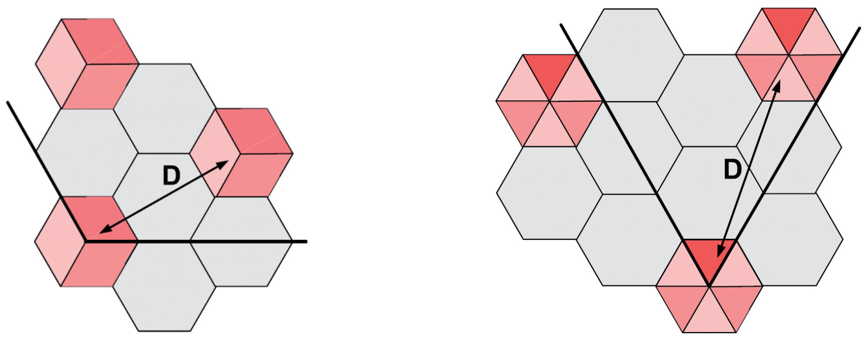

(a) 3-sectored cell using $CO = 4$ **(b)** 6-sectored cell using $CO = 7$

Figure 6.3: Different shapes and positions of sectors

sector area only, Eq. (6.11) calculates the resulting interference correction factor that can be applied to the result from a model where interference is generated at the center of the sectored co-channel cell.
Tables 6.2 and 6.3 list the interference correction in percent for the LOS and the NLOS cases. Since the sector is always farther away from the interfered BS than the center of the cell is, the correction for any number of sectors per cell is always negative. This means that the mean interference generated by the whole sector is lower than the interference generated by a single source assumed located at the center of the co-channel cell.
Analog to a non-sectored network, the corrections under LOS propagation are smaller than with NLOS. For instance, in Table 6.2 the reduction for two or more sectors per cell lies between 8.52 % and 48.18 %, whereas Table 6.3 shows reductions between 11.7 % and 65.98 %. Furthermore, the values depend on the number of sectors and on CO. With increasing CO, the correction factor decreases. With an increased number of sectors per cell the correction factor increases.

6.1.3 Cellular Scenario

The considered cellular scenario consists of hexagonal cells with central BSs and a variable cell radius R, see Figure 6.1. The cell is covered by one to six sectors applying $CO = 3...12$. The SINR for DL and UL, respectively results in

$$
\begin{aligned}
SINR_{DL} &= \frac{S}{N+I} = \frac{P_{Rx}^{S}}{N + \sum_{i=1}^{6} P_{Rx}^{I}} \\
&= \frac{P_{Tx}^{S} * pathloss^{S}}{(N_{th} + NF) + \sum_{i=1}^{6} P_{Tx}^{I} * pathloss^{I}} \qquad (6.12) \\
SINR_{UL} &= \frac{P_{Tx}^{S} * pathloss^{S}}{N + \sum_{i=1}^{6} P_{Tx}^{I} * pathloss^{I} * correction\ factor} \qquad (6.13)
\end{aligned}
$$

where the received signal power P_{Rx}^{S} is calculated from the signal's transmit power P_{Tx}^{S} and the pathloss to the serving BS $pathloss^{S}$. The first tier of six interfering co-channel cells is considered. Their received interference power P_{Rx}^{I} is calculated from the interferers' transmit power P_{Tx}^{I} and the corresponding pathloss to the source of co-channel interference $pathloss^{I}$. In DL co-channel BSs interfere. In UL co-channel SSs interfere, hence Eq. (6.13) additionally considers the interference *correction factor* as introduced in Section 6.1.2, see Tables 6.2 and 6.3. Thermal noise N_{th} of -174 dBm/MHz and a noise figure NF of 5 dB is assumed.
Antenna gain is neglected at the receiver as well as at the transmitter, it will be considered in the capacity estimation in Section 6.4. For dimensioning purposes, especially the SINR at the cell border is of interest where the most robust MCS, i.e., BPSK 1/2 has to be used. The minimum receiver requirement for BPSK 1/2, i.e., 6.4 dB is taken from the 802.16 standard.
The cellular network operates in the upper 5 GHz frequency bands, see Fig. 3.2 licensed for indoor and outdoor WLANs. Eleven non-overlapping frequency channels with a bandwidth of 20 MHz are located between 5.47 and 5.725 GHz. In Europe, the maximum allowed EIRP within these bands is restricted to 1000 mW or 30 dBm. Accordingly both BSs and SSs transmit with 1000 mW.
The suburban C1 Metropol pathloss model from the IST - WINNER project was applied in the analysis. The DL and UL channels of the considered network are assumed orthogonal to each other. This is accomplished either by synchronized switching points that separate DL and UL transmissions all over the TDD network or by applying FDD. It is assumed that during

Table 6.4: Assumptions for dimensioning

Parameter	Value	Comment
thermal noise	-174 dBm/MHz	
noise figure	5 dB	
min. SINR	6.4 dB	required for BPSK 1/2
frequency band	5.47 - 5.725 GHz	
bandwidth	20 MHz	
transmit power	1000 mW	for SS and BS
pathloss model	suburban C1 Metropol	
	LOS and NLOS	see Eq. (6.10) and (6.9)

a transmission, every co-channel cell transmits too and thus generates interference. This worst case analysis is valid for the broadcast phases in a synchronized network and for DL as well as for UL unicast transmission in an fully loaded network.

Figure 6.4 shows the SINR of an example scenario where the cell radius is $R = 1000\,\mathrm{m}$ and $CO = 7$. This results in a co-channel distance of $D = 4583\,\mathrm{m}$. Figure 6.4a shows the DL SINR over the surface area of the scenario. The BS transmitting to a SS in the cell is located in the center while six co-channel BSs interfere this SS. It can be seen that the SINR in the cell's center is quite high but it decreases, substantially, with increasing distance from the BS owing to co-channel cells' interference. Figure 6.4b plots the SINR for a SS traversing the cell across the x-axis. One can see the BS position and the cell border. The two stems, whose height indicates the minimum receiver requirement for BPSK1/2, mark the cell border. It can be seen that the actual SINR level at the border, which is 6.46 dB, is a little above its minimum requirement. Thus, $CO = 7$ has a sufficient SINR throughout the cell, but there is hardly any SINR margin left at the border.

In the following two sections only the SINR level at the cell border is evaluated. The cell radius R is varied and the corresponding SINR at the cell border is plotted. Different COs and number of sectors per cell are considered.

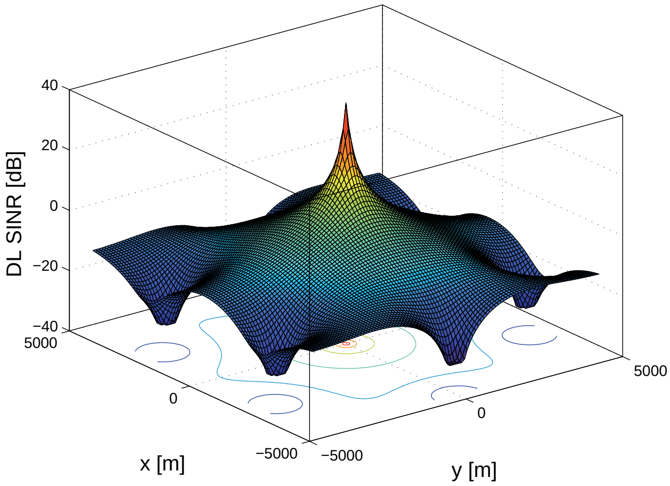

(a) DL SINR over cell surface area

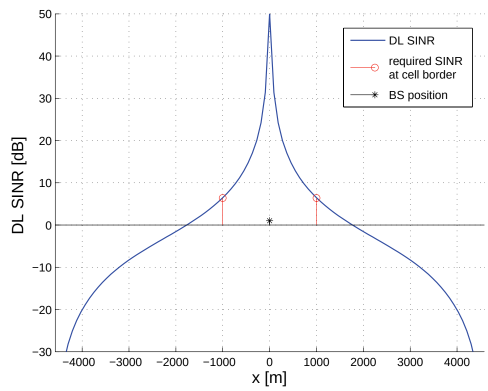

(b) DL SINR while traversing the scenario

Figure 6.4: DL SINR in a cellular network (cell radius 1000 m, $CO = 7$)

6.1.4 Downlink Transmission

In DL, the central BS transmits to the most distant SS, which is located at the cell border. For dimensioning purposes the **SINR at the cell border**, as calculated by Eq.(6.12) is relevant. So it is plotted versus the cell radius in the Figures 6.5 and 6.6. The maximum cell radius (SINR of 6.4 dB) is highlighted by stems.

Figure 6.5 shows the DL SINR at the cell border in the LOS scenario according to Table 6.4. In general, the SINR at the cell border decreases with an increasing cell radius. This is due to the influence of thermal noise. Figure 6.5a shows that the SINR at the cell border increases with increasing CO. The maximum cell radius (SINR of 6.4 dB) is increases accordingly. This is due to the increasing co-channel distance. However, it can be seen that $COs \leq 4$ do not provide a sufficient SINR level at the cell border. For $CO = 7$ and $CO = 12$ the maximum cell radius reaches 1000 m and 1475 m, respectively.

In DL, sectorization reduces the number of interferers simultaneously received at the SS and therewith the interference power level. Figure 6.5b shows the respective SINR at the cell border in a cellular network with $CO = 7$. In the investigated scenario the coverage range can be extended from 1000 m without sectorization to 1625 m with two sectors per cell. A radius of up to 1775 m can be reached when six sector antennas are applied. Note that with

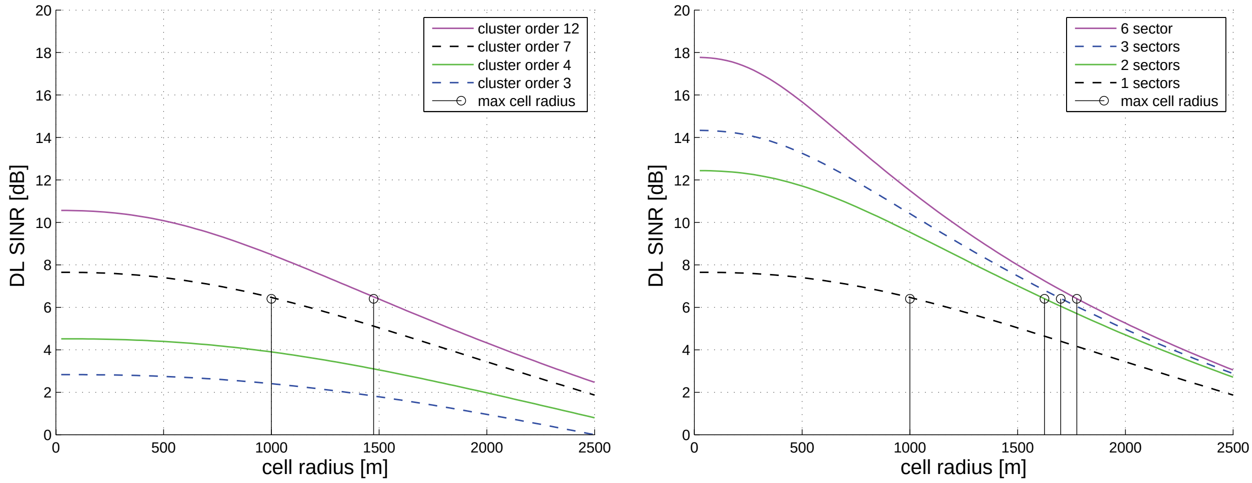

(a) Varying CO **(b)** Different number of sectors ($CO = 7$)

Figure 6.5: DL SINR at the cell border in a cellular LOS scenario

sectorization even $CO = 3$ and $CO = 4$ provide sufficient SINR.
Figure 6.6 shows comparable results under NLOS propagation, where the pathloss coefficient γ is nearly two times higher than under LOS propagation, see Eq. (6.9)). Accordingly, the interference of co-channel cells is substantially reduced. Neglecting noise, inequality (6.14) can be derived from Eq. (6.2) saying that the SIR under NLOS propagation is always higher than with LOS, owing to the difference $\Delta\gamma$ of the respective pathloss coefficient.

$$\left(\frac{S}{I}\right)_{NLOS} = \frac{1}{6}\left(\frac{D}{R}\right)^{(1+\Delta)\gamma} = \left(\frac{S}{I}\right)_{LOS}\left(\frac{D}{R}\right)^{\Delta\gamma} > \left(\frac{S}{I}\right)_{LOS} \qquad (6.14)$$

Figure 6.6a shows the DL SINR at the cell border for NLOS propagation. Compared to Figure 6.5a the SINR at small radii is increased owing to a higher attenuation of interference power. COs down to three may be used for cells with radii smaller than 160 m. However, the carrier and interference signal values attenuate under NLOS faster with distance and are, generally, lower than under LOS propagation. Hence, the influence of the fixed noise level is larger.
Since the level of interference in the NLOS example is rather low, it does not affect the SINR much. In the given NLOS scenario, see Table 6.4, the valid cell radii for different COs vary only between 160 and 190 m.

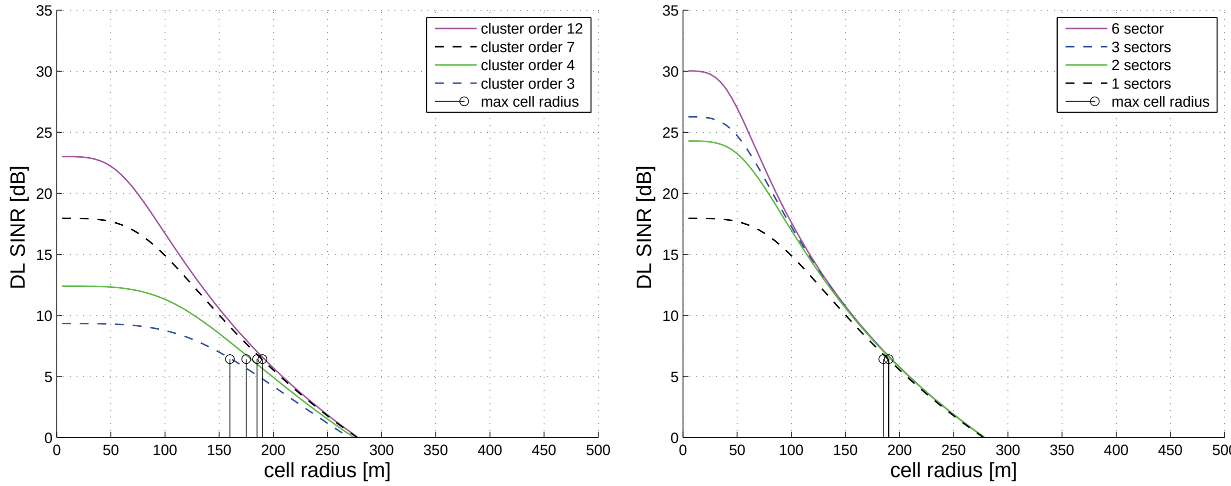

(a) Varying CO **(b)** Different number of sectors ($CO = 7$)

Figure 6.6: DL SINR at the cell border in a cellular NLOS scenario

Figure 6.6b plots the DL SINR at the cell border with $CO = 7$ and for a varying number of sectors. At small cell radii, sectorization tends to increase the SINR at the cell border. For larger radii, the contribution of sectorization to interference reduction is negligible. Sectorization increases the maximum cell radius of the example scenario with $CO = 7$ only from 185 to 190 m with any number of sectors.

Besides clustering and sectorization, several other technical measures may increase the SINR level and thus extend the DL coverage like

BS transmit power affects the SINR in noise-limited scenarios. There, higher power increases the DL coverage area.

DL subchannelization If BSs transmit on some subcarriers of an OFDMA system only, the number of interferers per subcarrier is reduced, benefiting interference-limited systems. If the BS transmit power can be focussed on some subcarriers, which is not allowed in the OFDM-based IEEE 802.16e, spectral density and thus the transmission range increases benefiting noise-limited systems.

BS transmit antenna gain According to Section 4.1.3, adaptive antennas reduce inter-cell interference. If regulations allow exceeding the EIRP by focusing the transmission power and thus increasing the spectral density, the received signal strength at the SSs is increased. This is especially useful in noise-limited systems, see also Section 8.2.1.1.

The techniques mentioned are only valid during the DL data transmission. During the broadcast phase of a synchronized cellular network, where all cells transmit omnidirectionally the interference is highest.

6.1.5 Uplink Transmission

In UL, SSs transmit to the central BS. The most distant SS located at the cell border has to be receive by the BS. Interference is generated by SSs of co-channel cells. As calculated by Eq. (6.13), Figures 6.7 and 6.8 show the SINR perceived at the central BS while the most distant SS located at the cell radius R is transmitting. The UL SINR is plotted versus the cell radius R assuming the parameters given in Table 6.4.

The UL SINR over the cell radius R is quite similar to that of the DL SINR, see Figure 6.5 in Section 6.1.4. On the one hand co-channel interference in UL is a little bit lower than in DL because in UL the receiver is located at the center of the cell and not at the border, which reduces the received interference. On the other hand co-channel interference is increased because in UL, SSs generate co-channel interference and not the central BSs. As it has been outlined in Section 6.1.2, their mean level of interference is slightly higher than that of co-channel BSs.

Figure 6.7a shows UL SINR over cell radius under LOS propagation. $CO = 3$ and 4 do not provide a sufficient SINR. $CO = 7$ and 12 allow for cell radii of 1050 and 1500 m, respectively. Here, the system is interference-limited.

In UL, sectorization reduces the number of SSs that are simultaneously received by the BS sector antenna and it reduces the interference power level (Sections 6.1.1 and 6.1.2). Figure 6.7b shows the UL SINR versus cell radius with $CO = 7$ under sectorization. The maximum cell radius is extended from 1050 m without sectorization to 1550 m with two sectors per cell. A radius of up to 1750 m can be reached with six sectors per cell.

Figure 6.8a shows the UL SINR in a NLOS scenario. Compared to LOS propagation the SINR is increased with small radii and all COs provide proper signal quality with cell radii smaller than 170 m. With larger cell radii, the cell-edge SINR decays rapidly due to the high pathloss coefficient and the resulting influence of noise. Similar to LOS results, the interference under NLOS is such small that the maximum cell radii for different COs are close between 170 and 190 m. Under NLOS propagation the system is noise-limited.

The UL SINR for $CO = 7$ and a varying number of sectors is plotted in

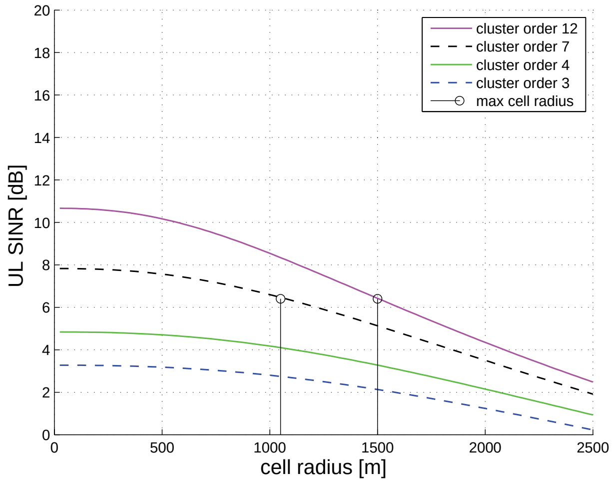

(a) Varying CO

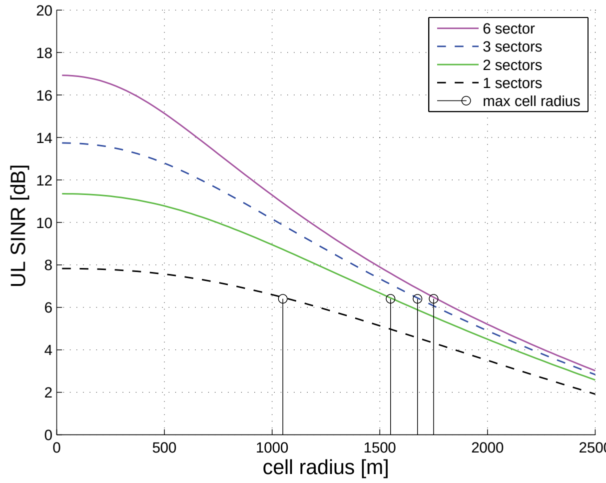

(b) Different number of sectors ($CO = 7$)

Figure 6.7: UL SINR of a SS at the cell border received at the BS in a cellular LOS scenario

Figure 6.8b. For small cell radii, sectorization increases cell-edge SINR, but for larger radii, the interference reduction by sectorization does not change the maximum cell radius much. Sectorization for the UL does not benefit in a noise-limited system: With two instead of one sector antenna per cell the cell border is increased from 185 to 190 m, more sectors do not change that. Besides clustering and sectorization, several other technical measures may increase the UL SINR and thus extend the UL range:

SS transmit power Mobile SSs may be battery powered and control transmit power, thereby reducing the carrier strength and co-channel interference. In an interference-limited system, the cell border is then nearly not affected. In a noise-limited system, reduced transmit power will lead to a reduced coverage range.

UL subchannelization is specified in [IEEE, 2004a]. For the contention-based access phase the standard allows focussing the transmit power to a subset of subcarriers increasing the spectral power density by 12 dB. Increasing the carrier signal and reducing interference, subchannelization is beneficial in both, interference and noise limited systems.

During UL data transmission the standard allows subchannelization but it restricts the spectral power density to stay constant at a level

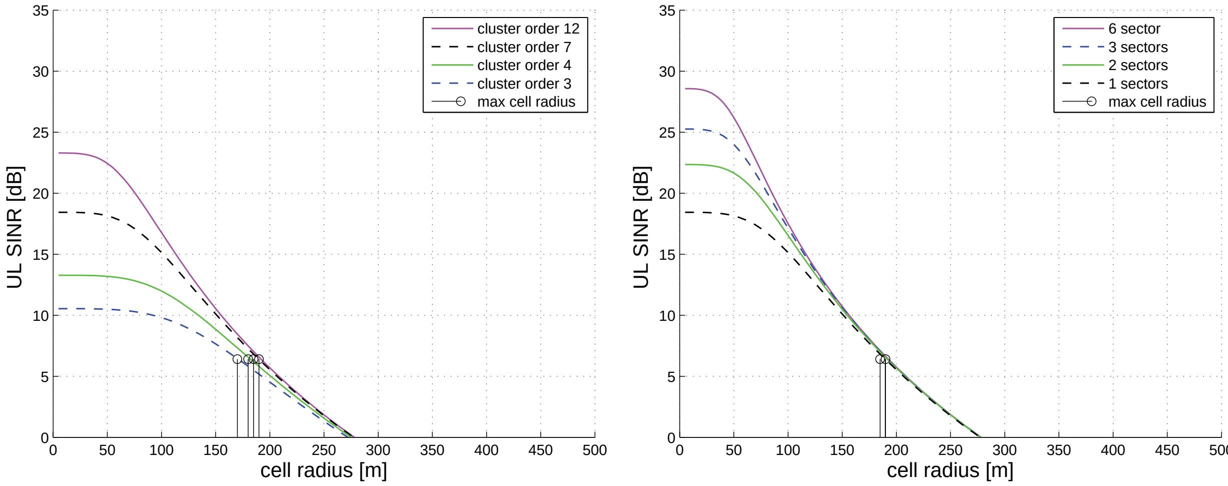

(a) Varying CO **(b)** Different number of sectors ($CO = 7$)

Figure 6.8: UL SINR of a SS at the cell border received at the BS in a cellular NLOS scenario

as if there were no subchannelization. Thus only interference-limited systems benefit from the reduced number of co-channel interferer per subcarrier.

BS receive antenna gain Similar to the observations made for the DL, receive antenna gain is well suited to increase the received carrier signal strength. Adaptive antennas can further reduce received co-channel interference.

Implementing the above mentioned technical measures, the UL transmission will not be the limiting factor in a cellular 802.16 network. A dimensioning approach should focus on the critical synchronized DL broadcast phase.

6.2 Dimensioning Cellular Multi-hop 802.16 Networks

This section investigates the SINR in cellular 802.16 networks that are enhanced by multi-hop transmissions thereby introducing Relay Enhanced Cells (RECs). Again, the UL and DL SINR from/ at the most distant SS is investigated since it is crucial for dimensioning.

6.2.1 Cellular Multi-hop Scenarios

The same parameters as used in the single-hop case were assumed to study multi-hop networks (see Table 6.4). Hence, hexagonal cells are regarded that are clustered according to a given *Cluster Order (CO)*. Inter-cell interference is considered from six co-channel cells of the first tier around the cell under study. The network operates in the 5 GHz spectrum using a channel bandwidth of 20 MHz. The transmit power applied is 1 W for BSs, SSs, and RSs according to the max. EIRP specified by regulations. LOS and NLOS propagation conditions are both taken into account.
DL and UL channels do not interfere each other according to TDD or FDD transmissions considered. According to the design of the multi-hop enabled MAC frame introduced in Section 5, transmissions on the first and the second hop, respectively are assumed perfectly separated in time.
The position of RSs in a REC w.r.t. the serving BS may vary according to the intended goals, namely maximization of either coverage or throughput capacity. The area covered by the RS in a REC is called RS subcell.

Coverage In order to maximize the coverage area of the cell, RS may be placed at the border of the BS's transmission range[1]. The distance between BS and RS is given by the cell radius R, Figure 6.9a. Three RSs at the corners are introduced there to extend the coverage of the BS by a factor of three.

$$A_{multi\,hop} = 3\frac{3}{2}\sqrt{3}R^2 = 3 * A_{single\,hop} \tag{6.15}$$

Due to the extended coverage area of a REC, the co-channel distance D is enlarged by a factor of $\sqrt{3}$, compared to Eq. (6.1).

$$D = 3R\sqrt{CO} \tag{6.16}$$

Throughput By placing RSs within the original BS's coverage area, the SINR and therewith the throughput capacity is increased. A possible placement of 3 RSs is at a distance from the BS ar $R/2$, see Figure 6.9b. The co-channel distance D remains the same as before, see Eq. (6.1). The REC clustering equals that of the single-hop case. Thus,

[1]When assuming no antenna gain on the link BS-RS, the cell area is maximized in this configuration. When gain antennas are used on that link, RSs may be even positioned outside the dashed hexagon shown around the BS in Figure 6.9a

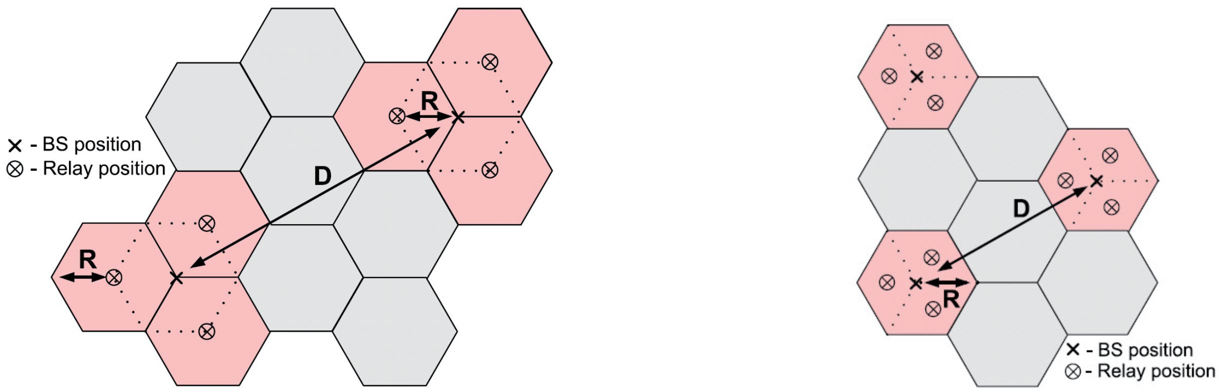

(a) Coverage scenario ($CO = 3$)

(b) Throughput scenario ($CO = 4$)

Figure 6.9: Multi-hop scenarios

the results given in Section 6.1 are directly applicable. Since all results are the same as that for single-hop cell deployments, we focus in the following only on coverage oriented RECs.

SSs are assumed to utilize omnidirectional antennas. In the following sectorization is not considered to be used in multi-hop scenarios although this would be possible. However, directive antennas are assumed as an option at the RS to reduce inter- and intra-cell interference. The antenna angle is then set to 240° with a look direction away from the central BS, see Figure 6.10. The directive antenna's backward signal power is assumed to be zero and the forward signal transmitted undistorted. Due to EIRP limitations no additional antenna gain is assumed for the directive antenna when compared to the omnidirectional one. Thus, the antenna characteristic is assumed perfect. According to Figure 6.10 the RS antenna angle has been chosen so that the other two RSs of the same REC are not affected and the number of co-channel interferers is reduced by a factor of $^2/_3$.

6.2.2 Mean UL Interference Generated by Multi-hop Subcells

In DL, co-channel interference is generated by BSs or by RSs whose positions results from the given cell radius and CO. In UL, interference is generated by SSs whose position may vary in the REC. In order to model co-channel interference generated by randomly positioned SS, in the following, UL co-channel interference is assumed to be generated by a planar transmitter

instead of a centrally located point source. The planar transmitter has the shape of the interfering BS or RS subcell.
A comparable model for interference calculation in multi-hop networks was introduced in [Wijaya, 2005]. However, circular instead of hexagonal cells are assumed there and noise is not considered. Directive antennas and simultaneous operation of RSs are not addressed there.
Analog to the single-hop dimensioning approach, see Section 6.1.2, the interference correction factors for co-channel subcells are calculated. Equations (6.4) to (6.7) can be applied directly. Only the shape of the RS subcell area and their relative position as shown in Figure 6.10 is different to the single-hop approach shown in Figure 6.3. Results are listed in Table 6.5. The value of the interference correction factor depends on the pathloss model, see Eq. (6.9 and 6.10), the scenario type and the antenna characteristic. The factors for omnidirectional antennas are positive. Hence, for omnidirectional antennas interference of a hexagonal planar transmitter is higher than that of a central point source. Apart from $CO = 1$, the corrections for directive antennas are negative. Thus, co-channel SSs are shielded by the RS sector antenna so that their interference level is lower.
In order to increase cell capacity, RSs might operate simultaneously in SDM. Under SDM operation a given RS transmits and receives in parallel to the other two RSs of the REC and in parallel to all RSs of the co-channel RECs. Then interference is generated by three different sources. In order to explain the sources, RSs are numbered 1 to 3 in Figure 6.10.
First, equally numbered subcells of co-channel cells interfere in UL. Like in the single-hop scenario, each co-channel subcell is equally distant from the interfered RS and the subcells look direction is equal to the subcell of interest, e.g., the antenna look direction of subcells numbered with 1 are all pointing to the upper right. Correction factors of these sources are listed in Table 6.5. It can be seen that directive antennas reduce UL interference compared to a point source, because in general, the SSs are located farther away from the interfered RS. Using omnidirectional antennas, the correction is comparable to the single-hop correction listed in Tables 6.2 and 6.3.
Second, in SDM operation, subcells with different numbers across co-channel RECs interfere as well in UL. The distance to the interfering subcells varies and they are located at different positions relative to the interfered RS. For instance, subcells numbered 2 are at the left hand side of the RS. So some interfering SSs are closer to the interfered RS, others are farther. Interference correction factors that take these effects into account are listed in Table 6.6.

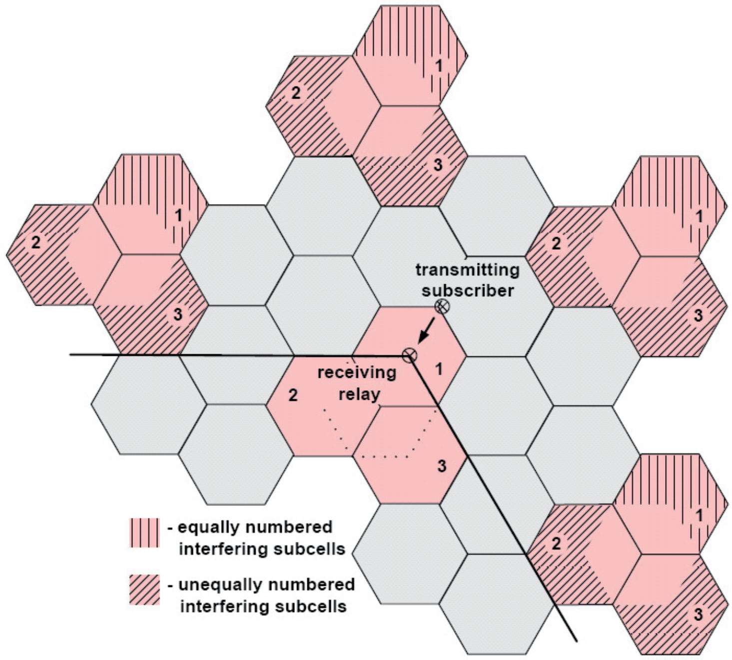

Figure 6.10: Coverage scenario with co-channel interferers (directional antennas, $CO = 4$)

Table 6.5: UL interference correction of equally numbered, distant multi-hop subcells within LOS and NLOS scenarios in [%], directive stays for RSs having 240° antennas, see Figure 6.10

		$ClusterOrder \rightarrow$	1	3	4	7	12
pathloss ↓	scenario ↓	antenna ↓					
LOS	coverage	omni	7.12	2.25	1.68	0.96	0.56
LOS	coverage	directive	-0.58	-2.61	-2.02	-1.20	-1.88
LOS	throughput	omni	5.21	1.68	1.26	0.72	0.43
LOS	throughput	directive	-2.16	-2.02	-2.39	-1.50	-1.42
NLOS	coverage	omni	21.82	6.55	4.86	2.74	1.59
NLOS	coverage	directive	7.62	-1.81	-1.51	-0.96	-2.53
NLOS	throughput	omni	15.64	4.86	3.61	2.05	1.19
NLOS	throughput	directive	2.56	-1.51	-2.59	-1.73	-1.93

Table 6.6: Averaged interference correction of unequally numbered, distant multi-hop subcells within LOS and NLOS scenarios in [%]

		$ClusterOrder \rightarrow$	1	3	4	7	12
pathloss ↓	scenario ↓	antenna ↓					
LOS	coverage	omni	91.29	22.66	15.42	8.37	4.72
LOS	coverage	directive	205.33	64.75	51.21	33.71	21.82
LOS	throughput	omni	82.74	15.42	11.36	6.13	3.49
LOS	throughput	directive	193.16	51.21	39.11	28.06	19.99
NLOS	coverage	omni	503.49	80.39	50.19	25.79	14.04
NLOS	coverage	directive	1033.30	185.50	126.00	74.60	45.80
NLOS	throughput	omni	500.44	50.19	36.09	18.44	10.25
NLOS	throughput	directive	1086.00	126.00	93.80	59	39.50

Table 6.7: Interference correction of multi-hop subcells of the same cell in [%]

	omni antenna	directive antenna
LOS	24.89	-18.15
NLOS	89.68	-16.47

Due to the varying distances, the values of the factors are higher than in Table 6.5.

Third, in SDM operation and with omnidirectional antennas, RSs of the same cell interfere. This interference is heavy since the interfering SSs are close to the interfered RS. Table 6.7 lists the correction factors for planar transmitters to be added to that of point sources.

6.2.3 Time Division Multiplex of RS Subcells

This section outlines the dimensioning of the coverage scenario where the RSs operate orthogonal to each other in TDM. RS are assumed here to use omnidirectional antennas. Figure 6.11 presents the DL SINR for this scenario as calculated with Eq. (eq:sinrDL) and (eq:sinrUL). Instead of co-channel BSs, co-channel RSs interfere during the relay DL subframe and co-channel SSs located in the RS subcell interfere in the relay UL subframe. UL interference correction factors are taken from Tables 6.5, 6.6, and 6.7.

A SS is always assumed served by the best server, i.e., either the BS or the RS. Figure 6.11a shows four SINR peaks at the locations of the central BS and three RSs. The perceived DL SINR of a SS that traverses the REC on line drawn through BS and one RS is plotted in Figure 6.11b. It shows SINR peaks at the positions of the BS and the RS at a distance of 1000 m. The height of the stems at the cell border reflects the minimum required SINR.

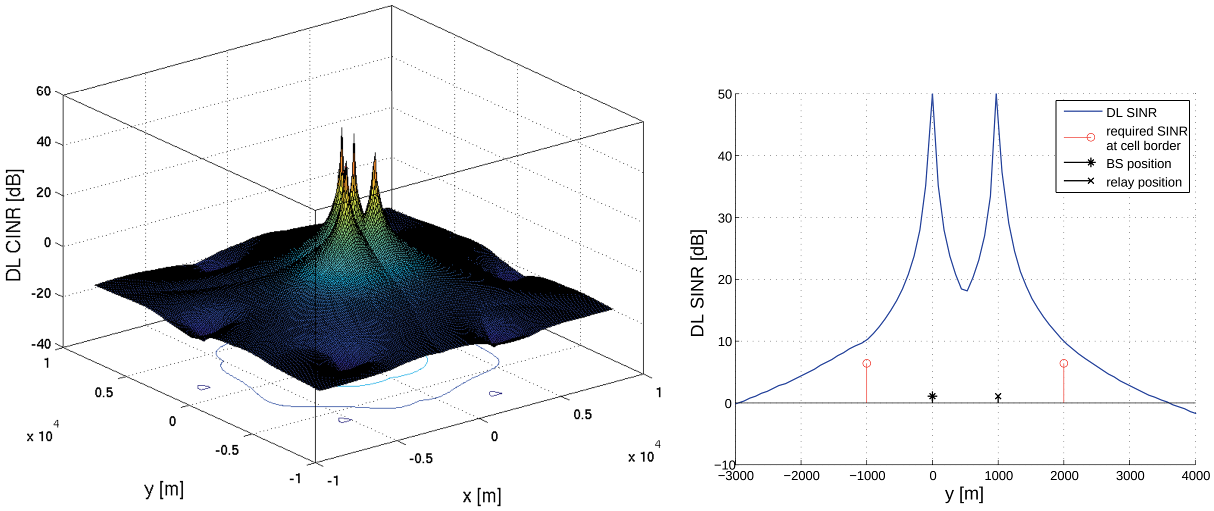

(a) DL SINR

(b) DL SINR while traversing the scenario

Figure 6.11: DL SINR in a cellular multi-hop scenario (TDM, omni antennas, LOS, $CO = 7$))

Since the actually perceived SINR is higher than the minimum required one, all SSs of that particular scenario are able to receive at least with the most robust MCS.

Figure 6.12 shows the DL best server for $CO = 7$, i.e., the BS or RS providing the best SINR level to a potential SS in its vicinity. Additionally, circles are plotted, whose radii R are the central BS and RS subcell radii as depicted in Figure 6.9a. The best server analysis shows that the inner part of the REC is covered by the BS while the outer areas are covered by RSs. Here, RSs use omni antennas, so that the points where BS and RS provide equal SINR levels are inside the BS's subcell.

For dimensioning cellular coverage, the signal quality of the most distant or most interfered SS has to be considered. In a REC, this position is at the outer border of a RS subcell. In Figure 6.12 this is at the coordinates $x = 0\,\mathrm{m}$, $y = 2 * \mathrm{cell\,radius}$. In DL, the most interfered SS is located at the subcell's border of a RS. In UL, the highest interference results if a SS at the outer border of a RS subcell transmits while a close by co-channel SS (or more of them) transmit, too.

In Figure 6.13, the DL and UL SINR that is perceived by a SS at the RS subcell border and the respective RS is plotted versus the BS subcell radius R, which is equal to the RS subcell radius. Note that, the BS radius is the

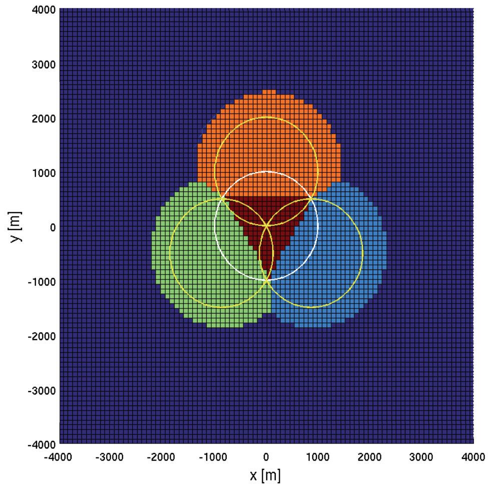

Figure 6.12: DL best server (TDM, omni antennas, LOS, 1000 m cell radius, $CO = 7$)

radius of the inner cell. The overall coverage of the REC is extended by the RS at best to a radius of $2 * R$, see Figure 6.9a.

Figure 6.13a plots the DL case. For $CO > 1$, a valid cell radius can be given. The valid cell radii increases with CO. For single-hop cells, only $CO > 4$ have been found valid, Figure 6.5a. Compared to single-hop cells (1000 m) the maximum cell radii is extended to 1675 m for $CO = 7$. Note that in the REC the most distant SS is 3350 m away from the BS. The overall coverage area of the BS is extended by 3 RSs from 2.598 km^2 to 21.868 km^2, Eq. (6.15). Thus, for $CO = 7$, three RSs extend the coverage area by a factor of 8.4.

The UL, Figure 6.13b, shows very similar SINR values. Like with single-hop cells, REC under LOS propagation are interference-limited. By increasing CO, the inter-cell interference is decreased. This improves the SINR and thus extends the maximum possible cell radius.

Figure 6.14 shows respective results for NLOS propagation conditions. Again, DL and UL signal quality do not differ much. Valid cell radii are smaller than for LOS conditions that range range up to 1675 m instead of 192 m for $CO = 7$. Compared to single-hop cells introduced in Section 6.1 the maximum BS subcell radius cannot be significantly increased (only from 185 m to 192 m for $CO = 7$). However, three RSs increase the coverage area of a single-hop cell from 0.0889 km^2 to 0.287 km^2, which is a factor of 3.23. Under NLOS propagation, the system is noise limited for $CO > 1$, because

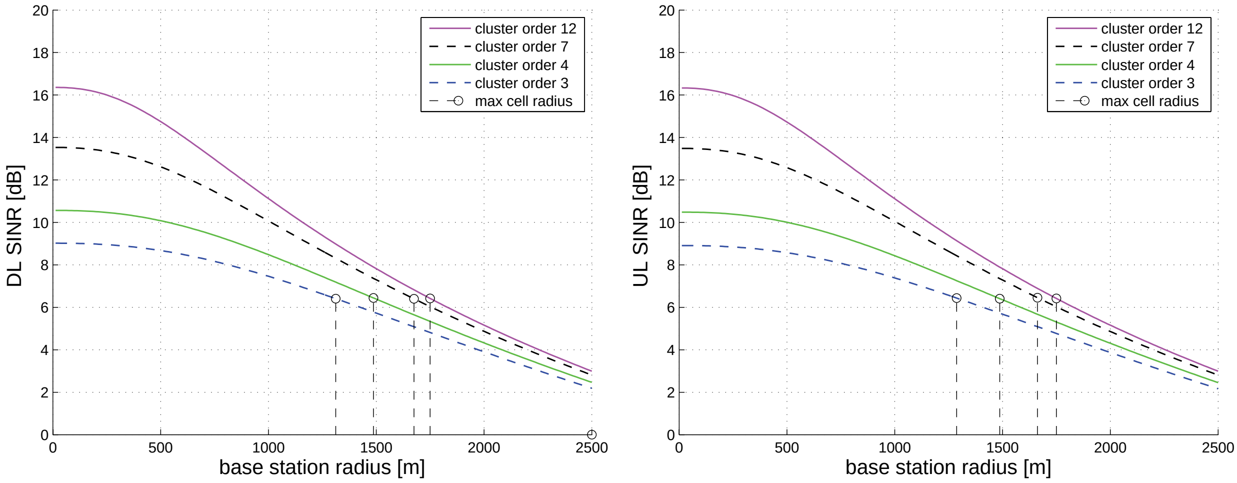

(a) DL SINR **(b)** UL SINR

Figure 6.13: DL and UL SINR at the RS subcell border in a cellular multi-hop scenario (TDM, omni antennas, LOS)

varying CO does not affect the maximum cell radius much. The NLOS attenuation of co-channel interference allows $CO = 1$ to provide a valid cell radius of approximately 150 m.

6.2.4 Space Division Multiplex of RS Subcells

Operating RSs in TDM results in high signal quality and large coverage. However, this way of operation shortens the portion of the MAC frame dedicated to BSs, RSs, and SSs. The MAC frame capacity can be increased by operating RSs simultaneously in time. Then, the frame is divided only into two parts, one dedicated to the BS, the other dedicated for simultaneous use by RSs as explained in Section 5.5.3, Figure 5.6. In the following we study the same scenario as considered in Section 6.2.3, except that the three RSs and their associated SSs transmit and receive concurrently.

Figure 6.15 shows the best server in a REC for $CO = 7$ and a cell radius of 1000 m. Again, the inner part of the cell is covered by the BS. Since the BS operates in a separate subframe, its coverage is equal to the one in the TDM approach. But, the SINR in the RS subcell significantly changed. Only the inner areas of the RS subcells perceive sufficient SINR. In the outer areas of the RS subcells, the SINR drops below 6.4 dB because of increased co-channel interference. Under SDM operation, the number of interferers

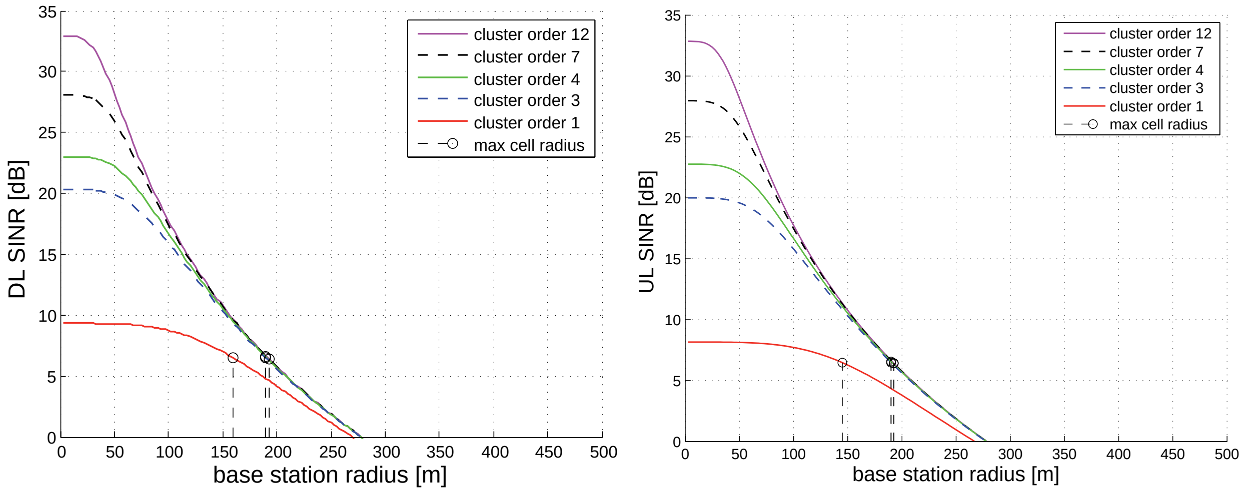

(a) DL SINR **(b)** UL SINR

Figure 6.14: DL and UL SINR at the RS subcell border in a cellular multi-hop scenario (TDM, omni antennas, NLOS)

is more than tripled and especially the two RSs of the same cell are quite close. A REC with a subcell radius of 1000 m cannot be sufficiently covered under SDM operation.

Figure 6.16 plots the DL and UL SINR at the RS subcell border versus the BS subcell radius of the SDM scenario. For the DL case shown in Figure 6.16a only $CO = 12$ is valid. The maximum cell radius is 650 m. For $CO < 12$ the SINR never reaches the minimum threshold of 6.4 dB.

Furthermore it can be seen that the curves for $CO = 7$ and 12 have a knee around 750 m. In REC with small subcell radii (left of the knee), the RS serves the SS located at its subcell border. In REC with larger subcell radii (right of the knee), the SS at the RS subcell border is served by the central BS even if the distance to a RS is much shorter. The interference during the RS subframe is so high that the perceived SINR from the BS surpasses the SINR from the RS. The shape of the curves for $CO \leq 4$ indicates that the SS at the RS subcell border is always covered best by the central BS.

In UL, the results are similar. Only $CO = 12$ allows valid cell radii ranging up to 663 m. The inter- and intra-cell interference degrade the SINR during the RS phase. In UL co-channel interference is even worse, since the sources of interference, i.e., the co-channel SSs might be closer to the interfered receiver than in DL, see Tables 6.5, 6.6, and 6.7.

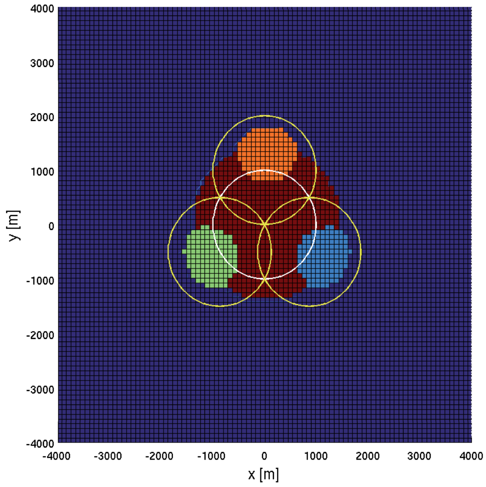

Figure 6.15: DL best server (SDM, omni antennas, LOS, 1000 m cell radius, $CO = 7$)

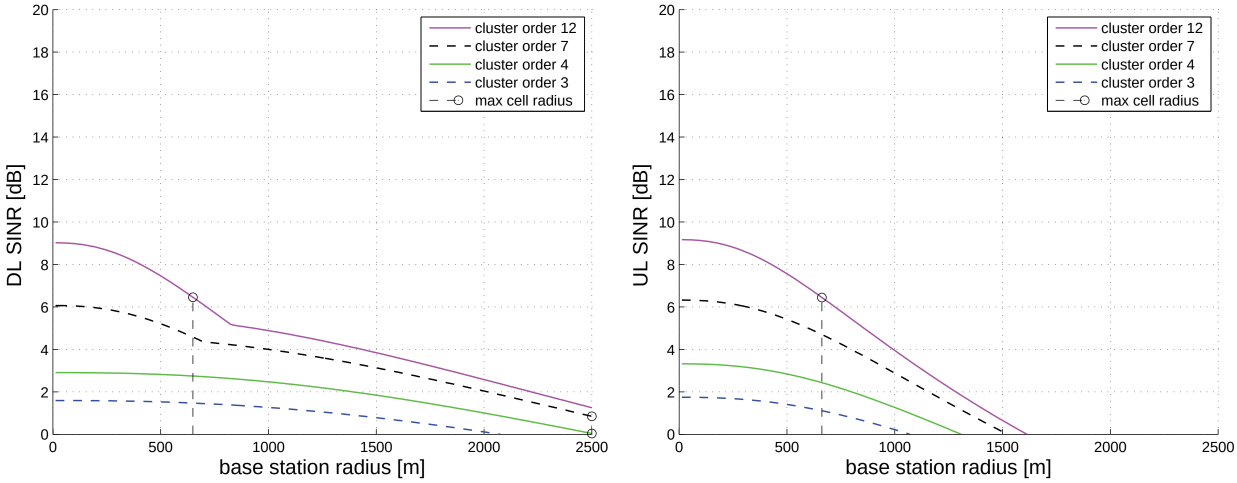

(a) DL SINR **(b)** UL SINR

Figure 6.16: DL and UL SINR at the RS subcell border in a cellular multi-hop scenario (SDM, omni antennas, LOS)

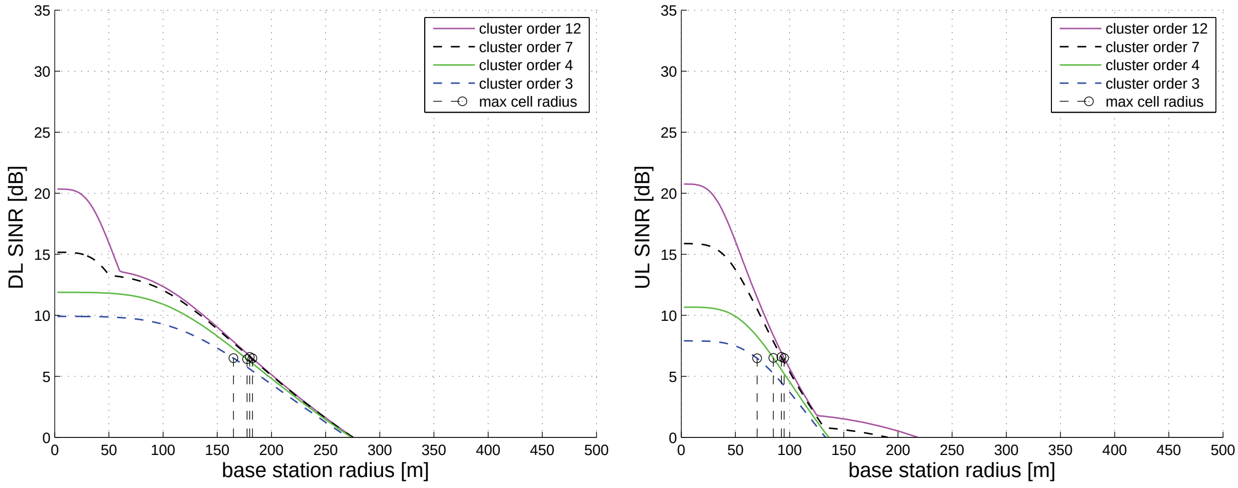

(a) DL SINR **(b)** UL SINR

Figure 6.17: DL and UL SINR at the RS subcell border in a cellular multi-hop scenario (SDM, omni antennas, NLOS)

Figure 6.17 plots results for the SDM scenario under NLOS conditions. The high pathloss degrades inter- and intra-cell interference so that even $CO = 3$ results in a valid deployment. Under NLOS the system is noise-limited. In DL, all CO allow nearly the same maximum cell radius of about 175 m. The UL interference is higher and the valid radius ranges only up to 95 m.

6.2.5 Space Division Multiplex in Combined LOS-NLOS Scenarios

Section 6.2.4 showed that a simultaneous operation of multiple RSs within one cell cannot be recommended due to heavy mutual interference of SSs and RSs. However, in some environments the mutual interference can be limited.

In urban Manhattan-like scenarios, the source and the destination have direct LOS connection along the streets. In contrast, the first tier of interferers is shadowed behind buildings, thus a NLOS path results. The same effect occurs in wide-area scenarios when the BSs are deployed with an antenna tilt. Then, the SSs of the cell have a LOS connection to the BS while the SSs of co-channel cells perceive NLOS attenuation. In both deployments, the carrier signal is attenuated by LOS propagation, while interfering signals are attenuated with NLOS pathloss.

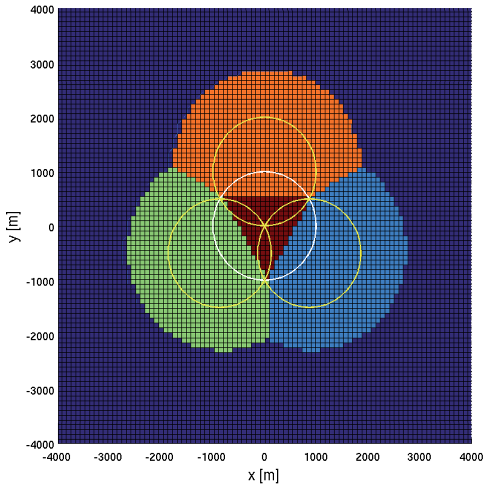

Figure 6.18: DL best server (SDM, omni antennas, LOS-NLOS, 1000 m cell radius, $CO = 7$)

Figure 6.18 plots the best server of such a combined LOS-NLOS scenario. omnidirectional antennas are used throughout. NLOS propagation applies to co-channel interference from distant cells and to intra-cell interference of RSs of the same cell. Thus, the coverage of the REC is extended far beyond the cell border indicated by circles in Figure 6.18. In contrast to the TDM operation, the RSs' coverage areas of the same cell adjoin.

Figure 6.19 plots the DL and UL SINR versus the BS radius of the LOS-NLOS scenario. The curves differ that shown in Figure 6.16 and 6.17. Deploying RECs with small subcell radii, the interferers are close and the system is interference-limited. With larger subcell radii, the interference attenuates faster than the carrier signal, because of its higher pathloss. Due to the relative increase of the carrier signal compared to the interference, the SINR increases, resulting in a maximum of the SINR curve.

Increasing the subcell radius further, the interference becomes more dominated by the noise level and the behavior of the system switches to noise-limited where SINR becomes independent of CO. The attenuation of the carrier signal decreases the SINR. The maximum subcell radius lies far beyond the switching point between interference and noise-limited operation. For all COs the maximum radius in DL is 1825 m. Even $CO = 1$ is valid and results in the same coverage range than all other COs.

The UL SINR, Figure 6.19b, shows a similar behavior, which results in the same maximum cell radius of 1825 m. Only $CO = 1$ restricts the radius to

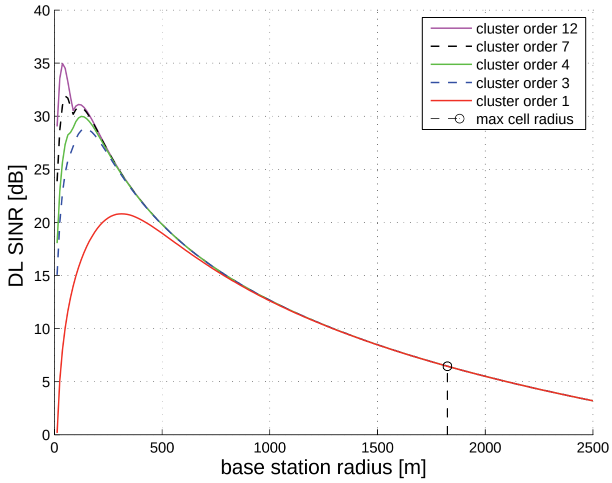

(a) DL SINR

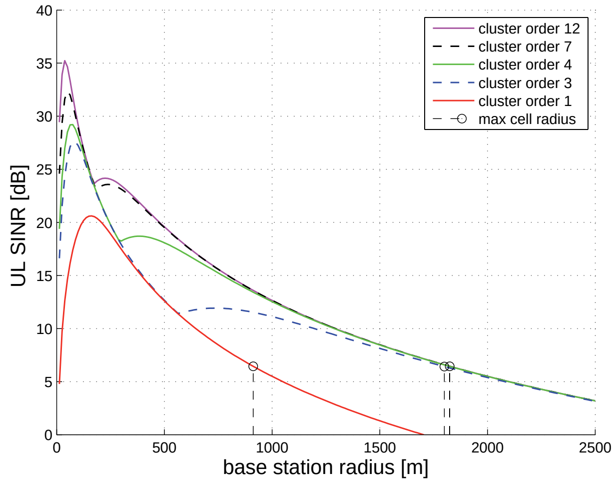

(b) UL SINR

Figure 6.19: DL and UL SINR at the RS subcell border in a cellular multi-hop scenario (SDM, omni antennas, LOS-NLOS)

910 m.

6.2.6 Space Division Multiplex with Directive Antennas

In order to control interference in SDM operation in pure LOS and pure NLOS scenarios, directive antennas can be used at the RSs. As shown in Figure 6.10, the directive antenna may cover the entire RS subcell area but RSs do not interfere with other subcells of its own REC.

Figure 6.20 plots the best server of the scenario shown in 6.10. Since the BS uses omnidirectional antennas and its operation is TDM, the BS coverage area is not affected by directive RS antennas. However, the RS coverage is improved. A SS at the outer RS subcell border can be served up to the example radius of 1000 m. The antenna angle of 240° is visible in Figure 6.20. Due to the ideal antenna shape assumed, the RS does not cover the inner BS subcell.

Figure 6.21 plots the SINR at the outer RS subcell border versus the BS subcell radius, which is equal to the RS subcell radius, under LOS propagation. Compared to SDM operation with omni antennas, see Figure 6.16, the SINR is improved. $COs = 7$ and 12 allow for radii up to 1640 m. This range is close to that of TDM operation shown in Figure 6.13a. However, $CO < 7$ is not sufficient here.

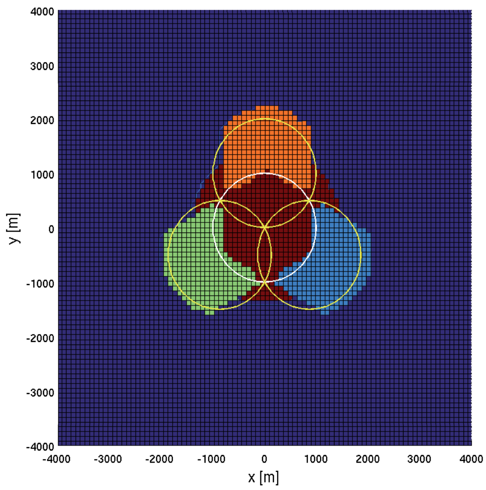

Figure 6.20: DL best server (SDM, directional antennas, LOS, 1000 m cell radius, $CO = 7$)

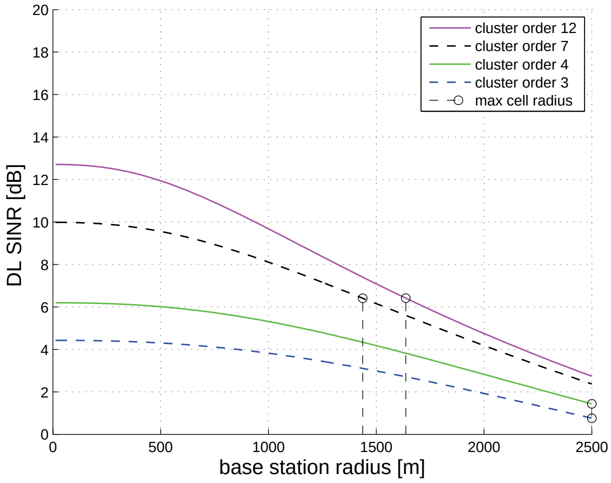

(a) DL SINR

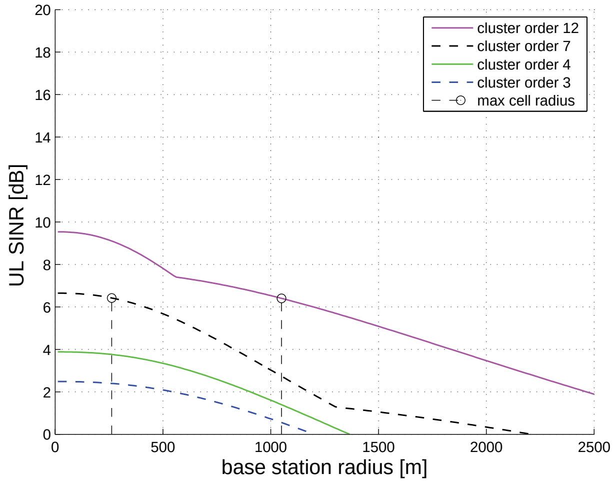

(b) UL SINR

Figure 6.21: DL and UL SINR at the RS subcell border in a cellular multi-hop scenario (SDM, directional antennas, LOS)

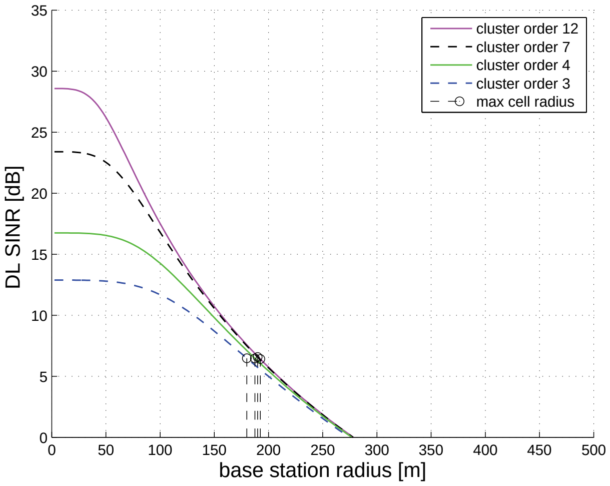

(a) DL SINR

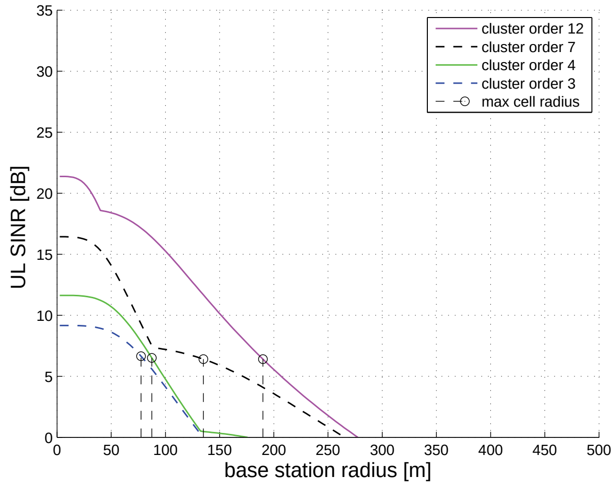

(b) UL SINR

Figure 6.22: DL and UL SINR at the RS subcell border in a cellular multi-hop scenario (SDM, directional antennas, NLOS)

In UL, the same COs are valid, but the achievable range is much smaller, see Figure 6.21b, caused by the random positions of interfering SSs. However, the UL SINR is not the limiting factor, because it can be improved by subchannelization, as introduced in Section 6.1.5.

Under NLOS propagation, Figure 6.22, the system is noise-limited and the reduced interference does nearly not affect the cell size. $CO > 1$ allows for subcell radii of up to 960 m. Compared to TDM operation (Section 6.2.3) cell sizes are approximately the same, a network with $CO = 1$ is not possible. Besides $CO = 12$, Figure 6.21b shows minor performance on UL compared to DL. The transition of the serving station from the BS to the RS at the knee of the curve causes the large variance in valid UL subcell radii.

In LOS-NLOS scenarios, as introduced in Section 6.2.5, the usage of directional antennas causes only a marginal improvement of the coverage range. Within these environments, co-channel interference is already so low that a further reduction by means of directional antennas is not necessary.

Table 6.8: Maximum BS coverage area in cellular single-hop and multi-hop networks (DL, $CO = 7$)

	single-hop coverage		multi-hop coverage		
pathloss	1 sector*	3 sectors	TDM	SDM omni anten.	SDM dir. anten.
NLOS	0.0889 km^2	0.0938 km^2	0.287 km^2	0.253 km^2	0.281 km^2
LOS	2.5981 km^2	7.2892 km^2	21.868 km^2	**	16.117 km^2
LOS-NLOS	8.6533 km^2	8.6533 km^2	25.960 km^2	25.960 km^2	25.960 km^2

* applicable to multi-hop *throughput scenario*
** no valid cell radius

6.3 Coverage Areas of Cellular Single-hop and Multi-hop 802.16 Networks

Table 6.8 summarizes the resulting coverage areas in cellular multi-hop and single-hop deployments. The table contains results for different scenarios using $CO = 7$. In order to calculate the coverage area from Eq. (6.6) and (6.15) subcell radii have been taken from the presented analysis. The maximum valid subcell radii were indicated by stems in the UL and DL SINR figures. Note that, the coverage of the multi-hop throughput scenario equals the single-hop case. SDM operation using omnidirectional antennas in a LOS environment does not result in a valid cell radius. However, Section 6.4 explains that by combining SDM and TDM, the same coverage area as with TDM operation can be achieved.

6.4 Capacity of Cellular Single-hop and Multi-hop 802.16 Networks

The resulting cell capacity can be derived from the SINR in a cell. The link capacity at a certain position $Cap(x,y)$ is a function of the perceived SINR. Gross data rates for each MCS in the scenario as described in Table 6.4 are known from [Hoymann, 2005]. If perfect link adaptation is assumed, the perceived signal quality (SINR) can be converted into the correspondent achievable throughput capacity, see Figure 6.23.
SSs served by RSs perceive a data rate influenced by the link capacity of both hops involved in tandem. The overall capacity can be calculated by Eq. (6.17), where $Cap_{hop\,1}$ is the capacity of the BS-RS link and $Cap_{hop\,2}$ is the RS-SS link capacity [Irnich et al., 2003]. In order to increase the link

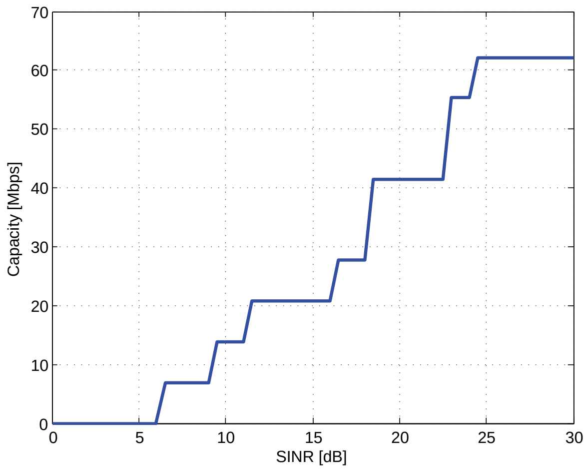

Figure 6.23: Link capacity vs. SINR

capacity on the first hop, the RS may apply receive antenna gain [Esseling et al., 2005], where whereby by the SINR on the first hop is improved and a higher MCS could be applied.

$$\frac{1}{Cap_{overall}} = \frac{1}{Cap_{hop\,1}} + \frac{1}{Cap_{hop\,2}} \tag{6.17}$$

Using the relation between SINR and capacity in Figure 6.23, from Eq. (6.17) the capacity of a SS traversing a REC can be calculated. Figure 6.24 shows the DL-LOS capacity of a SS traversing the REC, Figure 6.9, for different assumptions made for the antennas. The route of the SS is a straight line from one cell border via BS and RS to the opposite cell border. The positions of BS, RS and cell edge are marked. The dashed line shows the TDM case with omniantennas that corresponds to Figure 6.11b. It can be seen that the main cell is covered by the BS and the RS extends the coverage area to the right hand side.
If the RS applies receive antenna gain, it can improve its SINR on the first hop, as visible from the solid line graph in Figure 6.24 resulting from 14 dBi receive antenna gain.
The dashed-dotted line in Figure 6.24 shows that SDM operation of RSs reduces channel capacity when using omnidirectional antennas. However, since three RSs operate simultaneously, the dotted line represents the tripled SDM capacity. It can be seen that at some distance SDM is favorable. Later it will be shown that the overall cell capacity can be increased in some

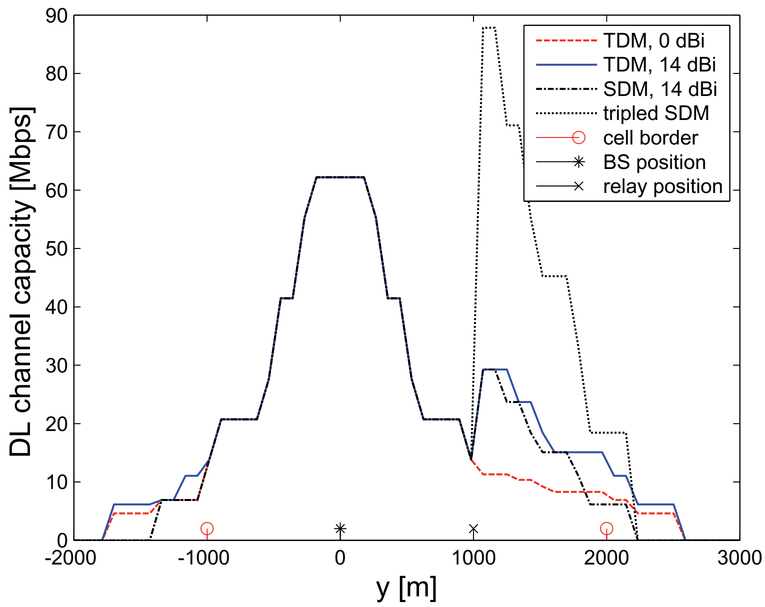

Figure 6.24: DL capacity while traversing the scenario (omni antennas, LOS)

scenarios due to the SDM operation.
The additional interference from SDM operation affects the maximum coverage range: the cell border cannot be covered completely. To avoid this drawback, operation could be switched from SDM to TDM at large distance. The link capacity of the SS traversing the REC would then follow the envelope of the better of both curves and the entire cell area is covered then. From the capacity of a single SS at a given position, the mean cell throughput capacity can be calculated. Equation (6.18) gives the reciprocal cell capacity of a circular single-hop cell as the integral of the reciprocal capacities at distance r to the BS [Habetha, 2002]. The variable to be integrated (ρ) is the distance to the BS r normalized to the cell radius R.

$$\frac{1}{Cap_{cell}} = \int_0^1 \frac{1}{Cap(\rho)} 2\rho \, d\rho \quad with \qquad \rho = \frac{r}{R} \tag{6.18}$$

An ideal single-hop cell has the shape of a hexagon. A REC has an area size of three hexagons (see Figure 6.9a). Thus, the REC capacity can be calculated from its constituents, namely single-hop and multi-hop throughput

Table 6.9: Cell capacity and area spectral efficiency of a single-hop cell ($CO = 7$, LOS/LOS-NLOS: $R = 1000\,\mathrm{m}$, NLOS: $R = 150\,\mathrm{m}$)

	cell capacity [Mbps]		area spectral efficiency [$^{\mathrm{bps}}/_{\mathrm{Hz\ km}^2}$]	
	1 sector	3 sectors	1 sector	3 sectors
LOS	12.9747	21.0642	0.2497	0.4054
LOS-NLOS	28.9193	28.9193	0.5566	0.5566
NLOS	44.2868	47.9382	37.879	41.003

capacity.

$$\frac{1}{Cap_{cell}} = \int_{cell\,area} \frac{1}{Cap(x,y)}\,dxdy \tag{6.19}$$

Note that, the DL SINR values and therewith the actual link capacity $Cap(x,y)$ have been calculated assuming none of the options contained in the IEEE 802.16 standard, like subchannelization and Advanced Antenna System (see Sections 6.1.4 and 6.1.5). That would improve SINR and thereby cell capacity.

Tables 6.9, 6.10, and 6.11 give the cell capacity Cap_{cell} and the area spectral efficiency for single-hop and multi-hop cells. The coverage area depends on the propagation conditions. According to the valid (sub-)cell radii calculated in Sections 6.1 and 6.2 for $CO = 7$, the BS (sub-)cell radius under LOS and LOS-NLOS conditions is set to $R = 1000\,\mathrm{m}$. Under NLOS conditions the cell radius is set to $R = 150\,\mathrm{m}$. Single-hop cell and multi-hop *throughput* RECs cover areas of $2.598\,\mathrm{km}^2$ and $0.0585\,\mathrm{km}^2$, respectively, see Eq. (6.6). Multi-hop *coverage* RECs triple the coverage area resulting in $7.7942\,\mathrm{km}^2$ and $0.1754\,\mathrm{km}^2$, respectively, see Eq. (6.15)
Table 6.9 gives the cell capacity and the area spectral efficiency for single-hop cells. Table 6.10 addresses multi-hop *throughput* REC, where RSs may operate in TDM or SDM and where RSs may take advantage of 14 dBi receive antenna gain.
Figure 6.25 gives the cell capacity of single-hop cells and multi-hop *throughput* REC. Single-hop cells under LOS conditions benefit from sectorization to increases cell capacity significantly. Under NLOS condition the benefit of sectorization decreases. In LOS-NLOS scenarios sectorization does not improve capacity at all. Under NLOS conditions cell capacity reaches its maximum, but the coverage area of the cell is small.

Table 6.10: Cell capacity and area spectral efficiency of a *throughput* REC ($CO = 7$, LOS/LOS-NLOS: $R = 1000\,\mathrm{m}$, NLOS: $R = 150\,\mathrm{m}$)

			cell capacity [Mbps]		area spectral efficiency [$^{\mathrm{bps}}/_{\mathrm{Hz\ km}^2}$]	
			gain 0 dBi	gain 14 dBi	gain 0 dBi	gain 14 dBi
LOS	TDM	omni	15.4676	20.0534	0.2977	0.3859
LOS	SDM	omni	13.0587	13.6253	0.2513	0.2622
LOS	SDM	directive	17.0894	20.4717	0.3289	0.3940
LOS-NLOS	TDM	omni	29.6229	32.1805	0.5701	0.6193
LOS-NLOS	SDM	omni	39.9708	45.8409	0.7692	0.8822
LOS-NLOS	SDM	directive	39.9888	45.8647	0.7696	0.8827
NLOS	TDM	omni	31.6841	35.0398	27.1005	29.9707
NLOS	SDM	omni	32.0656	32.7795	27.4268	28.0374
NLOS	SDM	directive	38.5744	42.1917	32.9940	36.0880

Looking at TDM modes of multi-hop *throughput* RECs, it can be seen that receive antenna gain at the RS can improve the cell capacity under all propagation conditions when compared to no gain. When using omnidirectional antennas, SDM operation of RSs is only beneficial under LOS-NLOS propagation conditions. Under pure LOS and pure NLOS propagation, the cell capacity of SDM operation drops below that of TDM.
SDM combined with directive antennas under NLOS propagation increases the cell capacity compared to TDM operation. Under LOS condition, directive antennas increase cell capacity up to that of TDM operation.
Comparing single-hop cells and multi-hop *throughput* REC, it can be seen that under LOS and NLOS conditions, the multi-hop capacity is less or equal to the single-hop capacity. When taking the MAC overhead into account needed to control multi-hop transmissions, a single-hop deployment is preferential. In deployments where RS subcells are highly shadowed from each other, i.e., under LOS-NLOS conditions, a multi-hop deployment increases cell capacity, especially in SDM mode. However, the additional MAC overhead and the cost for deploying and operating RSs must be faced.

Table 6.11 gives the cell capacity and the area spectral efficiency of the multi-hop *coverage* REC. Figure 6.26 visualizes these results. Like in the multi-hop *throughput* deployments, RS receive antenna gain increases cell capacity of the multi-hop *coverage* deployment under all propagation conditions. Since RSs in the *coverage* deployment are farther away from the BS compared to the *throughput* deployment, the advantage from receive antenna gain on the

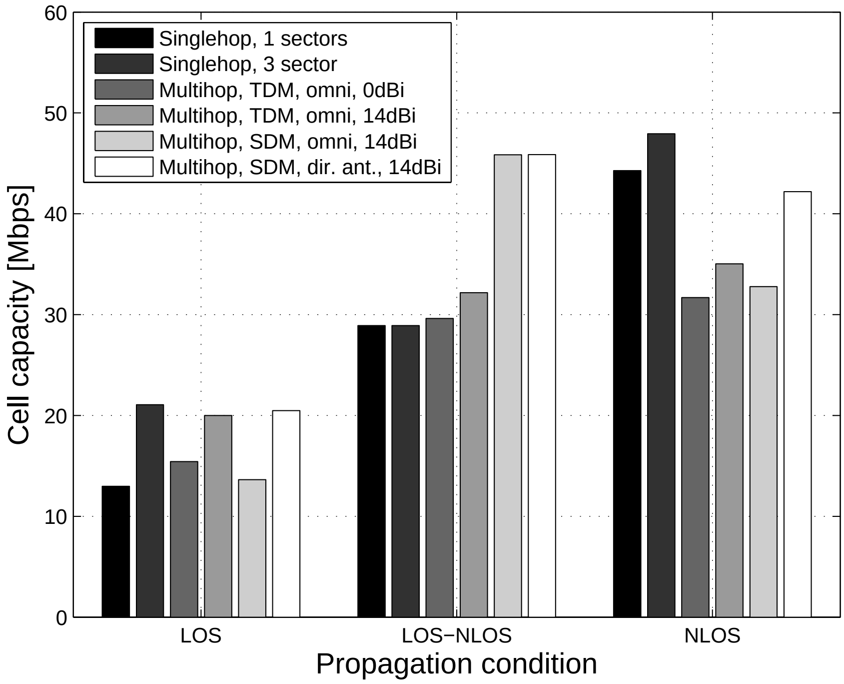

Figure 6.25: Cell capacity of single-hop cells and multi-hop *throughput* REC as given in Tables 6.9 and 6.10

Table 6.11: Cell capacity and area spectral efficiency of a *coverage* REC ($CO = 7$, LOS/LOS-NLOS: $R = 1000\,\mathrm{m}$, NLOS: $R = 150\,\mathrm{m}$)

			cell capacity [Mbps]		area spectral efficiency [$^{\mathrm{bps}}/_{\mathrm{Hz\ km}^2}$]	
			gain 0 dBi	gain 14 dBi	gain 0 dBi	gain 14 dBi
LOS	TDM	omni	11.8409	19.1668	0.0760	0.1230
*LOS	SDM	omni	15.1573	17.3118	0.0972	0.1110
**LOS	SDM	omni	11.3091	14.1873	0.0725	0.0910
LOS	SDM	directive	21.1643	29.4440	0.1358	0.1889
LOS-NLOS	TDM	omni	16.7554	22.9660	0.1075	0.1473
LOS-NLOS	SDM	omni	27.0160	44.6449	0.1733	0.2864
LOS-NLOS	SDM	directive	27.0160	39.2832	0.1733	0.2520
NLOS	TDM	omni	13.4483	24.1832	3.8342	6.8949
NLOS	SDM	omni	23.0167	34.6783	6.5623	9.8872
NLOS	SDM	directive	25.4360	41.2509	7.2521	11.7611

* 15.2% uncovered cell area

** uncovered area served in TDM, omni mode

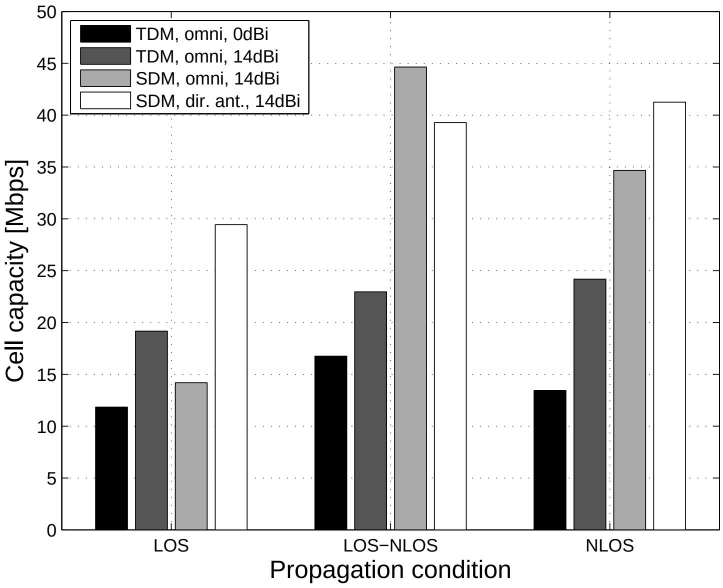

Figure 6.26: Cell capacity of multi-hop *coverage* REC as given in Table 6.11

first hop is larger.

SDM operation of RSs applying omnidirectional antennas further increases the cell capacity under LOS-NLOS and NLOS conditions since interference is attenuated there much more than under LOS propagation. Additionally, the distance between simultaneously operating RSs is larger in the *coverage* scenario compared to the *throughput* scenario. Again, omnidirectional antennas at the RSs generate too much inter- and intra-cell interference in the LOS environment so that the cell capacity with SDM operation drops below that of TDM.

SDM operation of RSs with directive antennas outperforms all other modes of operation under LOS and NLOS conditions. A significant capacity increase is visible. Under LOS-NLOS conditions, the mutual interference of concurrently operating RSs is negligible even with omnidirectional antennas owing to their large distance and NLOS attenuation of interference. Thus, the reduced RS coverage area (240° instead of 360° with directive antennas) reduces cell capacity.

In order to finally compare single-hop and multi-hop *coverage* deployments, the different sizes of their coverage areas have to be considered. By simply comparing area spectral efficiency, single-hop deployments appear beneficial because of higher cell capacity and smaller coverage area. Under all propagation conditions, the maximum area spectral efficiency of multi-hop *coverage* deployments (LOS: 0.1889 $^{\mathrm{bps}}/_{\mathrm{Hz\ km}^2}$, LOS-NLOS: 0.2864 $^{\mathrm{bps}}/_{\mathrm{Hz\ km}^2}$, NLOS: 11.761 $^{\mathrm{bps}}/_{\mathrm{Hz\ km}^2}$) is lower than the efficiency of single-hop deployments even without sectorization (LOS: 0.2497 $^{\mathrm{bps}}/_{\mathrm{Hz\ km}^2}$, LOS-NLOS: 0.5566 $^{\mathrm{bps}}/_{\mathrm{Hz\ km}^2}$, NLOS: 37.879 $^{\mathrm{bps}}/_{\mathrm{Hz\ km}^2}$). Hence, the benefit of multi-hop deployments is the cost-efficient coverage of a service area. Thus, a fair comparison must take Capital Expenditure (CAPEX) and Operational Expenditure (OPEX) into account, which is out of scope of this thesis.

CHAPTER 7

Simulation Environment - Wireless Network Simulator

The WNS is a sophisticated framework for event driven, stochastic system level simulation. Its highly modular structure allows for performance evaluation of various wireless systems such as IEEE 802.16, IEEE 802.11, UMTS, and the WINNER Protocol Stack (WinProSt). It has been developed at ComNets and contains a wide range of modules to analyze cellular mobile radio networks at almost any level of detail. The WNS provides modules for the following layers:

1. *Multimedia load generator*, e.g. voice, video, and web browsing
2. *Transport Layer*, e.g., Transmission Control Protocol (TCP) and User Datagram Protocol (UDP)
3. *Network Layer*, IP
4. *Radio Access Technology* including Logical Link Control (LLC), Radio Link Control (RLC), and MAC
5. *Interference Calculation* including smart antennas and the link-to-system interface

To enable the fast and reliable development of new modules, WNS provides a set of support libraries. A simulator finally consists of one or more modules loaded at runtime by the runtime environment. Each module has a specific task and roughly fits into one of the above categories. The set of support libraries includes:

1. SDL Performance Evaluation Tool Class Library (SPEETCL)
   A library used by simulators implemented in the Specification and Description Language (SDL). SPEETCL functionality currently in use by non-SDL based simulators is the event scheduler, probes, random number generation, and basic data types for communication protocols.
2. Radio Interference Simulation Engine (RISE)
   A library supporting the simulation of radio interference. Modules

for interference calculation are based on this library. It provides the beamforming antennas as described in Chapter 4.

3. WNS support library (libWNS)
   Among others, it features the following functionality:
   - Module handling support.
   - Logging system.
   - Configuration facilities.
   - Access to SPEETCL mechanisms including probes, probability distributions and event queuing.
   - Template based containers, extending those available in the Standard Template Library (STL)
   - Layer Development Kit (LDK) - The FUN based toolbox to model different radio access technologies.

The remainder of this chapter details the most important WNS modules used for the performance evaluation of the SDMA enabled IEEE 802.16 system in Chapter 8.

7.1 Functional Units in a Functional Unit Network

In the last years, a significant amount of research at ComNets has focused on flexible and reconfigurable protocol stacks [Berlemann et al., 2005; Schinnenburg et al., 2005]. To achieve a high degree of flexibility, a framework for modeling protocol stacks is proposed in [Schinnenburg et al., 2005]. Especially the DLC layer of the ISO/OSI reference model is targeted by using a network of small building blocks, called Functional Units (FUs). Each FU is supposed to contribute just a single cohesive functionality. As all FUs have to provide the same interface and data handling functions, they can be almost arbitrarily aggregated to form a Functional Unit Network (FUN). A FUN models an entire protocol layer.
PDUs together with Protocol Control Information (PCI) are bundled into an entity that is called a *compound*. Outgoing data is fed into a FU by means of a *DATAreq()* function whereas incoming data is indicated by the *DATAind()* function. Whenever a compound arrives, a FU may choose to mutate, drop, buffer or forward the compound or even inject new compounds into the FUN. PCI is encapsulated into the compounds in a way that allows a FU to provide a transparent service to a connected FU. That means a FUs does not need to interpret the PCI of another FU unless it aims to

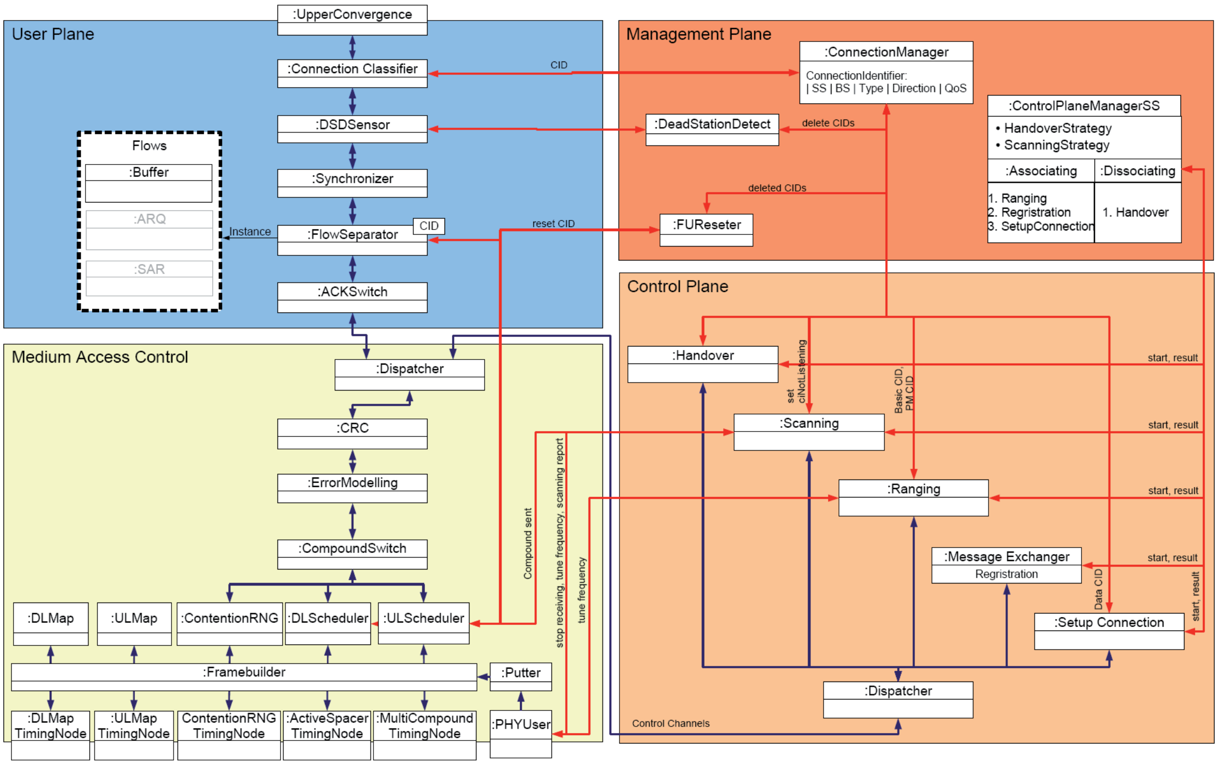

Figure 7.1: WiMAC Functional Unit Network representing the MAC layer at the BS

use it. FUNs are the basis of the WNS implementations for IEEE 802.16, WinProSt, IP, or TCP.
To facilitate the implementation of new protocols, the library LDK has been developed. It contains protocol functions like ARQ and SAR used in various systems' access protocols. Each function is implemented as a FUs or FUNs.

7.2 WiMAX MAC Layer

Figure 7.1 shows the structure of the BS FUN of the WiMAX MAC Layer (WiMAC). The multimedia traffic generator, the transport and the network layer on top, as well as the PHY layer including interference calculation below the WiMAC are not shown in the figure. The WiMAC module can be separated into a Radio Link Control (RLC) and a Medium Access Control (MAC) sublayer. The RLC sublayer is further subdivided into a user plane, control plane and management plane.

7.2.1 User Plane

The user plane handles user data and performs the corresponding RLC layer functionality such as classification of SDU to connections, QoS control, SAR, ARQ, and flow control.
The traffic generator requests data transmissions through the Data Link Layer (DLL) SAP which directs SDUs to the upper convergence FU of the station. There, the SDU enters the WiMAC, see Figure 7.1. First, the header is prepended which transforms an SDU into a PDU. The classifier FU identifies PDUs with the help of the Connection Manager. The classifier marks the PDU with the CID that the connection manager has reported. Depending on the CID the flow separator FU directs the PDU to the corresponding buffer FU. The PDU stays in the buffer until the scheduler requests a compound. Then, the respective PDU passes the SAR and the ARQ FUs.
Other FUs, e.g., the Synchronizer, or the ACK Switch are used for internal purposes, such as flow control of compounds.

7.2.2 Medium Access Control

Access to the radio resource is controlled by the MAC. It offers transmission services to the user plane as well as to the control plane. PDUs carrying user data and PDUs carrying control information pass the CRC and the error modeling FUs. A CRC is appended used at the receiver to detect erroneous PDUs. Besides its higher priority, there is no difference in the handling, transmission and reception of a control and a data PDU.
The basic part of the WiMAC is the frame configuration framework, which is composed of the frame builder and its corresponding FUs. Having passed the DL scheduler PDUs are sent through the respective timing node.
Incoming traffic takes the reverse path through the FUN. Payload PDUs go through the error modeling FU which determines a Packet Error Ratio (PER) for each PDU received. The CRC FU drops the PDU if a bit error has been detected. Finally, PDUs carrying user data are forwarded to the user plane while PDUs carrying control information are forwarded to the control plane.

7.2.2.1 Frame Configuration Framework

The frame configuration framework, see Figure 7.2, allows modeling frame based protocols. The MAC frame is constructed from subsequent logical

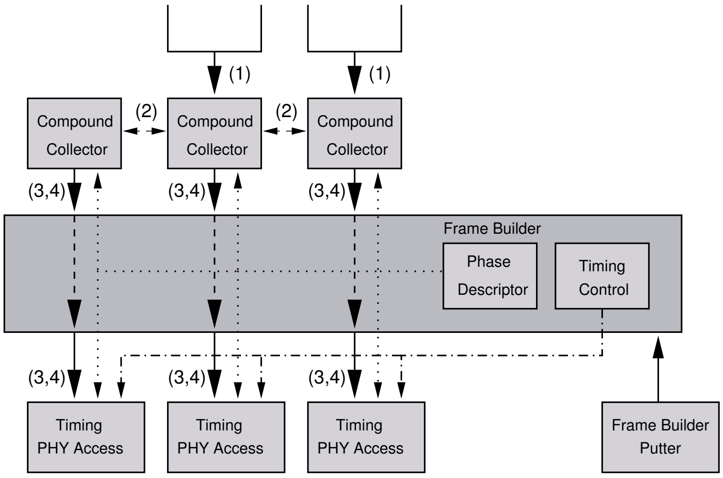

Figure 7.2: Frame Configuration Framework

phases. For instance, a phase might be the DL data phase, the broadcast phase, or the contention access phase, as shown in Figure 3.10. Some of these phases generate compounds themselves, e.g., the broadcast phase generates control information. Other phases just processes compounds from upper FUs, e.g., the DL data phase transmits DL MAC PDUs. In single-hop systems, each phase usually occurs only once in a MAC frame. In multi-hop networks, some phases might occur several times, e.g., one DL data phase might be configured to handle data on the first hop and a another one to handle data on the second hop.

Compound Collector FU is created in WiMAC for each phase, see Figure 7.2. It completely specifies the type of compounds to be created or handled during the specific phase. A set of compound collectors fully describes the whole MAC frame. The timing nodes provide access to the PHY layer and receive / transmit the given compounds at the specified time instants.

Timing control manages the correct sequence of phases. The Phase Descriptor is the central configuration element of a phase. With its help, the frame builder connects compound collectors and timing nodes and sets duration of phases and related policies. An example processing of a frame is given by the numbers and arrows in Figure 7.2. During the previous frame, compounds are collected (1). Before the frame start, compounds are scheduled and the resulting resource allocation is exchanged between Compound Collectors (2). At the frame start, phases are activated subsequently and the corresponding compounds are transmitted via the Timing nodes (3,4).

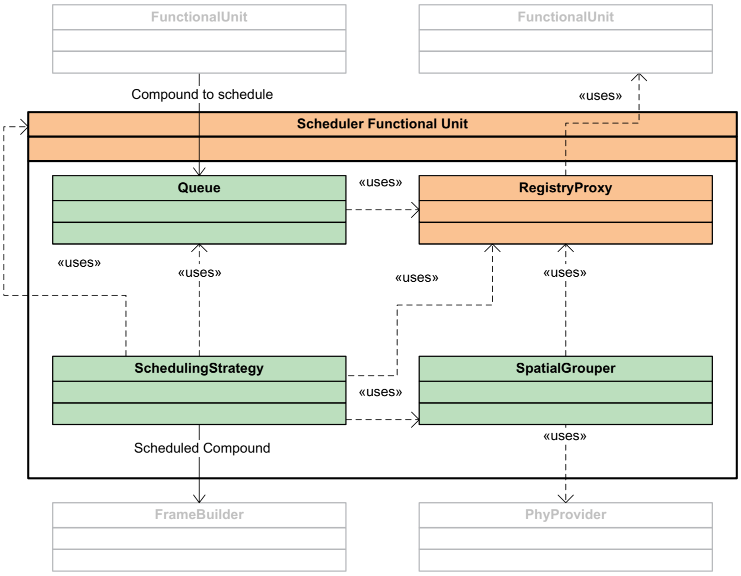

Figure 7.3: Internal structure of scheduler module

7.2.2.2 SDMA Scheduler

Compound Collectors of the frame configuration framework schedule UL and DL data transmissions. Hence, a combined TD-/SDMA scheduler is located there. The scheduler is a single FU offering the standard FU interface. Internally, the Scheduler FU consists of four modules, see Figure 7.3.
The scheduler FU creates, configures, and connects the internal modules. It provides the standard-FU functions to control the flow of compounds in the WiMAC FUN. Flow control calls are forwarded to the Queue module. The scheduler FU also provides functions for the FrameBuilder in order to create the signaling information to be transmitted in DL and UL MAPs.

Spatial Grouper implements the grouping algorithm, see Section 4.4. It takes the set of currently active SSs and the group size limit as input parameters and returns a data structure that contains the groups of SSs to be served. For each SS a SINR estimation and a pointer to the SS-specific beamforming pattern is returned. The pattern is adapted to each SS and takes the other group members into account. SINR estimation and thus the grouping differs for DL and UL.

Queue receives packets or compounds from the scheduler FU to store them until they are scheduled for transmission. Each queue module contains multiple queues, one for each CID known.

Scheduling Strategy performs the actual packet scheduling. It receives the set of available resources and triggers all other scheduler modules. After the strategy has decided when and how to schedule a compound, it provides this information by means of a packet transmission start and end point in time, the used beamforming pattern, and MCS to the scheduler FU.

Registry Proxy hides system specifics by forwarding and translating system queries. For instance, CIDs are mapped onto system specific values.

7.2.3 Control Plane

The control plane is realized based on control FUs. These FUs are only connected downwards (see Figure 7.1) because they generate compounds, so called MAC management messages themselves. The peer control plane will react to a control message received. Management messages are handed to the MAC via the dispatcher FU, where they are multiplexed with regular PDUs carrying user data.
The main function of the control plane is mobility support. The functionality to support communication of mobile SSs is contained in the following FUs.

Scanning is the process of measuring the carrier signal strength of BSs received. Measurement results are used to initiate a handover. Scanning FUs control the scanning process. IDs of potential BSs and the scan duration are exchanged between peer entities. Since a SS does not receive during the scanning phase, the FU cuts the SS off from the scheduling process. The scanning FU activates the tuning to the desired frequency and the following measurements.

Handover control FUs control handover and disassociation of the corresponding SS prior to this. All connections of the SS are being shut down.

Ranging serves for time synchronization of a SS's transmitter. In addition, the basic and primary management connections are allocated. After ranging the FU tunes the SS back to the BS's carrier frequency and re-establishes the connections. In case of a handover the SS is tuned to the carrier frequency of the target BS.

Connection Setup serves to establish a new connection with a specified QoS category. Therefore, the respective FU exchanges management messages and creates the corresponding CIDs.

7.2.4 Management Plane

The management plane offers information services to both, user and control plane, see Figure 7.1. It does is not implemented by means of FUs since it neither creates nor exchanges any compounds. The management plane is composed of two basic modules, the connection manager and the control plane manager. In addition it hosts two modules for internal purposes and error recovery functions.
The control plane manager resides in the SS where it manages handover and association to a BS. Therefore, the respective FU comprises strategies for handover, scanning, association and disassociation.
The connection manager stores connection specific data. It allocates unique CIDs to connections and provides methods for appending, changing and deleting connections. Besides the CID classification rule, QoS related data, e.g, measured interference levels are stored. The scheduler of the transmitting station needs an estimate of the interference level at the receiving station to be able to select the appropriate MCS. The SINR values measured at the receiver are averaged by Eq. (7.1) and stored in the cache of the connection manager. $\hat{\mu}_{SINR}$ denotes the averaged SINR value. $SINR(k)$ is the actual measured value that is written to the cache. The variable α_{avg} controls the influence of old measurement values.

$$\hat{\mu}_{SINR}[k] = \begin{cases} SINR[k] & k = 0 \\ (1-\alpha_{avg})\hat{\mu}_{SINR}[k-1] + \alpha_{avg} SINR[k] & k > 1 \end{cases} \tag{7.1}$$

7.3 Link-to-System Interface

In system level simulation, such as the WNS, the PHY layer is decoupled from the protocol stack. Separate link level simulations are performed in advance and their results are used to model the PHY layer behavior in system level simulation. This section describes the link level simulator and the link-to-system interface that has been used in conjunction with the WNS. A link level simulator implements all relevant transmit and receive blocks such as randomizer, coder, interleaver, modulator etc. as shown in Figure 7.4 and realistically models the wireless channel. Noise is artificially generated according to a given distribution, e.g., Additive White Gaussian Noise. The result is represented by link level curves showing the Bit Error Ratio (BER) versus the Signal to Noise Ratio (SNR) of an interference free channel.

The system level simulator takes all simultaneous ongoing transmissions w.r.t. the receiver into account and calculates the mean SINR of a received PDU. The influence of interference is considered equal to that of noise the SINR can be considered as SNR. Then the BER can be looked up in a table mapping the curves mentioned to get the particular SNR. Assumed that single bit errors are randomly distributed over a packet, the PER can be calculated by

$$PER = 1 - (1 - BER)^L \tag{7.2}$$

where L is the PDU length in bits. The distribution of bit errors per packet follows the binomial distribution.

$$P(n) = \binom{L}{n} p^n (1-p)^{L-n} \tag{7.3}$$

$P(n)$ gives the probability that n bit errors occur in a packet of length L bits, where p is the single BER.
The IST project STRIKE developed a link level simulation chain [Hutter et al., 2004; IST-STRIKE]. The chain can be used to calculate the expected performance gain by multi- compared to single-antenna transmission. The chain supports the OFDM specifications of both, the MAN standards HiperMAN and IEEE 802.16 as well as the LAN standards HiperLAN/2 and IEEE 802.11. The STRIKE simulation chain is based on SystemC with its basic building blocks shown in Figure 7.4. All relevant blocks of an OFDM transmission chain needed in transmitter and receiver as shown in Figure 3.5 are contained supplemented by a block Performance Meter for evaluation.
Simulation runs using the STRIKE link level chain gave evidence that bit errors are not equally distributed over a packet but occur in bursts. Figure 7.5 compares a histogram of values measured by the chain shown as bars with the binomial distribution (Eq. 7.3) shown as dots that do not match.
The simulation results presented in Figure 7.5 have been found from 3000 packets transmitted when $p = 7.8717 \cdot 10^{-4}$. Each packet contains 50 OFDM symbols or 38,392 bits. Additive White Gaussian Noise (AWGN) was assumed present resulting in an SNR of 18 dB so that the MCS 64QAM 2/3 was used. From Figure 7.5 it can be concluded that bit errors are bursty. To characterize the PHY at the link-to-system interface groups of bits instead of single bits should be focussed at. The constraint length of the convolutional coder used in WiMAX is six, so that a bit error influences up to six bits

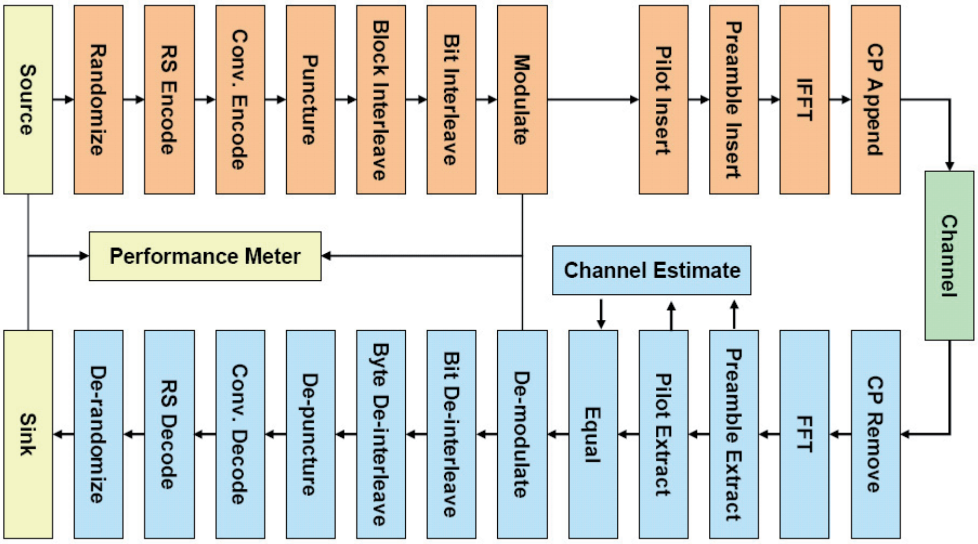

Figure 7.4: IST-STRIKE simulation chain

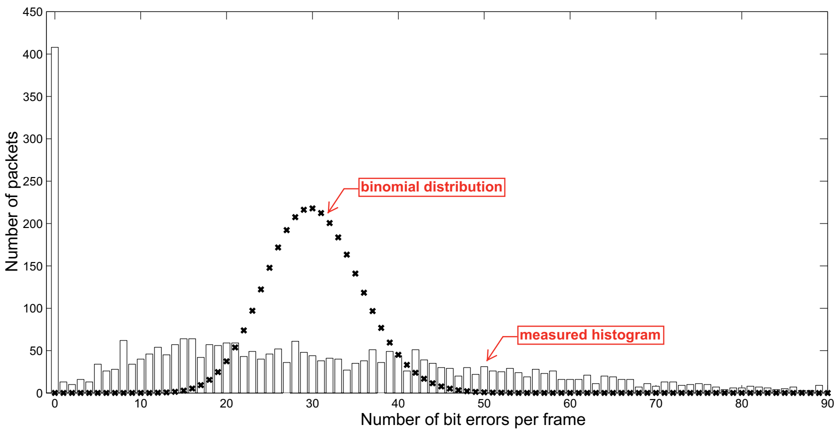

Figure 7.5: Distribution of bit errors per 38,392 bit packet

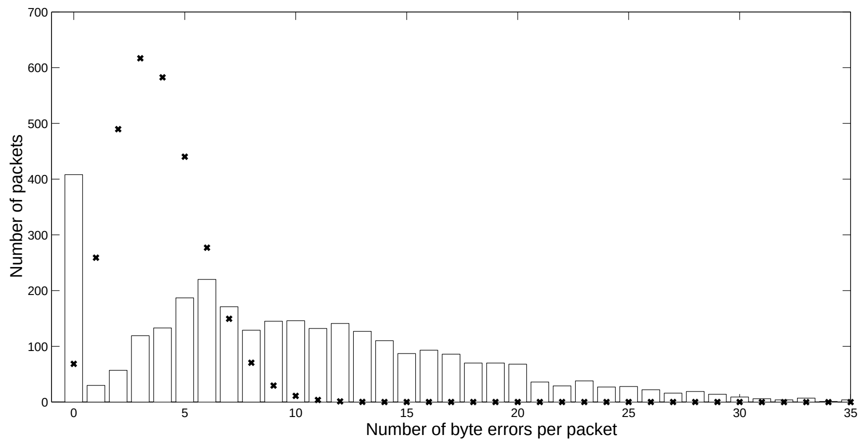

Figure 7.6: Distribution of byte errors per frame

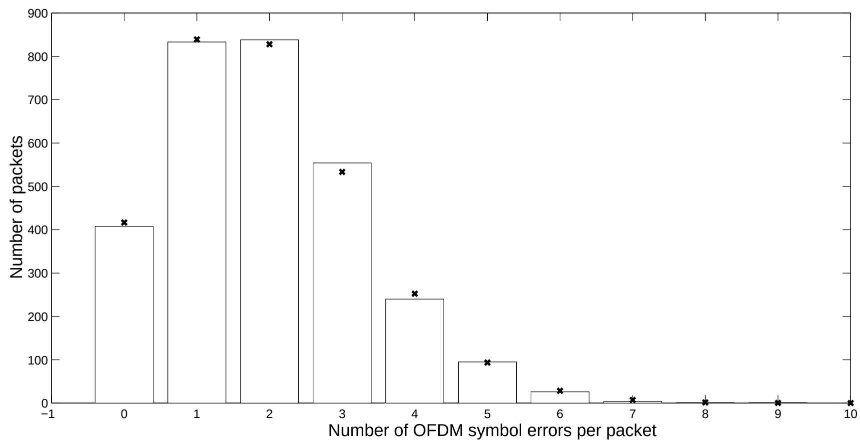

Figure 7.7: Distribution of OFDM symbol errors per frame

following. Thus, the best suited group of bits is a byte.
Simulations to evaluate errors on byte level result in Figure 7.6 showing the histogram of byte errors per packet and the binomial distribution of byte errors per packet using Eq. (7.3) with byte error ratio $p = 2.1 \cdot 10^{-3}$) and the length of a packet in byte L. Again the measured and calculated distributions do not match, so the unit byte appears not to be useful, too.
The Reed Solomon decoder of WiMAX is working on byte level. It either corrects the entire byte or it fails and the whole byte is in error. The next larger group of bits to consider is an OFDM symbol. Figure 7.7 shows that the distribution calculated and the histogram measured from the chain representing OFDM symbol errors per packet match well. Thus, if the

mean OFDM symbol error ratio for a particular SNR level is taken from link level simulation results the error distribution of a real PHY layer can be represented. Simulation runs with different MCSs and different SNR levels confirm this finding. The link-to-system level interface of the WiMAC simulator is modeled accordingly. The OFDM symbol error ratio is denoted Block Error Ratio (BLER) in the following.

7.3.1 Influence of SDMA Interference

A link level simulator considers one link connecting one transmitter and one receiver. Noise is added in the channel model. But during system level simulations, inter-cell interference is taken into account that results from co-channel cells. To do so, co-channel interference is assumed to have the same influence on BLER as noise so that the SINR calculated in the system level simulator can be taken as the SNR input to the mapping tables to read out the BLER.

Under SDMA operation, the SINR partly results from intra-cell interference generated by the same BS (DL) or by SSs of the same cell (UL). In the following, the influence of intra-cell interference and noise on the BER is investigated. To do so, the STRIKE simulation chain is advanced to support SDMA with a four-antenna ULA with an antenna spacing of $\lambda/2$. The MVDR beamforming algorithm calculates the optimal antenna weight vectors for two SSs, which are simultaneously receiving. Figure 7.8 presents the BER of one user versus the SINR for a two user scenario. The angle between both SSs is varied between 2 and 30°. Additionally, one curve shows the single user case, where no intra-cell interference is introduced. In the single user case, the SINR is equivalent to the SNR.

In the WiMAC system level simulator, the different signals (carrier, inter- and intra-cell interference, as well as noise) are independently modeled (method 1), meaning that only the single user curve of Figure 7.8 is used. 7.9 shows the optimized antenna patterns for an exemplary two-user scenario. α_{11} is the amplitude factor of the pattern optimized for SS 1 and received by SS 1. α_{21} is the amplitude factor of a beam pattern optimized for SS 2 at the angle of SS 1. The resulting SINR can be calculated as

$$SINR = \frac{S}{N+I} = \frac{S_{Rx} \cdot \alpha_{nn}^2}{N + S_{Rx} \cdot \alpha_{kn}^2} \tag{7.4}$$

S_{Rx} is the received signal strength considering pathloss and BS transmit

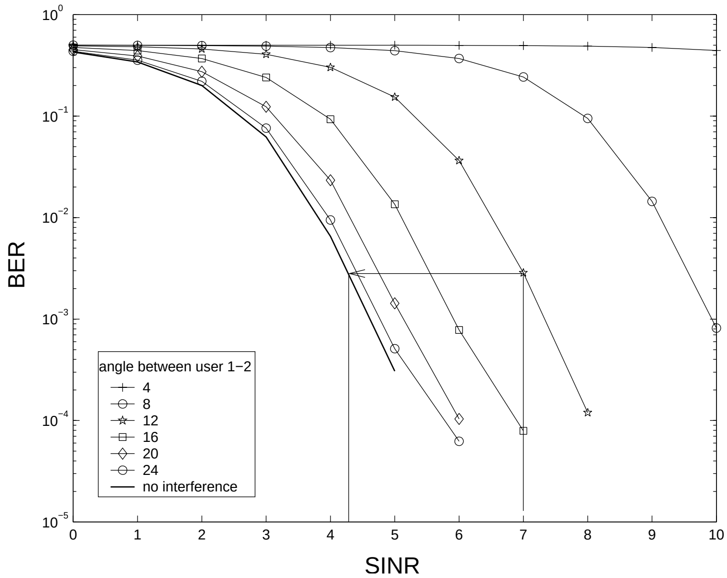

Figure 7.8: Simulated and calculated SINR in a two-SS scenario

power. For example, if SSs are 12° apart, the amplitude factors, as calculated by the beamforming algorithm (MVDR), are $\alpha_{11} = 0.72767$ and $\alpha_{21} = 0.003133$. Assuming a noise level of $N = -105.5dBm$ (7 MHz bandwidth), an SNR of 7 dB, and a signal power S of -98.5 dBm Eq. (7.4) results in $SINR = 4.2385$ dB. Looking at the single-user curve, the SINR input results in a BER of $2.8 \cdot 10^{-3}$.
In the STRIKE link level chain the signals of two users can be modeled jointly (method 2), meaning that the two-user curves of Figure 7.8 are available. With two SSs at an angle of 12° the resulting BER with a given SNR of 7 dB is $2.85 \cdot 10^{-3}$, see Figure 7.8.
The resulting BER values of both methods match each other. Various comparisons for different SNR levels and MCSs confirm the statement. Thus, the system level approach of calculating the SINR from Eq. (7.4) and mapping it to the corresponding BER value of single-user mapping tables is validated.

The influence of noise and of interference can be seen in the IQ-plane processed by the demodulator. Figure 7.10 shows the influence of noise on the position of the received symbols in the IQ-plane. The originally transmitted symbols modulated with 16QAM are disturbed by random noise. Results were gained with the STRIKE simulation chain in a single user

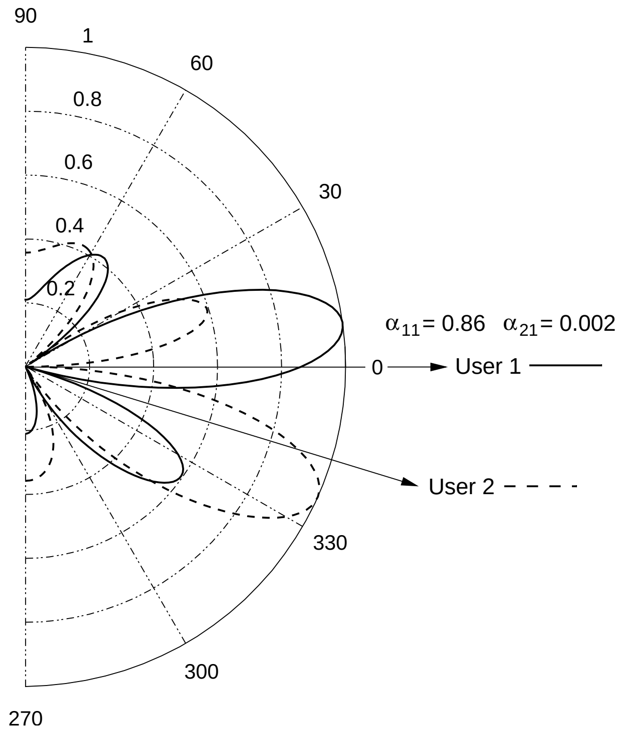

Figure 7.9: Amplitude factor α in a two SS scenario with two optimized beam patterns

setup.

In a two-user simulation without noise SDMA operation introduces intra-cell interference. The left hand side of Figure 7.11 shows the receiver's IQ-plane for a 64 QAM modulation. The right hand side figure focusses on one enlarged constellation point. It shows that a symbols received by SS 1 is disturbed by intra-cell interference resulting from the signal sent to the second user. Interference is not random in nature, but has a regular structure. The total IQ-plane of the signal transmitted to SS 2 is visible as interference signal to that of SS 1; but it is attenuated and rotated. The rotation results from the OFDM symbol delay introduced by the antenna weights. The attenuation results from the superposition of phase-shifted signals transmitted.

7.3.2 Wireless Channel Models

The STRIKE link level simulation chain models the channels as specified by the IEEE 802.16 Broadband Wireless Access Working Group [Erceg et al.,

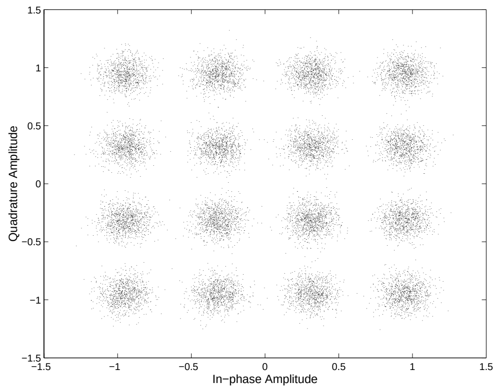

Figure 7.10: IQ-plane with Additive White Gaussian Noise

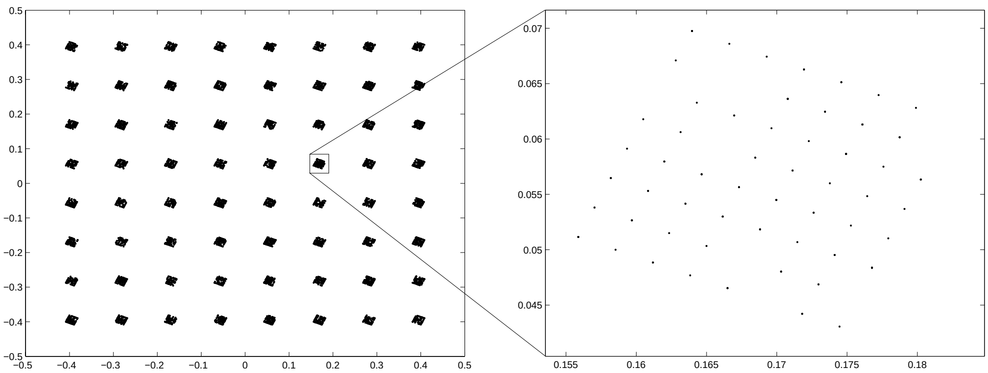

Figure 7.11: IQ-plane with intra-cell interference

2001]. The characteristics of wireless channel models are briefly discussed in the following.

7.3.2.1 Characteristics of Wireless Channels

For the purpose of explaining the representation of real world signal propagation by a channel model as used in the STRIKE simulation chain, components of models for radio propagation are briefly reviewed in the following.
In ideal free space the signal power is attenuated with the inverse square of distance d between receiver and transmitter. This attenuation is called pathloss. The signal power is given by:

$$P_r = P_t \left(\frac{\lambda_c}{4\pi d} \right)^2 G_t G_r \tag{7.5}$$

where P_r is the received and P_t the transmitted power. λ_c is the wavelength and G_t and G_r are the power gains of the receive and transmit antennas.
The received signal is subject to fluctuations in signal level called fading. There are two types of fading, macroscopic and microscopic fading, overlaid to each other.

Macroscopic fading (also called shadowing or slow fading) is caused by obstacles such as hills, trees, or buildings. The statistical distribution of the local mean was found experimentally to be influenced by the antenna height, the operating frequency and the specific type of environment. The received power averaged over the microscopic fading follows a normal distribution when plotted on a logarithmic scale, called a log-normal distribution.

Microscopic fading (also called fast fading) refers to the rapid fluctuations of the received signal in space, time and frequency caused by the superposition of a large number of independent multipath components. The in-phase and the quadrature components of the received signal can be assumed as independent zero mean Gaussian processes. The envelope of the received signal has a Rayleigh density function:

$$f(x|\sigma) = \frac{x}{\sigma^2} e^{-\frac{x^2}{2\sigma^2}} \tag{7.6}$$

where $2\sigma^2$ is the average received signal power. If a LOS path is present, the signal envelope follows a Ricean distribution instead:

$$f(x) = \frac{x(K+1)}{\sigma^2} e^{-(K+\frac{(K+1)x^2}{2\sigma^2})} I_o\left(2x\sqrt{\frac{K(K+1)}{2\sigma^2}}\right) \tag{7.7}$$

Again, $2\sigma^2$ is the mean receive power and $I_o(x)$ is the zero-order modified Bessel function. The K-factor denotes the ratio of the signal energy received from the LOS path and the multipath (NLOS) components. If $K = 0$ there is no direct path and the Ricean Probability Density Function (PDF) reduces to the Rayleigh distribution.

Figure 7.12 shows an example for mean propagation loss, microscopic and macroscopic fading. The monotonically decreasing mean received signal level is caused by pathloss. Its slope depends on the pathloss coefficient, which varies between 2 (free space) and 4 (urban environment). The fluctuation of the dotted line reflects slow fading and the oscillating solid line is caused by the additional fast fading process.

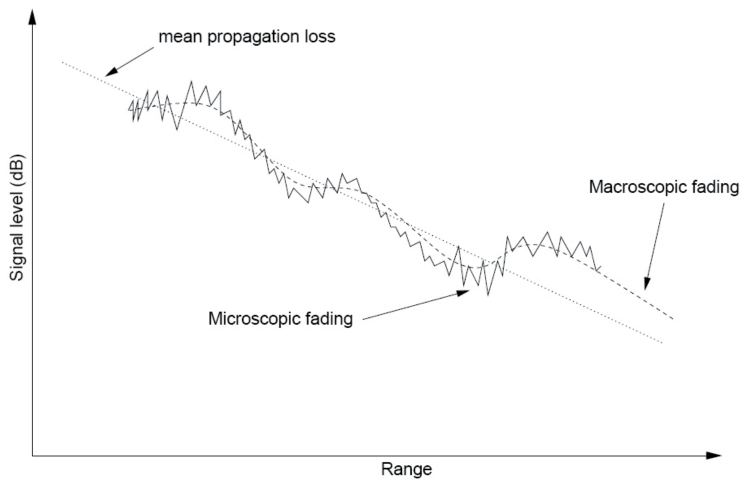

Figure 7.12: Macroscopic and microscopic fading

7.3.2.2 AWGN Channel

The AWGN channel is a model where white Gaussian noise is added to the input signal, resulting in a certain Signal to Noise Ratio (SNR). The energy per coded bit per noise power spectral density of an AWGN channel is

$$E_b/N_0 = 10 \cdot \log_{10}(\frac{10^{\frac{SNR}{10}}}{ModulOrder \cdot CodeRate}) \tag{7.8}$$

7.3.2.3 Flat-LOS Channel

Since the flat fading LOS channel has only one dominant path, Ricean fading occurs. Its configuration corresponds to the first path of the Stanford University Interim (SUI)-1 channel model, resulting in a K-factor of 4 dB.

7.3.2.4 SUI Channels

SUI channels model multipath propagation with three dominant paths, each represented by a tap, resulting in a frequency-selective channel response. Each tap has a different Doppler spread and its own K-factor. Different types of SUI channels are defined for several terrain types. The maximum path loss category is hilly terrain with moderate-to-heavy tree densities (Category A). The minimum path loss category is mostly flat terrain with light tree densities (Category C). Intermediate path loss condition is captured in Category B [Erceg et al., 2001]. The STRIKE link level chain implements the SUI channels 1, 3, and 5.

7.3.3 Link Level Lookup Tables

Figure 7.13a plots the uncoded BER obtained by comparing the input of the block *modulate* and the output of the module *de-modulate* (see Figure 7.4) versus the SNR. Since the channel coder has no influence on the BER, the curves for a given modulation scheme do not depend on the code rate. Higher order modulation schemes perceive a higher BER with a given SNR. The distance of constellation points in the IQ-plane depends on the modulation so that robust schemes such as BPSK are less affected by noise and interference than higher order schemes like 64QAM.

When comparing input and output bits of the modules *randomize* and *de-randomize* in Figure 7.4, the coded BER can be obtained. Figure 7.13b shows that the concatenation of a convolutional and a RS coder significantly reduces the BER. A code with a small rate, say 1/2, introduces more redundant bits than a code with a high rate, say 3/4, and therefore is more robust against noise.

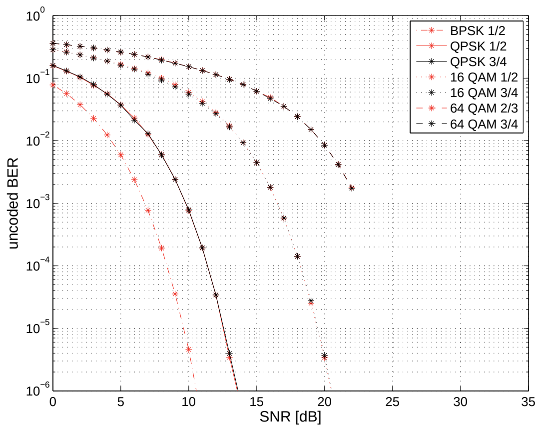

(a) Uncoded BER

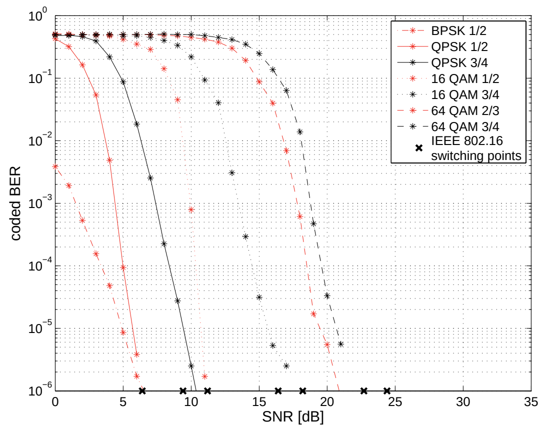

(b) Coded BER and SNR thresholds

Figure 7.13: Coded and Uncoded BER for AWGN channels and IEEE 802.16 SNR thresholds

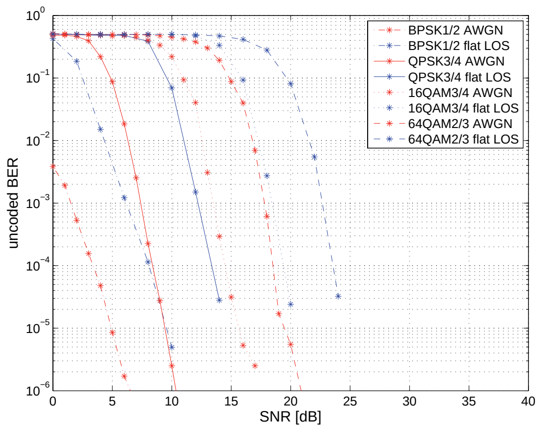

(a) AWGN compared to flat fading LOS

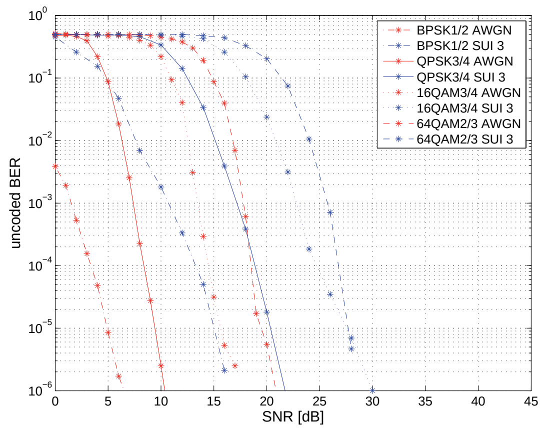

(b) AWGN compared to SUI-3

Figure 7.14: Coded BER for AWGN, flat fading LOS, and SUI-3 channels

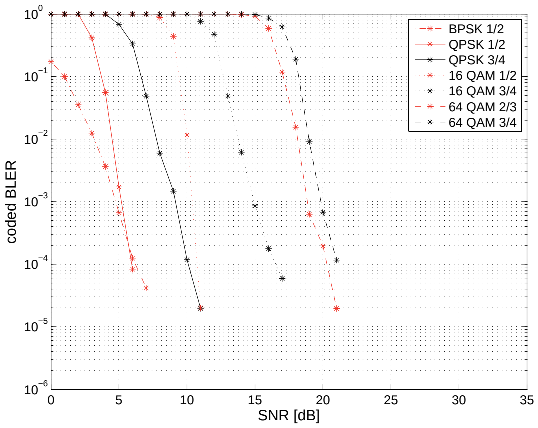

Figure 7.15: Coded BLER for AWGN channels

The influence of Rice fading can be observed in Figure 7.14a, where the BER of an AWGN channel is compared to that of a flat fading LOS channel. Deep fades occurring in the signal strength cause a higher BER of the flat fading channel. This is getting worse for frequency-selective channels, Figure 7.14b, where the AWGN is compared with the 3-tap SUI-3 channel. Signal fluctuations caused by multipath propagation are worse than those of a flat Ricean channel.

IEEE 802.16 standard requires that the BER measured after FEC shall always be less than 10^{-6} in AWGN channels. Hence, MCSs must be selected appropriately, depending on SINR, as indicated in Figure 7.13b by crosses on the abscissa. It can be seen that the coded BER fulfills the IEEE requirement. The link adaptation mechanism of the scheduler selects the MCS of each transmission according to the (estimated) BER.

In the introduction of Section 7.3 it has been explained that packet errors are related to OFDM symbol errors and the Block Error Ratio (BLER) is the best parameter to characterize the quality of the channel. Figure 7.15 presents the BLER versus SNR, namely the information contained in the link level look-up table used in the WNS to convert the SINR calculated there into the packet error ratio.

CHAPTER 8

Performance Evaluation by Simulation

This chapter evaluates to what extend SDMA improves the performance of IEEE 802.16 systems. Therefore, the SDMA enabled 802.16 protocol stack is implemented in the WNS as described in Section 7. The WNS is an event-driven simulator comprising emulation of a protocol stack that is embedded in an simulation environment that cares for stochastic processes representing the real radio propagation and data communications world. Influences of traffic characteristics, varying interference and the behavior of protocol related algorithms can be jointly analyzed in WNS.
The focus in this chapter is on the improvement of the system's cell throughput capacity and packet delay that can be achieved by using SDMA. Configurations where an adaptive BS antenna is used for SFIR and others using omnidirectional BS antennas are studied and the respective results are compared.

8.1 Simulation Scenario and Simulation Setup

8.1.1 Cellular Single-hop Scenario

In this evaluation we focus on a suburban environment where LOS propagation due to over-the-rooftop radio propagation between antennas is assumed. According to the analysis presented in Section 6.1 (Figure 6.5a) $CO = 7$ is chosen to meet the required DL SINR of 6 dB. The cell radius is set to 750 m. The distance to the co-channel cells is $D = 3437$ m. Different from the assumptions made in Section 6 (Table 6.4), 20 SSs are randomly positioned per cell, equally distributed over the cell area.
The scenario consists of seven hexagonal cells, each with a central BS and 20 SSs as shown in red and black in Figure 8.1a. Measurements are only performed in WNS for the central (black) cell at the corresponding BS and SSs. Stations in the first tier of co-channel cells (red) are not evaluated, they only serve to generate interference to the central cell. Nevertheless, the same event driven stochastic simulation, with identical average traffic load, and

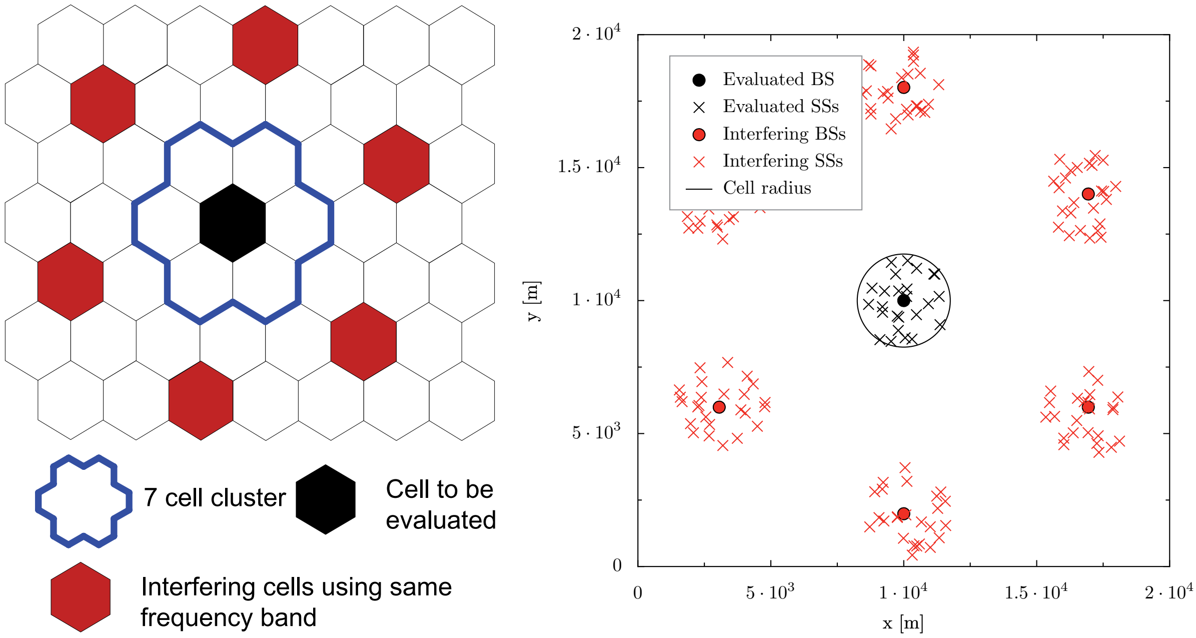

(a) Cell cluster with $CO = 7$ **(b)** Positions of BSs and SSs

Figure 8.1: Multicell scenario

with the same degree of detail, is conducted at all 7 BSs and 140 SSs. All BSs are assumed to operate synchronously in TDD. In order to avoid fatal BS-to-BS and SSs-to-SSs interference, UL and DL subframes are assumed to occur simultaneously in the seven cells of the network studied.
White cells in Figure 8.1a are assumed to operate on different frequency channels not producing any interference to the central cell. A snapshot of the locations of BSs and SSs is shown in Figure 8.1b. The SSs' positions in the cells continuously change during simulation time according to the chosen mobility model.

8.1.2 Performance Metrics

In order to assess the performance of the scenario different metrics are defined.

MAC Throughput The amount of user data of all MAC frames (packets) successfully arriving at the WiMAX MAC SAP during a fixed time window. The throughput is measured at the destination station in Megabits per Second (Mbps). Separate values are measured for packets traveling to/from every SS in UL/DL direction.

Delay Measured at the destination station's MAC SAP for all packets that are successfully transmitted. Defined as the time elapsed between entering the sender's WiMAX protocol layer until leaving it at the receiver's MAC SAP. In overload condition, the mean delay is not meaningful since packets that are never transmitted are not included then.

Interference Measured at the destination station's receiver (in dBm). All concurrent transmissions in co-channel cells (inter-cell interference) and all concurrent transmissions of the own cell (intra-cell interference) are accounted for. The interference level is averaged during packet reception. It also includes the thermal noise and the noise figure of the receiver.

Carrier Signal strength during packet reception measured at the destination station's receiver (in dBm). Transmit as well as receive antenna gain is taken into account. The carrier signal is averaged during packet reception.

SINR Calculated as the ratio between carrier and interference signal strength in dB.

Grouping gain A performance metric that measures the achieved SDMA throughput relative to that without SDMA see Eq. (4.35).

8.1.3 Link Adaptation and Error Modeling

The scheduling strategy controls link adaptation based on the SINR estimates provided by the spatial grouper. For each packet scheduled for transmission to a SS, a MCS is chosen according to the SINR threshold values shown in Table 8.1. These values are taken from the IEEE 802.16 WiMAX standard [IEEE, 2004a]. The SINR threshold values aim at a target BER of 10^{-6}. In order to avoid transmission errors, conservative SINR thresholds are chosen compared to those shown in Figure 7.13b on the abscissa. Thus, as long as the SINR is estimated accurately, transmission errors are kept even below 10^{-6} in our simulation studies. One problem is that higher throughput could be achieved if link adaptation use other switching thresholds resulting in higher BER and respective BLER.

Table 8.1: Modulation and Coding Schemes and corresponding switching thresholds

Modulation	Code rate	Min. SINR [dB]	PHY data rate [Mbps]
BPSK	1/2	6.4	6.91
QPSK	1/2	9.4	13.82
QPSK	3/4	11.2	20.74
16 QAM	1/2	16.4	27.65
16 QAM	3/4	18.2	41.47
64 QAM	2/3	22.7	55.30
64 QAM	3/4	24.4	62.21

8.1.4 WiMAX Frame Structure and Overhead

The IEEE 802.16 WiMAX frame as introduced in Section 3.3.2.2 is represented in very detail the WNS. The total WiMAX MAC frame duration is assumed to be 10 ms. According to the symmetric traffic load assumed, the frame is equally divided between DL and UL user data phases.
At the start of the DL subframe, the BS transmits the DL-preamble (2 OFDM symbols) and the FCH (1 OFDM symbol). The FCH is followed by the first DL burst containing DL and UL MAPs. The WNS-based implementation is assumed to transmit FCH, DL and UL MAPs without errors. This idealization allows evaluating the SDMA-enabled network even when the control signaling would have been the system's bottleneck (see Sections 8.2.4.1 and 8.2.4.2). UL and DL MAPs are always transmitted using omnidirectional antennas and the most robust MCS BPSK 1/2.
RTG and TTG occupy two OFDM symbols each. The UL subframe contains 16 OFDM symbols (two slots with eight symbols each) for the contention-based initial ranging and 10 OFDM symbols (two slots with five symbols each) for bandwidth requests. 192 data carriers are available in 20 MHz channel bandwidth. Each OFDM symbol is 13.89 10^{-5} s long, resulting in a total of 720 OFDM symbols in each 10 ms frame [Hoymann, 2005].

8.1.5 WiMAX Protocol Settings

The combined TD-/SD-/OFDM scheduler at the BS uses the proportional fair scheduling algorithm that offers the best trade-off between fairness and capacity Ellenbeck [2006]. The spatial grouper uses the tree-based SINR

heuristic introduced in Section 4.4.2.3 because it offers a good trade-off between runtime efficiency and grouping performance. The BS scheduler allocates resources in DL as well as in UL direction.
In order to eliminate other influencing factors when evaluating the performance of SDMA neither Segmentation and Reassembly (SAR) nor Automatic Repeat Request (ARQ) protocols are used.

8.1.6 UL Scheduler

Initial simulation studies indicated that interference in UL is much worse than in DL, with higher mean and larger variance. This is due to SSs transmitting with full power (1 W) in the Reference Scenario. When co-channel BSs schedule multiple concurrent UL transmissions, the overall inter-cell interference is multiplied as well. In contrary, the overall DL Tx power of the BS is constant (1 W) no matter how many streams are scheduled simultaneously, since it is equally shared among the streams.
High mean inter-cell interference result in low SINR and high variance leads to unpredictable interference at the scheduler so that SINR estimates tend to be random. Assigning too robust or too weak MCSs either wastes bandwidth or causes high PER or even unserved SSs.
It has been found useful for overcoming these problems to schedule SSs even if the predicted SINR falls below the minimum threshold of 6.4 dB. Although this leads to an increased number of packets errors, it prevents SSs from being discarded by the scheduler.

8.1.7 Simulation Parameters

All simulation studies are performed with a fixed packet size of 576 Bytes representing the network's Maximum Transmission Unit (MTU). The Inter-Arrival Time (IAT) of packets is controlled so that the desired offered traffic is achieved. It follows a negative exponential distribution. For all SSs a symmetric traffic load in DL and UL is assumed. To achieve a total (DL + UL) cell traffic load ($Traffic$), the IAT is set to the following mean value:

$$IAT[s] = \frac{\#(SS) * PacketSize * 2}{Traffic} \quad \frac{[Bit]}{[Bit/s]} \tag{8.1}$$

Each BS is equipped with a 9-element uniform circular antenna array used to serve the whole cell without sectorization. SSs are equipped with omnidi-

Table 8.2: Simulation parameter and values assumed

Parameter	Value	Comment
Antenna array/elements	UCA / 9	Only at the BS
Transmit power	1 Watt	fixed for both, BS and SS
Link adaptation	adaptive	SINR threshold in Table 8.1
Cluster Order	7	One tier of interferer cells
SSs per cell	20	
Cell radius	750 [m]	BPSK 1/2 the cell border
Mobility	Brownian motion velocity = 3 m/s	intra-cell mobility only
Mid frequency	5.470 GHz	CEPT band B
Bandwidth	20 MHz	
Pathloss	$23.8\ \log(d) + 41.9$	WINNER LOS C1 Metropolitan suburban
Traffic load UL/DL	Symmetric	
Packet size	576 Byte	Fixed
Inter arrival time	Mean in Eq. (8.1)	Neg. Exp. distributed
MAC Frame length	10 ms	720 OFDM symbols
Number of subcarriers	192	for data transmission
OFDM symbol duration	13.89 μs	according to IEEE [2004a]

rectional antennas. For both BS adn SS, the transmit power is 1 Watt and no power control is applied. A bandwidth of 20 MHz with a mid frequency of 5.47 GHz is used. Thermal noise (-174 dBm/MHz) is considered and a noise figure of 5 dB is added to that.
In order to eliminate the influence of particular SSs' positions, SSs are slowly moving inside their cell area. SSs follow a brownian motion with a pedestrian speed of 3 m/s, not leaving the coverage area of their BS so that handovers need not to be considered.
As a rooftop deployment of BSs and SSs antennas is assumed, the LOS pathloss model introduced in Eq. (6.6) applies. The "C1 LOS" pathloss model, see Eq. (6.10), as derived from measurements in [IST-WINNER, 2006] is used for the suburban environment studied in the following. Neither shadowing nor fast fading are considered.
Table 8.2 presents all relevant simulation parameters together with the values assumed.

8.2 Performance of a Smart Antenna Enhanced IEEE 802.16 System

8.2.1 Reference Scenario

The system configuration studied in this section is named "Reference Scenario" where three modes of operation are compared. Figure 4.6 visualizes the three modes:

Omni omnidirectional antennas at the BSs

Spatial Filtering for Interference Reduction (SFIR) Steerable antenna array at the BS to control both, transmit and receive antenna patterns. Only one single SS is served at a time (Section 4.1.3).

Space Division Multiple Access (SDMA) Adaptive antenna patterns are used at the BS to transmit/ receive data streams to/ from multiple SSs concurrently, separated in space (Section 4.1.4). Since a different number of maximum simultaneous streams can be supported, this mode is addressed by the number of maximum data streams supported, e.g., "2 streams".

Results of the Reference Scenario are compared to that from other scenarios, see Sections 8.2.3, 8.2.4, 8.2.5, and 8.2.6.

8.2.1.1 Performance Improvement

The mean DL MAC throughput of 20 SSs shown in Figure 8.2a is the lowest for "omni" operation and can be significantly enhanced by both, SFIR and SDMA allowing 2 simultaneous streams. The throughput capacity visible at the offered traffic value where the throughput no longer increases linearly with increased traffic, is 7 Mbps for "omni" and doubled to 15 Mbps for SFIR whilst two stream operation reaches a capacity of about 26 Mbps. Compared to the omni mode SDMA with two streams increases the capacity by 270%.
Figure 8.2b shows that the UL MAC throughput can be significantly enhanced by SFIR and two stream SDMA, too. The capacity of omnidirectional transmissions is more than doubled with SFIR and SDMA with a maximum of two concurrent streams gives a further increase by 40%. The throughput capacity measured is slightly below that of the DL.
The individual DL MAC throughput of the 20 SSs is shown in Figure 8.3 and the individual UL MAC throughput is shown in Figure 8.4, which is

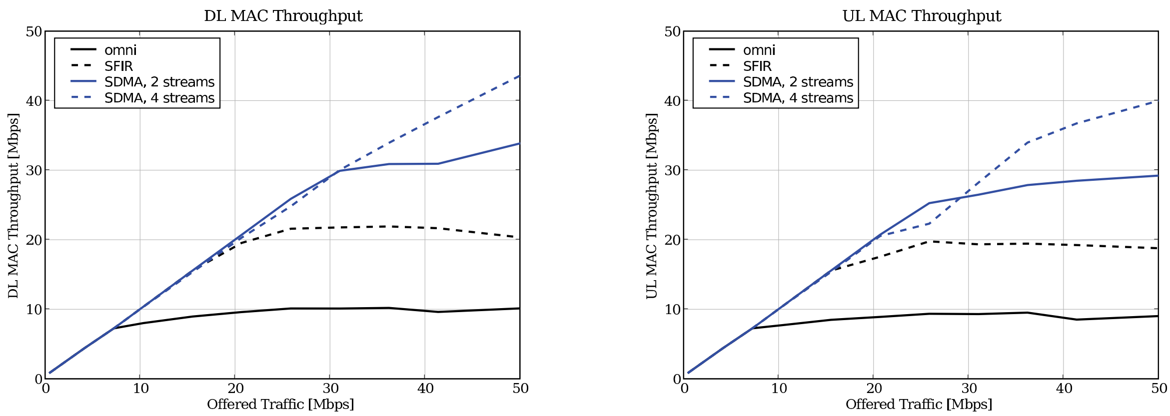

(a) Mean DL MAC throughput **(b)** Mean UL MAC throughput

Figure 8.2: Mean MAC throughput aggregated per cell

slightly lower than in DL. Up to the individual saturation point, each SS can transmit the offered traffic using the MCS applicable at its location. Beyond the saturation point, the proportional fair scheduler cannot assign enough radio resources to all SSs, whose individual throughput diverge. The scheduler maximizes the system capacity under SDMA operation while considering fairness. All SSs can be seen to benefit from SFIR and SDMA. Although the cell throughput for up to four SDMA streams is much larger than that of two streams (refer to Figures 8.2a and 8.2b), some SSs start to saturate earlier. In DL, individual SS saturate around 15 Mbps with two stream SDMA (see Figure 8.3d) compared to individual saturation around 10 Mbps with four stream SDMA (see Figure 8.3c). In UL, individual SSs of the four stream system start to saturate around 10 Mbps offered traffic, which is approximately 10 Mbps less than for two streams (see Figures 8.4c and 8.4d).

In DL the effect of early individual saturation is caused by the varying interference level in combination with a weak carrier signal especially under SDMA where the BS transmit power is shared among streams (refer to section 8.2.1.2). In UL, the carrier signal is rather good no matter how many SS are served in SDMA mode. However, the inter-cell interference in UL is much higher and even more varying than in DL (refer to section 8.2.1.3).

The mean packet delay shown in Figure 8.5 is clearly dependent on the MAC throughput. For all but the four stream mode, mean DL delay starts at a

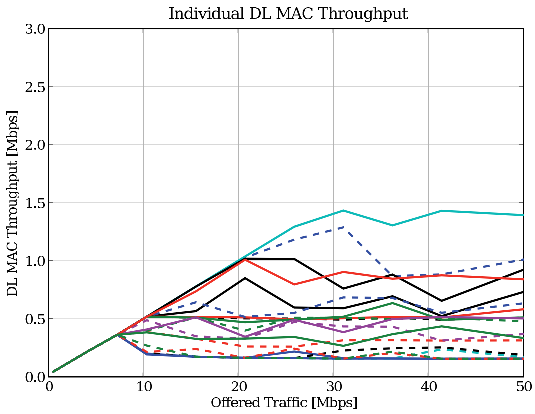

(a) Omnidirectional transmission

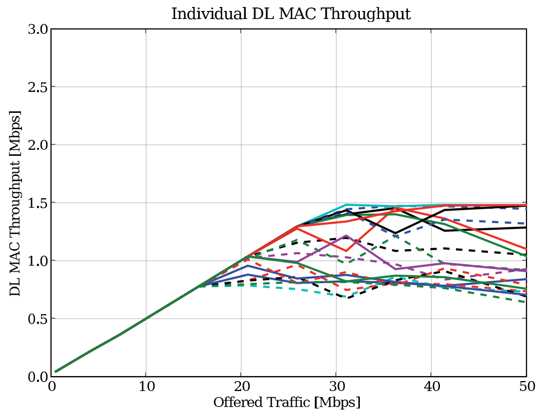

(b) SFIR

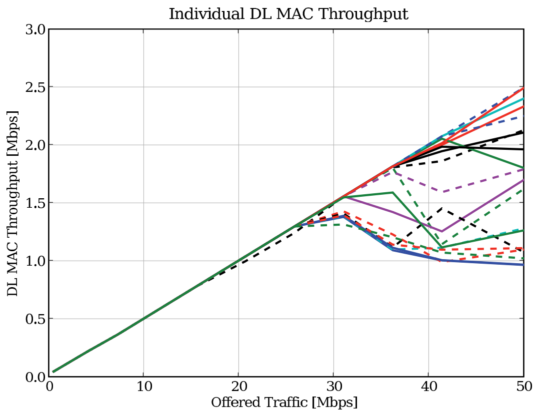

(c) SDMA with 2 streams

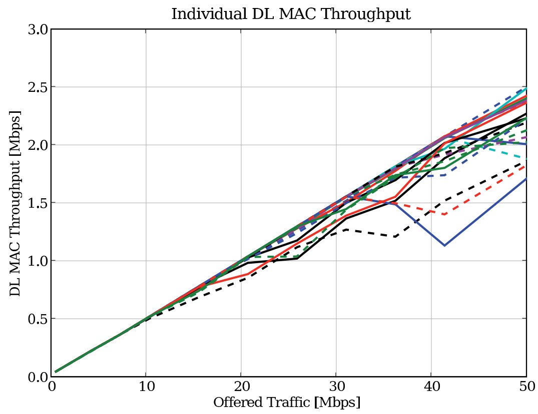

(d) SDMA with 4 streams

Figure 8.3: Mean DL MAC throughput of individual SSs for omni, SFIR, and SDMA mode

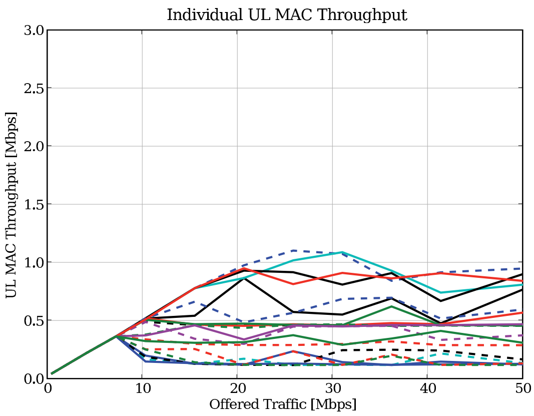

(a) Omnidirectional transmission

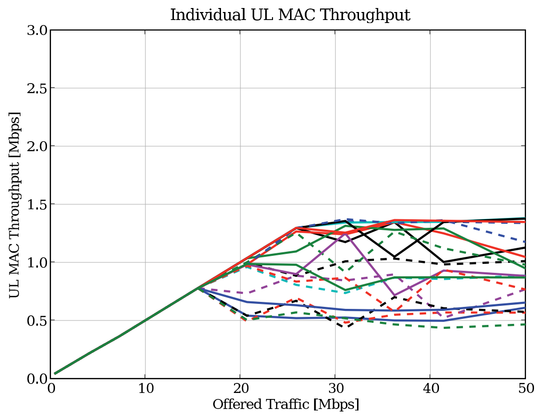

(b) SFIR

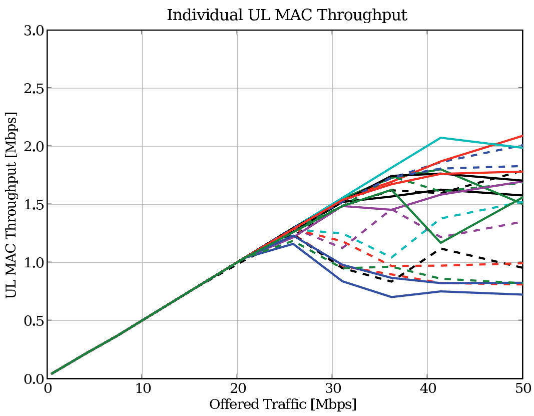

(c) SDMA with 2 streams

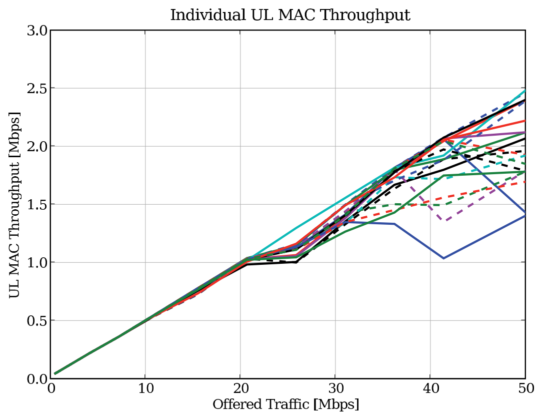

(d) SDMA with 4 streams

Figure 8.4: Mean UL MAC throughput of individual SSs for for omni, SFIR, and SDMA mode

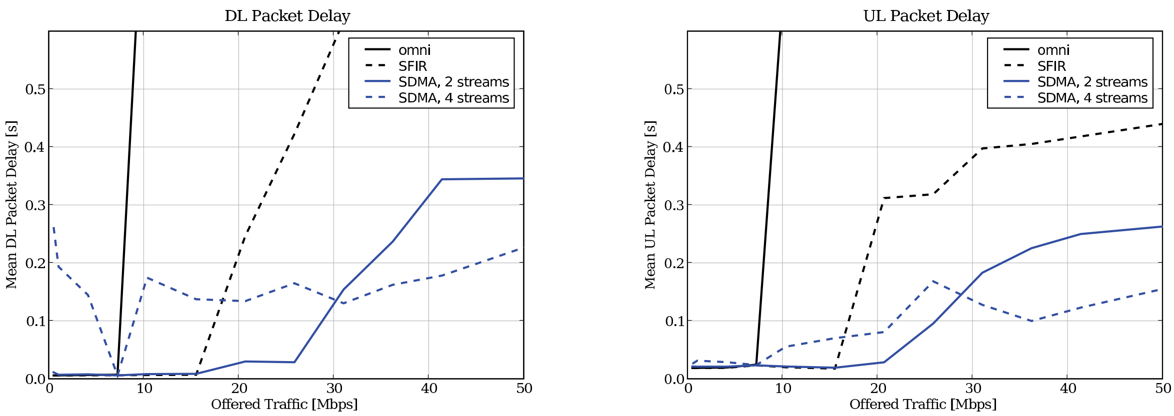

(a) Mean DL packet delay **(b)** Mean UL packet delay

Figure 8.5: Mean packet delay

level of about 10 ms under sufficiently low load and increases rapidly once the system saturates. With four stream SDMA the mean DL packet delay starts at a higher level because several SSs are scheduled infrequently.
In UL, all transmission modes start with a mean packet delay around 10 ms. Compared to the omnidirectional transmission, SFIR and SDMA with a maximum of two streams improves the packet delay by shifting the overload to higher traffic regions. SDMA with a maximum of four streams does not shift the starting point of higher mean packet delay values, but it modifies the behavior of the packet delay. Due to the high inter-cell interference some SSs cannot receive their offered traffic constantly while others still can.
Figure 8.6a shows the CCDF of the DL packet delay for a low system load of 1 Mbps (50 kbps per SS), Figure 8.6b shows the UL packet delay respectively. The figures confirm that nearly all packets (omni, SFIR, and 2 stream SDMA) are transmitted in the first MAC frame. Only SDMA with four streams cause higher packet delays.
In DL, 20% of all DL packets perceive a delay larger than 80 ms (8 MAC frames) and 10% of all packets are delayed for more than 500 ms. The reason is the substantial probability of low SINR conditions leading to large periods where a particular SS is not scheduled at all. Low SINR levels result from Tx power sharing among SDMA streams in conjunction with highly varying intra-cell interference (refer to Section 8.2.1.2).
In UL only 5% of all packets perceive a delay larger than 50 ms under 4

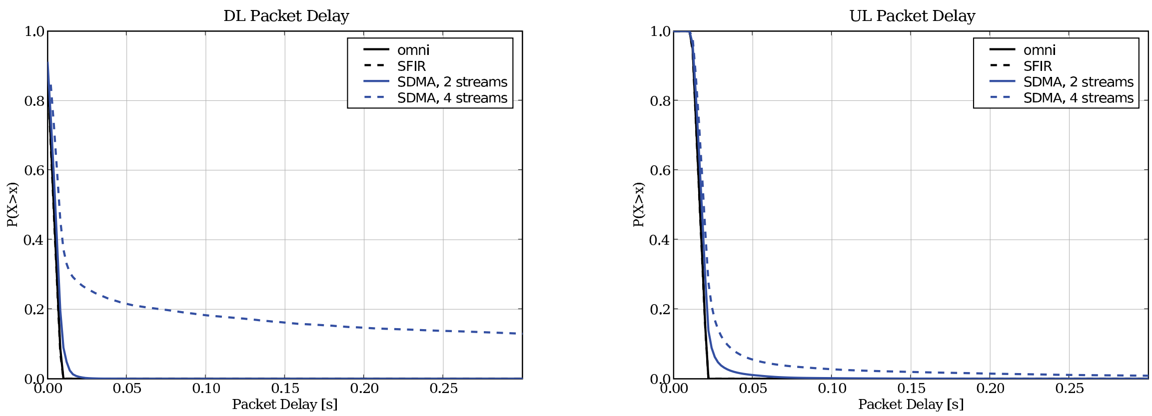

(a) DL packet delay **(b)** UL packet delay

Figure 8.6: CCDF of packet delay (1 Mbps offered traffic)

stream SDMA. The unpredictable inter-cell interference level causes this behavior (refer to Section 8.2.1.3).

8.2.1.2 Reasons for the DL Performance Gains

The performance increase of SFIR and of SDMA results from an increased SINR level. Figure 8.7a gives evidence that the mean SINR can be increased compared to the omni mode by approx. 8 dB for SFIR and approx. 5 dB for SDMA with two streams. SDMA with a maximum of four streams has 2 dB higher SINR at low load but a lower SINR at high load.
Figure 8.7b shows the CCDF of SINR at a low system load of 1 Mbps. It can be seen that all packets perceive SINR levels higher than the 6.4 dB threshold required, as long as SDMA with four data streams is not considered. There the SINR drops with some probability below 6.4 dB, owing to a reduced carrier strength and a too high intra-cell interference level.
Although the SINR levels of SDMA are lower than that of SFIR, the SDMA capacity is higher because multiple SSs can be served in parallel. Figure 8.8 shows that the mean DL grouping gain increases to 1.5 and 2.3 when up to two and four concurrent streams are allowed, respectively. For single-user modes such as omni or SFIR the grouping gain is 1.
But why can the SINR be increased so significantly when using antenna arrays? Due to the adaptive antenna pattern at the BS most of the transmitted energy is directed towards the receiving SSs. The CCDF of the

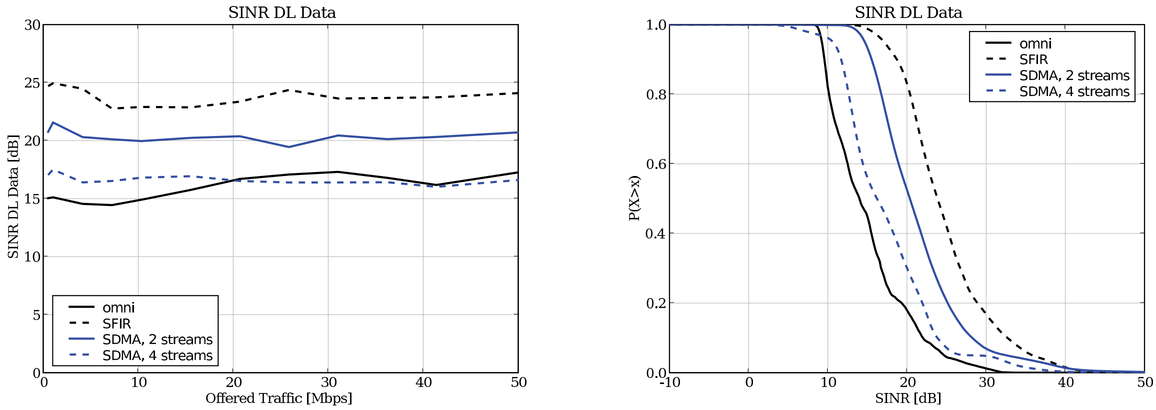

(a) Mean SINR **(b)** CCDF at 1 Mbps offered traffic

Figure 8.7: SINR of received DL packets

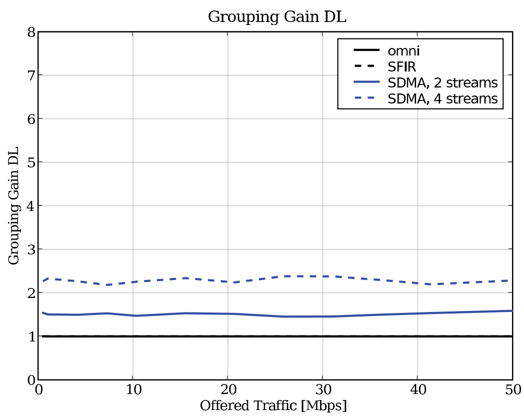

Figure 8.8: Mean DL grouping gain

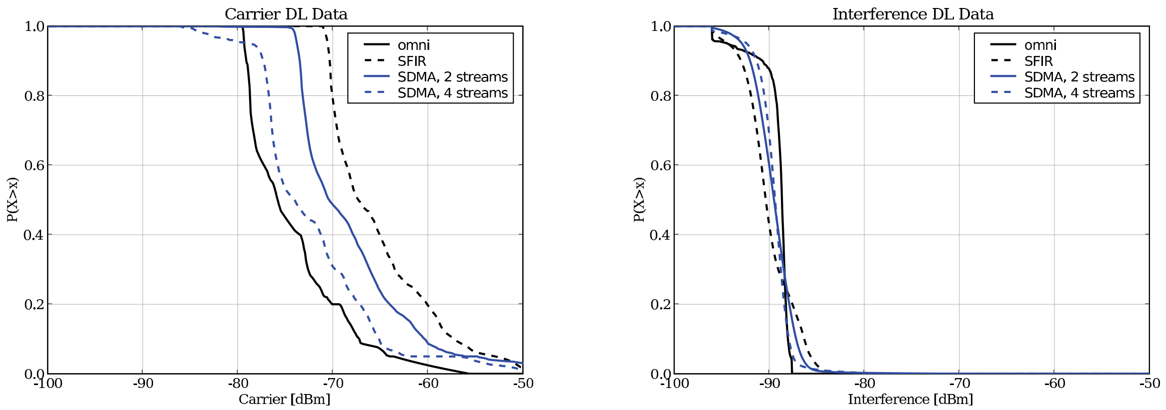

(a) DL carrier **(b)** DL interference

Figure 8.9: DL Carrier and interference levels (CCDF at 1 Mpbs offered traffic)

carrier strength, Figure 8.9a, shows that the mean carrier strength can be increased by approx. 9 dB for SFIR when compared to omnidirectional transmission. With SDMA the mean carrier strength is increased by 2 dB and 5 dB with two and four streams, respectively. This is much less than with SFIR since in SDMA mode, nulls in the antenna characteristic are steered towards simultaneously receiving SSs leading to smaller main beams and lower transmit antenna gain. Since the BS transmit power is shared among simultaneous SDMA streams the power per stream is inverse to the number of streams leading to a reduced carrier strength.

Besides the carrier strength the inter- and intra-cell interference is affected when using adaptive antenna arrays. The CCDF of interference, Figure 8.9b, shows that interference is only slightly reduced by SFIR and SDMA when compared to the omni mode. This is due to the overall BS Tx power being constant, only the antenna pattern is different. Thus, the total co-channel interference stays constant independent of the mode of operation.

Adaptive antenna patterns cause the variance of the interference to be increased for SFIR and SDMA. Most of the time a SS is lucky because no co-channel BS's main beam is pointing in its directions so that its interference level is lower than with omnidirectional transmission. With some lower probability, however, the main beam of a co-channel BS is steered towards the SS leading to an interference level that is higher than with omni transmission.

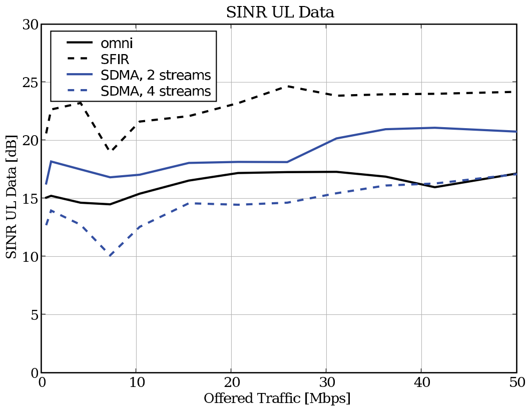

(a) Mean SINR

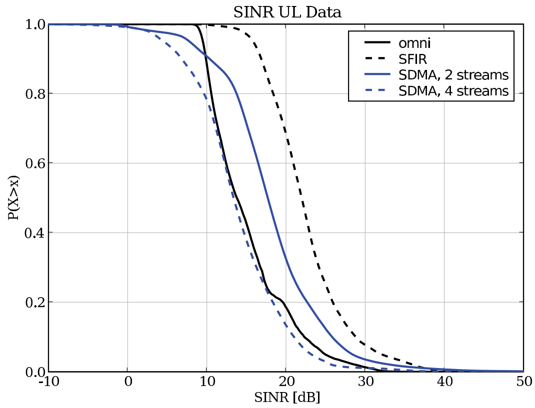

(b) CCDF at 1 Mbps offered traffic

Figure 8.10: SINR of received UL packets

8.2.1.3 Reasons for the UL Performance Gains

Like in DL, the increased UL MAC throughput and the improved packet delay of SFIR results from the increased SINR of received packets shown in Figure 8.10a. The performance increase of SDMA with up to two streams is due to the increased SINR and due to the simultaneous transmission of data. Note that the SINR for SDMA is increased compared to the omnidirectional transmission mode but reduced when compared to SFIR mode: the more streams are allowed to be scheduled, the lower the mean SINR becomes. Allowing four streams to be scheduled, the SINR even drops below the omnidirectional case.

Figure 8.11 shows the UL grouping gain, which is one for the omnidirectional and the SFIR mode because only a single stream is transmitted at a time. Allowing a maximum of two concurrent streams the mean grouping gain is approximately two indicating that nearly always two SSs are scheduled for concurrent transmission. The grouping gain in UL is higher than in DL where the scheduler does not schedule the maximum allowed number of streams that often because the carrier strength weakens too much. In UL the carrier signal is not affected and the scheduler nearly always exploits the maximum number of streams. Due to the predicted high level of inter-cell interference, intra-cell interference due to additional SDMA streams does not carry weight. Inter-cell interference is always dominating.

The CCDF of the SINR of received UL packets shows that using SDMA

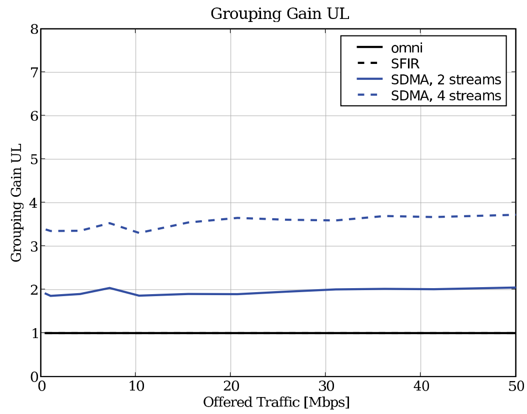

Figure 8.11: Mean UL grouping gain

several packets are received with an SINR lower than 6.4 dB, which is recommended for BPSK 1/2. These packets perceive a higher error probability and packet losses might occur.

Again, the question is why the SINR can be increased so significantly by using antenna arrays. In UL the receiving BS steers the adaptive antenna pattern so that the main beam points towards the transmitting SS resulting in improved receive antenna gain. At the same time the BS steers nulls towards SSs which are simultaneously transmitting suppressing intra-cell interference. The antenna pattern is optimized with the goal to maximize the received SINR.

Due to the adaptive antenna pattern the received carrier signal strength is increased for SFIR and SDMA. The mean receive antenna gain lies between 5 and 8 dB (see Figure 8.12a). SFIR and SDMA have nearly the same carrier level.

An increased interference level can be observed in SDMA (refer to Figure 8.12b). In SDMA mode, several SSs are transmitting in co-channel cells which multiplies inter-cell interference level. Additionally, intra-cell interference occurs which is generated by concurrently transmitting SSs in the same cell. Thus, the average interference level in the SDMA mode is between 3 and 5 dB higher than in SFIR or omnidirectional mode. In SFIR the mean inter-cell interference stays nearly constant when compared to the omnidirectional reception.

The variance of the UL interference in SFIR and SDMA is increased compared to the omnidirectional mode. Especially in SDMA the variance is increased

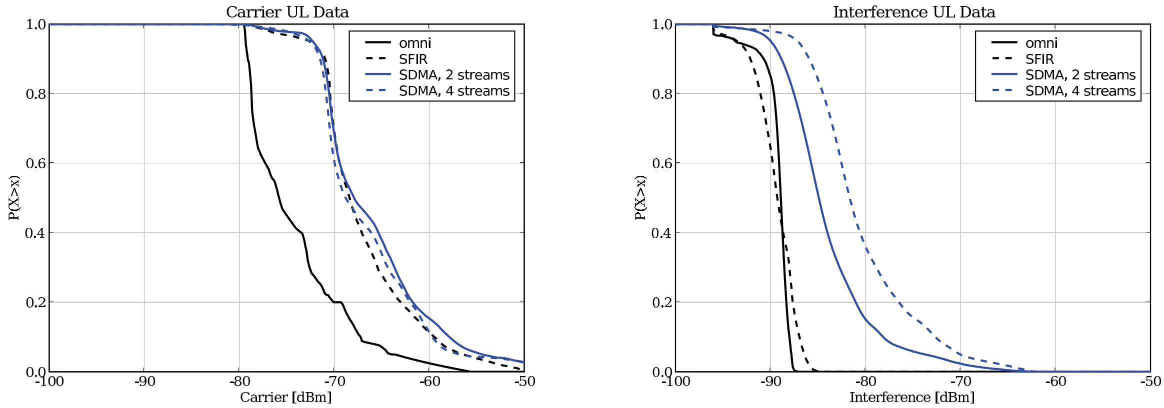

(a) UL Carrier **(b)** UL interference

Figure 8.12: UL carrier and interference levels (CCDF at 1 Mbps offered traffic)

significantly.

8.2.1.4 Conclusion

It is concluded that the SDMA-enabled scheduling algorithm used is able to increase the MAC throughput by leveraging the enhanced capacity offered by the multi-antenna based PHY layer. In the Reference Scenario considered in this section, a 9-element Uniform Circular Array can double the cell throughput in DL and UL when dynamically steering the main antenna beam in the direction of the receiving SS. SDMA with two concurrent data streams further increases throughput by 70% in DL and by 40% in UL. Due to the fairness control by the scheduler all SSs benefit from this and packet delay is decreased for the majority of SSs.
When the BS transmit power is kept fixed under SDMA, it has to be shared among simultaneous streams and hence the individual link quality degrades. The number of simultaneous SDMA data streams has to be adapted carefully to the needs of the application served in terms of, especially, delay variance. The limiting factor in UL appears to be the increasing inter-cell interference due to simultaneous transmissions in co-channel cells. Predicting the highly varying SINR becomes a challenging task for the BS scheduler. Some level of long-term persistency or coordination with co-channel BSs might help to mitigate that problem.

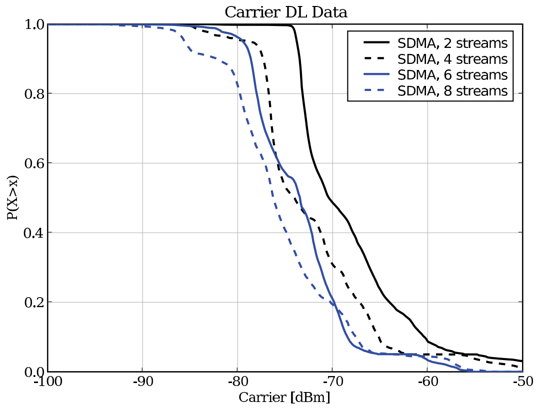

(a) DL carrier

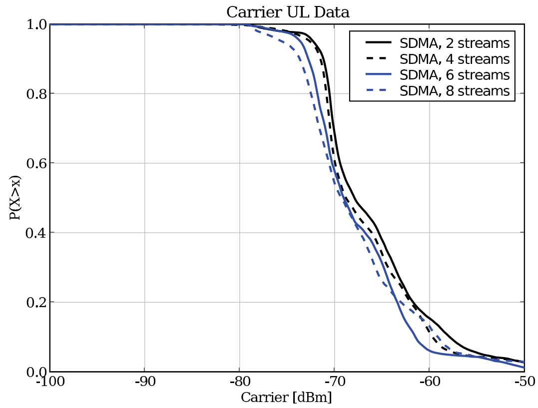

(b) UL carrier

Figure 8.13: Carrier signal strength for different limits of concurrent SDMA data streams (CCDF at 1 Mbps offered traffic)

8.2.2 SDMA with Multiple Streams

Nine antenna elements at the BS antenna array allow for up to nine concurrent streams, in principle. Eight degrees of freedom may be used to set eight nulls, and the ninth degree is needed to steer the main beam in the right direction. When exploiting all nine degrees of freedom, no measures remain to control interference transmitted by or received via side lobes. Further, the quality of nulls and the gain of the main beam degrade with an increased number of streams scheduled. The following simulation study makes this visible.

Figure 8.13a shows that the DL carrier signal strength degrades with an increased number of concurrent streams since the BS Tx power is shared. In UL, the carrier signal is nearly independent of the operation mode, since with with an increasing number of nulls in the pattern the receive antenna array gain decreases slightly.

In DL, multiple streams transmitted by a co-channel BS do not increase the inter-cell interference level, since the overall Tx power of the BS stays constant. The slight increase in the DL interference level visible in Figure 8.14a results from the intra-cell interference introduced by SDMA.

In UL, multiple simultaneously transmitting co-channel SSs multiply inter-cell interference. Figure 8.14b shows that the interference significantly increases with the number of SDMA streams. The minority of that increase

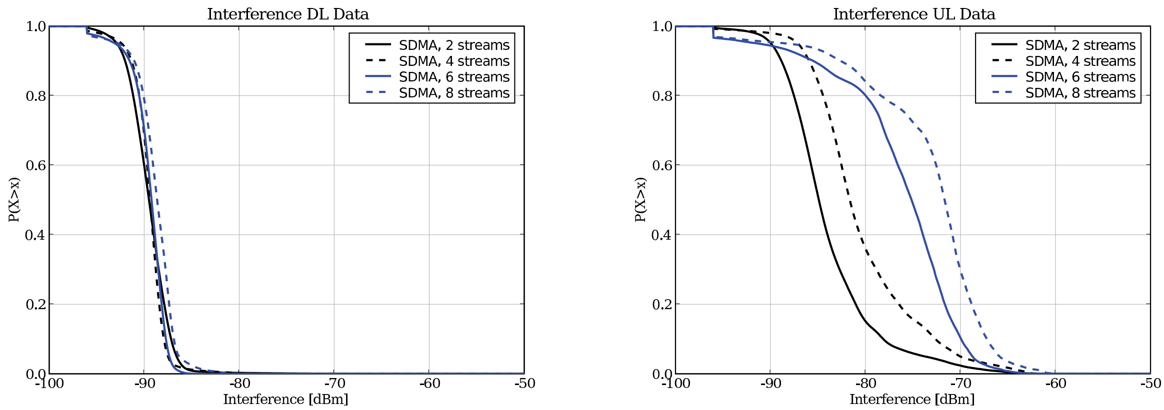

(a) DL interference **(b)** UL interference

Figure 8.14: Interference level for different limits of concurrent SDMA data streams (CCDF at 1 Mbps offered traffic)

results from intra-cell interference.

Both, the growing interference level in UL with increased number of streams and in line with this the decreasing carrier strength in DL result in decreased SINR levels, see Figures 8.15a and 8.15b. This degrades the performance of the individual links.

The more streams are scheduled concurrently the higher is the grouping gain, see Figures 8.16a and 8.16b. The gain increases in DL and UL with an increasing number of streams scheduled, but the absolute values differ much. In DL the grouping gain is up to three for eight streams indicating that on average three streams are scheduled in parallel. Even if more streams were allowed the scheduler would avoid that because the carrier signal would be too weak. In UL the mean grouping gain is close to the maximum number of streams allowed in the corresponding scenario, indicating that the scheduler allocates the maximum number of streams frequently.

A decreased SINR leads to a decreased link capacity, however, an increased grouping gain leads to an increased system capacity. The resulting MAC throughput shown in Figures 8.17a and 8.17b indicate that 4 streams are preferable since the saturation throughput is the highest.

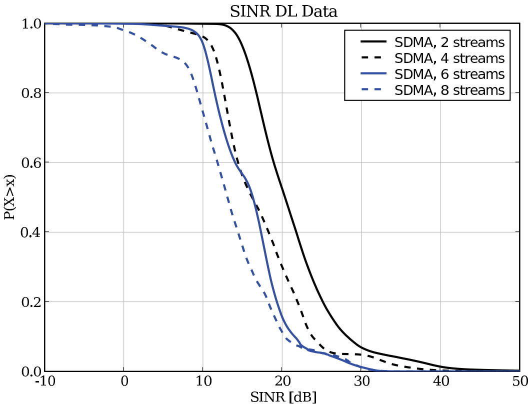

(a) DL SINR

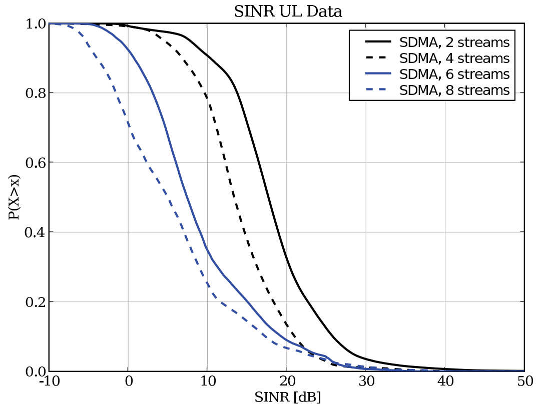

(b) UL SINR

Figure 8.15: Perceived SINR values for different limits of concurrent SDMA data streams (CCDF at 1 Mbps offered traffic)

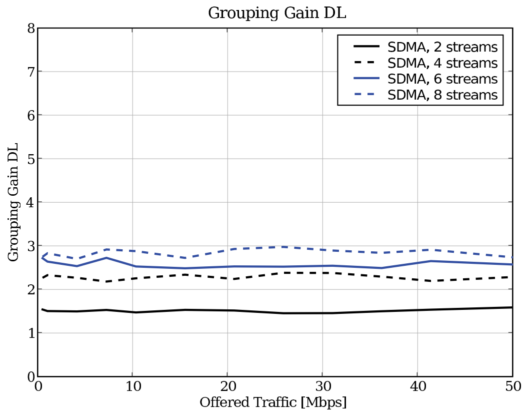

(a) Mean DL gain

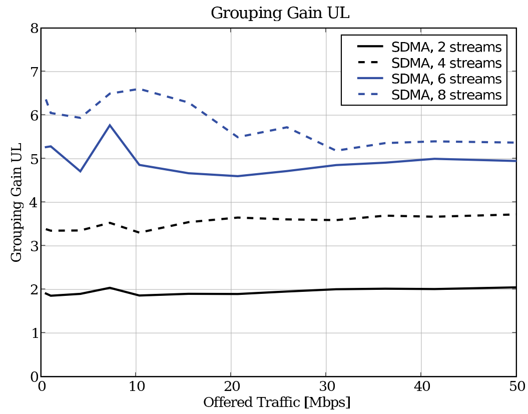

(b) Mean UL gain

Figure 8.16: Grouping gain for different limits of concurrent SDMA data streams

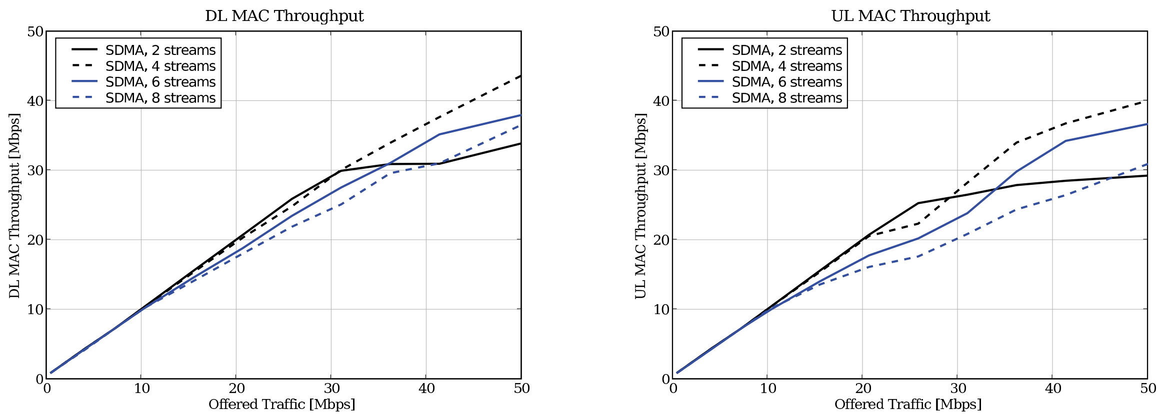

(a) Mean DL MAC Throughput **(b)** Mean UL MAC Throughput

Figure 8.17: DL and DL MAC Throughput for different limits of concurrent SDMA data streams

8.2.3 EIRP Limitation

The Equivalent Isotropic Radiated Power (EIRP) of a transmitter is the amount of power that would have to be emitted by an isotropic antenna in order to produce the same peak power density as it is observed in the direction of the maximum antenna gain of that particular transmitter. Regulation restricts EIRP in certain frequency bands to limit exposure of humans to electromagnetic fields and to minimize the interference range.
An antenna array adaptively forms antenna patterns of varying shape. The maximum antenna gain is not pre-defined but it results from the number and directions of desired and undesired signals. Once the weights per antenna element are calculated by the beamforming algorithm the shape of the antenna pattern and therewith the maximum antenna gain is fixed. In order to stick to potential EIRP restrictions the Tx power of the BS must be adjusted. With a single stream, the Tx power is adjusted so that the main beam meets the EIRP limits. With multiple streams, the signal energy of all antenna patterns sums up and the total must follow the EIRP limit.
The EIRP limit applies to the DL only, reducing Tx power at the BS. In the following, the DL of the Reference Scenario is evaluated in an EIRP limited frequency band. The EIRP limit is set to 1 W, which is the limit in the upper 5 GHz WLAN bands specified for outdoor usage in Germany. Omnidirectional antennas always meet the 1 W EIRP limit. Thus, only the

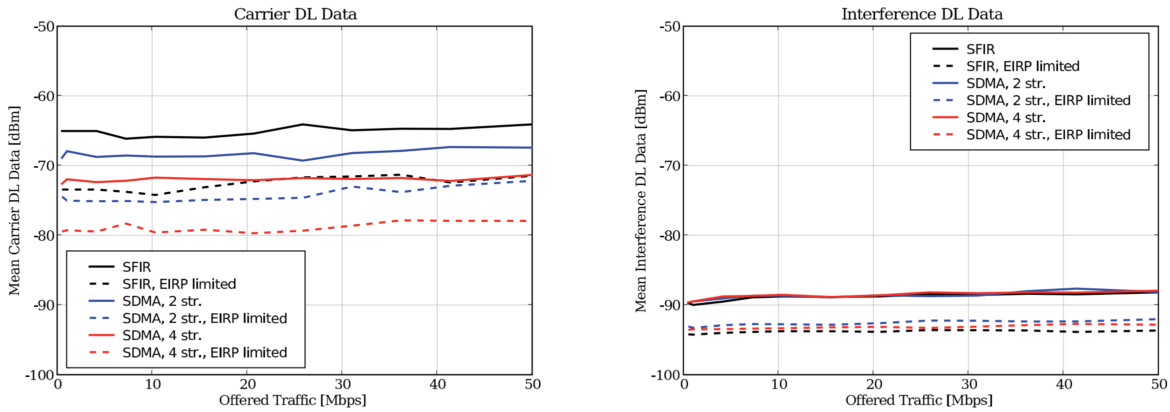

(a) Mean DL carrier **(b)** Mean DL interference

Figure 8.18: Carrier and interference reduction due to EIRP limitations

SFIR and SDMA modes need to be discussed in this section.
Figure 8.18a shows that the EIRP limitation decreases the mean carrier strength in DL by 6 to 7 dB when compared to the unlimited scenario. Apparently, the mean antenna gain of the main beam is in the range of 6 to 7 dBi and this is what needs to be compensated for by reducing the BS's Tx power. The Tx power reduction leads to a reduced interference level. Figure 8.18b indicates that the mean interference level is reduced by 5 to 6 dB. An advantageous side effect of the EIRP restriction is that the variance of the inter-cell interference is decreased as well easing estimation of the proper MCS.
When following the EIRP limit, the carrier strength reduces slightly more than the interference level, but the influence of noise increases. Since the noise level stays constant while the carrier and the interference are decreasing, SINR is further reduced so that the resulting DL SINR is weakened by the EIRP limitation. From Figure 8.19a can be seen that SINR drops by 1 to 3 dB when compared to unlimited EIRP.
The lower signal quality leads to lower throughput capacity. It is observed that the DL MAC throughput in Figure 8.19b saturates with lower offered traffic under EIRP limitation. Independent of EIRP limits, smart antennas in general can improve system capacity significantly.

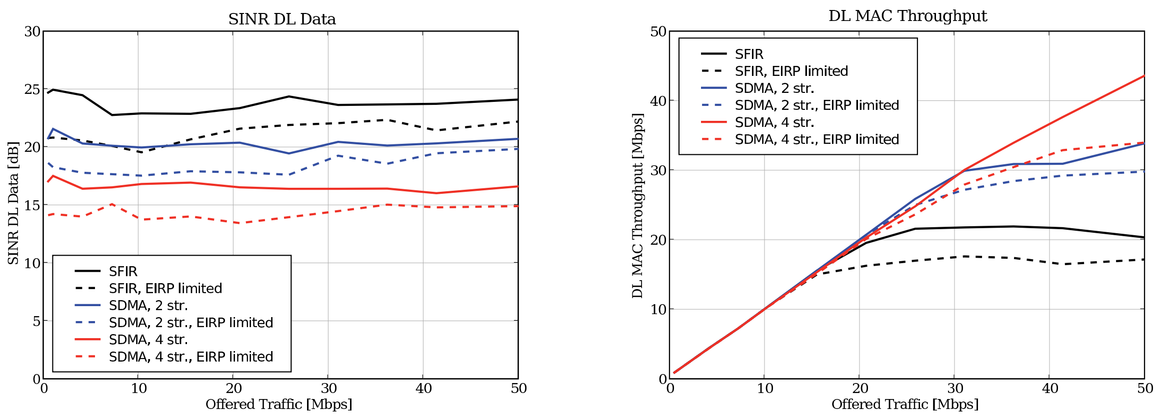

(a) Mean DL SINR **(b)** Mean DL MAC throughput

Figure 8.19: DL SINR and DL MAC throughput with and without EIRP limitations

8.2.4 Network Deployment

In cellular networks, cell radius and Cluster Order (CO) are the main parameters determining cost and performance. Other parameters, such as sectorization, antenna hight and tilt, number of antennas, etc. may have a substantial impact, too. The following, we investigate the influence of the cell radius, the CO and the number of antennas on the overall system performance. Other simulation parameters are set according to the Reference Scenario, see Table 8.2. Operation is limited to a maximum of four concurrent SDMA streams.

8.2.4.1 Cell Radius

A larger cell radius leads to a wider coverage per BS so that less BSs have to be deployed to cover a given area. This is extremely important from an economical point of view because the costs for sites and equipment scales with the number of deployed BSs. However, the cell radius cannot be chosen arbitrarily large. In noise limited systems, cell-edge SSs would perceive insufficient SINR leading to blocked SSs. In interference limited systems, the BS would not be able to satisfy the increasing traffic load per cell leading to unsatisfied users.
The maximum cell radius to achieve a specified minimum signal quality at receivers of broadcast control signaling is analyzed in Chapter 6. The

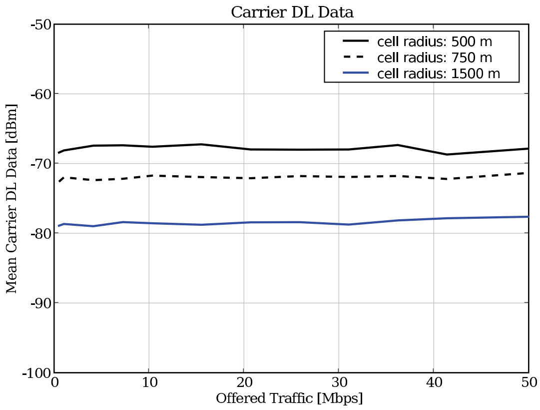

(a) Mean DL carrier strength

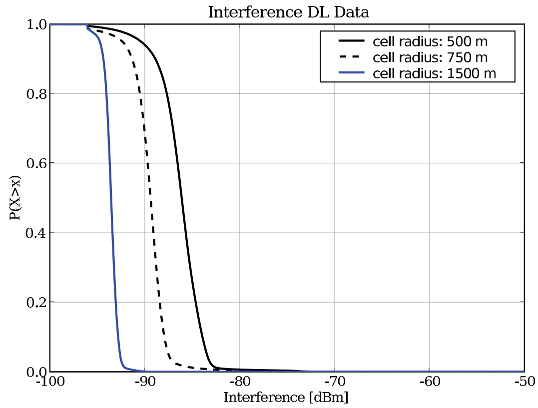

(b) CCDF of DL interference (1 Mbps total offered traffic)

Figure 8.20: Carrier and interference for different cell sizes ($CO = 7$, 4 streams)

following simulation study focuses on user data transmission where adaptive antennas are used for supporting multiple data streams. While varying the cell radius, the number of SSs per cell is kept constant. When doing so, the cell throughput of scenarios with different cell radii can be compared. Necessary control signaling, such as FCH and MAPs, is assumed to be error-free. The perceived control channel SINR is analyzed separately.

Figure 8.20a shows the mean carrier strength during reception of DL data. The carrier strength increases by about 4 dB when the cell radius is decreased from 750 to 500 m. It decreases by about 7 dB when the cell radius is increased from 750 to 1500 m owing to higher or lower pathloss.

In large cells, $R = 1500\,\text{m}$, co-channel BSs are far away leading to low interference, see Figure 8.20b. In small cells, $R = 500\,\text{m}$, co-channel BSs are close leading to high interference.

In DL, both carrier signals and interference are relatively low so that noise significantly influences SINR. In small cells (500 m) signals are stronger than in the reference case (750 m) increasing the SINR by 0.5 to 1 dB, see Figure 8.21a. In large cells (1500 m) the SINR decreases by 2 to 3 dB.

The MAC throughput reflects the SINR behavior. The DL MAC throughput in Figure 8.21b is reduced with increasing cell radius.

In UL, carrier signals and interference are higher than in DL so that noise has nearly no influence on the SINR and the mean UL SINR remains independent of the cell radius. Since the UL MAC throughput is not affected, UL results

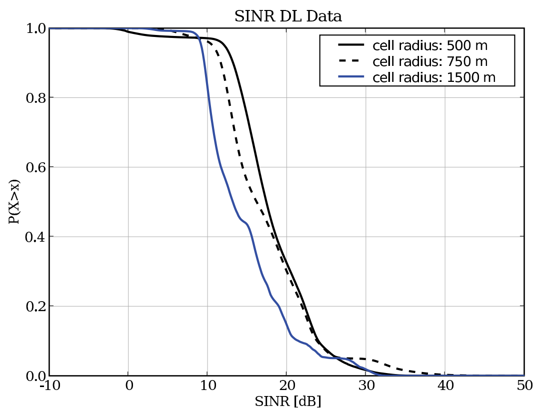

(a) CCDF of DL SINR (1 Mbps offered traffic)

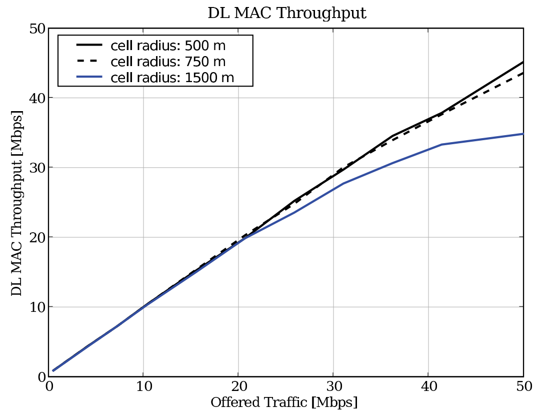

(b) Mean DL MAC throughput

Figure 8.21: SINR and corresponding MAC throughput for different cell sizes ($CO = 7$, 4 streams)

are not shown here.
Broadcast control signaling is transmitted by omnidirectional antennas, no adaptive antenna gain can be applied. In TDD mode, co-channel cells operate synchronously. Chapter 6 outlined that the SINR of the broadcast control phase is a crucial parameter especially when dimensioning networks that use adaptive antennas. Figure 8.22 shows that for a cell radius of 500 and 750 m the SINR is always above the minimum SINR required for BPSK 1/2. For $R = 1500$ m SINR might drop below 6.4 dB leading to packet errors. These simulative results match the analytical results shown in Figure 6.5a. Considering signal quality during the data phase, an operation with large cell radii is possible. Adaptive antennas at the BS overcome the enlarged pathloss. But considering the quality of the broadcast control signaling, this phase becomes the limiting factor. We can conclude that the control channels of WiMAX does not match to the data channels when applying adaptive antennas.

8.2.4.2 Cluster Order

The channel bandwidth and the Cluster Order (CO) determine the total amount of spectrum that an operator needs to run a wireless communication system. Because spectrum suitable for cellular systems is a scarce and highly

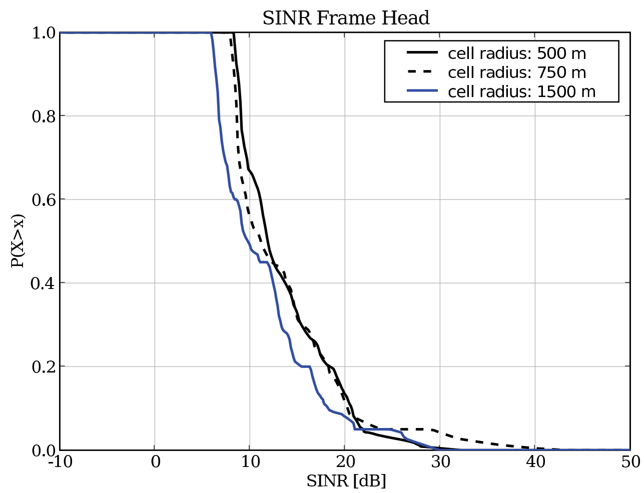

Figure 8.22: SINR of broadcast control signaling (CCDF at 1 Mbps offered traffic)

expensive resource, it is desirable to squeeze as much capacity as possible out of spectrum licensed to an operator. Therefore it is preferable to use low COs. Especially a frequency reuse of one is the goal of most network planners. However, a low CO leads to a high co-channel interference and low SINR.

The minimum CO that can be operated can be calculated from the minimum required SINR of the broadcast control channel, see Chapter 6. The following simulation study focuses on the user data phase where adaptive antenna patterns are applied. Necessary control signaling is assumed to be error-free. The interference distribution in DL under low load (1 Mbps) is shown in Figure 8.23a. When compared to $CO = 1$, $CO = 3$ decreases the mean DL interference by 7 dB. $CO = 12$ decreases it by 12 dB.

Figure 8.23b illustrates the corresponding UL interference distribution. Compered to $CO = 1$, $CO = 3$ decreases the mean UL interference by 5 dB while $CO = 12$ decreases it by 9 dB. Although the mean interference decreases with increased CO, the variance increases, so that the link quality is less predictable.

When the cell radius is kept constant the CO has no impact on the strength of the carrier signal. Thus, the resulting SINR reflects the interference distribution. The resulting mean MAC throughput is shown in Figures 8.24a and 8.24b. With $CO = 1$ the DL capacity derived from saturation level is 15 Mbps. In the Reference Scenario ($CO = 7$) the capacity is about

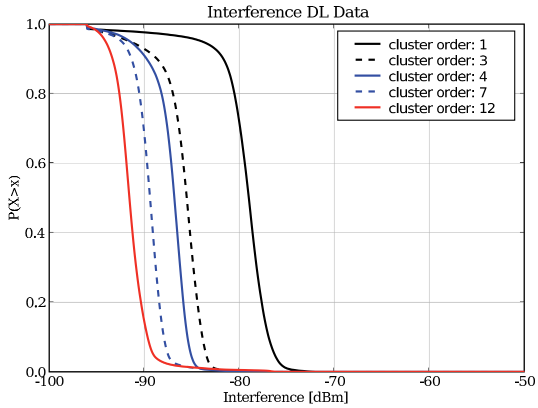

(a) DL interference **(b)** UL interference

Figure 8.23: CCDF of interference with different COs (1 Mbps offered traffic)

30 Mbps, although some cell-edge SSs suffer quite early from undesirable SINR conditions, refer to Section 8.2.1.1. The UL capacity of an SDMA-enabled system with $CO = 1$ is around 8 Mbps and can be increased up to 20 Mbps with $CO = 7$, see Figure 8.24b.

The above results show that the mean MAC throughput can roughly be doubled when increasing CO from one to seven. At the same time, the spectrum needs increases by a factor of seven, so that the system spectral efficiency in general goes down by a factor of 3.5 when increasing CO from one to seven.

Like in the previous subsection, the SINR of broadcast control signaling is the parameter that strictly limits the reduction of CO. SSs need to receive broadcast control signals periodically with an SINR above the BPSK 1/2 threshold of 6.4 dB. Figure 8.25 confirms the analytical results given in Section 6.1 (see Figure 6.5a): $COs = 7$ and $COs = 12$ guarantee the required SINR of 6.4 dB with probability one. With a lower CO the 6.4 dB value of SINR is failed by the broadcast signals in 24% (40%) with $CO = 4$ ($CO = 3$). With $CO = 1$ SINR falls below the threshold of 6.4 dB for 70% of all broadcast transmissions thus preventing the OFDM-based WiMAX system from a reuse one deployment.

Although a system setup using low COs lead to reasonable SINR during data transmissions, the broadcast channel becomes the limiting factor. The Reference Scenario (under the assumptions made) has therefore the minimum

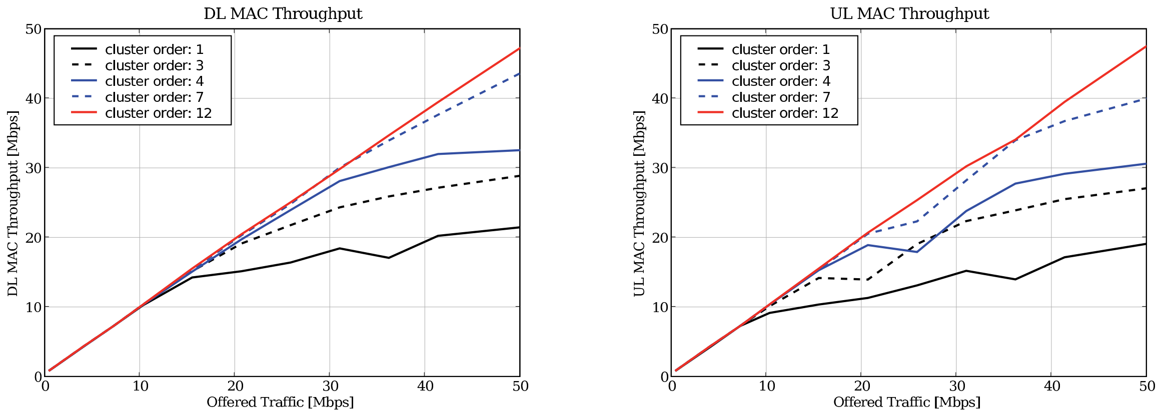

(a) Mean DL MAC throughput **(b)** Mean UL MAC throughput

Figure 8.24: Mean MAC throughput for different COs

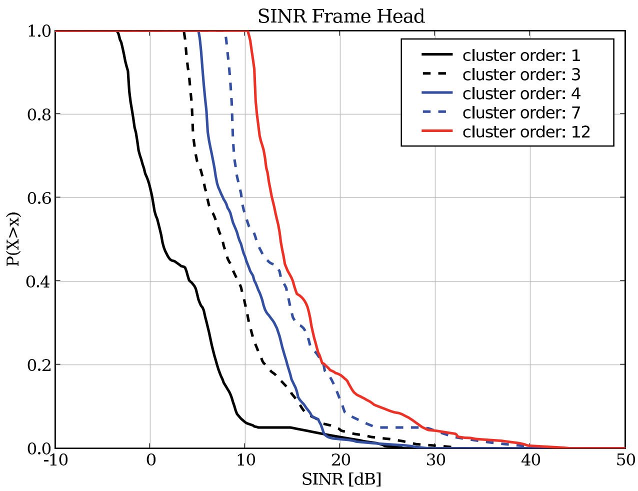

Figure 8.25: CCDF of broadcast channel SINR (1 Mbps offered traffic)

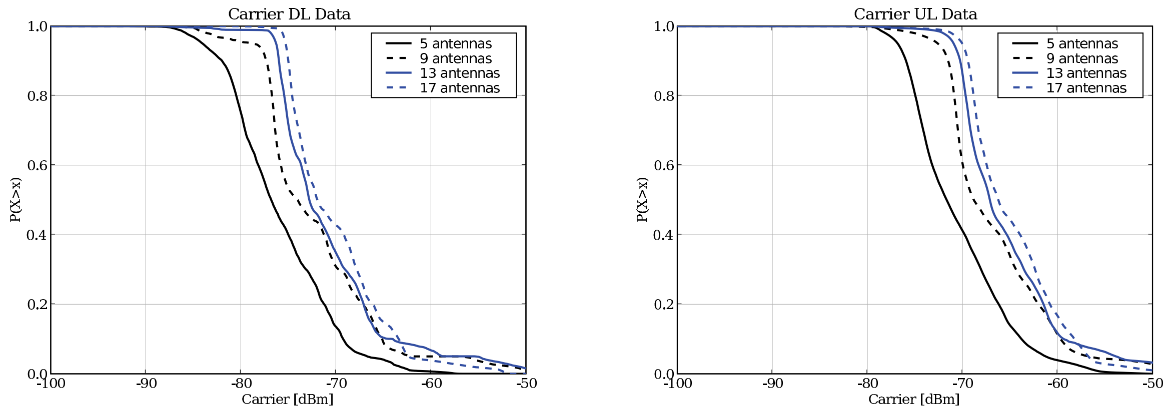

(a) DL carrier   **(b)** UL carrier

Figure 8.26: CCDF of carrier signal strength for a variable number of BS antenna elements (1 Mbps offered traffic)

CO (= 7) that can be operated in a real world system. In order to allow for a smaller CO sectorization as introduced in Section 6.1 can be applied. Furthermore, the OFDMA-based PHY specification of WiMAX specifies optional repetition codes for the broadcast phase that reduce the required SINR threshold to about 0 dB, so that operation with $CO = 3$ becomes feasible.

8.2.4.3 Impact of Number of Antennas

The number of antenna elements determines the capability of the BS to steer beams to desired SS and to set nulls towards undesired SSs. Although the number of antenna elements linearly increases the array efficiency, multi-antenna arrays are expensive, complex in signal processing, and occupy much space at the BS site and, therefore must be optimized. In the following we evaluate the Reference Scenario (up to four concurrent SDMA streams) using a variable number of antenna elements at the BS.

The gain of the main beam determines the carrier signal strength. The more antenna elements are deployed the higher the antenna gain is. In DL, the carrier strength is reduced by 4 dB when the number of antennas is reduced from nine to five (see Figure 8.26a). The signal strength increases by 1 dB when four elements are added to the 9-element UCA. Four more elements give another 1 dB gain. The UL carrier strength, whose CCDF is shown in

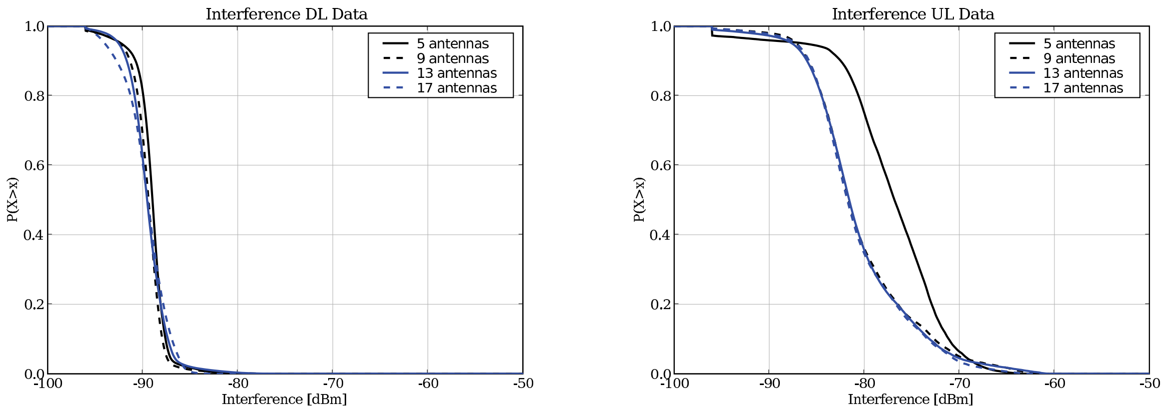

(a) DL interference **(b)** UL interference

Figure 8.27: CCDF of interference for a variable number of BS antenna elements (1 Mbps offered traffic)

Figure 8.26b, varies in almost the same manner.

In the Reference Scenario up to four streams can be scheduled simultaneously. Having five antenna elements there is only one degree of freedom left for further optimization of the antenna pattern. With nine antenna elements more than five degrees of freedom are available to optimize the patterns. More than nine elements allow for even higher gain but the increase in carrier strength (with four concurrent streams) is getting smaller. Using twice the number of antenna elements compared to the number of concurrent data streams appears to be a good choice.

The quality of nulls steered towards concurrently active SSs in the same cell determines the intra-cell interference. The mean level of inter-cell interference in DL is independent of the number of antenna elements, while the mean UL inter-cell interference scales with the number of concurrently active SSs. The CCDF of DL interference, which is composed of inter- and intra-cell interference is shown in Figure 8.27a. The number of antenna elements does not affect the mean value although the variance is increased slightly with more elements. This result indicates that the quality of the nulls steered towards undesired SSs of the same cell is excellent already with nine elements. Furthermore, the DL scheduler can adapt the schedule to the capability of the antenna array. With less elements available, less terminals are scheduled simultaneously degrading the grouping gain. It was found by simulation

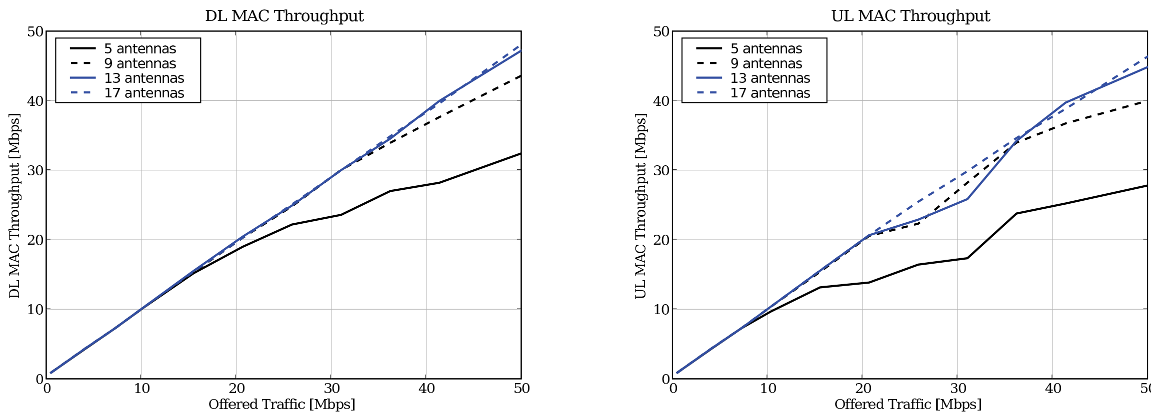

(a) Mean DL MAC throughput **(b)** Mean UL MAC throughput

Figure 8.28: Mean MAC throughput for a variable number of BS antenna elements

that with five elements the mean grouping gain is 1.8 compared to 2.3 in the Reference Scenario using nine antennas.

Simulation results further show that the mean UL grouping gain stays around 3.5 independent of the number of antennas. Due to high UL inter-cell interference in general, the UL scheduler cannot react as sensitive to intra-cell interference as possible in DL. The CCDF of UL interference in Figure 8.27b shows that interference drops by more than 3 dB if the number of antennas is increased from five to nine. This results from an increased quality of nulls steered towards SSs of the same cell that are simultaneously transmitting using different beam patterns. Adding more than five elements does not affect the interference any more. Hence, with nine elements at the BS the quality of the nulls is excellent as well. As in DL, using twice as many antenna elements compared to the number of concurrent data streams appears to be a good choice.

The MAC throughput shown in Figure 8.28 much depends on the number of antenna elements. With five elements, the system runs into saturation at about 8 Mbps in UL while 15 Mbps are reachable in DL. DL saturation is caused by the weak carrier and the low grouping gain, UL saturation is caused by high interference. With nine elements the throughput is more than doubled, i.e., 20 and 30 Mbps in UL and DL respectively. Increasing the number of elements up to 13 or 17 elements appears not to increase throughput substantially. From the results presented in this chapter it can be concluded that the number of antenna elements should be twice as high as the number of concurrent data streams.

8.2.5 Influence of Estimation Error on Performance

Simulation studies in the previous sections are assumed to have perfect channel knowledge at the time of the scheduling decision. Then the precise Direction of Arrival (DoA) and Direction of Departure (DoD) of all SSs of the same cell can be easily extracted. The delay between the time instant of an actual channel measurement during UL burst reception in the respective subframe and the time instant of the scheduling decision has been neglected in the results presented so far. This delay depends on the frame duration and on the frequency of UL transmissions in successive MAC frames by a given SS. The scheduler determines the final schedule at the beginning of each frame, i.e, the end of the UL subframe, in order to broadcast the DL and UL MAPs. The time delay between the scheduling decision and the actual transmission is taken into account: 5 ms at maximum for the DL and 5 to 10 ms for the UL, since DL is served first in the frame.

Positions of SSs outside a given cell are not known at all, i.e., DoA estimation cannot be done for co-channel SSs. Their interference is measured at the time of reception. In the following the influence of DoA and DoD estimation errors on system performance is evaluated.

Estimation errors occur due a number of imperfections: The channel cannot be perfectly estimated due to inter-cell interference and noise during reception of training symbols (preamble and pilot symbols). The SINR of training symbols is further reduced by Inter Carrier Interference (ICI) due to Doppler shift, or by Inter Symbol Interference (ISI) due to not perfectly synchronized clocks. The quality of the channel state information is degraded by quantization errors. The quantized channel knowledge is then used to optimize the adaptive antenna pattern. The time delay between the generation of a channel estimate and its actual application for forming the adaptive pattern introduces inaccuracies that are due to slow and fast fading processes of the wireless channel caused by moving SSs and by mobile objects in the environment. Last but not least imperfectly calibrated BS equipment distorts an adaptive beam. All these imperfections finally lead to DoA and DoD estimation errors.

This section models estimation errors by explicitly adding Gaussian noise with zero means to the correct DoA and DoD. The variance is set to 3°, 6°

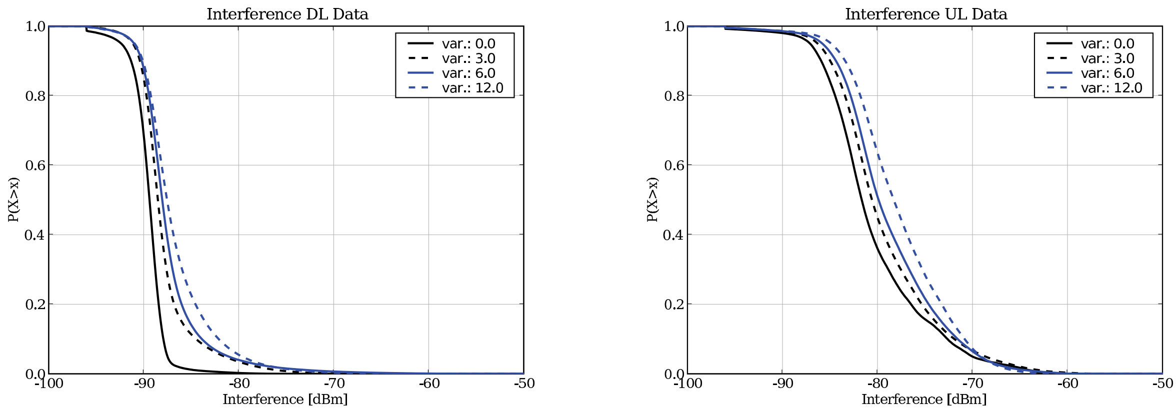

(a) DL interference **(b)** UL interference

Figure 8.29: CCDF of interference under DoA and DoD estimation error (zero-mean AWGN with variance of 0 to 12 square degree, 1 Mbps offered traffic)

and 12° resulting in a standard deviation of 1.73, 2.45, and 3.46, respectively. These three values can be seen as typical for scenarios where the angular spread is low (due to LOS condition), the training sequence is large (UL preamble and UL pilot symbols) and the SINR during channel estimation are high [Fuhl, 1997]. A reference for zero variance is provided as well for the simulation results presented in the following.

DoA and DoD estimation errors lead to incorrect beam steering. A main beam that does not steer towards the desired SS reduces the carrier signal strength. A null that does not point towards a simultaneously active SS increases intra-cell interference. The level of inter-cell interference is not affected by direction estimation errors because the adaptive antenna pattern is not optimized to consider SSs of co-channel cells in our simulator.

It was found by simulation that the mean carrier strength in UL and DL is nearly independent of the estimation errors. The main beam seems to be quite broad so that small inaccuracies of the DoA and DoD estimates can be neglected. Beams of an antenna pattern, e.g. as shown in Figure 4.4b, are usually broader than nulls. Consequently, estimation errors increase the intra-cell interference more than they reduce the carrier signal. Figures 8.29a and 8.29b show the CCDF of DL and UL interference under different direction estimation errors. The mean interference level increases up to 2 dB

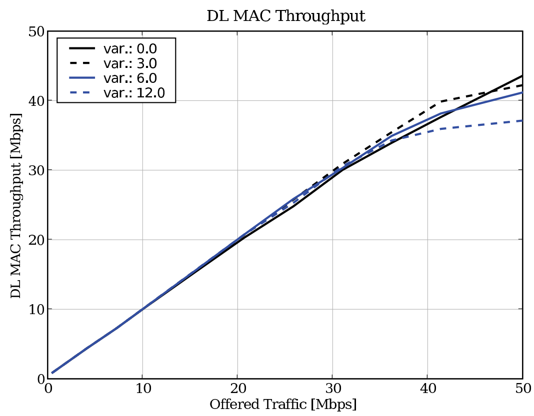

(a) Mean DL MAC throughput

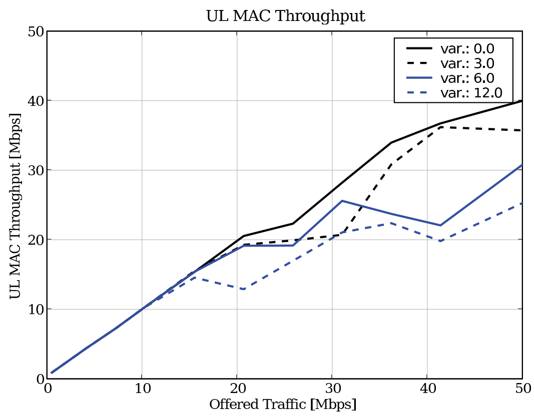

(b) Mean UL MAC throughput

Figure 8.30: Mean DL and UL MAC throughput with DoA and DoD estimation errors (variance of zero-mean Gaussian error between 0 and 12 square degree)

in UL and up to 3 dB in DL with the highest variance of 12 square degree. In DL the overall interference level is lower than in UL so that the increased intra-cell interference has a larger effect: especially, the worst 20% of DL interference significantly increase. In UL, the overall interference level is rather high and extra intra-cell interference influences the majority of SSs equally. The worst 10% are nearly not affected.

The increased intra-cell interference that results from direction of patterns errors is expected to degrade the SINR and system performance. In DL, the scheduler reduces the number of concurrently scheduled SSs due to the enhanced interference. The mean grouping gain degrades from 2.3 (perfect estimation) to 1.8 (12° error) so that the DL MAC throughput is slightly reduced, see Figure 8.30a.

In UL the grouping gain is less affected than in DL. The UL is much more sensitive to interference variation and the UL MAC throughput degrades much more than the DL MAC throughput resulting in a reduced system capacity. When operated beyond the saturation capacity the system behaves incalculably.

It can be concluded that the DL of an SDMA enhanced WiMAX system can tolerate DoA and DoD estimation errors as long as the capacity limit in not exceeded. However, the UL capacity is reduced by such errors. In real cellular systems mobile stations move faster than 3.6 $^{km}/_{h}$, as assumed here, and NLOS propagation conditions are expected to lead to a much lower quality of channel estimations and large estimation errors. This is expected to cause serious performance degradation, especially in UL.

8.2.6 Adaptive Space-Time Sectorization

The general idea of adaptive STS (see Section 4.5.1) is to group all SSs of a cell into logical sectors. Logical sectors are served in subsequent time slots while SSs within a logical sector are served by the adaptive antenna array in SDMA mode. This offers the same potential to reduce inter-cell interference as fixed sectorization. One drawback is that fixed sector antennas do have smaller side lobes than adaptive antennas. However, STS is more flexible because the number and the shape of the sectors can be modified just by re-grouping SSs. Logical sectors do not need to cover a continuous area, they can be divided into subsectors for better spatial separation of SSs served in SDMA (see Figure 4.23). The hierarchical TD-SD-OFDM scheduler introduced in Section 4.4 is suited to support STS by respecting logical groups of SS while performing spatial grouping.

When applying adaptive STS the DL and UL carrier signal strength do not change: SSs are served with the same array and the same beam steering algorithm so that the resulting antenna pattern allows for the same transmit and receive antenna gain.

In DL, STS sectors do not reduce the mean interference as shown in Figure 8.31a. Apparently, the probability that a SS is hit by a co-channel main beam or side lobe does not depend on number of logical STS sectors and subsectors.

Figure 8.32 shows that both, the DL and UL grouping gain are reduced with increased number of STS sectors: with two logical sectors, only half of the SSs are available to be served in a given time slot. This lowers the probability of finding multiple SSs to be served in a given logical group that are separable in space. This observation corresponds to the fact that the trunking gain under sectorization is reduced Walke [2001]. Dividing sectors into spatially separated subsectors does not affect the grouping gain much.

The mean UL interference shown in Figure 8.31b degrades with an increasing number of STS sectors because the UL grouping gain is reduced. Sectorization reduces the number of SSs that can be scheduled simultaneously. The number of potential SSs to be served is the smaller the higher the number of sectors

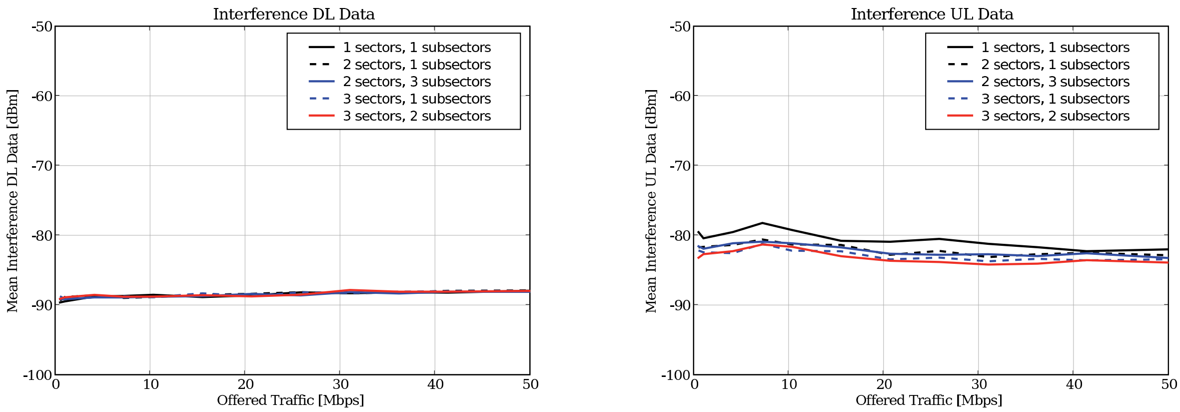

(a) Mean DL interference **(b)** Mean UL interference

Figure 8.31: Influence of STS on the interference level

is thereby reducing the UL grouping gain, Figure 8.32b and in turn inter-cell interference, Figure 8.31b.

A DL grouping gain reduced in comparison to the Reference Scenario, together with an unchanged DL SINR level results in a DL MAC throughput degradation when using STS. Figure 8.33a shows that the mean MAC throughput degrades with the number of sectors as expected from the reduced grouping gain. Subsectors do not have the expected effect of increasing the SDMA throughput capacity. In UL, STS reduces the grouping gain but increases the UL SINR. Figure 8.33b shows that the reduced grouping gain dominates increased SINR leading to reduced UL MAC throughput.

The results presented give evidence that STS appears unable to increase the throughput capacity in SDMA-enabled WiMAX networks. Apparently, adaptive antenna patterns are sufficient to reduce undesired interference so that STS cannot improve capacity further. An attempt to engineer the inter-cell interference by means of STS appeasr not to be beneficial. More promising would be an attempt to explicitly consider specific co-channel SSs when shaping an an actual antenna pattern. Then, nulls could be steered towards currently active co-channel SSs. This would require a sophisticated information exchange for coordination between BSs.

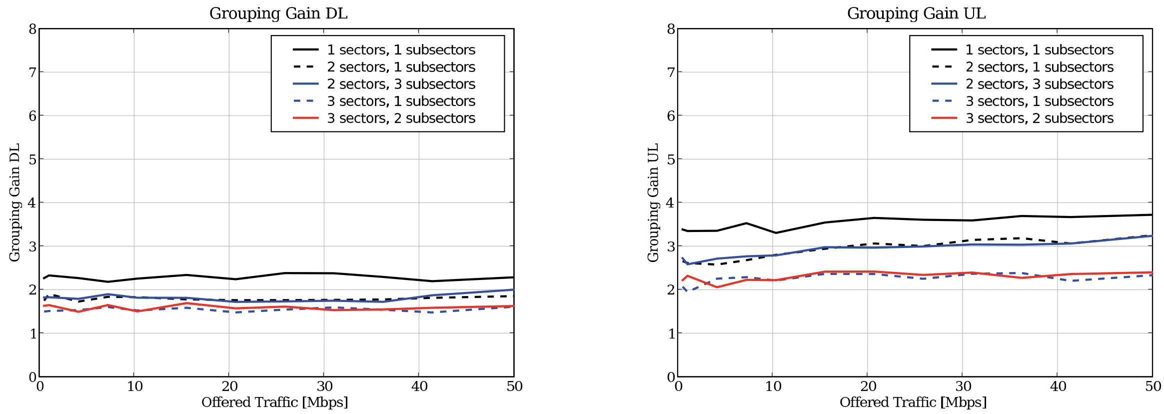

(a) Mean DL grouping gain **(b)** Mean UL grouping gain

Figure 8.32: Grouping gain reduction due to STS

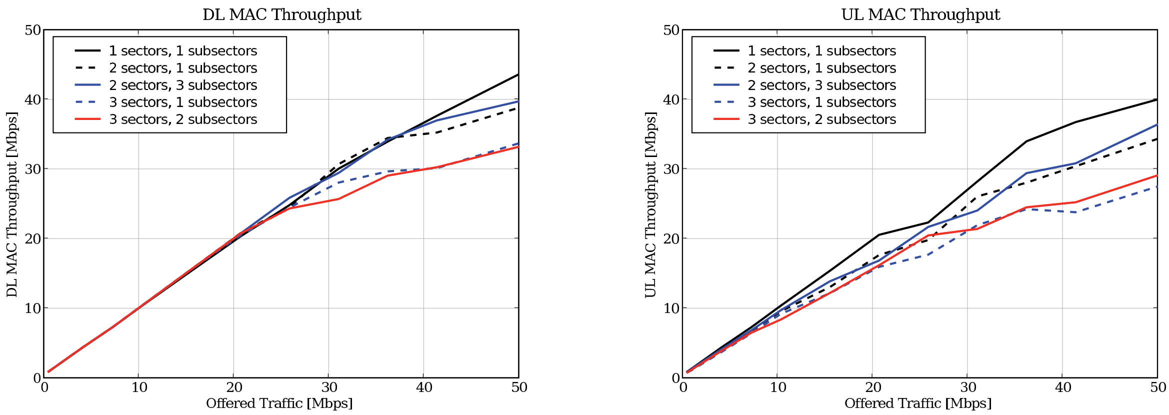

(a) Mean DL MAC throughput **(b)** Mean UL MAC throughput

Figure 8.33: DL and UL MAC throughput using Space-Time Sectorization

8.3 Conclusion

The simulation results presented prove that SDMA is well suited to boost system capacity. The SDMA-enabled scheduling algorithm introduced is able to increase the MAC throughput and decrease packet delay substantially when compared to operation without SDMA. In the Reference Scenario a 9-element Uniform Circular Array at the BS with adaptive control has been shown to double DL and UL cell throughput compared to an omnidirectional antenna. And SDMA with two concurrent data streams has been shown to further increase throughput by about 70% in DL and 40% in UL, respectively. In DL the capacity limiting factor is the BS transmit power shared among simultaneous streams. In UL the increased and highly varying interference causes the capacity limits. The SDMA-enabled scheduler is making decisions based on unreliable SINRs prediction values. To improve its behavior, the BS scheduler should apply a long-term persistent behavior to not overreact to random signal fluctuation reported. In addition, coordination of beam control between BSs is expected to reduce interference and increase capacity. The optimum number for an upper limit of simultaneous data streams depends on the number of antenna elements at the BS. For the investigated Reference Scenario a maximum of four concurrent streams appeared optimum with a 9-element UCA at the BSs.

For dimensioning the cell radius and the CO of SDMA-enabled networks the omnidirectional broadcast control phase is the limiting factor. During user data phases adaptive antennas may be able to support much larger large cell radii and much lower COs than required for the broadcast channels to be effective. In the Reference Scenario, even a frequency reuse one appeared possible for the data phase. However, the broadcast control phase limits both, the minimum CO and the maximum cell radius. The synchronized, non-sectorized, cellular Reference Scenario studied requires $CO = 7$ and allows a maximum radius of less than 1000 m. Thus, future effort should be spend to increase robustness of broadcast transmission in SDMA-enabled WiMAX networks.

CHAPTER 9

Summary & Conclusion

9.1 Summary

Broadband Wireless Access (BWA) is one of the key drivers of the telecommunications industry today. In metropolitan areas, fixed BWA offers a cost-effective alternative to wired access such as DSL and cable modems. Especially in rural areas BWA technology offers market potential to extend access to telecommunication services for portable and mobile terminals.

Standard IEEE 802.16, supported by the WiMAX forum, is a promising radio technology that offers fixed and mobile BWA. WiMAX promises high performance similar to that of wired systems and it allows for covering large geographic regions. One key feature of WiMAX is the support of multi-antenna techniques, especially, the support for beamforming and SDMA. The results presented in this thesis motivated the IEEE 802.16 group to accept the SDMA support for the OFDM-based air interface as proposed by the author.

The thesis describes a comprehensive system concept to fully integrate SDMA technology into the WiMAX system. SDMA affects a large portion of the IEEE 802.16 system: Multiple antennas are required in the PHY layer to form adaptive patterns. Through the new PHY SAP specified in this thesis, a multi-antenna PHY layer offers enhanced services to MAC layer entities. The MAC protocol is extended to take the spatial dimension into account. The proposed hierarchical TD-SD-OFDM scheduling algorithm optimizes resource allocation while observing strict real-time constraints.

For multi-hop transmissions, a MAC extension is worked out and evaluated. By leveraging SDMA at the BS, the proposed MAC structure strengthens the feeder link between BS and RS, which is seen to be the bottleneck. Interference suppression by means of beamforming at the RS allows for a tight spatial reuse on the access link.

Analytical models are used to evaluate the upper bound of the OFDM-based IEEE 802.16 system in terms of cellular coverage and throughput.

It compares single-hop and multi-hop scenarios and illustrates the advantages of multi-hop operation. The thesis also introduces a prototypical implementation of an SDMA-enabled IEEE 802.16 system, especially of the TD-SD-OFDM scheduler, which is embedded in an event-driven system level simulator. The simulation tool comprises all aspects of the WiMAX system that are affected by SDMA operation.
The performance evaluation results gained by means of computer simulation show the potential gains of beamforming and SDMA technologies in terms of throughput, packet delay, and extended coverage range of the SDMA-enhanced WiMAX system. The major parameters that influence the system performance are identified and evaluated.

9.2 Conclusion

The WiMAX system offers all key features that characterize future wireless communication systems: Its OFDM based physical layer is optimized to operate on large channel bandwidth and under challenging multipath propagation conditions. Its TDMA/OFDMA multiple access scheme allows to exploit the time- and frequency-selective wireless channel. The MAC layer provides QoS support according to the needs of multimedia services.
Advanced antenna systems are the ultimate feature to boost link and system capacity. However, the integration of advanced antenna techniques into wireless communication systems involves more than just the physical layer. Instead cross layer functions have to be considered and optimized. The introduction of beamforming and SDMA has a deep impact on both PHY and MAC layer protocols and its corresponding algorithms.
The analytical evaluation performed underlines that SDMA operation has consequences for the dimensioning and planning of networks. Current networks tend to be noise or interference limited. Due to adaptive antennas, interference can be reduced and carrier signals can be strengthened. Hence, multi antenna systems become limited in range by broadcast signaling phases that require omnidirectional transmission. Especially the DL broadcast control phase in synchronized and EIRP limited networks appears to be the reason for limiting the cell radius.
Simulation results validate these limiting factors for dimensioning multi antenna networks. The SINR distribution resulting from the adaptive antenna supported data phase is fundamentally better compared to the

SINR during the broadcast phase. The data phase could be operated with large cell radii or with low COs and frequency reuse one is possible. In contrast, the broadcast phase of the Reference Scenario requires $CO = 7$ and a maximum cell radius smaller than 1000 m.
The simulation based performance evaluation results show the potential of beamforming technologies. However, results also indicate that an SDMA-enhanced WiMAX system has to be carefully configured. In DL, carrier strength weakens when the BS transmit power is shared amongst concurrent SDMA streams. In UL, interference scales with the number of simultaneously active SDMA SSs. Nevertheless, in the Reference Scenario a 9-element Uniform Circular Array at the BS with adaptive control has been shown to double DL and UL cell throughput capacity compared to an omnidirectional antenna. SDMA with two concurrent data streams has been shown to further increase throughput by about 70% in DL and 40% in UL, respectively. These gains clearly indicate why multi-antenna techniques and especially beamforming and SDMA are an essential part of modern wireless communication systems.

LIST OF ABBREVIATIONS

1xEVDO Evolution Data-Optimized
2G 2nd Generation
3G 3rd Generation
3GPP 3rd Generation Partnership Project
3GPP2 3rd Generation Partnership Project 2
AAS Advanced Antenna System
ACK Acknowledgment
AMC Adaptive Modulation and Coding
AP Access Point
ARQ Automatic Repeat Request
ATM Asynchronous Transfer Mode
ATS Abstract Test Suite
AWGN Additive White Gaussian Noise
BE Best Effort
BER Bit Error Ratio
BLAST Bell Labs Layered Space Time
BLER Block Error Ratio
BPSK Binary Phase Shift Keying
BRAN Broadband Radio Access Networks
BS Base Station
BSID BS Identifier
BSN Block Sequence Number
BTC Block Turbo Code
BWA Broadband Wireless Access
CAPEX Capital Expenditure
CC Convolutional Code
CCDF Complementary Cumulative Distribution Function
CDM Code Division Multiplex
CDMA Code Division Multiple Access
CEPT European Conference of Postal and Telecommunications Administrations
CID Connection Identifier
CO Cluster Order
CP Cyclic Prefix
CPS Common Part Sublayer
CPU Central Processing Unit
CQI Channel Quality Indicator
CRC Cyclic Redundancy Check
CS Convergence Sublayer

CSI	Channel State Information
CTC	Convolutional Turbo Code
dB	Dezibel
DC	Direct Current
DCD	Downlink Channel Descriptor
DFS	Dynamic Frequency Selection
DIUC	Downlink Interval Usage Code
DL	Downlink
DLC	Data Link Control
DLFP	Downlink Frame Prefix
DLL	Data Link Layer
DoA	Direction of Arrival
DoD	Direction of Departure
DSA	Dynamic Service Addition
DSC	Dynamic Service Change
DSD	Dynamic Service Deletion
DSL	Digital Subscriber Line
e.g.f.	Exponential Generating Function
ECC	Electronic Communications Committee
E-DCH	Enhanced Dedicated Transport Channel
EIRP	Equivalent Isotropic Radiated Power
EKS	Encryption Key Sequence
ETSI	European Telecommunications Standards Institute
E-UTRA	Evolved UTRA
E-UTRAN	Evolved UTRAN
FCC	Federal Communications Commission
FCH	Frame Control Header
FDD	Frequency Division Duplex
FDMA	Frequency Division Multiple Access
FEC	Forward Error Correction
FFT	Fast Fourier Transform
FPC	Fast Power Control
FSN	Fragment Sequence Number
FTP	File Transfer Protocol
FU	Functional Unit
FUN	Functional Unit Network
GPCS	Generic Packet Convergence Sublayer
GSM	Global System for Mobile Communication
HARQ	Hybrid ARQ
HCS	Header Check Sequence
HFDD	Half-Duplex FDD

HiperACCESS	High Performance Radio Access Network
HiperLAN/2	High Performance Local Area Network Type 2
HiperMAN	High Performance Metropolitan Area Network
HoL	Head of the Line
HRPD	High Rate Packet Data
HSDPA	High Speed DL Packet Access
HS-DSCH	High Speed DL Shared Channel
HSPA	High Speed Packet Access
HSUPA	High Speed UL Packet Access
HUMAN	High Speed Unlicensed MAN
IAT	Inter-Arrival Time
ICI	Inter Carrier Interference
IE	Information Element
IEEE	Institute of Electrical and Electronics Engineers
IFFT	Inverse Fast Fourier Transform
IMT	International Mobile Telecommunications
IP	Internet Protocol
IPv4	IP Version 4
ISI	Inter Symbol Interference
ISO	International Organization for Standardization
IST	Information Society Technologies
ITU	International Telecommunications Union
ITU-R	ITU Radiocommunications Sector
kbps	Kilobits per Second
LAN	Local Area Network
LDK	Layer Development Kit
LLC	Logical Link Control
LOS	Line-of-Sight
LTE	Long-Term Evolution
MAC	Medium Access Control
MAN	Metropolitan Area Network
Mbps	Megabits per Second
MCS	Modulation and Coding Scheme
MIB	Management Information Base
MIMO	Multiple Input Multiple Output
MISO	Multiple Input Single Output
ML	Maximum Likelihood
MMSE	Minimum Mean Squared Error
MPEG	Moving Pictures Experts Group

MRC	Maximum Ratio Combining
MS	Mobile SS
MSE	Mean Squared Error
MTU	Maximum Transmission Unit
MU	Multi User
MVDR	Minimum Variance Distortionless Response
NLOS	Non Line-of-Sight
nrtPS	Non-Real-Time Polling Service
OEIS	On-Line Encyclopedia of Integer Sequences
OFDM	Orthogonal Frequency Division Multiplex
OFDMA	Orthogonal Frequency Division Multiple Access
OPEX	Operational Expenditure
OSI	Open Systems Interconnection
PAPR	Peak to Average Power Ratio
PC	Personal Computer
PCI	Protocol Control Information
PDA	Personal Digital Assistant
PDF	Probability Density Function
PDU	Protocol Data Unit
PER	Packet Error Ratio
PF	Proportional Fair
PHS	Payload Header Suppression
PICS	Protocol Implementation Conformance Statement
PMP	Point-to-Multipoint
PPP	Point-to-Point Protocol
PSK	Phase Shift Keying
PTP	Point-to-Point
QAM	Quadrature Amplitude Modulation
QoS	Quality of Service
QPSK	Quadrature Phase Shift Keying
RAN	Radio Access Network
RCT	Radio Conformance Tests
REC	Recommendation
REC	Relay Enhanced Cell
RF	Radio Frequency
RISE	Radio Interference Simulation Engine
RLC	Radio Link Control
RNG-REQ	Ranging Request
RNG-RSP	Ranging Response
RR	Round Robin
RS	Relay Station
RS	Reed-Solomon
RTD	Round Trip Delay
RTG	Receive / Transmit Transition Gap
rtPS	Real-Time Polling Service
Rx	Receiver

SA Standards Association
SAP Service Access Point
SAR Segmentation and Reassembly
SC Single Carrier
SCa Single Carrier below 11 GHz
SDL Specification and Description Language
SDM Space Division Multiplex
SDMA Space Division Multiple Access
SDU Service Data Unit
SFC Space Frequency Coding
SFID Service Flow Identifier
SFIR Spatial Filtering for Interference Reduction
SIMO Single Input Multiple Output
SINR Signal to Interference plus Noise Ratio
SIR Signal to Interference Ratio
SISO Single Input Single Output
SME Small and Medium-Sized Enterprise
SNR Signal to Noise Ratio
SOHO Small Office, Home Office
SPEETCL SDL Performance Evaluation Tool Class Library
SS Subscriber Station
STBC Space Time Block Code
STC Space Time Coding
STL Standard Template Library
STRIKE Spectrally Efficient Fixed Wireless Network based on Dual Standards
STS Space-Time Sectorization
STTC Space Time Trellis Code
SUI Stanford University Interim
SVD Singular Value Decomposition
TCP Transmission Control Protocol
TDD Time Division Duplex
TDM Time Division Multiplex
TDMA Time Division Multiple Access
TSS&TP Test Suite Structure and Test Purposes
TTA Telecommunications Technology Association
TTG Transmit / Receive Transition Gap
Tx Transmitter
UCA Uniform Circular Array

UCD	Uplink Channel Descriptor
UDP	User Datagram Protocol
UGS	Unsolicited Grant Service
UIUC	Uplink Interval Usage Code
UL	Uplink
ULA	Uniform Linear Array
UMTS	Universal Mobile Telecommunications System
U-NII	Unlicensed National Information Infrastructure
UTRA	UMTS Radio Access
UTRAN	UMTS Radio Access Network
VCI	Virtual Connection Identifier
VoIP	Voice over IP
VPI	Virtual Path Identifier
WCDMA	Wideband CDMA
WiBro	Wireless Broadband
WiMAC	WiMAX MAC Layer
WiMAX	Worldwide Interoperability for Microwave Access
WINNER	Wireless World Initiative New Radio
WinProSt	WINNER Protocol Stack
WLAN	Wireless Local Area Network
WNS	Wireless Network Simulator
WWW	World Wide Web

BIBLIOGRAPHY

CEPT/ERC/REC 12-05 E, Harmonized radio frequency channel arrangements for digital terrestrial fixed systems operating in the band 10.0 - 10.68 GHz, 1996.

CEPT/ERC/REC 13-04, Preferred frequency bands for fixed wireless access in the frequency range between 3 and 29.5 GHz, 1998.

ERC/DEC (99)15, ERC decision on the designation of the harmonised frequency band 40.5 to 43.5 GHz for the introduction of Multimedia Wireless Systems (MWS), including Multipoint Video Distri-bution Systems (MVDS), 1999.

ERC/REC (00)05, Use of parts of the band 24.5-26.5 GHz for fixed wireless access, 2000.

ERC/REC (01)03, Use of parts of the band 27.5-29.5 GHz for fixed wireless access (FWA), 2001.

3GPP. 3GPP TR 25.913, Technical Specification Group Radio Access Network; Requirements for Evolved UTRA (E-UTRA) and Evolved UTRAN (E-UTRAN), March 2006a.

3GPP. 3GPP TR 25.814; Technical Specification Group Radio Access Network; Physical layer aspects for evolved Universal Terrestrial Radio Access (UTRA), June 2006b.

3GPP2. 3GPP2 C.S0024-0 v4.0; cdma2000 High Rate Packet Data Air Interface Specification, October 2002.

3GPP2. 3GPP2 C.S0024-A v2.0; cdma2000 High Rate Packet Data Air Interface Specification, July 2005.

3GPP2. 3GPP2 C.S0024-B v2.0; cdma2000 High Rate Packet Data Air Interface Specification, March 2007.

S. Alamouti. A Simple Transmit Diversity Technique for Wireless Communications. *IEEE Journal on Select Areas in Communications*, 16(8): 1451–1458, October 1998.

A. Alexiou and M. Haardt. Smart antenna technologies for future wireless systems: trends and challenges. *Communications Magazine, IEEE*, 42(9): 90–97, Sept. 2004.

F. Altman and W. Sichak. A Simplified Diversity Communication System for Behind-the-Horizon Links. *IRE Transactions on Communications Systems*, pages 50–55, March 1956.

Diego Bartolomé Calvo. *Fairness Analysis of Wireless Beamforming Schedulers.* PhD thesis, Universitat Politècnica de Catalunya (UPC), Department of Signal Theory and Communications, Nov 2004.

Nico Bayer, Dmitry Sivchenko, Bangnan Xu, Veselin Rakocevic, and Joachim Habermann. Transmission timing of signalling messages in IEEE 802.16 based Mesh Networks. In *Proceedings of European Wireless*, 2006.

L. Berlemann, R. Pabst, M. Schinnenburg, and B. Walke. A flexible protocol stack for multi-mode convergence in a relay-based wireless network architecture. In *Proceedings of PIMRC*, page 6, Berlin, Germany, Sep 2005. ISBN 3-8007-2909-1. URL `http://www.comnets.rwth-aachen.de`.

V. Bharghavan, Songwu Lu, and T. Nandagopal. Fair queuing in wireless networks: issues and approaches. *Personal Communications, IEEE [see also IEEE Wireless Communications]*, 6(1):44–53, Feb. 1999.

Balvinder Bisla, Roger Eline, and Luiz M. Franca-Neto. RF System and Circuit Challenges for WiMAX. *Intel Technology Journal*, 8(3):189–200, August 2004.

H. Bölcskei and A. Paulraj. Space-Frequency Coded Broadband OFDM Systems. *Proc. IEEE Intl. Symp. Inf. Theory*, June 2001.

S.M. Cherry. The wireless last mile. *Spectrum, IEEE*, 40(9):18–22, Sep 2003.

C. Cicconetti, L. Lenzini, E. Mingozzi, and C. Eklund. Quality of service support in IEEE 802.16 networks. *Network, IEEE*, 20(2):50–55, March-April 2006.

E. G. Coffman, Jr., M. R. Garey, and D. S. Johnson. *Approximation algorithms for NP-Hard Problems*, chapter Approximation algorithms for bin packing - a survey, pages 46–93. PWS Publishing, 1997.

R. Compton. *Adaptive Antennas, Concepts and Performance.* Prentice Hall, 1988.

Thomas H. Cormen, E. Leiserson, Charles, and Ronald L. Rivest. *Introduction to Algorithms.* MIT Press, 1990.

Erik Dahlman, Stefan Parkvall, Johan Skold, and Per Beming. *3G Evolution: HSPA and LTE for Mobile Broadband.* Academic Press, August 2007.

M. Döttling, J.-P. Javaudin, K. Kalliojärvi, G. Klang, T. Sälzer, U. Schwark, A.i Sorri, and C. Wijting. D6.13.2, state-of-the-art evaluation (issue 1). Deliverable, IST-4-027756 WINNER II, June 2006.

J. Eberspächer and H.J. Vögel. *GSM Global System for Mobile Communication.* Teubner Verlag Stuttgart, 1999.

H. Ekstrom, A. Furuskar, J. Karlsson, M. Meyer, S. Parkvall, J. Torsner, and M. Wahlqvist. Technical solutions for the 3G long-term evolution. *Communications Magazine, IEEE*, 44(3):38–45, March 2006.

Jan Ellenbeck. Performance Evaluation of Combined TD-/FD-/SDMA Medium Access Strategies to Support Relay-Enhanced Broadband Cells. Master's thesis, Chair of Communication Networks (ComNets), RWTH Aachen University, April 2006.

Marc Engels, editor. *Wireless OFDM Systems: How to Make Them Work?*, volume 692 of *The International Series in Engineering and Computer Science*. Springer, 2002.

V. Erceg, KVS Hari, MS Smith, DS Baum, et al. Channel models for fixed wireless applications. *IEEE 802.16. 3 Task Group Contributions, Doc. IEEE 802.16. 3. c-01/29r4*, 2001.

N. Esseling, H. Vandra, and B. Walke. A forwarding concept for hiperlan/2. In *Proceedings of European Wireless 2000*, volume 0, pages 13–18, Sep 2000.

N. Esseling, B. Walke, and R. Pabst. *Emerging Location Aware Broadband Wireless Adhoc Networks*, chapter Fixed Relays For Next Generation Wireless Systems, pages 71–91. Springer Science+Buisness Media, Inc., New York, USA, 2005. ISBN 0-387-23070-x.

ETSI. Broadband Radio Access Networks (BRAN); HIPERACCESS; Cell based Convergence Layer; Part 1: Common Part; TS 102 115-1; V1.1.1, September 2002a.

ETSI. Broadband Radio Access Networks (BRAN); HIPERACCESS; Cell based Convergence Layer; Part 2: UNI Service Specific Convergence Sublayer (SSCS); TS 102 115-2; V1.1.1, October 2002b.

ETSI. Broadband Radio Access Networks (BRAN); HIPERACCESS; DLC protocol specification; TS 102 000; V1.4.1, July 2004.

ETSI. Broadband Radio Access Networks (BRAN); HIPERACCESS; PHY protocol specification; TS 101 999; V1.1.1, April 2002c.

ETSI. Broadband Radio Access Networks (BRAN); HIPERACCESS; Packet based Convergence Layer; Part 1: Common Part; TS 102 117-1; V1.1.1, September 2002d.

ETSI. Broadband Radio Access Networks (BRAN); HIPERACCESS; Packet based Convergence Layer; Part 2: Ethernet Service Specific Convergence Sublayer; TS 102 117-2; V1.1.1, October 2002e.

ETSI. Broadband Radio Access Networks (BRAN); HIPERLAN Type 2;

Data Link Control (DLC); Part 1: Basic Transport Functions; TS 101 761-1; V1.3.1, 2001.

ETSI. Broadband Radio Access Networks (BRAN); HIPERMAN; Data Link Control (DLC) Layer, TS 102 178, 2003a.

ETSI. Broadband Radio Access Networks (BRAN); HIPERMAN; Physical (PHY) Layer, TS 102 177, 2003b.

D. Falconer, A. Alexiou, S. Kaiser, M. Haardt, and T. Jämsä. *Technologies for the Wireless Future - Wireless World Research Forum (WWRF)*, volume 2, chapter New Air-interface Technologies and Deployment Concepts, pages 131–226. Wiley & Sons, Ltd, 2006.

H. Fattah and C. Leung. An overview of scheduling algorithms in wireless multimedia networks. *Wireless Communications, IEEE [see also IEEE Personal Communications]*, 9(5):76–83, Oct. 2002.

B. Fong, N. Ansari, A.C.M. Fong, and G.Y. Hong. On the scalability of fixed broadband wireless access network deployment. *Communications Magazine, IEEE*, 42(9):S12–S18, Sept. 2004.

Ingo Forkel. *Performance Evaluation of the UMTS Terrestrial Radio Access Modes*. PhD thesis, RWTH Aachen University, Lehrstuhl für Kommunikationsnetze, November 2005. URL `http://www.comnets.rwth-aachen.de`.

G. Foschini. Layered Space-Time Architecture for Wireless Communication in a Fading Environment when Using Multiple Antennas. *Bell Labs Technical Journal*, 1(2):41–59, 1996.

M. Fuchs, G. Del Galdo, and M. Haardt. A novel tree-based scheduling algorithm for the downlink of multi-user MIMO systems with ZF beamforming. In *IEEE International Conference on Acoustics, Speech, and Signal Processing*, volume 3, 2005.

Josef Fuhl. *Smart Antennas for Second and Third Generation Mobile Communications Systems*. PhD thesis, Institut für Nachrichtentechnik und Hochfrequenztechnik, TU Wien, March 1997.

A. Ghosh, D.R. Wolter, J.G. Andrews, and R. Chen. Broadband wireless access with WiMax/802.16: current performance benchmarks and future potential. *Communications Magazine, IEEE*, 43(2):129–136, Feb 2005.

R. Giuliano, F. Mazzenga, and F. Vatalaro. Smart cell sectorization for third generation CDMA systems. *Wireless Communications and Mobile Computing*, 2(3):253–267, 2002.

L.C. Godara. Applications of antenna arrays to mobile communications. I.

Performance improvement, feasibility, and system considerations. *Proceedings of the IEEE*, 85(7):1031–1060, 1997a. ISSN 0018-9219.

L.C. Godara. Application of antenna arrays to mobile communications. II. Beam-forming and direction-of-arrival considerations. *Proceedings of the IEEE*, 85(8):1195–1245, 1997b. ISSN 0018-9219.

Ronald L. Graham, Donald E. Knuth, and Oren Patashnik. *Concrete Mathematics: A Foundation for Computer Science*. Addison-Wesley Longman Publishing Co., Inc., Boston, MA, USA, 1994. ISBN 0201558025.

J. Habetha. *Entwurf eines cluster-basierten ad hoc Funknetzes*. PhD thesis, RWTH Aachen University, Lehrstuhl für Kommunikationsnetze, Jul 2002. URL `http://www.comnets.rwth-aachen.de`.

J. Habetha and J. Wiegert. Network capacity optimisation, part 1: Cellular radio networks. In *10th Symposium on Signal Theory*, pages 125–132, Aachen, Sep 2001.

Seung Hee Han and Jae Hong Lee. An overview of peak-to-average power ratio reduction techniques for multicarrier transmission. *Wireless Communications, IEEE [see also IEEE Personal Communications]*, 12(2):56–65, April 2005.

Y. Hara. Time Slot Assignment Algorithms for SDMA/TDMA System Based on Estimated SINR. *IEICE TRANSACTIONS on Communications*, 84 (2):220–227, 2001.

C. Hartmann. Channel allocation and handover for the HSCSD service in SDMA systems. In *15th IEEE International Symposium on Personal, Indoor and Mobile Radio Communications, PIMRC 2004*, volume 2, pages 1486–1490, September 2004.

M.J. Ho, GL Stuber, and MD Austin. Performance of switched-beam smart antennas for cellular radiosystems. *Vehicular Technology, IEEE Transactions on*, 47(1):10–19, 1998.

C. Hoymann. Analysis and Performance Evaluation of the OFDM-based Metropolitan Area Network IEEE 802.16. *Computer Networks*, 49(3): 341–363, Oct 2005.

C. Hoymann. MAC Layer Concepts to Support Space Division Multiple Access in OFDM based IEEE 802.16. *Wireless Personal Communications*, 36(4):363–385, March 2006. ISSN 0929-6212.

C. Hoymann and K. Klagges. MAC Frame Concepts to Support Multihop Communication in IEEE 802.16 Networks. In *Proceedings of the 16th Wireless World Research Forum*, page 6, Shanghai, China, Apr 2006.

C. Hoymann and P. Piggin. Extended IE format for concurrent transmission of bursts. IEEE 802.16 Standard Contribution, Mar 2004.

C. Hoymann and B. Wolz. Adaptive Space-Time Sectorization for Interference Reduction in Smart Antenna Enhanced Cellular WiMAX Networks. In *Proceedings of the 64th IEEE Vehicular Technology Conference*, page 5, Montreal, Canada, Sep 2006. ISBN 1-4244-0063-5.

C. Hoymann, A. Ibing, and I. Forkel. MAC Layer Concepts to Support Space Division Multiple Access in Wireless Metropolitan Area Networks (IEEE 802.16a). In *10th Wireless World Research Forum (WWRF) Meeting*, volume 0, New York, USA, Oct 2003.

C. Hoymann, K. Klagges, and M. Schinnenburg. Multihop Communication in Relay Enhanced IEEE 802.16 Networks. In *Proceedings of the 17th IEEE PIMRC*, page 4, Helsinki, Finland, Sep 2006a. ISBN 1-4244-0330-8.

C. Hoymann, Haiqiang Meng, and Jan Ellenbeck. Influence of SDMA-Specific MAC Scheduling on the Performance of IEEE 802.16 Networks. In *Proceedings of 12th European Wireless Conference 2006*, page 7, Apr 2006b.

C. Hoymann, J. Ellenbeck, R. Pabst, and M. Schinnenburg. Evaluation of Grouping Strategies for an Hierarchical SDMA/TDMA Scheduling Process. In *Proceedings of IEEE International Conference on Communications (ICC)*, Glasgow, UK, June 2007.

A. Hutter, C. Hoymann, B. Wächter, E. Cianca, and N. Cassiau. Advanced Link Level Techniques for Broadband MIMO Metropolitan Area Networks. In *Proceedings of The Seventh International Symposium on Wireless Personal Multimedia Communications*, pages V3, 310–315, Abano Terme, Italy, Sep 2004.

IEEE. IEEE Std 802.16-2001, IEEE Standard for Local and Metropolitan Area Networks, Part 16: Air Interface for Fixed Broadband Wireless Access Systems, Apr. 2002.

IEEE. IEEE Std 802.16-2004, IEEE Standard for Local and metropolitan area networks, Part 16: Air Interface for Fixed Broadband Wireless Access Systems, Oct. 2004a.

IEEE. IEEE Std 802.16.2-2001, IEEE Recommended Practice for Local and Metropolitan Area Networks, Coexistence of Fixed Broadband Wireless Access Systems, Sep. 2001.

IEEE. IEEE Std 802.16.2-2004, IEEE Recommended Practice for Local and Metropolitan Area Networks, Coexistence of Fixed Broadband Wireless Access Systems, Mar. 2004b.

IEEE. IEEE Std 802.16/Conformance01-2003, IEEE Standard for Conformance to IEEE 802.16, Part 1: Protocol Implementation Conformance Statement (PICS) Proforma for 10-66 GHz WirelessMAN-SC Air Interface, Aug. 2003a.

IEEE. IEEE Std 802.16/Conformance02-2003, IEEE Standard for Conformance to IEEE 802.16, Part 2: Test Suite Structure and Test Purpose for 10-66 GHz WirelessMan-SC Air Interface, Feb. 2004c.

IEEE. IEEE Std 802.16/Conformance03-2004, IEEE Standard for Conformance to IEEE 802.16, Part 3: Radio Conformance Tests (RCT) for 10-66 GHz WirelessMAN-SC Air Interface, Jun. 2004d.

IEEE. IEEE Std 802.16/Conformance04-2006, IEEE Standard for Conformance to IEEE 802.16, Part 4: Protocol Implementation Conformance Statement (PICS) Proforma for Frequencies below 11 GHz, Jan 2007a.

IEEE. IEEE Std 802.16a-2003, IEEE Standard for Local and Metropolitan Area Networks, Part 16: Air Interface for Fixed Broadband Wireless Access Systems - Amendment 2: Medium Access Control Modifications and Additional Physical Layer Specifications for 2-11 GHz, Apr. 2003b.

IEEE. IEEE Std 802.16c-2002, IEEE Standard for Local and Metropolitan Area Networks, Part 16: Air Interface for Fixed Broadband Wireless Access Systems - Amendment 1: Detailed System Profiles for 10-66 GHz, Jan. 2003c.

IEEE. IEEE Std 802.16e-2005, IEEE Standard for Local and Metropolitan Area Networks, Part 16: Air Interface for Fixed and Mobile Broadband Wireless Access Systems Amendment for Physical and Medium Access Control Layers for Combined Fixed and Mobile Operation in Licensed Bands, Feb. 2006.

IEEE. IEEE Std 802.16f-2005, IEEE Standard for Local and Metropolitan Area Networks, Part 16: Air Interface for Fixed Broadband Wireless Access Systems - Amendment 1: Management Information Base, Dec. 2005.

IEEE. IEEE Std 802.16g-2006, IEEE Standard for Local and Metropolitan Area Networks, Part 16: Air Interface for Fixed and Mobile Broadband Wireless Access Systems - Amendment 2: Management Plane Procedures and Services, Dec 2007b.

IEEE. IEEE 802.16j/D3, Draft Standard for Local and Metropolitan Area Networks Part 16: Air Interface for Fixed and Mobile Broadband Wireless Access Systems Multihop Relay Specification, Feb 2008.

Intel. OFDMA PHY SAP Interface Specification for 802.16 Broadband Wireless Access Base Stations, Sep. 2006. URL `www.intel.com/netcomms/technologies/wimax/PHY_SAP_API_229.pdf`. Version 2.29.

T. Irnich, D. Schultz, R. Pabst, and P. Wienert. Capacity of a relaying infrastructure for broadband radio coverage of urban areas. In *Proceedings of Vehicular Technology Conference (VTC fall)*, page 5, Orlando (FL), USA, Oct 2003. ISBN 0-7803-7955-1. URL `http://www.comnets.rwth-aachen.de`.

IST-STRIKE. URL `www.ist-strike.org`.

IST-WINNER. D5.4, Final Report on Link Level and System Level Channel Models. Deliverable, IST-4-027756 WINNER II, September 2006.

W. Jakes. *Microwave Mobile Communications*. Wiley, 1974.

J.F. Kepler, T.P. Krauss, and S. Mukthavaram. Delay spread measurements on a wideband MIMO channel at 3.7 GHz. In *Vehicular Technology Conference, 2002. Proceedings. VTC 2002-Fall. 2002 IEEE 56th*, volume 4, pages 2498–2502, 24-28 Sept. 2002.

J. Kim and J. Cioffi. Spatial Multiuser Access with Antenna Diversity Using Singular Value Decomposition. *Proc. IEEE Int. Conf. Commun. (ICC)*, 2000.

I. Koffman and V. Roman. Broadband wireless access solutions based on OFDM access in IEEE 802.16. *Communications Magazine, IEEE*, 40(4): 96–103, April 2002.

I. Koutsopoulos, T. Ren, and L. Tassiulas. The impact of space division multiplexing on resource allocation: a unified approach. In *INFOCOM 2003. Twenty-Second Annual Joint Conference of the IEEE Computer and Communications Societies. IEEE*, volume 1, pages 533–543, 2003.

M. Lampe, T. Giebel, H. Rohling, and W. Zirwas. PER-prediction for PHY mode selection in OFDM communication systems. In *Global Telecommunications Conference, 2003. GLOBECOM '03. IEEE*, volume 1, pages 25–29, Dec. 2003.

J. Liberti and T. Rappaport. *Smart Antennas for Wireless Communications: IS-95 and Third Generation CDMA Applications*. Prentice Hall, 1999.

T. Mansour. Restricted permutations by patterns of type (2,1), 2002. URL `http://www.citebase.org/cgi-bin/citations?id=oai:arXiv.org:math/0202219`.

Andreas Molisch. *Wireless Communications*. John Wiley & Sons, Ltd., 2005. ISBN 0-470-84888-X.

A. M. Odlyzko. Asymptotic Enumeration Methods. In R.L. Graham,

M. Grötschel, and L. Lovász, editors, *Handbook of Combinatorics*, volume 2, pages 1063–1229. North-Holland, Amsterdam, 1995. ISBN 0-444-82351-4.

openWNS. open wireless network simulator, December 2007. URL `http://www.openwns.org`.

F. Orthman. *WiMAX Handbook, Building 802.16 Wireless Networks*. McGraw-Hill, 2005.

R. Pabst, B. Walke, D. Schultz, and et al. Relay-Based Deployment Concepts for Wireless and Mobile Broadband Radio. *IEEE Communications Magazine*, pages 80–89, Sep 2004. ISSN 0163-6804. URL `http://www.comnets.rwth-aachen.de`.

R. Pabst, J. Ellenbeck, M. Schinnenburg, and C. Hoymann. System Level Performance of Cellular WiMAX IEEE 802.16 with SDMA-enhanced Medium Access. In *Proceedings of IEEE Wireless Communications & Networking Conference*, page 5, Hong Kong, China, Mar 2007. ISBN 1-4244-0659-5.

pari/gp. PARI/GP, 2006. URL `http://pari.math.u-bordeaux.fr/`.

A. Pauraj, R. Nabar, and D. Gore. *Introduction to Space-Time Wireless Communications*. Cambridge University Press, July 2003.

G. Raleigh and J. Cioffi. Spatio-Temporal Coding for Wireless Communications. *IEEE Trans. Commun.*, 46(3), March 1998.

T. Rappaport. *Wireless Communications: Principles and Practice*. Prentice Hall, 2001.

CU Saraydar and A. Yener. Adaptive cell sectorization for CDMA systems. *Selected Areas in Communications, IEEE Journal on*, 19(6):1041–1051, 2001.

M. Schinnenburg, F. Debus, A. Otyakmaz, L. Berlemann, and R. Pabst. A Framework for Reconfigurable Functions of a Multi-Mode Protocol Layer. In *Proceedings of SDR Forum 2005*, page 6, Los Angeles, U.S., Nov 2005. URL `http://www.comnets.rwth-aachen.de`.

F. Shad, T.D. Todd, V. Kezys, and J. Litva. Dynamic slot allocation (DSA) in indoor SDMA/TDMA using a smart antenna basestation. *IEEE/ACM Transactions on Networking*, 9(1):69–81, 2001. ISSN 1063-6692.

N. J. A. Sloane. The On-Line Encyclopedia of Integer Sequences, 2006. URL `http://www.research.att.com/{\char126\relax}njas/sequences/`.

V. Tarokh, N. Seshadri, and A. Calderbank. Space-Time Codes for High Data Rate Wireless Communications: Performance Criterion and Code Construction. *IEEE Trans. Inf. Theory*, 44(2):744–765, 1998.

V. Tarokh, H. Jafarkhani, and A. Calderbank. Space-Time Block Codes from Orthogonal Designs. *IEEE Trans. Inf. Theory*, 45:1456–1467, 1999.

Emre Telatar. Capacity of Multi-Antenna Gaussian Channels. *European Transactions on Telecommunications*, 10(6):585–595, November 1999.

Richard van Nee and Ramjee Prasad. *OFDM for Wireless Multimedia Communications*. Artech House, Inc., Norwood, MA, USA, 2000. ISBN 0890065306.

U. Vornefeld. Packet Scheduling in SDMA Based Wireless Networks. volume 0, Boston, USA, Sep 2000. URL `http://www.comnets.rwth-aachen.de`.

U. Vornefeld, C. Walke, and B. Walke. SDMA techniques for wireless ATM. *Communications Magazine, IEEE*, 37(11):52–57, Nov. 1999.

B. Walke and R. Briechle. A Local Cellular Radio Network for Digital Voice and Data Transmission at 60GHz. volume 0, pages 215–225, Online London, Nov 1985. URL `http://www.comnets.rwth-aachen.de`.

Bernhard Walke. *Mobile Radio Networks - Networking and Protocols*. John Wiley & Sons, November 2001.

Bernhard Walke, Stefan Mangold, and Lars Berlemann. *IEEE 802 Standardized Systems: Protocols, Multi-hop Relaying/Mesh, Traffic Performance and Spectrum Coexistence*. Wiley, 2006.

H. Wijaya. *Broadband Multi-Hop Communication in Homogeneous and Heterogeneous Wireless LAN Networks*. PhD thesis, RWTH Aachen University, Lehrstuhl für Kommunikationsnetze, Feb 2005. URL `http://www.comnets.rwth-aachen.de`.

WiMAX Forum. Worldwide interoperability for microwave access, 2006a. URL `http://www.wimaxforum.org`.

WiMAX Forum. Mobile WiMAX - Part II: A Comparative Analysis, May 2006b. URL `http://www.wimaxforum.org`.

Hujun Yin and Hui Liu. Performance of space-division multiple-access (SDMA) with scheduling. *IEEE Transactions on Wireless Communications*, 1(4):611–618, 2002. ISSN 1536-1276.

Ruifeng Zhang. Scheduling for maximum capacity in SDMA/TDMA networks. In *Acoustics, Speech, and Signal Processing, 2002. Proceedings. (ICASSP '02). IEEE International Conference on*, volume 3, 2002.

W. Zirwas, T. Giebel, N. Esseling, E. Schulz, and J. Eichinger. Broadband multi hop networks with reduced protocol overhead. In *Proc. European Wireless 2002*, volume 1, pages 333–339, Florence, Italy, Feb 2002. URL `http://www.comnets.rwth-aachen.de`.

ACKNOWLEDGEMENT

This thesis is the result of five years research at the Chair of Communication Networks (ComNets) at the RWTH Aachen University, Germany. During this time I had the pleasure to work for Prof. Dr.-Ing. Bernhard Walke. I am deeply grateful to him for his support, the inspiring work environment he provided and the freedom in research.

Furthermore, I would like to thank Prof. Dr.-Ing. Bernhard Rembold from the Chair of High Frequency Technique (IHF), RWTH Aachen University, Germany, for his support as second examiner.

Special thanks go to my colleagues at ComNets: Dr. Peter Stuckmann for being my mentor in the first years. Dr. Ingo Forkel for the teamwork in the IST STRIKE project. Benedikt Wolz for the collaboration in IST FIREWORKS, and DFG TakeOFDM (supported by Daniel Martini (IHF)). Marc Schinnenburg, Ralf Pabst, and Karsten Klagges for the support while working with the WNS. Stephan Göbbels for daily discussions. All colleagues for the comfortable and inspiring work environment.

Many thanks go to all students that contributed to my research at ComNets, especially to Markus Grauer, Karsten Klagges, Jan Ellenbeck, Benedikt Wolz, Haiqiang Meng, Budi Hartono, Victor Bermúdez Llamusí, Björn Wächter, Andreas Ibing, Holger Rosier, Michael Dittrich, and Markus Püttner.

I like to thank my friends and family for having them on my side. Special thanks go to my parents for their never ending support.

Finally, I would like to thank my wife, Annabell, for her love, mental support and patience during the preparation of the thesis.

Aachen, July 2008 Christian Hoymann

CURRICULUM VITAE

Name:	Christian Hoymann
Date of birth:	May 10, 1976
Place of birth:	Essen
Nationality:	German

09/1986 - 06/1995	Erzbischöfliches St.-Angela Gymnasium, Wipperfürth
10/1996 - 01/2002	Studies in Electrical Engineering at RWTH Aachen University
10/1998 - 03/2005	Studies in Business Administration at RWTH Aachen University and at Fern-Universität Hagen
10/2000 - 04/2001	Internship at Siemens Corporate Research, Princeton, NJ, USA
03/2002 - 03/2007	Research Engineer at Chair of Communication Networks, RWTH Aachen University
04/2007 - 05/2007	Senior Systems Design Engineer at PureWave Networks, Mountain View, CA, USA
since 06/2007	Senior Research Engineer at Ericsson Research